GHENT
UNIVERSITY

FACULTY OF
PHARMACEUTICAL SCIENCES

Synthesis and biological evaluation of novel bivalent GPCR ligands

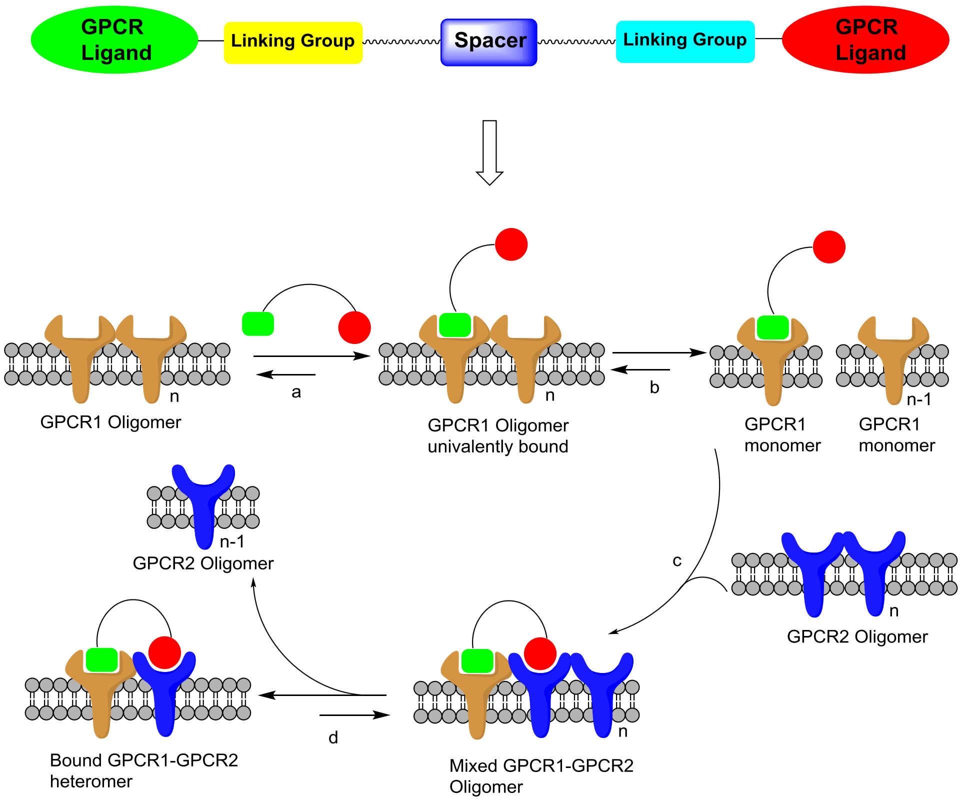
GPCR Ligand
Linking Group
Spacer
Linking Group
GPCR Ligand
n
GPCR1 Oligomer
a
n
GPCR1 Oligomer univalently bound
b
GPCR1 monomer
n-1
GPCR1 monomer
n-1
GPCR2 Oligomer
c
n
GPCR2 Oligomer
Bound GPCR1-GPCR2 heteromer
d
n
Mixed GPCR1-GPCR2 Oligomer

Mingcheng Qian

Promoter:
Prof. Dr. S. Van Calenbergh

Academic year 2018-2019

Thesis submitted in fulfillment of the requirements for the degree of Doctor in Pharmaceutical Sciences

Synthesis and biological evaluation of novel bivalent GPCR ligands

Mingcheng Qian

Ghent University
Faculty of Pharmaceutical Sciences
Department of Pharmaceutics
Laboratory for Medicinal Chemistry

Promoter:
Prof. Dr. S. Van Calenbergh

Academic year 2018-2019

Thesis submitted in fulfillment of the requirements for the degree of Doctor in Pharmaceutical Sciences

Composition of the jury

Promoter:
Prof. Dr. Serge Van Calenbergh
Laboratory for Medicinal Chemistry, Faculty of Pharmaceutical Sciences, Ghent University

Co-promoter:
Prof. Dr. Kathleen Van Craenenbroeck
Laboratory of toxicology, Faculty of Pharmaceutical Sciences, Ghent University

Chairman:
Prof. Dr. Filip De Vos
Laboratory of Radiopharmacy, Faculty of Pharmaceutical Sciences, Ghent University

Members of the Examination Committee:
Prof. Dr. Francisco Ciruela Alférez
Unitat de Farmacologia, Departament de Patologia i Terapèutica Experimental, Facultat de Medicina i Ciències de la Salut, Universitat de Barcelona, Spain

Prof. Dr. Patrick Vanderheyden
Research Group of Molecular and Biochemical Pharmacology, Faculty of Sciences and Bioengineering Sciences, Vrije Universiteit Brussel

Prof. Dr. Karolien De Bosscher
Receptor Research Laboratories, Nuclear Receptor Lab (NRL) and Cytokine Receptor Lab (CRL), VIB-UGent Center for Medical Biotechnology, Ghent University

Prof. Dr. Bruno De Geest
Biopharmaceutical Technology Unit, Laboratory of Pharmaceutical Technology, Faculty of Pharmaceutical Sciences, Ghent University

Prof. Dr. Christophe Stove
Laboratory of Toxicology, Faculty of Pharmaceutical Sciences, Ghent University

Table of Contents

Summary i

Samenvatting ii

List of Abbreviations iii

I. Introduction 1

I.1. General introduction of GPCR 1

I.1.1 Structure of GPCR 1

I.1.2 Classification of GPCR 2

I.1.3 GPCR signaling 2

I.1.4 GPCR dimerization 5

I.1.5 Techniques used to study GPCR dimerization 6

I.2. Bivalent ligands of G protein-coupled receptors (GPCRs) 13

I.2.1 Concept and design of bivalent GPCR ligands 14

I.2.2 Functionalized pharmacophore, attachment point and linking groups 14

I.2.3 Spacer Length. 16

I.2.4 Conformational flexibility and hydrophilicity of the Spacer 20

I.2.5 Bivalent ligands may enhance selectivity and binding affinity 24

I.2.6 How to estimate if a bivalent ligand bridges the receptor dimer? 26

I.2.7 In vivo relevance of bivalent ligands 33

I.2.8 Conclusion 37

Reference 39

II. Objectives 61

III. Design, synthesis and biological evaluation of bivalent ligands targeting Dopamine D_2-like receptors and the µ-opioid receptor 67

III.1. Abstract 67

III.2. Introduction 67

III.3. Design of heterobivalent ligands based on structure of D_2-likeR ligands and µOR ligands 68

III.4. Results and Discussion 70

III.4.1. Chemistry 70

III.4.2. Ligand binding assays 72

III.4.3. Functional assays 77

III.5. Conclusions 81

III.6. Experimental Section 82

III.6.1. Chemistry 82

III.6.2. Plasmids and receptor fusion constructs 90

III.6.3. Cell culture and transfection 91

III.6.4. Membrane Preparation and Protein Determination. 91

III.6.5. [^{3}H]Spiperone Binding. 91

III.6.6. [^{3}H]Raclopride Binding. 91

III.6.7. [^{3}H]Diprenorphine Binding. 92

III.6.8. Data Analysis. 92

III.6.9. MAPK phosphorylation 92

III.6.10. β-arrestin2 recruitment 93

References: 94

III.7. Supporting information (SI) 99

IV. Synthesis toward bivalent ligands for the dopamine D$_2$ and metabotropic glutamate 5 receptors 121

IV.1. ABSTRACT 121

IV.2. Introduction 121

IV.3. Results and Discussion 124

IV.3.1. Design of heterobivalent ligands 124

IV.3.2. Synthesis 126

IV.3.3. Pharmacological evaluation 128

IV.4. Conclusion 138

IV.5. Experimental Section 139

IV.5.1. Chemistry 139

IV.5.2. Generation of the stable D2s-mGluR5 co-expressing cell line 146

IV.5.3. Cell culture and transfection 146

IV.5.4. Membrane Preparation and Protein Determination. 147

IV.5.5. [^{3}H]Spiperone Binding. 147

IV.5.6. [^{3}H]Raclopride Binding. 147

IV.5.7. [^{3}H]MPEP Binding. 148

IV.5.8. Data Analysis. 148

IV.5.9. MAPK phosphorylation 148

IV.5.10. GloSensor cAMP protocol 149

IV.5.11. Computational modeling 149

REFERENCES 150

IV.6. Supporting information 159

V. Synthesis and biological evaluation of fluorescent ligands targeting the metabotropic glutamate 5 receptor 187

V.1. Abstract 187

V.2. Introduction 187
V.3. Design of fluorescent mGluR5 ligands 187
V.4. Results and discussion 188
V.4.1. Chemistry 188
V.4.2. Preliminary evaluation of the synthesized fluorescent mGluR5 ligands 190
V.5. Conclusion 193
V.6. Experimental 194
V.6.1 Chemistry 194
V.6.2 Spectra 198
V.6.3 Relative emission 198
V.6.4 Single binding NanoBRET assay 198
V.6.5 Saturation binding NanoBRET assay 198
References 199
V.7. Supporting Information 200
VI. General Conclusion 213
VII. Broader International Context, Relevance, and Future Perspectives 219
VII.1. Marketed small-molecule drugs targeting GPCRs 219
VII.2. Bivalent ligands: tools par excellence to study receptor dimers 220
VII.3. From bivalent ligands to drug-like compounds targeting dimeric receptors 222
VII.3.1. Disadvantages of bivalent ligands 222
VII.3.2. From bivalent ligands to integrated dual acting ligands 222
VII.3.3. Towards drug-like compounds that selectively activate heterodimeric receptors 224
VII.4. Future Perspectives 224
References 229
Dankwoord ─ Acknowledgements 235
Scientific curriculum vitae 239
Overview of synthesized compounds 243

Summary

In many disease processes G protein-coupled receptors (GPCRs) are over- or understimulated, explaining why the pharmaceutical industry develops drugs (blockers or stimulators) to counteract this over- or understimulation. Almost half of the clinically used drugs today are interfering with GPCRs.

Chapter I gives a general introduction on GPCRs, such as GPCR structure, classification, signaling, as well as GPCR dimerization. Furthermore, an overview of bivalent ligands targeting GPCR dimers is given in this chapter, which mainly focuses on the recent studies on bivalent ligands. As a rule of thumb, bivalent ligands with a spacer of optimal length are envisaged to exhibit a potency that is greater than that derived from the sum of its two monovalent pharmacophores. They may allow targeting certain dimeric receptors, thereby increasing the selectivity of drug action. The design of such molecules requires the choice of appropriate pharmacophores, the selection of suitable attachment points for the spacer - and the length and chemical structure of the spacer. We also illustrated how a bivalent ligand bridges the GPCR dimer in vitro and in vivo by numerous recent studies.

The main objectives of this thesis are described in Chapter II.

Heterobivalent ligands have been proven useful molecular probes for confirming and targeting heteromeric receptors. Chapter III describes the design and synthesis of novel heterobivalent ligands for the dopamine D_2-like receptors (D_2-likeR) and the μ opioid receptor (μOR) and their biological evaluation using ligand binding and functional assays. To assess their functionality, D_2-likeR induced MAPK phosphorylation was quantified in the presence or absence of bivalent ligands. Furthermore, β-arre2 recruitment was studied via NanoBiT to evaluate stimulation of the μOR.

In Chapter IV we designed and synthesized a series of bivalent D_2R ligands and mGluR5 allosteric antagonists pharmacophores linked through spacers of varying length as tools to study the functional interaction between D_2-likeR and mGluR5. Ligand binding allowed to determine the affinity of the bivalent ligands for both protomers. In addition, cAMP and MAPK phosphorylation assay was utilized to assess the signal transduction for both receptors.

Chapter V describes the synthesis of fluorescently labeled ligands as potential pharmacological tools to study receptor localization, trafficking, and signaling processes via fluorescence imaging. They could also be employed in fluorescent binding assays to study ligand/receptor interactions. The BODIPY labeled mGluR5 fluorescent ligands were applied to investigate ligand-receptor interactions via a NanoBRET.

A general conclusion of this PhD work is given in Chapter VI.

Finally, Chapter VII is dedicated to the discussion of the broader international context of small-molecule drugs targeting GPCRs, relevance of recently reported bivalent GPCR ligands, as well as future perspectives regarding the design and evaluation of bivalent ligands.

Samenvatting

In veel ziekteprocessen worden G-proteïne gekoppelde receptoren (GPCRs) over- of onder gestimuleerd. Dit verklaart waarom de farmaceutische industrie (stimulerende of blokkerende) drugs heeft ontwikkeld om deze over- of onder stimulatie te normaliseren. Ongeveer de helft van de klinische drugs die tegenwoordig worden gebruikt, interfereren met de werking van deze GPCRs.

Hoofdstuk 1 biedt de algemene introductie van GPCRs, zoals de structuur van GPCRs, classificatie, signalisatie, alsook de GPCR dimerisatie. Verder wordt er in dit hoofdstuk ook een beperkt overzicht gegeven van bivalente liganden die GPCR-dimeren als doelwit hebben. In dit overzicht, wordt de nadruk hoofdzakelijk gelegd op de recente studies over deze bivalente liganden. Indien bivalente liganden zijn uitgerust met een linker van optimale lengte, kan een grotere potentie worden verkregen, in vergelijking met de potentie afkomstig van de som van de twee monovalente farmacoforen. Dit kan ervoor zorgen dat er preferentieel kan worden geinterageerd met bepaalde dimerische subtypes, wat de selectiviteit van de drugs doet stijgen. De ontwikkeling van zo'n molecule vereist de keuze van farmacoforen, de aanhechtingspunten van de linkers op de farmacofoor en de lengte en de chemische structuur van de linker. We tonen ook met meerdere recente studies aan hoe bivalente liganden binden met de GPCR-dimeren.

Hoofdstuk II beschrijft de kerndoelstellingen van dit proefschrift.

Het is reeds bewezen dat heterobivalente liganden zeer nuttige moleculen zijn voor de bevestiging van het bestaan van, alsook het *targeten* van heteromere receptoren. Hoofdstuk III beschrijft de ontwikkeling en de synthese van nieuwe heterobivalente liganden voor de dopamine D_2-like receptoren (D_2-likeR) en de µ-opiaatreceptor (µOR) en hun biologische evaluatie, op basis van radioactieve ligandbindingstechnieken en functioneel onderzoek. Voor dit laatstgenoemde werd de MAPK fosforylatietechniek geïmplementeerd om de D_2-likeR te testen in de aan- of afwezigheid van bivalente liganden. Verder werd de β-arre2 recrutering via de NanoBiT techniek toegepast om de signalisatietransductie van µOR te analyseren.

Hoofdstuk IV beschrijft het ontwerp en de synthese van een aantal bivalente liganden waarbij D_2-likeR agonist en mGluR5 antagonist farmacoforen, aan elkaar zijn gehecht met linkers van variërende lengte. Deze dimeren worden vervolgens gebruikt als *tools* om de functionele interactie tussen de D_2-likeR en mGluR5 te onderzoeken. Ligandbindingsexperimenten stelden ons in staat om de affiniteit van de dimere liganden voor beide promotoren te bepalen. Daarnaast werd een cAMP en MAPK fosforylatieassay gebruikt om de signaaltransductie voor beide receptoren te bestuderen.

Hoofdstuk V beschrijft de ontwikkeling van fluorescent gelabelde liganden als farmaceutische gereedschappen om receptorlokalisatie, -transport en –signalisatie te bestuderen via fluorescente beeldvormingstechnieken. Deze liganden worden ook toegepast bij fluorescente bindingstechnieken om ligand/receptor interacties te kunnen bestuderen. Er werd gebruik gemaakt van mGluR5 liganden gelabeld met BODIPY fluoroforen om de ligand-receptor interacties te onderzoeken via NanoBRET.

Het algemeen besluit van deze PhD thesis staat beschreven in hoofdstuk VI.

Hoofdstuk VII omvat de discussie van de brede context van *small-molecule* drugs die GPCRs als doelwit hebben, de relevantie van recent gerapporteerde bivalente GPCR-liganden, alsook de toekomstige perspectieven omtrent het ontwerp en de evaluatie van bivalente liganden.

List of Abbreviations

δOR	δ-opioid receptor;
κOR	κ-opioid receptor;
μOR	μ-opioid receptor;
δ	Chemical shift
J	Coupling constant
1,4-DAP	1,4-disubstituted aromatic piperazine
5-HT	Serotonin receptor
5-OH-DPAT	5-hydroxy-2-(dipropylamino)tetralin
A_{2A}R	Adenosine A_{2A} receptor
AC	Adenylyl cyclase
ATP	Adenosine triphosphate
BL	Bivalent ligand;
BODIPY	Boron dipyrromethene
BODIPY	Boron dipyrromethene
BRET	Bioluminescence resonance energy transfer
cAMP	Cyclic Adenosine monophosphate
CB	Cannabinoid receptor
CB1	Cannabinoid 1 receptor
CCK	Cholecystokinin
CCR, CXCR	Chemokine receptor
CFP	Cyan fluorescent protein
CHPG	(RS)-2-Chloro-5-hydroxyphenylglycine

Co-IP	Co-immunoprecipitation
CuAAC	Copper-catalyzed azide-alkyne cycloaddition
CXCR4	CXC chemokine receptor 4
d	Doublet
D_2-likeR	Dopamine D_2-like receptors
D_2R	Dopamine D_2 receptor
Da	Dalton
DA	Dopamine
DAG	Diacylglycerol
DCE	1,2-Dichloroethane
dd	Double doublet
ddd	Double double doublet
DHPG	(S)-3,5-Dihydroxyphenylglycine
DMAP	4-(Dimethylamino)-pyridine
DMEM	Dulbecco’s modified Eagle’s medium
DMF	N,N-Dimethylformamide
DMSO	Dimethyl sulfoxide
dt	Double triplet
E. coli	Escherichia coli
EDC	N-(3-Dimethylaminopropyl)-N′ -ethylcarbodiimide hydrochloride
ERK	Extracellular-signal regulated kinase
Et	Ethyl
Et2O	Diethyl ether

Et3N	Triethylamine
EtOAc	Ethyl acetate
EtOH	Ethanol
FRET	Fluorescence resonance energy transfer
g	Gram(s)
GABA	Gamma amino butyric acid
GDP	Guanosine disphosphate
GFP	Green fluorescent protein
GPCR	G protein coupled receptor
GRPR	Gastrin-releasing peptide receptor
GSHR	Apo-ghrelin receptor
GTP	Guanosine triphosphate
H	Histamine receptor
h	Hour(s)
HEK	Human embryonic kidney cell line
HM	Hydromorphone
Hz	Hertz
IC_{50}	Inhibitor concentration resulting in 50% inhibition of enzyme activity
IP3	Inositol triphosphate
K_i	Binding affinity
L-DOPA	L-3,4-dihydroxyphenylalanine
L-Glu	L-Glutamic acid
M	Molar

m	Multiplet
MAPK	Mitogen-activated protein kinase
mg	Milligram(s)
mGluRs	Metabotropic glutamate receptors
min	Minute(s)
mL	Milliliter(s)
mmol	Millimole(s)
MPEP	2-methyl-6-(phenylethynyl)pyridine
MS	Mass spectrometry
MTEP	3-[(2-methyl-4-thiazolyl)ethynyl]pyridine
NAc	Nucleus accumbens
NAM	Negative allosteric modulator
NanoBiT	NanoLuc Binary Technology
NK1	Neurokinin NK1 receptor
NMR	Nuclear magnetic resonance spectroscopy
NTS	Neurotensin receptor
NTX	Naltrexone
OT	Oxytocin receptor
PAGE	Polyacrylamide gel electrophoresis
PCR	Polymerase chain reaction
PEG	Polyethylene glycol
PI	Phosphoinositide
PKC	Protein kinase C

PLA	Proximity ligation assay
PLC	Phospholipase C
PLCγ	Phospholipase C-gamma
ppm	Parts per million
RT	Room temperature
s	Singlet
SAR	Structure-activity relationship
sat.	Saturated
SDS	Sodium dodecyl sulphate
SERT	Serotonin reuptake transporter
SFK	Src family kinase
SFM	Serum-free media
SSTR	Somatostatin receptor
t	Triplet
TBAF	Tetra-n-butylammonium fluoride
TBTA	Tris[(1-benzyl-1H-1,2,3-triazol-4-yl)methyl]amine
TFA	Trifluoroacetic acid
THF	Tetrahydrofuran
TLC	Thin-layer chromatography
TR-FRET	Time-resolved fluorescence resonance energy transfer
UV	Ultraviolet
v	Volume
YFP	Yellow fluorescent protein

CHAPTER I

INTRODUCTION

I. INTRODUCTION

I.1. General introduction of GPCR

Our body is composed of cells that need to communicate with each other for proper functioning. Towards this end cells contain many different receptors, involved in passing information from outside the cell to the intercellular environment and to control physiological processes (e.g, food digestion, muscle contraction, mood, etc.). By means of messengers (e.g. neurotransmitters or hormones), G protein-coupled receptors (GPCRs) represent the largest group of cell membrane receptors. In many disease processes GPCRs are over- or understimulated, explaining why the pharmaceutical industry develops drugs (blockers or stimulators) to compensate for this over- or understimulation. Almost half of today’s clinically used drugs act directly or indirectly on GPCRs.

I.1.1 Structure of GPCR

G protein-coupled receptors (GPCRs), which are also known as 7-transmembrane receptors, heptahelical receptors or serpentine receptors, constitute the largest protein family of cell surface receptors encoded by the human genome. Structurally, GPCRs consist of seven-transmembrane α-helices (7-TM) connected by three extracellular loops and three intracellular loops, with an extracellular N-terminal region and an intracellular C-terminus at each end of the 7-TM domain. GPCRs can recognize extremely diverse stimuli, including neurotransmitters, hormones, growth factors, chemokines and light, to receive messengers from outside the cell and transfer these into the activating internal signal transduction pathways and, ultimately, cellular responses.[1]

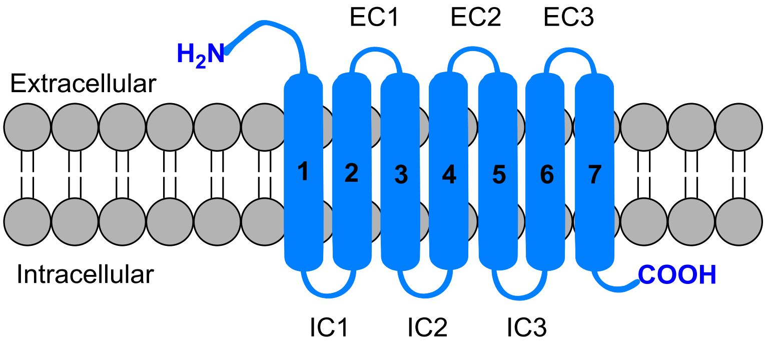

Figure 1. Schematic representation of a class A GPCR

All GPCRs consist of seven hydrophobic transmembrane domains separated by three intracellular (IC) and three extracellular (EC) loops. The N-terminus is exposed to the extracellular environment and often possesses N-glycosylation site(s). The C-terminal tail is located intracellularly.

GPCRs participate in a diversity of important physiological functions and are the targets of a large number of therapeutic agents.[2]

I.1.2 Classification of GPCR

Over the past decade, Fredriksson et al. performed large scale phylogenetic analyses of over 800 GPCRs in the human genome and divided these into five families on the basis of phylogenetic criteria. They proposed the GRAFS system to classify five main families termed Glutamate (G), Rhodopsin (R), Adhesion (A), Frizzled/Taste2 (F) and Secretin (S).[3] In the more classical A-F system, GPCRs are divided into six subfamilies based on sequence homology and functional similarity: rhodopsin-like (class A), secretin-like (class B), metabotropic glutamate (class C), fungal pheromone receptors (class D), cyclic AMP receptors (class E) and frizzled/taste2 (class F).[4]

The largest class A GPCR family (A-F system) contains more than 700 members that recognize particularly diverse ligands including inorganic ions, organic odorants, peptides, biogenic amines, lipids, proteins, nucleotides, and photons (rhodopsin, the first GPCR of which the structure was resolved).[5] These ligands can initiate downstream signals through either G protein or β-arrestin pathways. This family comprises very extensively studied GPCRs like adrenoceptors, chemokine receptors, adenosine receptors, opioid receptors and dopamine receptors. Class B GPCR members mostly bind large peptides and their N-terminus plays a key role in binding the ligand. Family C GPCRs are characterized by a long N-terminus, which plays a vital role in ligand recognition. The three other families are less studied.

I.1.3 GPCR signaling

I.1.3.1 G protein-dependent signaling

It is well known that G proteins are composed of α, β, and γ subunits, which are associated in an inactive state. The heterotrimeric G proteins are key in GPCR signaling.[6] Figure 2 shows the regulatory cycle of G proteins, i.e. activation/inactivation through GPCR ligand binding. In the inactive state, the Gα subunit is bound to a Gβγ dimer and GDP. G protein-dependent signaling starts by binding of an agonist that activates the GPCR. As a result of conformational changes, the activated GPCR catalyzes the exchange of GTP for GDP on the Gα subunit, which leads to the dissociation of the Gβγ dimer from Gα. Activated Gα and Gβγ proteins in turn bind to and modulate various effectors, which will influence the intracellular concentration of different second messengers. Finally, the intrinsic GTPase activity of Gα comes into play, which leads to the hydrolysis of bound GTP into GDP and hence the inactivation of G proteins cascade. GTPase activity of the Gα subunits may also be regulated by regulators of G proteins signaling (RGS proteins) as well as effectors.

The activated Gα subunit interacts and positively regulates numerous effectors such as potassium and calcium channels, phospholipase C (PLC), protein kinases and adenylyl cyclase (AC), which upon activation catalyzes the conversion of ATP into cAMP, a second messenger important in many biological processes.[7] It was discovered that the βγ subunits could also activate the muscarinic K^+ channel and positively regulate many effectors including AC, phospholipase C-β (PLC-β), phospholipase A_2 (PLA_2), phosphoinositide 3-kinase (PI3-kinase) and β-adrenergic receptor kinase.[8] Furthermore, Gβγ can activate Gα subunit. [9] It is now clear that many effectors are regulated by both α and βγ subunits.

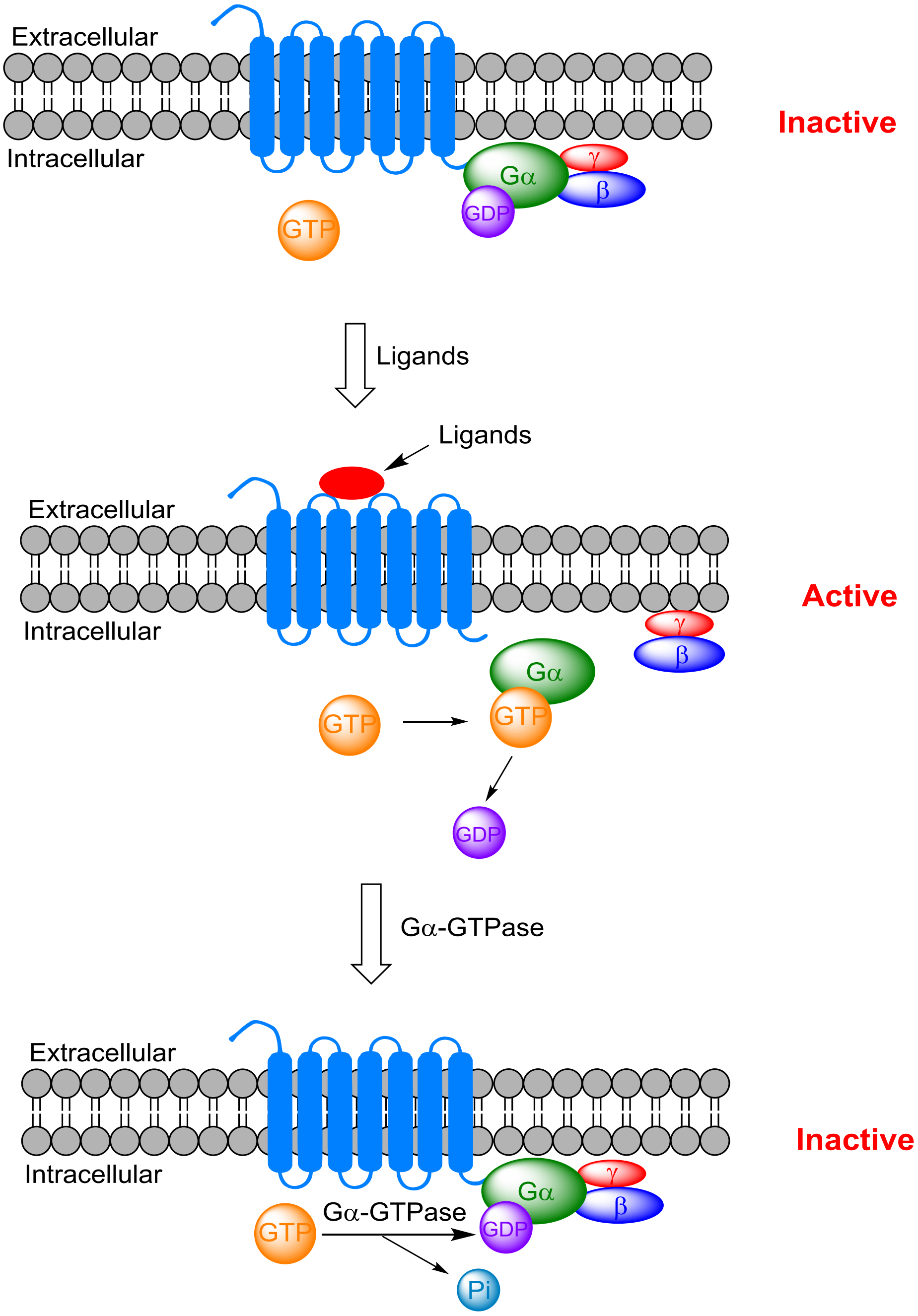
Extracellular
Intracellular
Gα
γ
β
GDP
GTP
Inactive
Ligands
Ligands
Extracellular
Intracellular
γ
β
Gα
GTP
GTP
GDP
Active
Gα-GTPase
Extracellular
Intracellular
Gα
γ
β
GTP
Gα-GTPase
GDP
Pi
Inactive

Figure 2. G protein-dependent signaling

In its inactive state the subunits of heterotrimeric G proteins (Gα and Gβγ) are associated and GDP is bound to Gα (Gα-GDP). Upon agonist binding, GPCRs undergo conformational changes, which lead to dissociation of Gα from Gβγ subunit. In the active state GTP is bound to Gα (Gα-GTP). Now free Gα and Gβγ have their own effectors to further transmit the signals and initiate unique intracellular signaling responses. Signal transduction ceases due to the intrinsic Gα-GTPase activity, which hydrolyzes the bound GTP (Gα-GTP) to GDP and Pi and inactivates the G protein complex by re-associating the Gα with Gβγ.

I.1.3.2 G protein-independent signaling

GPCRs may transduce their signals through G protein-independent mechanisms, and heterotrimeric G proteins may also play functional roles in non-GPCR signaling. β-arrestins are multifunctional proteins, which are very important regulators of GPCR function. There are two forms of β-arrestin, β-arrestin1 and β-arrestin2 (also known as arrestin2 and arrestin3, respectively). Most studies have focused on the consequences of β-arrestin2 recruitment. Specifically, β-arrestins are required for the termination of G protein signaling and the initiation of arrestin-mediated signal transduction by GPCRs. The termination of G protein signaling is promoted by phosphorylation of the intracellular loops of the activated GPCR via a G protein kinase (GRK). GPCR phosphorylation is involved in the recruitment and activation of β-arrestin, which triggers receptor internalization and sometimes initiation of the arrestin-mediated signaling cascade.[10]

β-arrestins can recruit catalytically active proteins to the activated receptors, amongst which p44/p42 mitogen-activated protein kinases (MAPK) are the most important ones.[11],[12] Some studies have focused on the significance of β-arrestins in the regulation of p44/42 MAPK phosphorylation.[11] β-arrestin-dependent and G protein-dependent phosphorylation of MAPK was shown for different GPCRs, among others angiotensin II type 1 receptors (AT_1Rs),[13],[14] neurokinin 1 receptor (NK_1)[15], parathyroid hormone receptor (PTHR)[16], vasopressin V_2 receptor (V_2R)[17], and β_2-adrenergic receptor (β_2AR)[18]. Studies involving AT_1Rs, PTHR and β_2AR suggest a common β-arrestin-mediated MAPK activation that exhibits different kinetics compared to G protein-mediated MAPK signaling. G protein-dependent MAPK activation occurs very rapid and transient, while β-arrestin-dependent MAPK activation is slower and more sustained.[16],[19],[20]

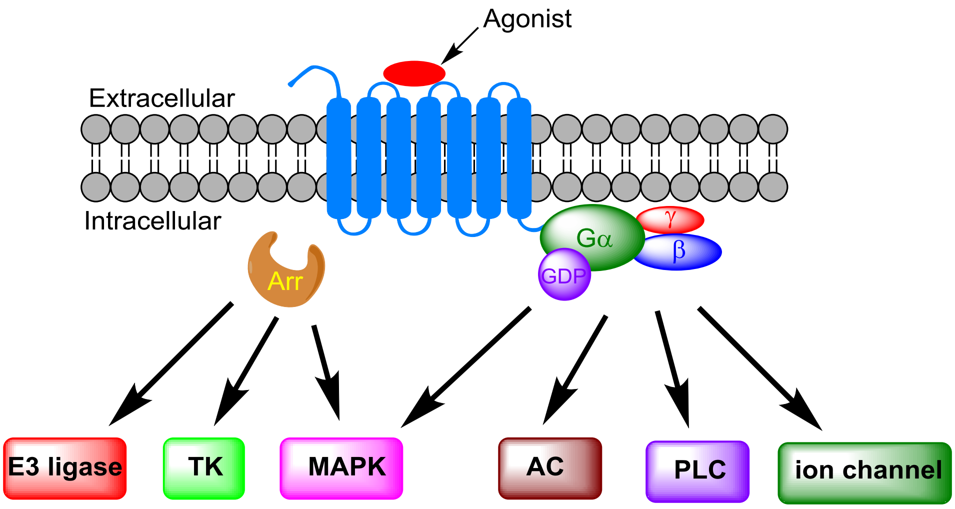

Figure 3. The G protein- and β-arrestin-mediated signaling

Activation of a GPCR can initiate two independent signaling pathways: 1) classical GPCR signaling pathway via heterotrimeric G proteins leads to the activation of membrane-delimited effectors like AC, phospholipase C isoforms (PLC), MAPK and ion channels that generate intracellular second messengers; 2) in the G protein-independent pathway β-arrestins (depicted in orange) can serve as scaffolds linking GPCRs to non-traditional effector pathways like non-receptor tyrosine kinases (TK), MAPK, and E3 ubiquitin ligases. β-arrestins can also inhibit G protein-coupling to the receptor, which makes the two pathways mutually exclusive.[91]

I.1.4 GPCR dimerization

For a long time, GPCRs have been considered to exist and function as monomers within the plasma membrane. However, in the past decades an increasing number of studies revealed that GPCRs are capable of forming dimers or even higher-ordered oligomers, which may modulate receptor function.[21],[22],[23]

The first hypothesis on GPCR heteromers was already raised in the early eighties after observations of neuropeptide-monoamine receptor-receptor interactions.[24],[25] The existence of heteromers was confirmed almost twenty years later for two non-functional GPCR monomers, i.e. the gamma amino butyric acid (GABA) receptors, GABA-B1 and GABA-B2, which assemble at the cell surface in a signaling heterodimer, the GABA-B receptor.[26] Now, dimerization has been described for many GPCRs in *in vitro* settings although evidence in native tissue is still sparse.[27],[28]

Both homodimers and heterodimers may exhibit properties distinct from those of the constituting protomers including distinct ligand binding properties, altered signaling and trafficking properties.[90] GPCR dimerization can result in altered binding properties that are not compatible with the model that one single GPCR binds one ligand. Studies on signaling assays such as receptor-mediated G-protein activity, adenylyl cyclase activity, MAPK phosphorylation, and β-arrestin-mediated signaling have provided evidence that dimerization can change signal transduction.[22] Moreover, dimerization plays an essential role in the regulation of receptor processing and trafficking, including receptor maturation, cell surface delivery, and ligand-mediated endocytosis.[21],[22]

I.1.5 Techniques used to study GPCR dimerization

Many techniques have been utilized to detect the GPCR dimers in living cells and tissues. Here we summarize some typical physicochemical (Coimmunoprecipitation, Co-IP), fluorescence-based (FRET, TR-FRET, BRET and PLA), and complementation-based techniques such as NanoBiT. Bivalent ligands that also have been frequently used as pharmaceutical tools to study GPCR dimerization will be discussed later.

I.1.5.1 Co-immunoprecipitation (Co-IP)

To investigate direct physicochemical interaction between two GPCRs, co-immunoprecipitation (co-IP) of differentially epitope-tagged receptors is one of the most broadly used techniques.[29] If suitable antibodies against the endogenous receptors are available, these can be used to immunoprecipitate endogenous receptors. Because it is often very difficult to find a good antibody against an endogenous receptor, this approach often uses differentially epitope-tagged (such as cMyc-, HA-, His-, or FLAG-tagged) receptors, which are co-expressed in heterologous cells, together with two specific antibodies. The potentially formed dimers are immunoprecipitated by a specific antibody against one epitope, followed by immunoblotting using a specific antibody against the other protomer. Typically, Co-IP is performed with total cell lysates, but when studying membrane proteins, modification of this technique is recommended. The principle of co-IP is described in Figure 4. Although co-IP reveals the presence of both receptors in the same complex, it does not provide evidence of physical interaction between the protomers. Therefore, co-IP is often complemented with fluorescence-based methodology to validate the obtained results.

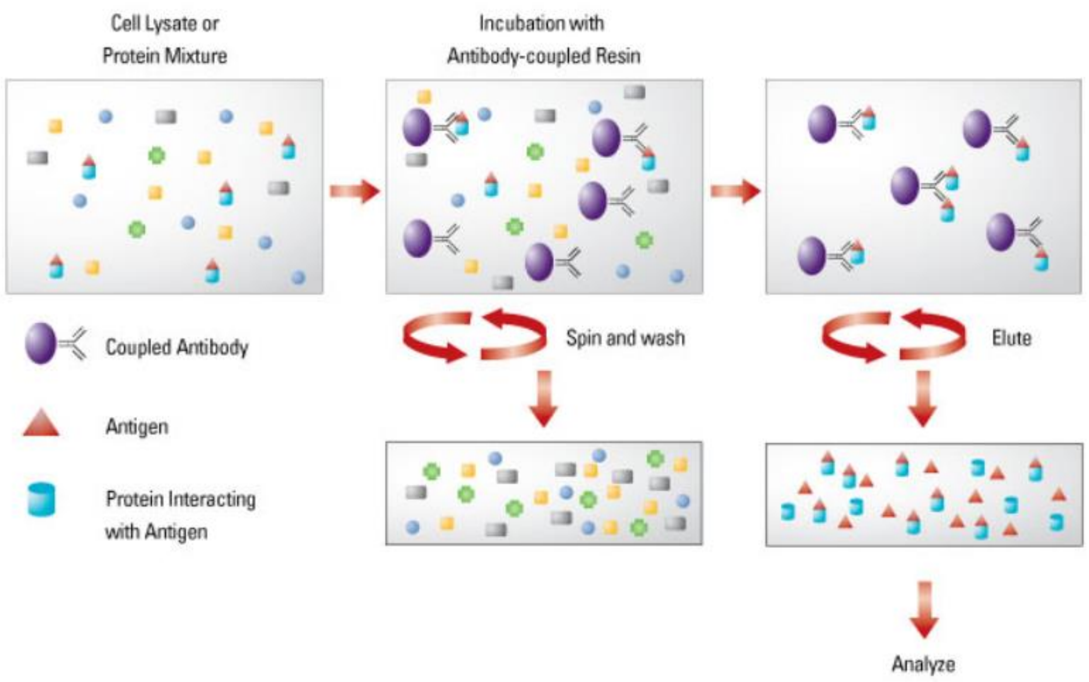
Cell Lysate or
Protein Mixture
Incubation with
Antibody-coupled Resin
Coupled Antibody
Antigen
Protein Interacting
with Antigen
Spin and wash
Elute
Analyze

Figure 4. Schematic summary of a standard co-immunoprecipitation assay. (Adapted from Thermo Fisher SCIENTIFIC)

A coupled antibody against a specific antigen conjugating a protein of interest forms an immune complex. Then the immune complex is captured, or precipitated on a beaded support. Next an antibody-bound protein is immobilized, and proteins not captured or precipitated on the beads will be washed away. In the end, the antigen (and antibody, if it is not covalently conjugated to the beads or when using buffers for denaturing) is eluted from the support.

I.1.5.2 FRET

Fluorescence resonance energy transfer (FRET) is based on energy transfer between donor and acceptor molecules in close proximity (Figure 5).[30] A distance smaller than 10 nm and an overlapping absorption spectrum of the acceptor with the emission spectrum of the donor are essential for efficient energy transfer. By exploitation of FRET, energy transfer-competent pairs of fluorescent proteins have been attached to the C-terminus of the GPCR (such as cyan fluorescent protein (CFP) as donor and yellow fluorescent protein (YFP) as acceptor). Background fluorescence from sample components like buffers, proteins, chemicals and cell lysate may hamper traditional FRET. Such background fluorescence is very transient (with a nanosecond range of lifetime) and can therefore be reduced by using time-resolved fluorescence resonance energy transfer (tr-FRET) as shown in Figure 6a.

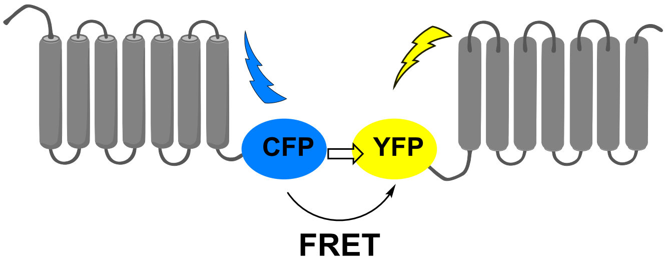

Figure 5. Schematic representation of the interaction of two different fluorescent proteins. Protein-protein interactions between GPCRs labeled fluorescent proteins bring cyan fluorescent protein and yellow fluorescent proteins in close enough proximity to allow for FRET to occur.

I.1.5.3 Ligand-tr-FRET

Ligand-tr-FRET makes use of fluorescently labeled ligands instead of labeled proteins. One ligand is coupled to an acceptor fluorophore, while the other ligand is coupled to a donor, causing energy transfer if both receptors are in close proximity.[31] The required ligand-fluorophore conjugates may be accessible from synthetic intermediates used for the construction of the heterobivalent ligands. (Ligand-)TR-FRET assays are sensitive, can be miniaturized and display reduced autofluorescence, but there is a limited choice of donor/acceptor pairs. Moreover, it might be challenging to label donor and/or acceptor/ligands without interfering with receptor binding affinity.

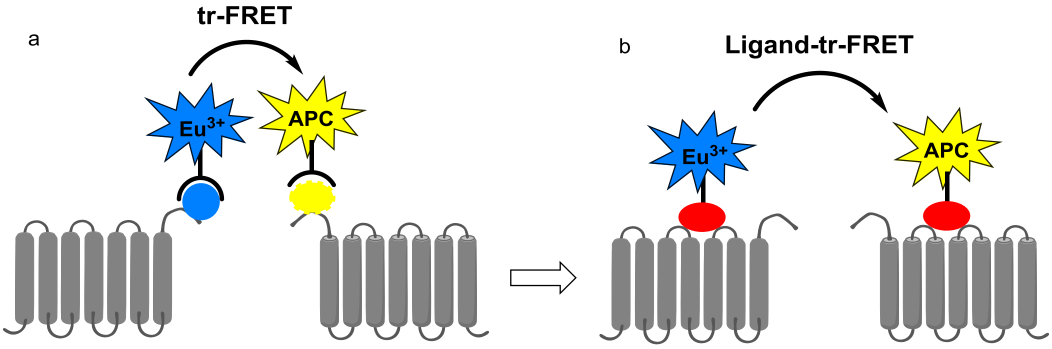

Figure 6. Fluorescence-based techniques.[92] a) tr-FRET strategies use lanthanide-labeled antibodies against N-terminal-tagged GPCRs to monitor receptor dimerization at the cell surface, which is based on the energy transfer between a lanthanide (e.g. Europium^{3+}, Eu^{3+}) and a compatible fluorophore (e.g. allophycocyanin, APC). Because of the long-lasting light emission of the lanthanides, tr-FRET provides a significantly improved signal-to-noise ratio. b) Ligand-tr-FRET uses fluorescently labeled ligands instead of labeled proteins.

I.1.5.4 BRET

The luminescent variant of FRET where energy transfer occurs between a luminescent donor and a fluorescent acceptor is called bioluminescence resonance energy transfer (BRET, Figure 7). The enzymatic oxidation of a substrate leads to the emission of energy from the donor, which means that no excitation light is needed in contrast to FRET. Moreover, the enzyme reaction does not produce a background signal and the assay is therefore more sensitive than FRET.[32] Taking advantage of BRET, a bioluminescent protein, commonly luciferase from Renilla reniformis (Rluc), has been used as an energy donor and a fluorescent protein (YFP, GFP2, or mOrange) as an acceptor.[33] Because of the fact that there is no requirement of a light source, the instrumentation for BRET[34] makes these assays applicable for high-throughput screening. Nevertheless, because of the large fluorescent and bioluminescent probes, it is necessary to consider which label to choose, how to label the ligand and/or receptor (with or without spacer), and to assess the effect of labeling on the binding properties.

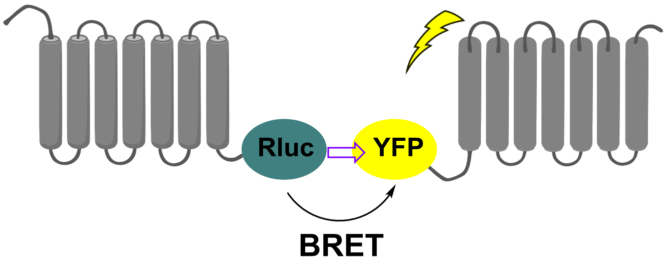

Figure 7. Schematic representation of BRET. Protein-protein interactions between GPCRs labeled with a luminescent donor and a fluorescent acceptor bring Rluc and YFP in close enough proximity to allow for BRET to occur.

I.1.5.5 Proximity ligation assay (PLA)

For in situ detection of heteromers PLA (Olink Bioscience) is a new technique, which has been optimized for brain tissue by the group of Javitch [35]. This technique is based on immunelabeling with two primary antibodies from different species and then with different species-specific secondary antibodies. The two secondary antibodies, each recognizing a specific species, are covalently coupled to oligonucleotides, the so-called proximity MINUS and PLUS probes. When both secondary antibodies are near to each other proximity-dependent ligation and rolling circle amplification of a circular DNA reporter molecule occurs, which can be visualized.[36]

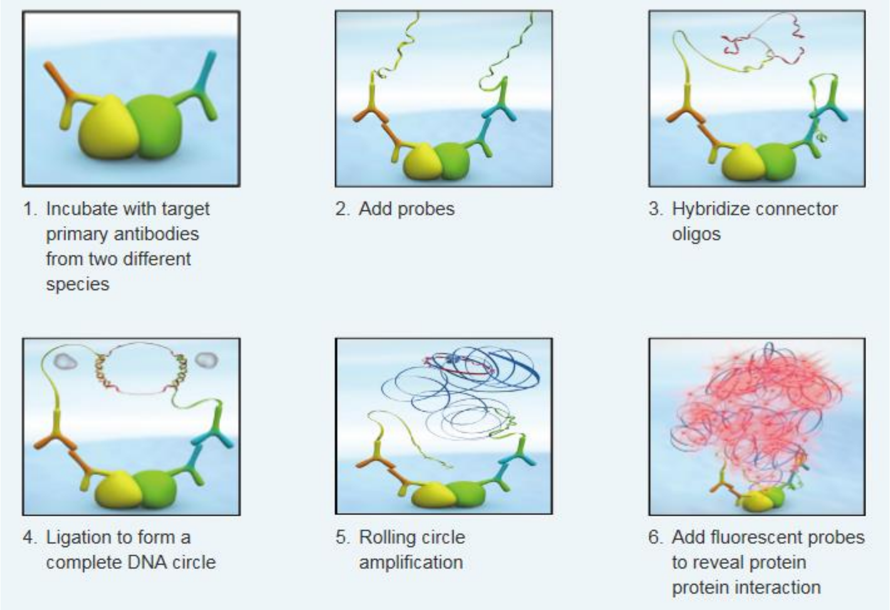
1. Incubate with target primary antibodies from two different species
2. Add probes
3. Hybridize connector oligos
4. Ligation to form a complete DNA circle
5. Rolling circle amplification
6. Add fluorescent probes to reveal protein protein interaction

Figure 8. Principle of Proximity Ligation Assay. (Adapted from Abnova)

I.1.5.6 NanoLuc Binary Technology (NanoBiT)

A new complementation-based approach termed NanoLuc binary technology (NanoBiT) was used to study protein-protein interactions in living cells.[37] It utilizes inactive subunits of NanoLuc luciferase, Large BiT (LgBiT; 18 kDa) and Small BiT (SmBiT; 1 kDa), which are coupled to two proteins of interest. Protein interaction promotes structural complementation of the subunits, thus restoring NanoLuc luciferase activity, which generates a bioluminescent signal in the presence of the furimazine substrate.

An optimized assay was established to be capable of detecting the dimerization of GPCRs (e.g. D_2R).[38] Candidate GPCRs are fused to SmBiT or LgBiT. Upon GPCR dimerization, the NanoBiT fragments come into close proximity resulting in NanoLuciferase reconstitution, which can convert the furimazine substrate leading to the emission of light.

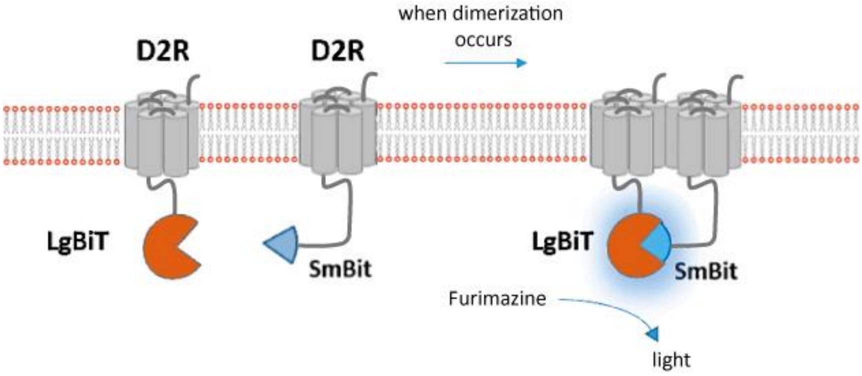
when dimerization occurs
D2R
D2R
LgBiT
SmBit
LgBiT
SmBit
Furimazine
light

Figure 9. Schematic representation of the NanoBiT system.[38]

Table 1 summarizes studies on GPCR dimerization containing at least one of the dopamine receptors, opioid receptors and metabotropic glutamate receptors.

Table 1. Examples of GPCR dimers

Dimer	Detection technique	Ref.	Dimer	Detection technique	Ref.
δOR−D_1R	FRET	[39]	D_1R−D_3R	BRET, Co-IP, FRET	[62],[63]
δOR−CB1	BRET, Co-IP	[40],[41]	D_2R −D_2R	FRET	[64]
δOR−CXCR2	BRET, Co-IP, TR-FRET	[42]	D_2R −D_3R	FRET, BRET	[65],[66]
δOR–CXCR4	FRET	[43]	D_2R −SSTR5	FRET	[67]
δOR−CCR5	nd	[43]	D_1R/D_2R −H3	BRET	[68]
δOR−κOR	Co-IP	[44]	D_2R-OTR	nd	[69],[70]
δOR−β2	Co-IP	[45]	D_2R-GSHR1a	nd	[71]
µOR−α_{2A}	FRET	[46]	D_1R-GSHR1a	Co-IP	[72],[73]
µOR-GRPR	Co-IP	[47]	D_2R-5-HT_{2A}	Co-IP, FRET	[74],[75]
µOR-NK1	Co-IP BRET	[48]	D_{2L}R−NTS1	Co-IP	[76]
µOR-mGlu5	BL	[49]	D_2R -CB1	FRET	[77],[78]
µOR-κOR	BRET, Co-IP	[50]	D_4R-D_{2S}R	nd	[79]
µOR−δOR	Co-IP, BRET, BL	[51],[52]	D_4R-α_{1B}AR	Co-IP	[80]
µOR−SSTR2A	Co-IP	[53]	D_4R-β_1AR	Co-IP	[80]
µOR−CB1	BRET	[54],[55]	D_2R-SSTR2	Co-IP	[81],[82]

	FRET				
μOR−CCK2	BRET	[56]	D_1R −A1	Co-IP	[83]
μOR−CCR5	Co-IP	[57]	D_2R −A_{2A}	BRET, Co-IP	[84],[85]
κOR–CXCR4	nd	[58]	mGluR1-A_1	Co-IP, FRET	[86]
κOR−CCR5	nd	[59]	mGluR2-5-HT_{2A}	Co-IP, FRET, BRET	[87]
D_1R −D_2R	FRET, Co-IP	[60],[61]	mGluR5-A_{2A}	Co-IP BRET	[88],[89]

Co-IP, coimmunoprecipitation; FRET, fluorescence resonance energy transfer; TR-FRET, time-resolved fluorescence resonance energy transfer; BRET, bioluminescence resonance energy transfer; BL, bivalent ligand; nd, not determined; δOR, δ-opioid receptor; D, dopamine receptor; CB, cannabinoid receptor; CCR, CXCR, chemokine receptor; κOR, κ-opioid receptor; β, β-adrenergic receptor; α, α-adrenergic receptor; GRPR, gastrin-releasing peptide receptor; NK1, neurokinin NK1 receptor; μOR, μ-opioid receptor; mGlu, metabotropic glutamate receptor; SSTR, somatostatin receptor; CCK, cholecystokinin; H, histamine receptor; OT, oxytocin receptor; M, muscarinic receptor; GSHR, Apo-ghrelin receptor; 5-HT, serotonin receptor; NTS, neurotensin receptor; A, adenosine receptor; nd, not determined.

I.2. Bivalent ligands of G protein-coupled receptors (GPCRs)

In classical pharmacology allosteric mechanisms were only discussed in terms of intramolecular interactions within a receptor between orthosteric and allosteric sites. Nowadays, there is mounting evidence that also intermolecular receptor-receptor interactions may result in altered receptor recognition, pharmacology and signaling. Bivalent ligands[93],[94],[95] have been proven useful molecular probes for confirming and targeting dimeric receptors, such as the κ opioid receptor (κOR)-δOR heteromers.[93] Bivalent ligands are valuable tools to demonstrate the existence of receptor dimers even in native tissue and can be used to study a specific GPCR dimer behavior without any receptor modification.[96],[97],[98] Such compounds may also evolve to useful pharmacological agents.[97]

Bivalent ligands with a spacer of optimal length are anticipated to exhibit a potency that is different from that derived from its two monovalent pharmacophores and may allow the targeting of certain dimeric subtypes, thereby increasing the selectivity of drug action.[98],[99],[100] Such synergy is based on the assumption that a bivalent ligand will first undergo univalent binding, followed by binding of the second pharmacophore to a recognition site on a neighboring receptor (Figure 10). When the bivalent ligand is in the univalently bound state, the pathway to bivalent binding should be favored over univalent binding of a second ligand because of the small containment volume of the tethered, unbound pharmacophore that is in the region of the unoccupied neighboring receptor site. The situation may be different in case the neighboring receptors are negatively allosterically coupled. In that case the binding enhancement may be mitigated.

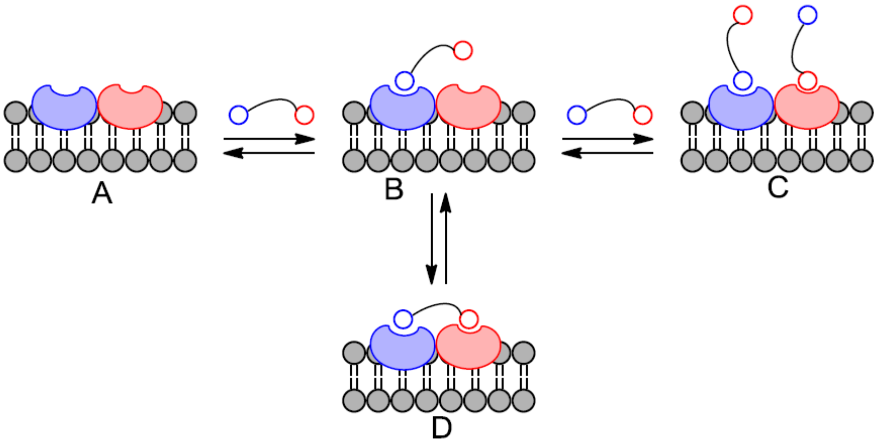

Figure 10. Bivalent ligand concept for bridging a receptor dimer.

The unoccupied dimer (A) undergoes univalent binding that leads to state B. The unoccupied site in B can be “bridged” to give D, which is entropically favored over binding of a second ligand to give the dimer with both sites occupied (C).

I.2.1 Concept and design of bivalent GPCR ligands

A typical bivalent GPCR ligand consists of three different components including two pharmacophores, two linking groups and a spacer of optimal length and nature (Figure 11). Specifically, the two pharmacophores are based on GPCR ligands, which could be the same (homo-bivalent ligands) or different (hetero-bivalent ligands). The selected GPCR ligands should be functionalized with a group, e.g. amine, carboxylic acid, alkyne or azide, to allow swift conjugation to the spacer. In addition, the spacer should also be equipped with appropriate ligation handles to couple with GPCR ligands. Overall, the design of such molecules requires the selection of the pharmacophores and attachment points, as well as the selection of appropriate length and chemical nature.

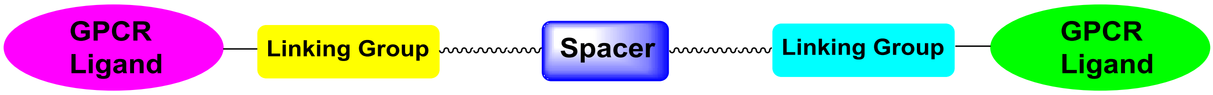

Figure 11. General Structure of Bivalent GPCR Ligands

I.2.2 Functionalized pharmacophore, attachment point and linking groups

Bivalent ligands represent very promising tools for the study of GPCR dimerization. Aspects such as pharmacophore identification, linker attachment site, length and composition of linker will be addressed in the following part.

The selection of the position and nature of the attachment points for linking the two pharmacophore units to the spacer depends on two criteria: the feasibility of the chemical modification and the compatibility of these modifications with receptor binding and intrinsic activity of the pharmacophore.

Preferred reactive groups (Table 2) for connecting two pharmacophoric units and spacers are hydroxyl, amine, and carboxylic groups,[101],[102] but also alkynes or azides may be employed to generate 1,4-substituted 1,2,3-triazole linking groups via a copper-catalyzed azide–alkyne cycloaddition (CuAAC) reaction.[103],[104],[105] The use of azides and terminal alkynes requires additional reaction steps, as these functional groups are usually not present in most pharmacophores. These functional moieties may be connected to the spacer via ether, amide and triazole moieties. In some studies, ester, amine or thioether functions are also described.

Table 2. Functionalized pharmacophores and linking groups used for bivalent ligands

Functionalized Pharmacophore	Linking group	References
	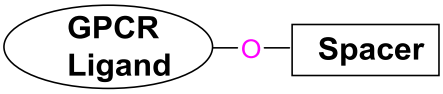	[106],[107]

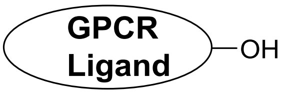	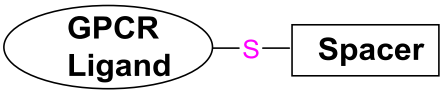	[106],[107]
	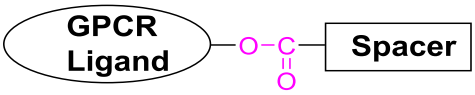	[108],[109]
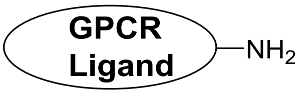	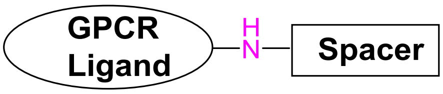	[108],[110]
	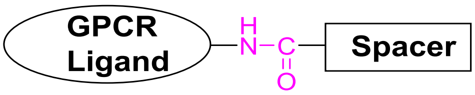	[111],[112],[113]
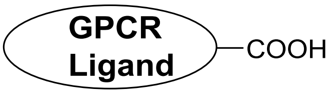	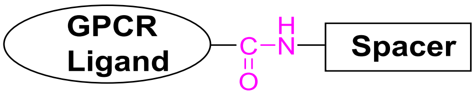	[111],[112],[114]
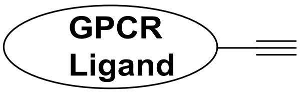	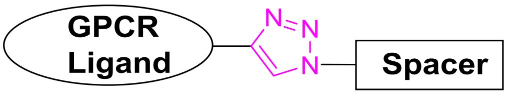	[103],[104],[105]

Normally, pharmacophores including the examples shown in Table 3 possess more than one functional group and the spacer has to be attached ideally without significantly disrupting the binding affinity or functionality of the parent compounds. Therefore, the most suitable spacer attachment position is preferentially chosen based on structure-activity relationship (SAR) data. For instance, the phenolic hydroxyl group of morphinans (Table 3), which is known to function as a hydrogen bond donor and to be crucial for appropriate receptor binding of these opioid receptor (OR) ligands, is excluded as a linker attachment point despite its reactive properties. Alternatively, the ketone portion of these OR ligands was chosen as the attachment point (Table 3), after conversion into an amine for connection to the spacer portions via an amide bond.[115]

Table 3. Pharmacophores, Targets, Attachment Points, and Linking Groups

Pharmacophore	Target	Linking Group	Ref.
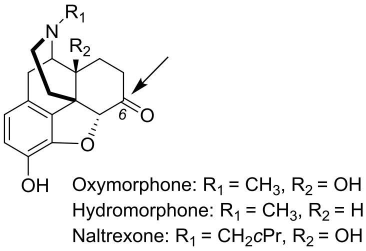 Oxymorphone: $R_1 = CH_3$, $R_2 = OH$ Hydromorphone: $R_1 = CH_3$, $R_2 = H$ Naltrexone: $R_1 = CH_2cPr$, $R_2 = OH$	μOR	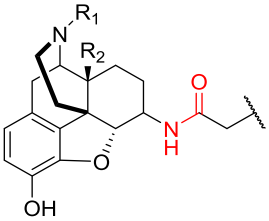	[115]
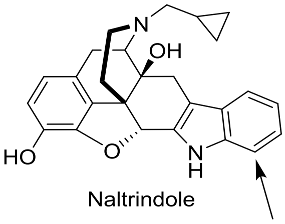 Naltrindole	δOR	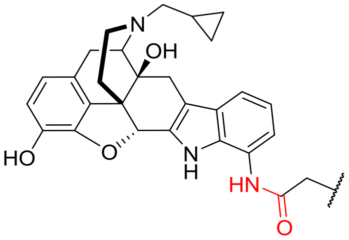	[116],[121]

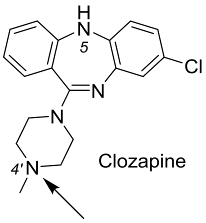 Clozapine	D$_2$R	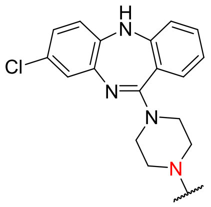	[120]
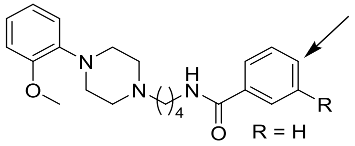 1,4-DAP	D$_2$-likeR	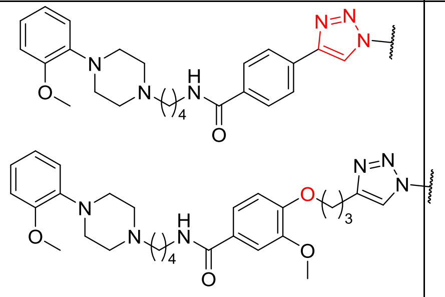	[103],[122], [123]
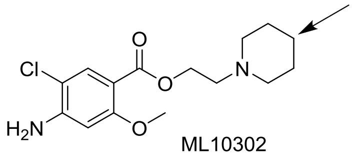 ML10302	5-HT4	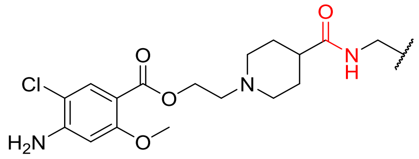	[124],[125]
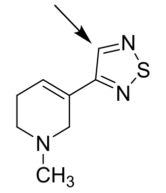 Thiadiazole analogue	Muscarinic receptors	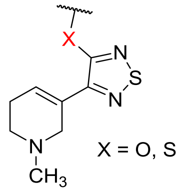	[106]
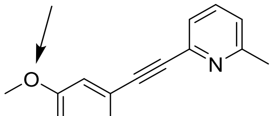 M-MPEP	mGluR5	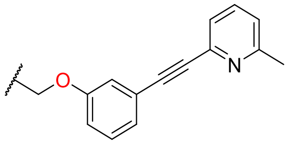	[118]
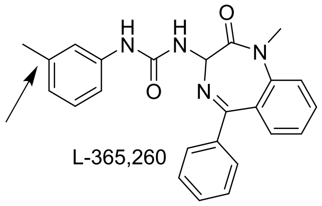 L-365,260	CCK2	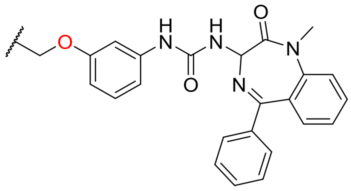	[115]
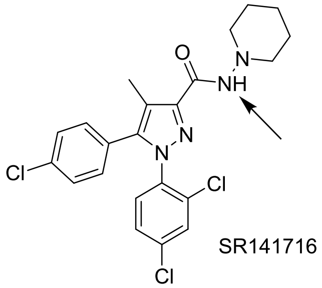 SR141716	CB1R	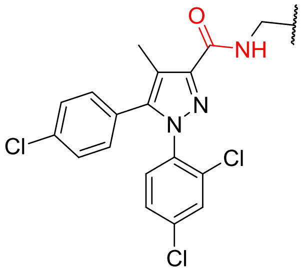	[126],[127]

Arrows represent acceptable attachment points of linking groups.

I.2.3 Spacer Length.

Both the length and composition of the spacer unit are critical for binding of bivalent ligands to their target receptors. Most successful studies on bivalent ligands revealed an impact of the spacer length on the binding affinity and functional activity, often leading to an optimal spacer length connecting the two pharmacophores.

In an early study of bivalent ligands targeting opioid receptors (μ, δ and κ dimers), Portoghese et al. showed that an optimal distance between the pharmacophores to bridge the GPCR dimer is 18 atoms (~20 Å).[36] A recently reported X-ray crystal structure of the μ opioid receptor reveals an optimal spacer length between 18 and 22 atoms to bridge the protomers.[129]

In recent studies, Portoghese and co-workers designed a number of heterobivalent ligands based on opioid receptors ligands.[115],[121] All these that show high potency compared to the monovalent ligands feature optimal spacer lengths of 18 to 22 atoms. The most convincing support for this 18−22 atom spacer requirement for bridging the μOR and CCK2 dimer employed BRET technology.[115] The data revealed that bivalent ligands **1.01a-c** (Figure 12) containing μOR agonist and CCK2 antagonist pharmacophores linked through 18−22 atom spacers efficiently induced physical association of coexpressed μOR and CCK2 receptors by shifting the equilibrium from homodimers to a heterodimer, whereas bivalent ligands with shorter spacers and monomeric ligands were not effective. While clearly established for these studies, the proper spacer length of other dimer spanning bivalent ligands relies on the dimer interface, which often remains ill defined, the structure of the pharmacophores, and the topicity of the attachment points.[130]

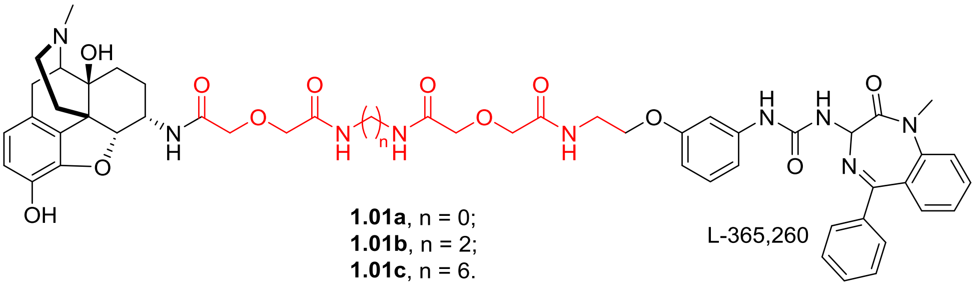

1.01a, n = 0;
1.01b, n = 2;
1.01c, n = 6.

Figure 12. Bivalent ligands targeting μOR and CCK2 receptors with spacer length between 16 and 22 atoms.[115]

Recently, the optimal attachment point for the synthesis of clozapine homobivalent ligands was identified as the N4′ position, which also incorporated a linking group between the nitrogen and the spacer.[120] Both functional and binding assays pointed toward a spacer length dependent effect, with the most active compounds (**1.02a** and **1.02b**) having total spacer lengths of 16 and 18 atoms, respectively. These compounds exhibited exceptional high binding affinity (K_i 1.41 and 1.35 nM) and remarkable functional activity (IC_{50} 23 and 44 nM) compared to the original pharmacophore, clozapine, i.e. 75-79-fold increase in affinity and 5-9-fold increase in potency. These clozapine propylamine bivalent ligands were used as pharmacological tools to investigate dopamine D_2R dimerization.

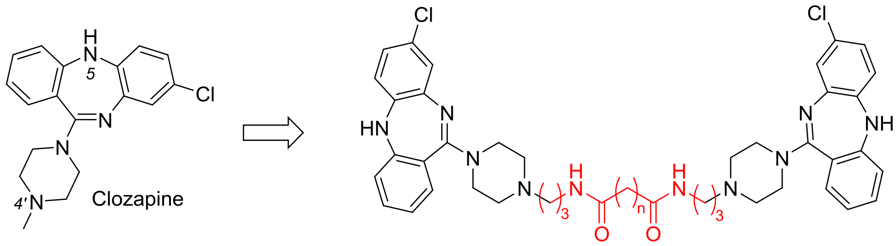

1.02a: n = 6;
1.02b: n = 8.

Figure 13. Bivalent ligands of clozapine at the N4′ position with optimal spacer lengths of 16 and 18 atoms.

A series of bivalent ligands was synthesized to target cannabinoid 1 (CB1) receptor dimers using two rimonabant (SR141716) pharmacophores connected by different linkers.[126] The potent and selective CB1 receptor antagonist was linked by alkylamine spacers of various lengths, and the resulting bivalent ligands were assessed in radioligand binding and functional assays. These ligands displayed a binding affinity that was spacer length dependent (Figure 15). Bivalent ligand **1.03** (n = 7, Figure 14) composed of a 15-atom spacer exhibited the highest gain in affinity as compared to the corresponding monovalent ligand. Thus, this novel compound may serve as a probe that enables further characterization of CB1 receptor dimerization and oligomerization.

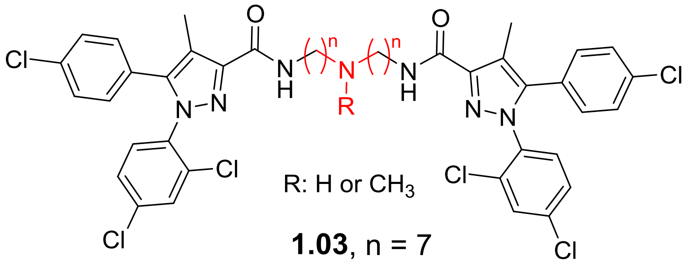

1.03, n = 7

Figure 14. Structure of homobivalent CB1R ligands from Zhang et al. [126] Spacer length calculated as 2n+1. Highest CB1R affinity with n=7 (15-atom): R=H (secondary amine): K_i (*h*CB1R)=12.3 nM; R=Me (tertiary amine): K_i (*h*CB1R)=17.3 nM.

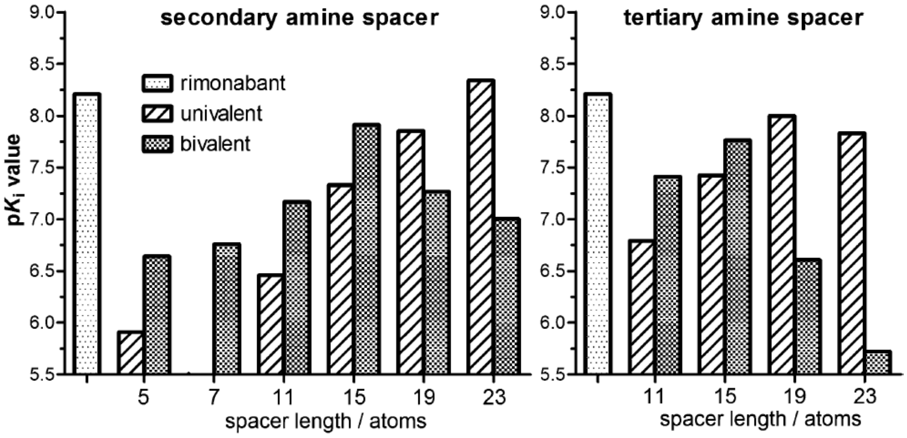

Figure 15. Correlation of spacer length and affinity at *h*CB1R for homobivalent CB1R ligands. Structures are shown above; K_i values are from Zhang et al.[126] The graphs are from Nimczick et al.[131]

In another recent example, Tanaka et al.[132] employed poly(L-prolines) as rigid spacers in the development of bivalent ligands targeting the CXC chemokine receptor 4 (CXCR4) homodimer. In this case, the bivalent ligand could be used as a "molecular ruler" approach to further understand the details of CXCR4 oligomer formation. Interestingly, more rigid linkers having an optimal length of approximately 6 nm were favored and displayed low nanomolar potency (Figure 16).

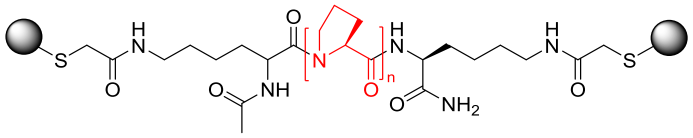

1.04

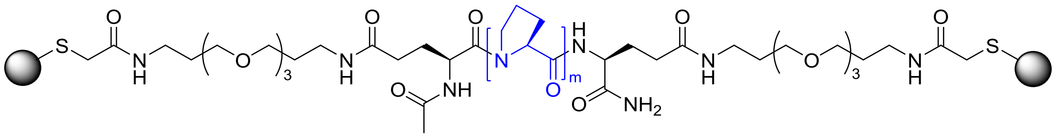

1.05

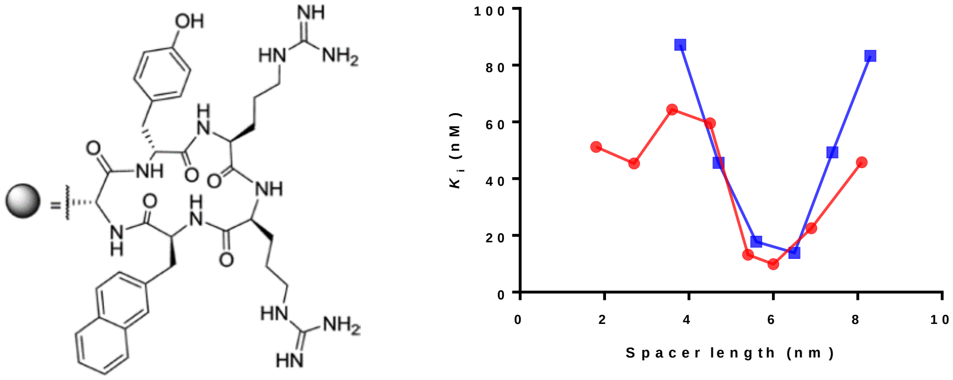

Figure 16. Oligoproline helices as molecular rulers. Graphic adapted from Tanaka et al.[132] showing the relationship between binding affinity of bivalent ligands targeting CXCR4 and the length of the spacer conjugating the two pharmacophores.

For their study on D_2R agonist/$A_{2A}R$ antagonist bivalent ligands, Soriano et al. [133] reported a minimum spacer length of 26 atoms, which could increase up to 118 atoms. No correlation was observed between spacer length and binding affinity of the bivalent ligands, which, however, exhibited a significant gain in affinity compared to their monovalent ligands. The bivalent ligands exhibited a Lys-Lys-(PEG/polyamide)$_n$-Lys-Glu spacer unit to span the vast distance between the dimeric binding sites (Figure 17). The advantage of this approach is the extreme length that can be obtained through multiple coupling steps. A disadvantage is the inability to extend the spacer groups incrementally to enable a methodical analysis of the exact distance between the binding sites of the dimer. Although this series of compounds are the first reported bivalent ligands targeting the $D_2R/A_{2A}R$ heterodimer, further optimization of the spacer is required to detect an optimal increase in binding affinity.

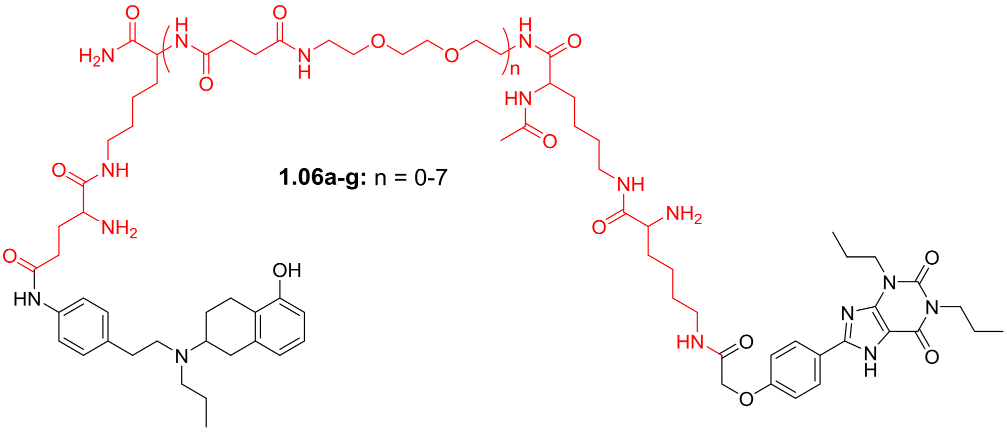

1.06a-g: n = 0-7

Figure 17. Bivalent $D_2R/A_{2A}R$ ligands with spacer lengths ranging from 26–118 atoms between the two pharmacophores.[133]

The above examples demonstrate that there are general no rules governing the optimal spacer distances to construct bivalent ligands for various dimeric GPCRs. However, several criteria on spacer length should be carefully considered to determine the optimal length of the connecting entity in a bivalent ligand: the binding mode of the chosen pharmacophore, the respective relative position of the two linker attachment points and the interface between the two protomers. Overall, in the absence of structural information of the targeted dimer, the optimal length of the spacer in a bivalent ligand may vary and needs to be determined empirically for each new pair of target receptors.

I.2.4 Conformational flexibility and hydrophilicity of the Spacer

In addition to spacer length, the chemical composition of the spacer may play an important role on the binding properties of the prospective bivalent ligands.

Generally, the spacer needs to be flexible enough to allow correct accommodation of each pharmacophore in the binding pocket of each protomer. Portoghese et al. investigated the effect of conformational rigidity of the spacer on opioid receptor activity. The conformational flexibility of the spacer was reduced by replacement of a succinyl group by a fumaryl moiety. Bivalent ligands containing two β-naltrexamine pharmacophores connected by a succinyl (**1.07a**, **1.07b**, Figure 18)[134] or fumaryl amide (**1.08a**, **1.08b**)[134] revealed significant differences in receptor selectivity. Bivalent ligand **1.07a** bearing the succinyl group was a potent and selective κOR antagonist, whereas the corresponding fumaryl analogue **1.08a** displayed no κ-antagonistic activity. Interestingly, a recovery of κ antagonism was observed upon increasing the conformational flexibility by introduction of an additional four glycine units (**1.07b** and **1.08b**).

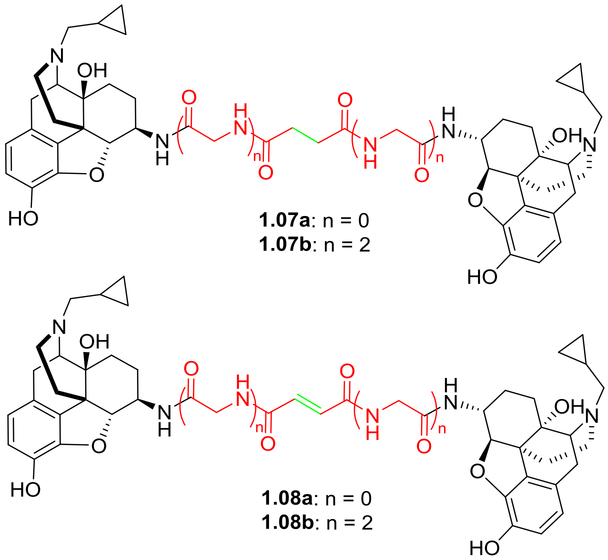

1.07a: n = 0
1.07b: n = 2

1.08a: n = 0
1.08b: n = 2

Figure 18. Bivalent naltrexamine ligands featuring succinyl or fumaryl groups in their spacers.[134]

Bivalent D_2-like receptor ligands (Figure 19) were synthesized using relatively rigid bismethyl-p-biphenyl spacers directly linked by 1,2,3-triazoles to 1,4-DAP pharmacophores. The para-substituted benzamides **1.09** [103] displayed poor binding affinities with K_i values between 70 and 2000 nM at the D_2-like subtypes. Interestingly, the ferrocenebenzamide **1.10** [103] displayed high binding affinities (K_i of 15, 14, 1.1, and 22 nM for D_{2long}, D_{2short}, D3, and D4, respectively), which were even surpassing that of bivalent ligand **1.11** with a more flexible methylene spacer.[122] These results clearly demonstrate the importance of conformational flexibility on the binding affinity of dimeric ligands. This study suggests that 1,1′-disubstituted ferrocenyl subunits may be used as molecular hinges when rotation of the cyclopentadienyl moieties enables the two pharmacophores to adopt an optimal orientation.[103]

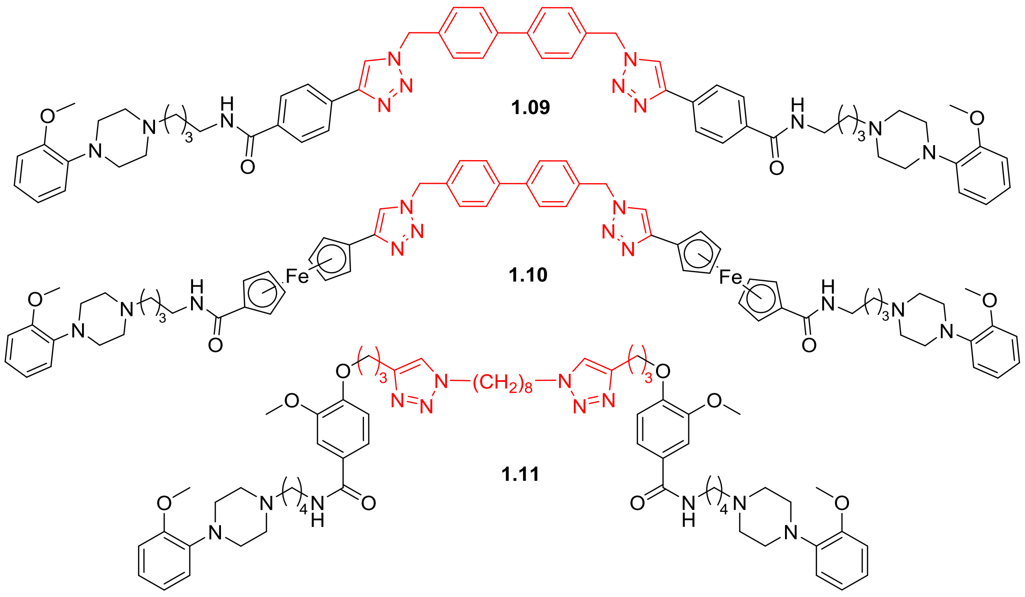

Figure 19. Ferrocene as a molecular hinge in bivalent D_2-likeR ligands.

A variety of spacer groups were used to synthesize 5-HT4 receptor bivalent ligands based on the highly potent and specific partial agonist ML10302 (Table 3), including polyalkyl chains, polyethylene glycol (PEG) units, polyamide chains, hydrophobic spacers, cyclic core alkyl spacers, flexible aromatic containing spacers, and constrained aromatic containing spacers (Figure 20). [135] Binding studies indicated that the optimal spacer length was 20–24 atoms for bivalent binding.[136] The rigidity of the spacer, represented in Figure 20 as number of rotatable bonds, is also of considerable interest as it can result in an 'all or nothing' approach as described by Bobrovnik,[137] whereby the appropriately designed rigid spacer can selectively increase the concentration of the pharmacophore to the active site of the binding pocket. Bonger et al.[138] successfully generated bivalent ligands targeting the gonadotropin releasing hormone receptor (GnRHR) with rigid benzene-based scaffolds (Figure 20).[139]

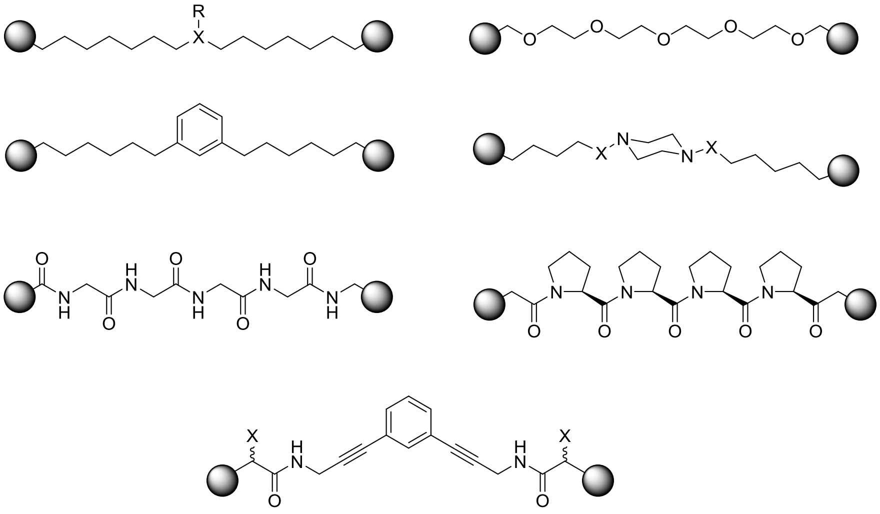

Figure 20. Bivalent 5-HT4 or GnRHR ligands with various spacers.

The above spacers could potentially be incorporated into any bivalent ligand. However, they all have their respective advantages and disadvantages. They mainly differ in lipophilicity and flexibility (number of rotatable bonds).

The polarity of the spacer unit contributes to the overall solubility of the bivalent ligand, which may be relevant, especially when the pharmacophore is very hydrophobic. Indeed, hydrophilic groups like polyamide or polyethylene glycol (PEG) units present in many spacers enhance aqueous solubility.[134],[141],[142] However, polyamide and polyethylene glycol units do not permit one-atom variations. Therefore, polyamide spacers, most commonly polyglycine units, are usually combined with alkyldiamine or methylenediacyl cores as in bivalent opioid receptor ligand **1.12** to combine high polarity with the possibility of one-atom variation.[143],[144],[145] In addition to hydrophilicity of the spacer, flexibility can also be improved using PEG spacers.

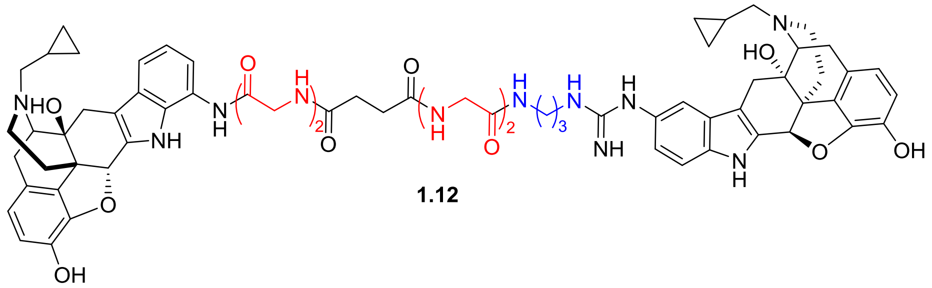

1.12

Figure 21. Incorporation of oligoglycine and diamine moieties into the spacer.[121]

Both lipophilicity and rigidity of the spacer are important factors when designing a bivalent ligand, and the linkers listed in Figure 20 can serve as a down list for the synthesis of bivalent ligands. Incorporation of piperazine into the spacer group can improve the hydrophilicity of the bivalent ligand, but is slightly less flexible than a polyalkyl chain and PEG spacer, but slightly more than polyamide chains.

I.2.5 Bivalent ligands may enhance selectivity and binding affinity

Bivalent ligands often possess receptor binding properties that differ substantially from those of the monovalent ligands. Several different mechanisms can contribute to their specific binding properties.[146] For instance, bivalent ligands can bind dimeric receptors on the cell surface. In this case, the cost for the translational entropy is paid with the first receptor–ligand contact and subsequent binding interactions proceed without additional penalties in the translational entropy (Figure 22a). Even in the case of receptors that are not dimeric, bivalent ligands can bind avidly to multiple receptors, a process that is facilitated by the two dimensional diffusion of receptors in the fluid bilayer (Figure 22b). As the result, the bivalent ligands can enhance binding affinity, agonist/antagonist potency and GPCR subtype selectivity.[146]

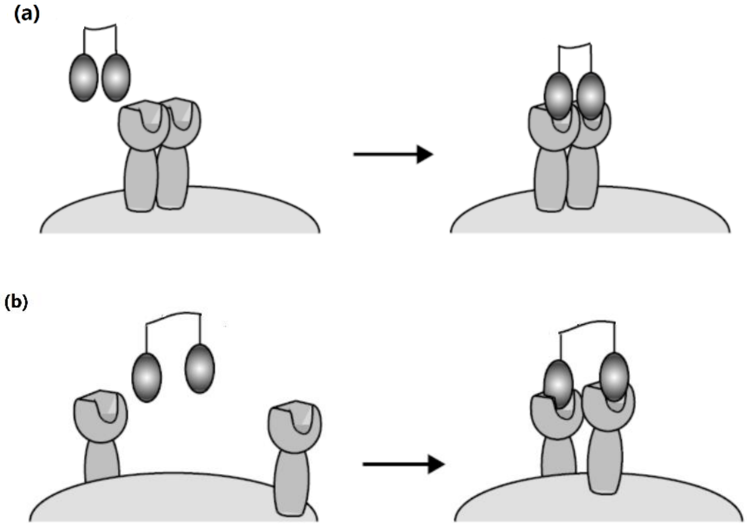

Figure 22. Mechanisms of bivalent ligand–receptor interactions. (a) Bivalent ligands can bind dimeric receptors by occupying multiple binding sites (chelate effect). (b) Bivalent ligands can cause receptors to cluster on the cell surface.

Andersen et al. has synthesized a series of bivalent serotonin ligands to reveal insight into substrate recognition in the serotonin reuptake transporter (SERT).[147] An optimized bivalent serotonin ligand **1.14** (Figure 23) containing a poly(ethylene glycol) spacer binds SERT with >3,700-fold higher affinity than serotonin (**1.13**), indicating that the human SERT has two distinct substrate binding sites.

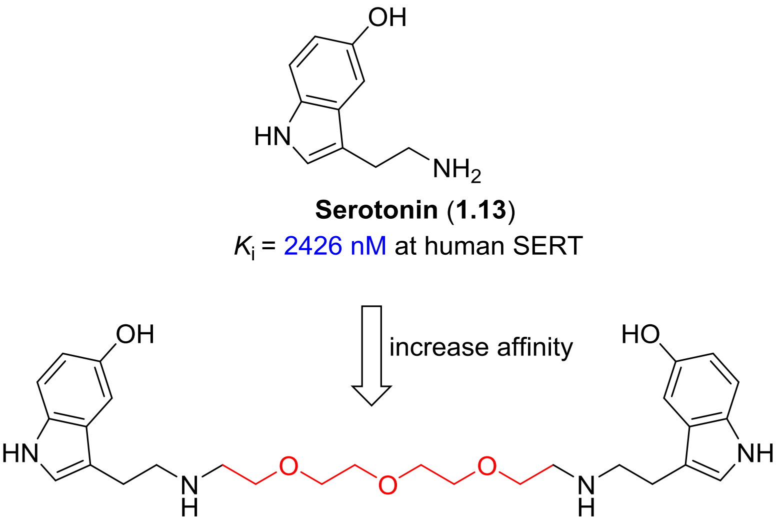

Serotonin (**1.13**)
K_i = 2426 nM at human SERT

Bivalent **serotonin** ligand (**1.14**)
K_i = 0.64 nM at human SERT

Figure 23. Structure of serotonin and the corresponding bivalent nd **1.14** and their affinities for the human SERT.

She et al. synthesized a series of homo- and hetero-bivalent ligands targeting muscarinic acetylcholine receptors M_1R−M_5R.[148] The heterodimeric ligand UR-SK75 (**1.16**, Figure 24) containing a MR dibenzodiazepinone antagonist and a M_1R/M_4R agonist (xanomeline) showed 20-480-fold selectivity for M_2R over the other four subtypes.

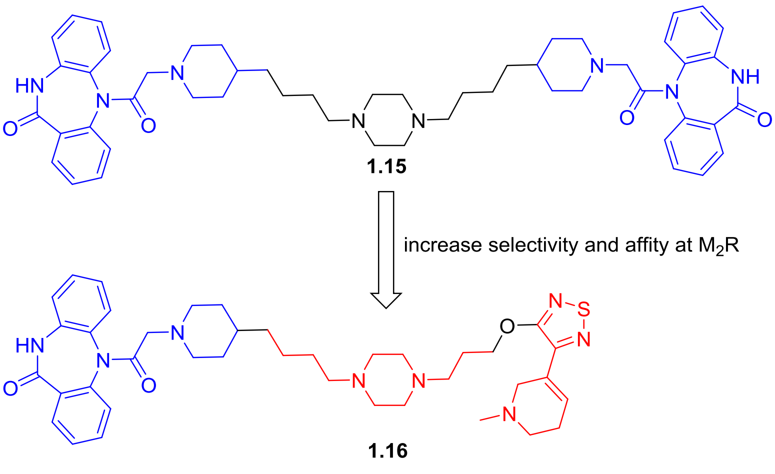

1.15

	K_i nM
M_1R	1.00
M_2R	0.31
M_3R	6.76
M_4R	1.07
M_5R	22.91

1.16

	K_i nM
M_1R	1.44
M_2R	0.07
M_3R	13.18
M_4R	2.57
M_5R	33.88

Figure 24. Bivalent ligands **1.15** and **1.16** targeting muscarinic acetylcholine receptor.

To increase the affinity and selectivity for the histamine H_2 receptor (H_2R), Pockes et al.[149] prepared bivalent H_2R alkylguanidine ligand **1.19** (Figure 25) that exhibits significantly higher affinity for hH_2R than for hH_1R, hH_3R, and hH_4R (Table 4). This hH_2R selectivity was much more pronounced than for the monomeric **1.18**. Furthermore, bivalent ligand **1.19** showed a higher functional activity at guinea pig H_2R (atrium) compared to **1.17** and **1.18** (Table 4).

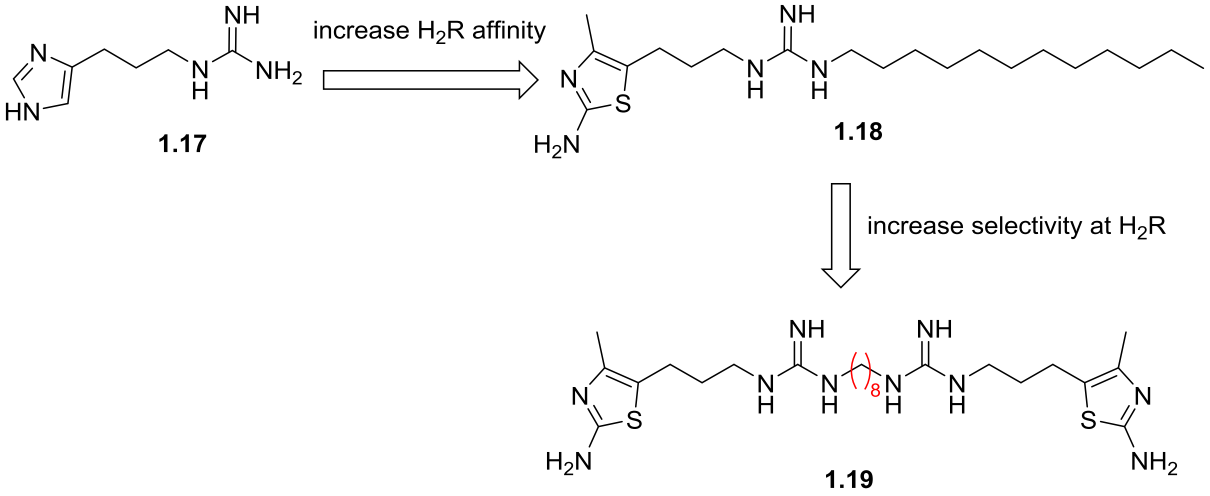

Figure 25. Structure of bivalent H_2R agonist **1.19**.

Table 4. Binding affinities at the human $H_{1,2,3,4}R$ and agonistic activities at the *gp*H_2R (atrium)

Compd	K_i (µM) for *h*H_1R	K_i (µM) for *h*H_2R	K_i (µM) for *h*H_3R	K_i (µM) or *h*H_4R	EC_{50} (µM) at *gp*H_2R (atrium)
1.17	>100	4.07	0.038	0.0074	6.92
1.18	>3.3	0.47	2.04	5.62	0.27
1.19	>3.3	0.047	5.62	10	0.0042

In case bivalent ligands show comparable or decreased binding affinities compared to the monovalent compounds this may be ascribed to suboptimal length or composition of the linker or the inadequate selection of the attachment points.

I.2.6 How to estimate if a bivalent ligand bridges the receptor dimer?

In pharmacology, positive cooperative binding is defined as the enhanced binding of a ligand to a receptor in the presence of another ligand binding to a different binding site of the same receptor. In competitive ligand binding assay, the slope of the binding curve is defined as Hill coefficient or Hill slope (n_H), which is indicative of the degree of cooperativity among multiple ligand binding sites. The Hill equation is commonly expressed as follows:

$$\theta = \frac{[\mathrm{L}]^n}{K_d + [\mathrm{L}]^n} = \frac{[\mathrm{L}]^n}{(K_A)^n + [\mathrm{L}]^n} = \frac{1}{\left(\frac{K_A}{[\mathrm{L}]}\right)^n + 1}$$

The equation's terms are defined as follows:

θ - Fraction of the ligand-binding sites on the receptor protein which are occupied by the ligand.

[L] - Free (unbound) ligand concentration.

K_d - Apparent dissociation constant derived from the law of mass action (the equilibrium constant for dissociation).

K_A - The ligand concentration producing half occupation (ligand concentration occupying half of the binding sites).

n - The Hill slope.

Competitive binding curves follow the law of mass action. A Hill slope of 1 indicates completely independent binding. A Hill slope greater than 1 indicates positive cooperativity binding, i.e. one ligand facilitates binding of subsequent ligands at other sites on the multimeric receptor complex. A value less than 1 suggests negative cooperativity. Antagonists tend to have Hill slope values close to 1 since they fail to show cooperativity, thereby following the general law of mass action for single site competition. Competition assays between agonists and radiolabeled antagonists are often characterized by shallow curves with Hill slopes between 0.5 and 0.7. [122]

Cross-talk between GPCRs forming a dimer can evoke positive cooperativity, which also can be induced by bivalent ligand owing to the thermodynamic advantage of sequential ligand binding. This effect was observed in the study of bivalent ligands of dopamine D_2 receptor (D_2R) based on 1,4-disubstituted aromatic piperazine (1,4-DAP). Competitive binding curves of monomeric antagonists such as the phenylpiperazine **1.20** [150] (Figure 26) usually show Hill slopes close to 1 ($n_H = 0.9{\sim}1.2$), indicating a binding mode whereby one monovalent ligand binds to one receptor protomer. Bivalent D_2R antagonist **1.21a** [150] displayed a remarkably increased Hill slope of 2.0, indicating positive cooperativity. Positive cooperativity is usually observed as an allosteric effect, which induces a conformational crosstalk within one receptor protomer or modulates the interaction between two protomers of a receptor dimer. Bivalent ligands addressing two adjacent binding sites of receptor dimers will also induce such positive cooperativity because bivalent binding of the second pharmacophore is significantly accelerated owing to its vicinity to the second binding site and the enrichment of its local concentration. Therefore, bivalent binding leads to the liberation of 2 equiv of radioligand and a substantial steepening of the competition curve.

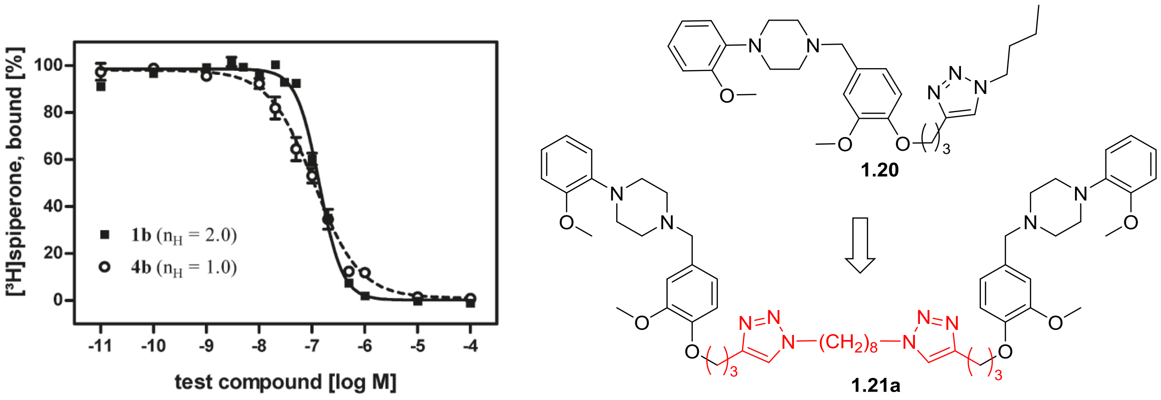

Figure 26. Bivalent and monovalent binding mode of **1.20 (4b)** and **1.21a (1b)** at the human dopamine D$_{2short}$ receptor.

Interestingly, bivalent agonists also exhibited steeper binding curves compared to their corresponding monovalent ligands. Monomeric D$_2$R agonists reveal shallow curves with Hill slopes of 0.5~0.7, suggesting negative cooperativity. While binding studies of bivalent D$_2$R agonist **1.21b** (Figure 27) revealed significantly increased Hill slopes of 1.3−1.4, indicating positive cooperativity and a bivalent binding mode.[122],[130],[151] Careful analysis of Hill coefficients may thus constitute a valuable approach to confirm a true bivalent binding mode.

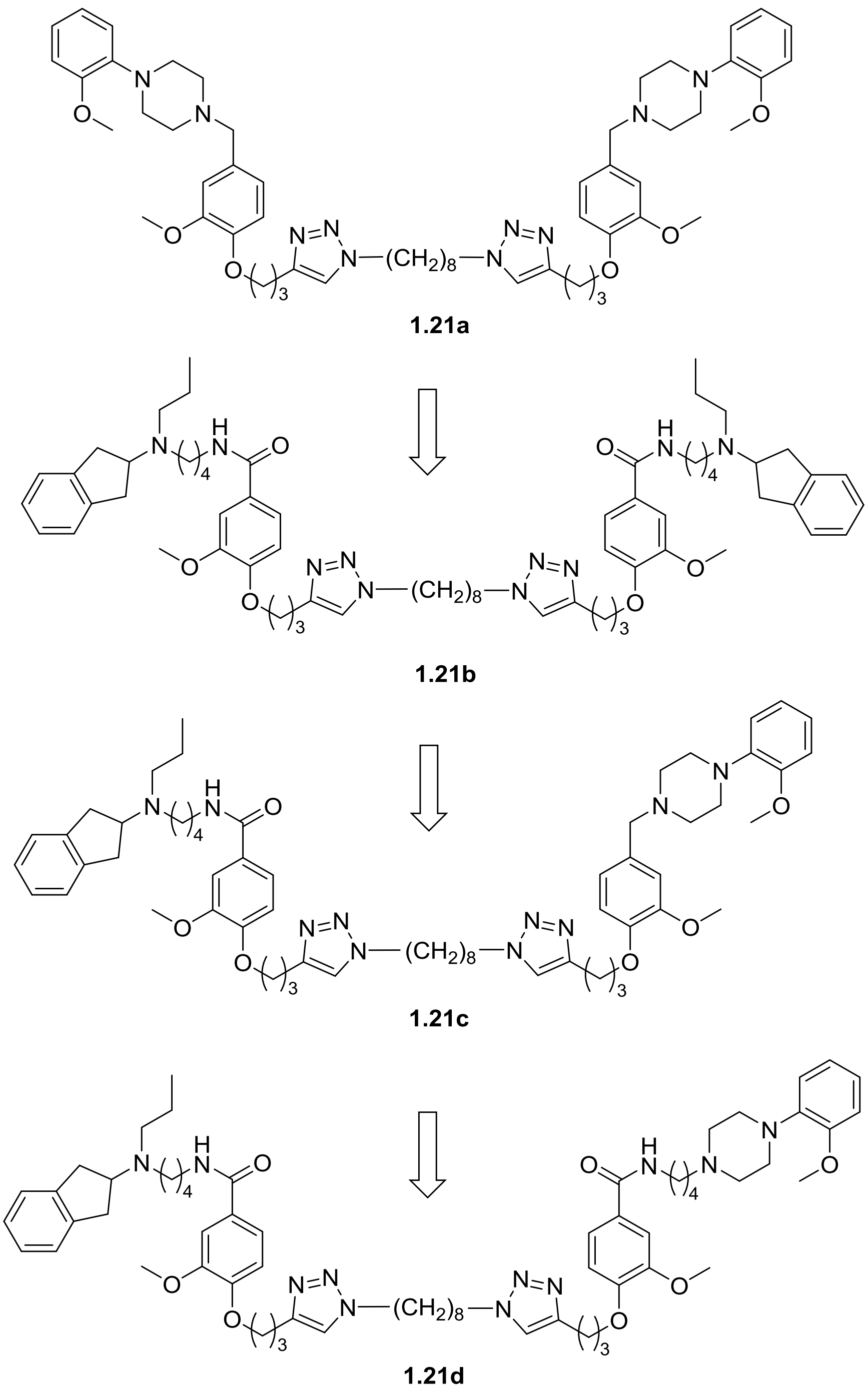

Figure 27. Structure of bivalent D_2R ligands.

Meanwhile, the heterobivalent ligands **1.21c** and **1.21d** containing a D_2R agonist (aminoindane pharmacophore) and a D_2R antagonist (phenylpiperazine pharmacophore) were also assessed for their ability to inhibit cAMP accumulation and induce D_2R internalization (Figure 28).[122] The results of cAMP assay revealed that **1.21c** shows weak partial D_2R agonist activity (Emax =13%), whereas **1.21d** exhibited D_2R antagonism. In addition, neither bivalent ligand could activate D_2R-mediated internalization. Therefore, these two heterobivalent ligands do not show D_2R biased agonisms (cAMP versus internalization).

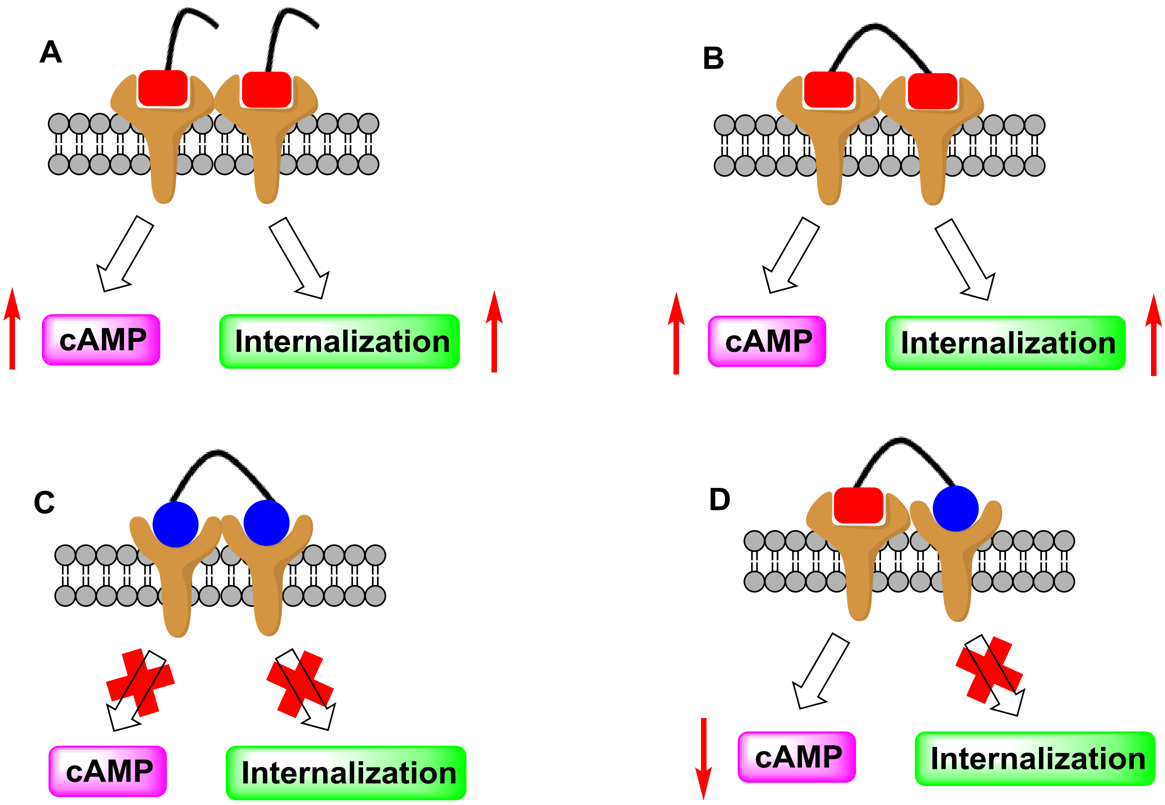

Figure 28. Bivalent D_2R ligands. A cartoon illustrating the effect of bivalent ligands binding to the D_2R dimer on D_2R-mediated cAMP formation and internalization. Red square and blue circle represent D_2R agonist and antagonist pharmacophores, respectively.

Four cartoons further clarified the influence of different bivalent ligands on the signal transduction of D_2R homodimer (Figure 28). Monovalent D_2R agonists binding to the D_2R homodimer could induce cAMP accumulation and activate the D_2R-mediated internalization (Figure 28A), as did the bivalent D_2R agonists (Figure 28B). Bivalent D_2R antagonists binding, on the other hand, blocked both cAMP formation and internalization (Figure 28C). Interestingly, heterobivalent ligands comprising a D_2R agonist and a D_2R antagonist lead to a very low efficacy of cAMP (Emax ≤15%), indicating partial D_2R agonism, and inhibit D_2R internalization (Figure 28D).

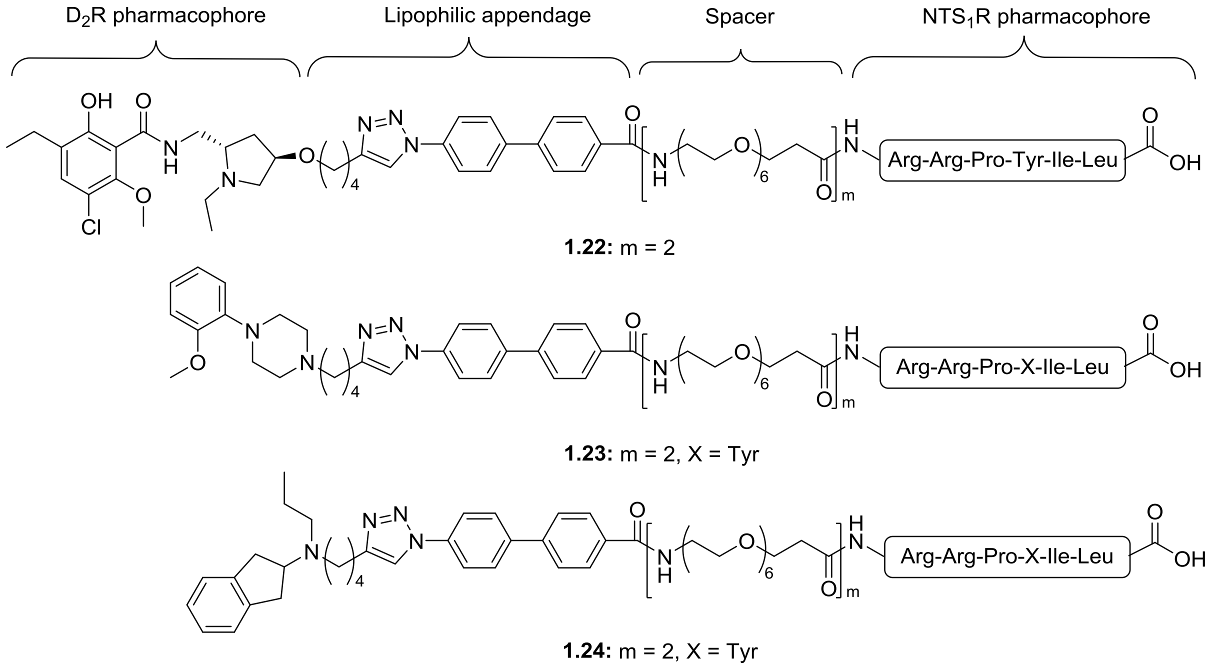
D2R pharmacophore
Lipophilic appendage
Spacer
NTS1R pharmacophore
Arg-Arg-Pro-Tyr-Ile-Leu
Arg-Arg-Pro-X-Ile-Leu
Arg-Arg-Pro-X-Ile-Leu

1.22: m = 2

1.23: m = 2, X = Tyr

1.24: m = 2, X = Tyr

Figure 29. Bivalent ligands (**1.22-1.24**) for D_2R and NTS_1R.

A recent study on bivalent D_2R agonist/antagonist and neurotensin NTS_1 receptor (NTS_1R) agonist ligands (Figure 29) afforded biphasic competition-binding curves when measuring $[^3H]$spiperone displacement.[153] Such biphasic-binding curves (two K_i values, Figure 30) were specifically observed with spacer lengths of 44 (m=2), 66 (m=3) or 88 (m=4) atoms at cell membranes coexpressing D_2R/NTS_1R. The $K_{i\ high}$ values correspond to a bivalent receptor-bridging binding mode to D_2R/NTS_1R heterodimers, while the $K_{i\ low}$ values reveal a monovalent-binding mode to D_2R.

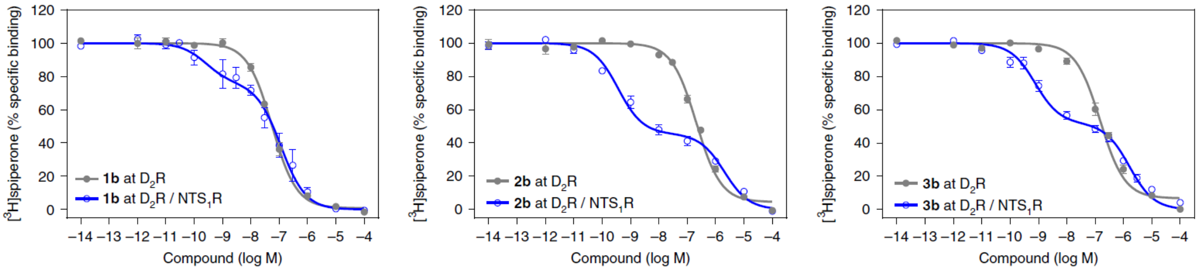

Figure 30. Biphasic competition-binding curves indicate a bivalent binding mode of **1.22** (1b), **1.23** (2b) and **1.24** (3b).

Similar binding assays were performed in the presence of an excess of NTS_1R agonist NT(8-13) (1 µM), which could prevent a biphasic binding mode of the bivalent compounds by hampering binding of their NT(8-13) pharmacophore to the NTS_1R. Indeed, co-incubation prevented high-affinity binding, resulting in typical sigmoidal monophasic curves (Figure 31a).

To confirm the bivalent receptor-bridging binding mode, reciprocal competition experiments were performed with the NTS_1R radioligand $[^3H]$neurotensin. Employing **1.24**, a biphasic-binding curve was observed with a $K_{i\ high}$ value of 0.11pM and a $K_{i\ low}$ at 1.7 nM, which was shifted to a monophasic sigmoidal binding curve in the presence of haloperidol (K_i 0.79 nM, Figure 31b). Incubation with this monovalent D_2R antagonist thus efficiently prevented the bivalent-binding mode. Affinities for this competition-enforced monovalent-binding mode were found to be in good agreement with results obtained with membranes from CHO-cells stably expressing NTS_1R only (K_i 0.86 nM). To further complement the results obtained with overexpressing heterologous cell lines with results from native brain tissue, competition binding assays with $[^3H]$spiperone and the bivalent ligand **1.24** were performed with membranes from porcine striatum (Figure 31c). Interestingly, compound **1.24** displayed a biphasic binding curve with a 140-fold preference for the high-affinity binding site over the low-affinity receptor population ($K_{i\ high}$ 2.8 nM, $K_{i\ low}$ 310 nM, high-affinity fraction 38%). In line with the results from heterologous cell lines, addition of 1 µM NT(8-13) reverted this biphasic binding curve to a sigmoidal binding isotherm with a K_i value of 28 nM. The superior binding of bivalent over monovalent ligands to D_2R/NTS_1R heterodimers was thus not only evident in heterologous cell lines but also in native tissue, though less pronounced, which might be explained by lower receptor expression levels leading to a lower propensity to form D_2R/NTS_1R heterodimers.

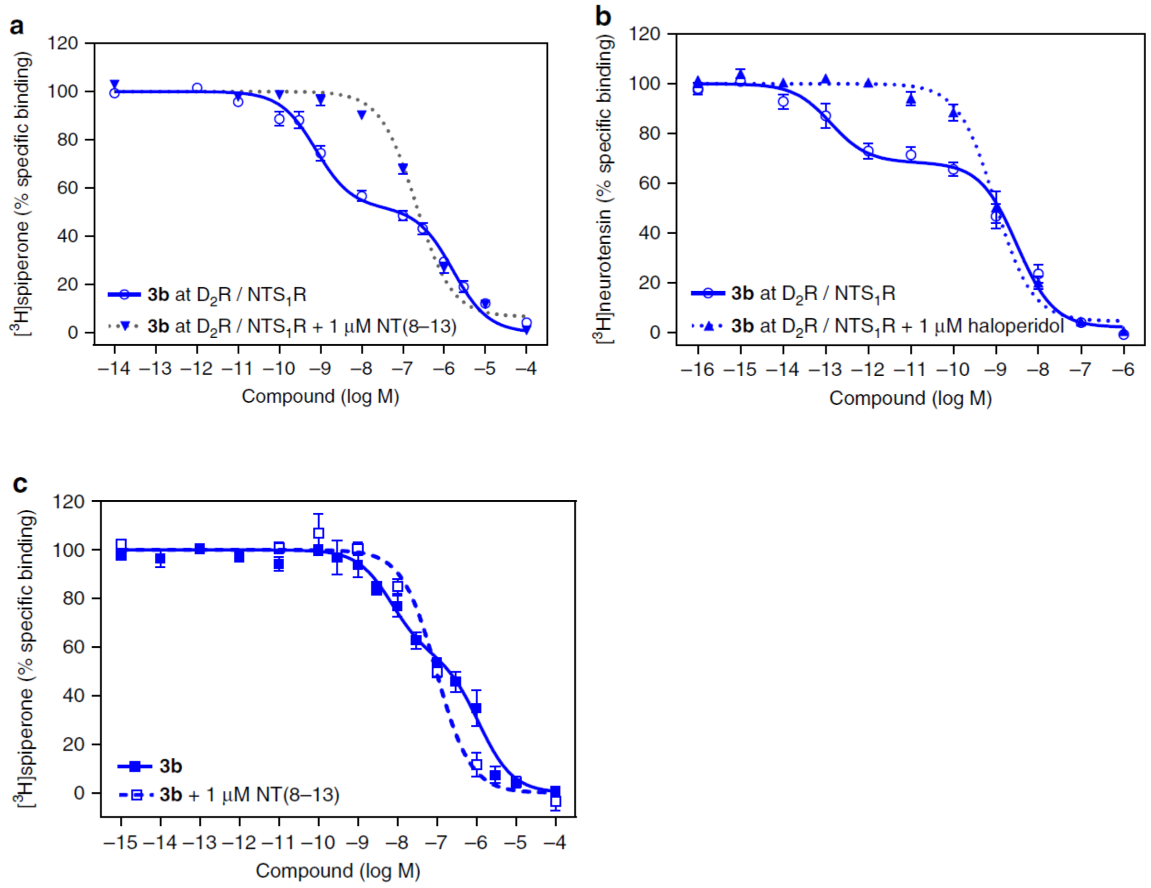

Figure 31. Prevention of bivalent binding mode abolishes biphasic competition curves. (a) Dopamine receptor binding of **1.24** (3b, *m*=2, 44-atom spacer) at D_2R/NTS_1R in the absence (blue open circles) or presence (blue inverted triangles) of 1 µM NT(8-13). Incubation with the monovalent NTS_1R agonist NT(8-13) prevents a bivalent binding mode and converts the biphasic-binding curve into a monophasic sigmoid competition curve. (b) Neurotensin receptor binding of **1.24** at D_2R/NTS_1R in the absence (blue open circles) or presence (blue filled triangles) of 1 µM haloperidol. Incubation with the monovalent D_2R antagonist prevents the bivalent binding mode, observed for the coexpression of D_2R/NTS_1R. (c) When radioligand displacement studies were performed with striatal membranes and $[^3H]$spiperone, biphasic binding mode was observed for the bivalent ligand **1.24** (blue filled squares) alone, but not in the presence of 1 µM NT(8-13) (blue open sqares).

I.2.7 In vivo relevance of bivalent ligands

Akgün et al. reported a series of bivalent ligands that contain a µOR agonist and a mGluR5 antagonist pharmacophore linked through spacers of varying length (10–24 atoms) to study the µOR/mGluR5 receptor interaction in vivo (Figure 32) [118]. Bivalent ligands (intrathecal administration) were evaluated for antinociception using the tail-flick and von Frey assays in mice pretreated with lipopolysaccharide (LPS) or in mice with bone cancer. In LPS-pretreated mice, **1.25** with a 21-atom spacer exhibited the highest potency (ED_{50} ~ 9 fmol per mouse), while bivalent ligands with shorter or longer spacers showed at least a 25-fold higher ED_{50}. The exceptional potency of **1.25** may be owning to the optimal bridging of protomers in the target µOR-mGluR5 heterodimer. Bivalent ligand **1.25** holds a $>10^6$ therapeutic ratio and may be a promising candidate for treatment of chronic, intractable pain via spinal administration.

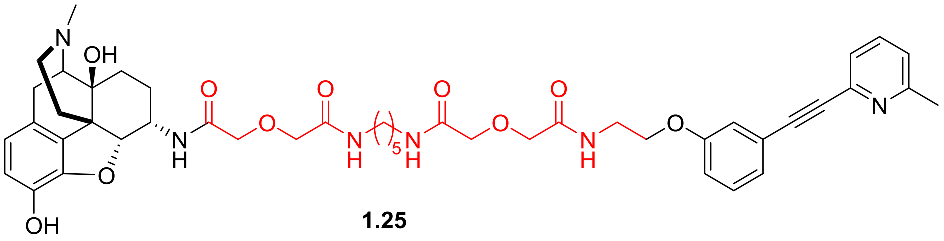
1.25

Figure 32. Bivalent µOR and mGluR5 ligand.[118]

Portoghese et al.[152] proposed a simple model for the induction of µOR-mGluR5 heterodimer by **1.25** that could contain the following steps (Figure 33): (a) univalent binding of **1.25** to a mGluR5 (or µOR) oligomer; (b) dissociation of **1.25**-bound to mGluR5 protomer from the oligomer; (c) association with a µOR oligomer via assistance of the free µOR agonist pharmacophore of **1.25**; (d) dissociation of the bridged **1.25**-bound oligomer from the µOR oligomer to give the **1.25**-bound µOR/mGluR5 heterodimer complex. Whereas many other models of induced heterodimer formation are also possible, the crucial feature for all would be the optimal length and nature of spacers incorporated into the bivalent ligand.

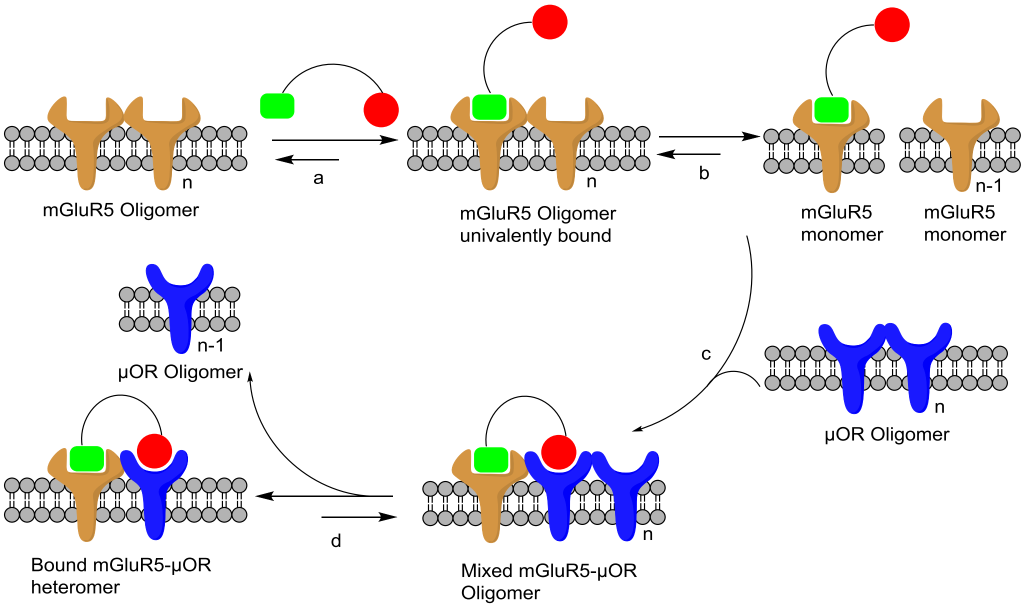
mGluR5 Oligomer
n
a
mGluR5 Oligomer
univalently bound
n
b
mGluR5
monomer
mGluR5
monomer
n-1
n-1
µOR Oligomer
c
µOR Oligomer
n
Bound mGluR5-µOR
heteromer
d
Mixed mGluR5-µOR
Oligomer
n

Figure 33. Illustration of the concept of µOR−mGluR5 heterodimer induced by **1.25**. Green square and red circle represent mGluR5 antagonist and µOR agonist pharmacophores, respectively.[152]

Cross-talk between opioid and chemokine receptors is initiated by chemokine release which, to some extent, leads to reduced potency of morphine in the treatment of chronic pain. Based on the probability that a µOR-CCR5 heteromer is involved in such cross-talk, Akgün et al.[119] synthesized a series of bivalent ligands that consist of µOR agonist and CCR5 antagonist pharmacophores linked through homologous spacers (14−24 atoms).

When tested on the lipopolysaccharide (LPS) inflamed mice, the bivalent ligand **1.26** (Figure 34) with a 22-atom spacer displayed excellent antinociceptive activity (i.t. ED50 = 0.0146 pmol/mouse) that was 2000-fold higher than morphine. Furthermore, **1.26** was approximately 3500-fold more potent than a combination treatment of the corresponding µOR agonist and CCR5 antagonist. These results clearly indicate that **1.26** bridges the protomers of a µOR-CCR5 heterodimer, which was supported by docking studies, and that the µOR-CCR5 heterodimer could act as a novel target for the treatment of chronic pain.

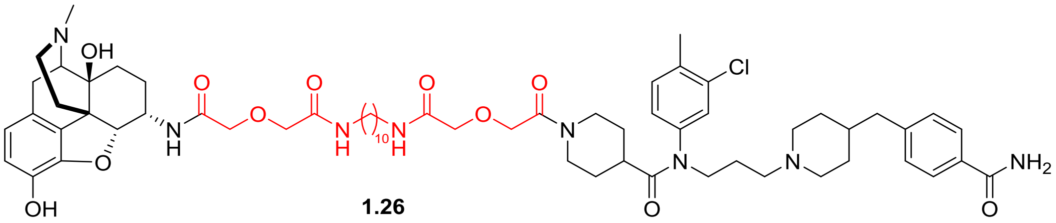

1.26

Figure 34. Bivalent ligand **1.26** bridging μOR and CCR5 receptors.[119]

Based on the above studies on opioid receptor, a main difference between the bivalent ligands and clinically used opioid ligands is their remarkable potency in both reducing hyperalgesia and strengthening antinociception without tolerance in inflamed mice. To further identify the targets of bivalent ligands **1.25** and **1.26**, Akgün et al. has undertaken a study upon i.t. administration recently.[154] The results showed that the high potency of **1.25** and **1.26** in LPS inflamed mice is partially owing to their contributions to directly blocking the activated spinal glia. Specifically, compound **1.25** displayed the potently enhanced antinociception due principally to selective inhibition of activated astrocytes, while **1.26** antinociception was owing mainly to blockage of induced spinal microglia.

Lacking μOR/δOR heterodimer-selective antagonists is the major limitation in the study of μOR/δOR dimerization. Hence, Olson et al. synthesized a series of varying length (15−41 atoms) bivalent peptides with selective but moderate/low-affinity pharmacophores for the μOR and δOR (Figure 35).[155] The pharmacological results showed a spacer length dependent μOR/δOR dimer affinity/potency profile in vitro, with the 24-atom spacer length **1.29** (D24M) generating the highest affinity/potency (<1 nM) at the μOR/δOR dimer and selectivity (≥89-fold relative to the μOR or δOR monomer). In addition, **1.29** displayed ≥200-fold higher potency than the monomeric compounds at the μOR/δOR heterodimer.

Subsequently, **1.29** was further evaluated in the tail flick test in mice, which exhibited a dose-dependently antagonized antinociception formed by the μOR/δOR agonists CYM51010 and Deltorphin-II, without antagonizing the monomer agonists DAMGO and DSLET. Interestingly, **1.29** was also observed to sharply reduce withdrawal behavior in models of acute and chronic morphine dependence.

These data strongly suggest that **1.29** is a first-in-class selective and high affinity/potency μOR/δOR heterodimer antagonist both in vitro and in vivo.

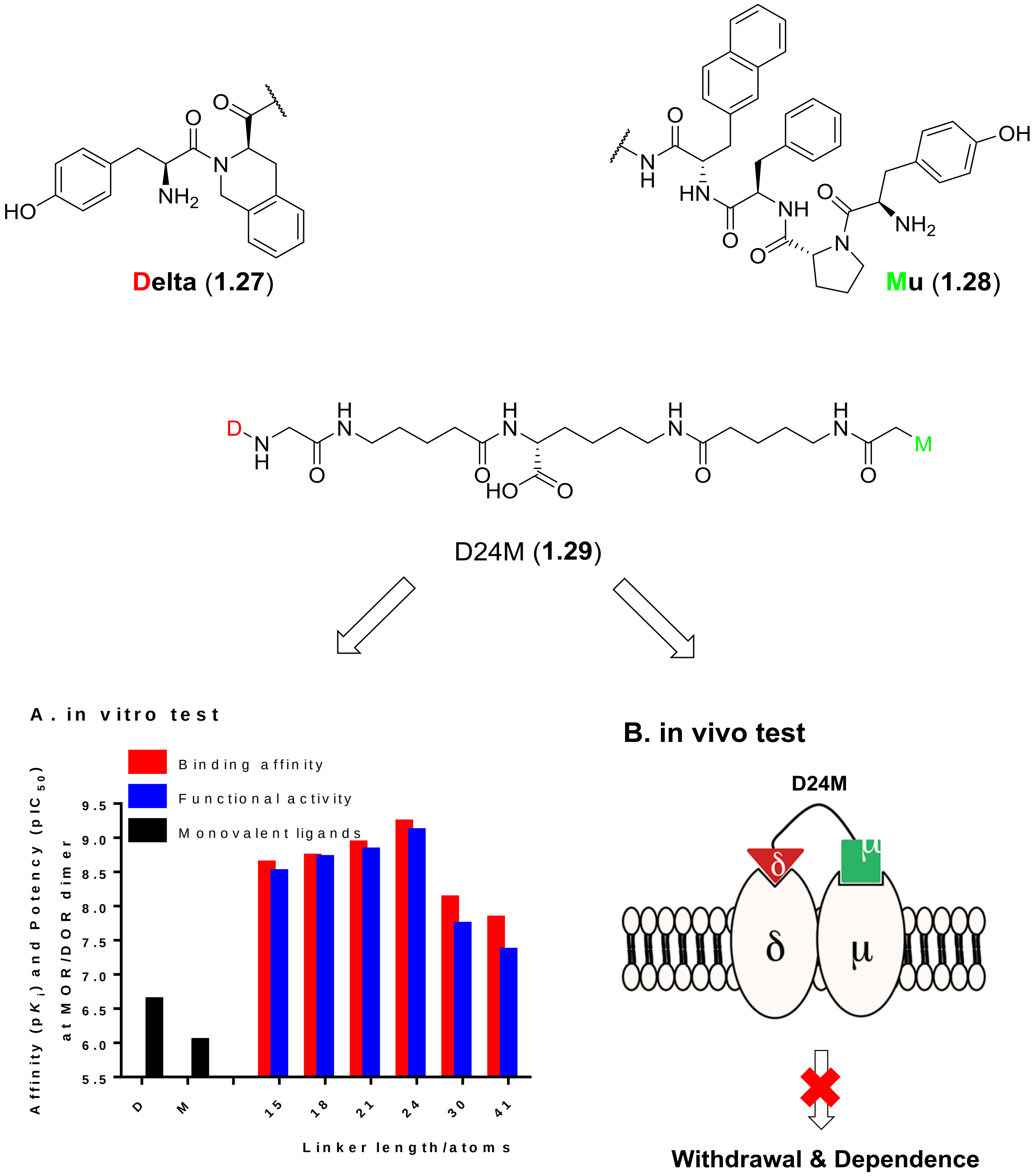
Delta (1.27)
Mu (1.28)
D
M
D24M (1.29)
A. in vitro test
Binding affinity
Functional activity
Monovalent ligands
Affinity (pKi) and Potency (pIC50) at MOR/DOR dimer
9.5
9.0
8.5
8.0
7.5
7.0
6.5
6.0
5.5
D
M
15
18
21
24
30
41
Linker length/atoms
B. in vivo test
D24M
δ
μ
Withdrawal & Dependence

Figure 35. Bivalent μOR/δOR antagonist ligands.

Busnelli et al.[156] reported bivalent ligands **1.30a** and **1.30b** comprising two identical oxytocin-mimetics (Figure 36) that induced a three order magnitude boost in G-protein signaling of oxytocin receptors (OTRs) in vitro and a 100- and 40-fold gain in potency in vivo in the social behavior of mice and zebrafish.

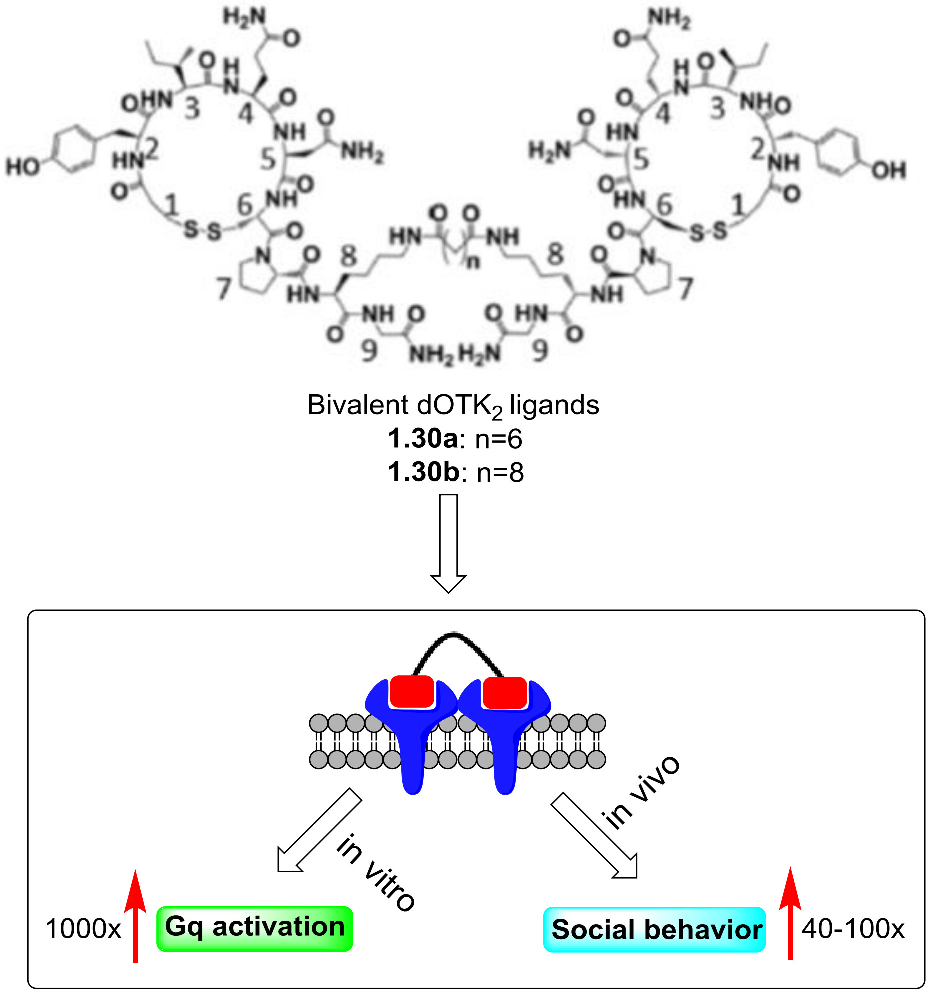

Figure 36. Bivalent OTR ligands **1.30a** and **1.30b** with high potency both in vitro and in vivo.

Through receptor mutagenesis and interference experiments with synthetic peptides mimicking transmembrane helices (TMH), they show that such superpotent behavior follows from the binding of the bivalent ligands to dimeric receptors based on a TMH1-TMH2 interface. Furthermore, in this arrangement, only the analogues with a well-defined spacer length (~25 Å) precisely fit inside a channel-like passage between the two protomers of the dimer. The newly discovered oxytocin bivalent ligands represent a powerful tool for targeting dimeric OTR in neurodevelopmental and psychiatric disorders and, in general, provide a framework to untangle specific arrangements of GPCR dimers.

I.2.8 Conclusion

Bivalent ligands are defined as compounds that contain two pharmacophores linked by an appropriate spacer. The design of such molecules requires the selection of potent and subtype-selective lead pharmacophores, appropriate attachment points to connect the spacer, and the length and composition of the spacer group. This overview mainly focused on the design of bivalent ligands recently described in the literature and used as specific pharmacological tools to investigate GPCR dimerization.

The advantages of the bivalent approach are numerous, including enhanced potency and receptor subtype specificity. However, the use of bivalent ligands as potential pharmacotherapeutics is limited by problematic molecular properties, such as high molecular weight and lipophilicity. In addition, the linker must be attached to the pharmacophore in a position that tolerates structural modification.

All the examples mentioned above strongly suggest that the length and nature of the linker are crucial factors for the optimal ligand-receptor interactions, which depend on the properties of the selected pharmacophores and binding sites of GPCRs.

Overall, these compounds possess great potential as pharmacological tools to investigate the GPCR dimerization in vitro and in vivo.

Reference

[1] Latorraca, N. R.; Venkatakrishnan, A. J.; Dror, R. O. GPCR Dynamics: Structures in Motion. *Chem. Rev.* **2017**, *117*, 139−155.

[2] Rask-Andersen, M.; Almén, M. S.; Schiöth, H. B. Trends in the exploitation of novel drug targets. *Nat. Rev. Drug Discov.* **2011**, *10*, 579-590.

[3] Fredriksson, R.; Lagerström, M. C.; Lundin, L. G.; Schiöth, H. B. The G-protein-coupled receptors in the human genome form five main families. Phylogenetic analysis, paralogon groups, and fingerprints. *Mol. Pharmacol.* **2003**, *63*, 1256–1272.

[4] Lagerström, M. C.; Schiöth, H. B. Structural diversity of G protein-coupled receptors and significance for drug discovery. *Nat. Rev. Drug Discov.* **2008**, *7*, 339–357.

[5] Schiöth, H. B.; Fredriksson, R. The GRAFS classification system of G-protein coupled receptors in comparative perspective. *Gen. Comp. Endocrinol.* **2005**, *142*, 94–101.

[6] Oldham, W. M.; Hamm, H. E. Heterotrimeric G protein activation by G-protein-coupled receptors. *Nat. Rev. Mol. Cell Biol.* **2008**, *9*, 60-71.

[7] Tuteja, N. Signaling through G protein coupled receptors. *Plant Signal. Behav.* **2009**, *4*, 942-947.

[8] Ford, C. E.; Skiba, N. P.; Bae, H.; Daaka, Y.; Reuveny, E.; Shekter, L. R.; Rosal, R.; Weng, G.; Yang, C. S.; Iyengar, R.; Miller, R. J.; Jan, L. Y.; Lefkowitz, R. J.; Hamm, H. E. Molecular basis for interactions of G protein betagamma subunits with effectors. *Science* **1998**, *280*, 1271-1274.

[9] Rondard, P.; Iiri, T.; Srinivasan, S.; Meng, E.; Fujita, T.; Bourne, H. R. Mutant G protein alpha subunit activated by Gbeta gamma: a model for receptor activation? *Proc. Natl. Acad. Sci. USA* **2001**, *98*, 6150-6155.

[10] Gurevich, V. V.; Gurevich, E. V. Structural determinants of arrestin functions. *Prog. Mol. Biol. Transl. Sci.* **2013**, *118*, 57-92.

[11] Shenoy, S. K.; Lefkowitz, R. J. β-Arrestin-mediated receptor trafficking and signal transduction. *Trends Pharmacol. Sci.* **2011**, *32*, 521-533.

[12] Shukla, A. K.; Xiao, K.; Lefkowitz, R. J. Emerging paradigms of β-arrestin-dependent seven transmembrane receptor signaling. *Trends Biochem. Sci*. **2011**, *36*, 457-469.

[13] Seta, K.; Nanamori, M.; Modrall, J. G.; Neubig, R. R.; Sadoshima, J. AT1 receptor mutant lacking heterotrimeric G protein coupling activates the Src-Ras-ERK pathway without nuclear translocation of ERKs. *J. Biol. Chem.* **2002**, *277*, 9268-9277.

[14] Tohgo, A.; Pierce, K. L.; Choy, E. W.; Lefkowitz, R. J.; Luttrell, L. M. beta-Arrestin scaffolding of the ERK cascade enhances cytosolic ERK activity but inhibits ERK-mediated transcription following angiotensin AT1a receptor stimulation. *J. Biol. Chem.* **2002**, *277*, 9429-9436.

[15] Jafri, F.; El-Shewy, H. M.; Lee, M. H.; Kelly, M.; Luttrell, D. K.; Luttrell, L. M. Constitutive ERK1/2 activation by a chimeric neurokinin 1 receptor-beta-arrestin1 fusion protein. Probing the composition and function of the G protein-coupled receptor "signalsome". *J. Biol. Chem.* **2006**, *281*, 19346-19357.

[16] Gesty-Palmer, D.; Chen, M.; Reiter, E.; Ahn, S.; Nelson, C. D.; Wang, S.; Eckhardt, A. E.; Cowan, C. L.; Spurney, R. F.; Luttrell, L. M.; Lefkowitz, R. J. Distinct beta-arrestin- and G protein-dependent pathways for parathyroid hormone receptor-stimulated ERK1/2 activation. *J. Biol. Chem.* **2006**, *281*, 10856-10864.

[17] Ren, X. R.; Reiter, E.; Ahn, S.; Kim, J.; Chen, W.; Lefkowitz, R. J. Different G protein-coupled receptor kinases govern G protein and beta-arrestin-mediated signaling of V2 vasopressin receptor. *Proc. Natl. Acad. Sci. U S A.* **2005**, *102*, 1448-1453.

[18] Shenoy, S. K.; Drake, M. T.; Nelson, C. D.; Houtz, D. A.; Xiao, K.;;; Madabushi, S.; Reiter, E.; Premont, R. T.; Lichtarge, O.; Lefkowitz, R. J. beta-arrestin-dependent, G protein-independent ERK1/2 activation by the beta2 adrenergic receptor. *J. Biol. Chem.* **2006**, *281*, 1261-1273.

[19] Wei, H.; Ahn, S.; Shenoy, S. K.; Karnik, S. S.; Hunyady, L.; Luttrell, L. M.; Lefkowitz, R. J. Independent beta-arrestin 2 and G protein-mediated pathways for angiotensin II activation of extracellular signal-regulated kinases 1 and 2. *Proc. Natl. Acad. Sci. U S A.* **2003**, *100*, 10782-10787.

[20] Ahn, S.; Shenoy, S. K.; Wei, H.; Lefkowitz, R. J. Differential kinetic and spatial patterns of beta-arrestin and G protein-mediated ERK activation by the angiotensin II receptor. *J. Biol. Chem.* **2004**, *279*, 35518-35525.

[21] George, S. R.; O'Dowd, B. F.; Lee, S. P. G-protein-coupled receptor oligomerization and its potential for drug discovery. *Nat. Rev. Drug Discov.* **2002**, *1*, 808−820.

[22] Milligan, G. G protein-coupled receptor dimerization: function and ligand pharmacology. *Mol. Pharmacol.* **2004**, *66*, 1−7.

[23] Maurice, P.; Kamal, M.; Jockers, R. Asymmetry of GPCR oligomers supports their functional relevance. *Trends Pharmacol. Sci.* **2011**, *32*, 514−520.

[24] Agnati, L. F.; Fuxe, K.; Zini, I.; Lenzi, P.; Hökfelt, T. Aspects on receptor regulation and isoreceptor identification. *Med. Biol.* **1980,** *58*, 182-187.

[25] Fuxe, K.; Agnati, L. F.; Benfenati, F.; Cimmino, M.; Algeri, S.; Hökfelt, T.; Mutt, V. Modulation by cholecystokinins of 3H-spiroperidol binding in rat striatum: evidence for increased affinity and reduction in the number of binding sites. *Acta Physiol Scand.* **1981,** *113* 567-569.

[26] White, J. H.; Wise, A.; Main, M. J.; Green, A.; Fraser, N. J.; Disney, G. H.; Barnes, A. A.; Emson, P.; Foord, S. M.; Marshall, F. H. Heterodimerization is required for the formation of a functional GABA(B) receptor. *Nature.* **1998,** *396*, 679-682.

[27] Fuxe, K.; Marcellino, D.; Woods, A. S.; Giuseppina, L.; Antonelli, T.; Ferraro, L.; Tanganelli, S.; Agnati, L. F. Integrated signaling in heterodimers and receptor mosaics of different types of GPCRs of the forebrain: relevance for schizophrenia. *J. Neural. Transm (Vienna).* **2009,** *116*, 923-939.

[28] Milligan, G. The role of dimerisation in the cellular trafficking of G-protein-coupled receptors. *Curr. Opin. Pharmacol.* **2010,** *10*, 23-29.

[29] Hiller, C.; Kühhorn, J.; Gmeiner, P. Class A G-protein-coupled receptor (GPCR) dimers and bivalent ligands. *J. Med. Chem.* **2013**, *56,* 6542−6559.

[30] de Jong, L. A.; Uges, D. R.; Franke, J. P.; Bischoff, R. Receptor-ligand binding assays: technologies and applications. *J. Chromatogr. B Analyt. Technol. Biomed. Life Sci.* 2005, *829*, 1–25.

[31] Albizu, L.; Cottet, M.; Kralikova, M.; Stoev, S.; Seyer, R.; Brabet, I.; Roux, T.; Bazin, H.; Bourrier, E.; Lamarque, L.; Breton, C.; Rives, M. L.; Newman, A.; Javitch, J.; Trinquet, E.; Manning, M.; Pin, J. P.; Mouillac, B.; Durroux, T. Time-resolved FRET between GPCR ligands reveals oligomers in native tissues. *Nat. Chem. Biol.* **2010**, *6*, 587-594.

[32] Pfleger, K. D.; Eidne, K. A. New technologies: bioluminescence resonance energy transfer (BRET) for the detection of real time interactions involving G-protein coupled receptors. *Pituitary* **2003,** *6*, 141-151.

[33] Milligan, G.; Bouvier, M. Methods to monitor the quaternary structure of G protein-coupled receptors. *FEBS J.* **2005**, *272*, 2914−2925.

[34] Milligan, G. Applications of bioluminescence- and fluorescence resonance energy transfer to drug discovery at G protein-coupled receptors. *Eur. J. Pharm. Sci.* **2004,** *21*, 397-405.

[35] Trifilieff, P.; Rives, M. L.; Urizar, E.; Piskorowski, R. A.; Vishwasrao, H. D.; Castrillon, J.; Schmauss, C.; Slättman, M.; Gullberg, M.; Javitch, J. A. Detection of antigen interactions ex vivo by proximity ligation assay: endogenous dopamine D2-adenosine A2A receptor complexes in the striatum. *Biotechniques* **2011**, *51*, 111-118.

[36] Ghirmai, S.; Azar, M. R.; Polgar, W. E.; Berzetei-Gurske, I.; Cashman, J. R. Synthesis and biological evaluation of alpha- and beta-6-amido derivatives of 17-cyclopropylmethyl-3, 14beta-dihydroxy-4, 5alpha-epoxymorphinan: potential alcohol-cessation agents. *J. Med. Chem.* **2008**, *51*, 1913-1924.

[37] Dixon, A. S.; Schwinn, M. K.; Hall, M. P.; Zimmerman, K.; Otto, P.; Lubben, T. H.; Butler, B. L.; Binkowski, B. F.; Machleidt, T.; Kirkland, T. A.; Wood, M. G.; Eggers, C. T.; Encell, L. P.; Wood, K. V. NanoLuc Complementation Reporter Optimized for Accurate Measurement of Protein Interactions in Cells. *ACS Chem. Biol.* **2016**, *11*, 400−408.

[38] Wouters, E.; Vasudevan, L.; Ciruela, F.; Saini, D. K.; Stove, C.; Van Craenenbroeck, K. Assessing GPCR dimerization in living cells: comparison of the NanoBiT assay with related bioluminescence- and fluorescence-based approaches. **2018** *Springer protocols (Neuromethods) book chapter 15*.

[39] van Rijn, R. M.; Harvey, J. H.; Brissett, D. I.; DeFriel, J. N.; Whistler, J. L. Novel screening assay for the selective detection of G protein-coupled receptor heteromer signaling. *J. Pharmacol. Exp. Ther.* **2013**, *344*, 179−188.

[40] Rozenfeld, R.; Bushlin, I.; Gomes, I.; Tzavaras, N.; Gupta, A.; Neves, S.; Battini, L.; Gusella, G. L.; Lachmann, A.; Ma'ayan, A.; Blitzer, R. D.; Devi, L. A. Receptor heteromerization expands the repertoire of cannabinoid signaling in rodent neurons. *PLoS One* **2012**, *7*, e29239.

[41] Rios, C.; Gomes, I.; Devi, L. A. mu opioid and CB1 cannabinoid receptor interactions: reciprocal inhibition of receptor signaling and neuritogenesis. *Br. J. Pharmacol.* **2006**, *148*, 387−395.

[42] Parenty, G.; Appelbe, S.; Milligan, G. CXCR2 chemokine receptor antagonism enhances DOP opioid receptor function via allosteric regulation of the CXCR2-DOP receptor heterodimer. *Biochem. J.* **2008**, *412*, 245−256.

[43] Pello, O. M.; Martínez-Muñoz, L.; Parrillas, V.; Serrano, A.; Rodríguez-Frade, J. M.; Toro, M. J.; Lucas, P.; Monterrubio, M.; Martínez-A, C.; Mellado, M. Ligand stabilization of CXCR4/delta-opioid receptor heterodimers reveals a mechanism for immune response regulation. *Eur. J. Immunol.* **2008**. *38*, 537–549.

[44] Jordan, B. A.; Devi, L. A. G-protein-coupled receptor heterodimerization modulates receptor function. *Nature* **1999**, *399*, 697−700.

[45] Jordan, B. A.; Trapaidze, N.; Gomes, I.; Nivarthi, R.; Devi, L. A. Oligomerization of opioid receptors with beta 2-adrenergic receptors: a role in trafficking and mitogen-activated protein kinase activation. *Proc. Natl. Acad. Sci. U.S.A.* **2001**, *98*, 343−348.

[46] a) Vilardaga, J. P.; Nikolaev, V. O.; Lorenz, K.; Ferrandon, S.; Zhuang, Z. J.; Lohse, M. J. Conformational cross-talk between α2A-adrenergic and μ-opioid receptors controls cell signaling. *Nat. Chem. Biol.* **2008**, *4*, 126−131. b) Walwyn, W. M.; Chen, W.; Kim, H.; Minasyan, A.; Ennes, H. S.; McRoberts, J. A.; Marvizón, J. C. Sustained suppression of hyperalgesia during latent sensitization by μ-, δ-, and κ-opioid receptors and α2A adrenergic receptors: role of constitutive activity. *J. Neurosci.* **2016**, *36*, 204-221.

[47] Liu, X. Y.; Liu, Z. C.; Sun, Y. G.; Ross, M.; Kim, S. Tsai, F. F.; Li, Q. F.; Jeffry, J.; Kim, J. Y.; Loh, H. H.; Chen, Z. F. Unidirectional cross-activation of GRPR by MOR1D uncouples itch and analgesia induced by opioids. *Cell* **2011**, *147*, 447-458.

[48] Pfeiffer, M.; Kirscht, S.; Stumm, R.; Koch, T.; Wu, D.; Laugsch, M.; Schröder, H.; Höllt, V.; Schulz, S. Heterodimerization of substance P and mu-opioid receptors regulates receptor trafficking and resensitization. *J Biol Chem.* **2003**, *278,* 51630-51637.

[49] a) Akgün, E.; Javed, M. I.; Lunzer, M. M.; Smeester, B. A.; Beitz, A. J.; Portoghese, P. S. Ligands that interact with putative MOR-mGluR5 heteromer in mice with inflammatory pain produce potent antinociception. *Proc. Natl. Acad. Sci. USA.* **2013**, *110*, 11595-11599. b) Akgün, E.; Lunzer, M. M.; Portoghese, P. S. Combined glia inhibition and opioid

receptor agonism afford highly potent analgesics without tolerance. *ACS Chem. Neurosci.* DOI: 10.1021/acschemneuro.8b00323. Publication Date: 15 Aug **2018**.

[50] a) Wang, D.; Sun, X.; Bohn, L. M.; Sadee, W. Opioid receptor homo- and heterodimerization in living cells by quantitative bioluminescence resonance energy transfer. *Mol. Pharmacol.* **2005**, *67*, 2173−2184. b) Turnaturi, R.; Aricò, G.; Ronsisvalle, G.; Parenti, C.; Pasquinucci, L. Multitarget opioid ligands in pain relief: New players in an old game. *Eur. J. Med. Chem.* **2016**,*108*, 211-228.

[51] Gomes, I.; Gupta, A.; Filipovska, J.; Szeto, H. H.; Pintar, J. E.; Devi, L. A. A role for heterodimerization of mu and delta opiate receptors in enhancing morphine analgesia. *Proc. Natl. Acad. Sci. U.S.A.* **2004**, *101*, 5135−5139.

[52] a) George, S. R.; Fan, T.; Xie, Z.; Tse, R.; Tam, V.; Varghese, G.; O'Dowd, B. F. Oligomerization of mu- and delta-opioid receptors. Generation of novel functional properties. *J. Biol. Chem.* **2000**, *275*, 26128−26135. b) Olson, K. M.; Keresztes, A.; Tashiro, J. K.; Daconta, L. V.; Hruby, V. J.; Streicher, J. M. Synthesis and evaluation of a novel bivalent selective antagonist for the mu-delta opioid receptor heterodimer that reduces morphine withdrawal in mice. *J. Med. Chem.* **2018**, *61*, 6075−6086.

[53] Pfeiffer, M.; Koch, T.; Schroder, H.; Laugsch, M.; Hollt, V.; Schulz, S. Heterodimerization of somatostatin and opioid receptors cross-modulates phosphorylation, internalization, and desensitization. *J. Biol. Chem.* **2002**, *277*, 19762−19772.

[54] Rios, C.; Gomes, I.; Devi, L. A. mu opioid and CB1 cannabinoid receptor interactions: reciprocal inhibition of receptor signaling and neuritogenesis. *Br. J. Pharmacol.* **2006**, *148*, 387−395.

[55] a) Hojo, M.; Sudo, Y.; Ando, Y.; Minami, K.; Takada, M.; Matsubara, T.; Kanaide, M.; Taniyama, K.; Sumikawa, K.; Uezono, Y. Mu-Opioid receptor forms a functional heterodimer with cannabinoid CB1 receptor: electrophysiological and FRET assay analysis. *J. Pharmacol. Sci.* **2008**, *108*, 308-319. b) Manduca, A.; Lassalle, O.; Sepers, M.; Campolongo, P.; Cuomo, V.; Marsicano, G.; Kieffer, B.; Vanderschuren, L. J.; Trezza, V.; Manzoni, O. J. Interacting cannabinoid and opioid receptors in the nucleus accumbens core control adolescent social play. *Front Behav. Neurosci.* **2016**,10,211.

[56] Zheng, Y.; Akgun, E.; Harikumar, K. G.; Hopson, J.; Powers, M. D.; Lunzer, M. M.; Miller, L. J.; Portoghese, P. S. Induced association of mu opioid (MOP) and type 2 cholecystokinin (CCK2) receptors by novel bivalent ligands. *J. Med. Chem.* **2009**, *52*, 247−258.

[57] Chen, C.; Li, J.; Bot, G.; Szabo, I.; Rogers, T. J.; Liu-Chen, L. Y. Heterodimerization and cross-desensitization between the mu-opioid receptor and the chemokine CCR5 receptor. *Eur. J. Pharmacol.* **2004**, *483*, 175−186.

[58] Finley, M. J.; Chen, X.; Bardi, G.; Davey, P.; Geller, E. B.; Zhang, L.; Adler, M. W.; Rogers, T. J. Bi-directional heterologous desensitization between the major HIV-1 co-receptor CXCR4 and the kappa-opioid receptor. *J. Neuroimmunol.* **2008**, *197*, 114-123.

[59] Pello, O. M.; Martínez-Muñoz, L.; Parrillas, V.; Serrano, A.; Rodríguez-Frade, J. M.; Toro, M. J.; Lucas, P.; Monterrubio, M.; Martínez-A, C.; Mellado, M. Ligand stabilization of CXCR4/delta-opioid receptor heterodimers reveals a mechanism for immune response regulation. *Eur. J. Immunol.* **2008**. *38*, 537–549.

[60] Urizar, E.; Yano, H.; Kolster, R.; Galés, C.; Lambert, N.; Javitch, J. A. CODA-RET reveals functional selectivity as a result of GPCR heteromerization. *Nat. Chem. Biol.* **2011**, *7*, 624−630.

[61] a) So, C. H.; Varghese, G.; Curley, K. J.; Kong, M. M.; Alijaniaram, M.; Ji, X.; Nguyen, T.; O'dowd. B. F.; George, S. R. D1 and D2 dopamine receptors form heterooligomers and cointernalize after selective activation of either receptor. *Mol. Pharmacol.* **2005**, *68*, 568−578. b) Frederick, A. L.; Yano, H.; Trifilieff, P.; Vishwasrao, H. D.; Biezonski, D.; Mészáros, J.; Urizar, E.; Sibley, D. R.; Kellendonk, C.; Sonntag, K. C.; Graham, D. L.; Colbran, R. J.; Stanwood, G. D.; Javitch, J. A. Evidence against dopamine D1/D2 receptor heteromers. *Mol. Psychiatry.* **2015**, *20*, 1373-85.

[62] a) arcellino, D.; Ferre, S.; Casado, V.; Cortes, A.; Le Foll, B.; Mazzola, C.; Drago, F.; Saur, O.; Stark, H.; Soriano, A.; Barnes, C.; Goldberg, S. R.; Lluis, C.; Fuxe, K.; Franco, R. Identification of dopamine D1-D3 receptor heteromers. Indications for a role of synergistic D1-D3 receptor interactions in the striatum. *J. Biol. Chem.* **2008**, *283*, 26016−26025. b) Galaj, E.; Ewing, S.; Ranaldi, R. Dopamine D1 and D3 receptor polypharmacology as a potential treatment approach for substance use disorder. *Neurosci. Biobehav. Rev.* **2018**, *89*, 13-28.

[63] a) Fiorentini, C.; Busi, C.; Gorruso, E.; Gotti, C.; Spano, P.; Missale, C. Reciprocal regulation of dopamine D1 and D3 receptor function and trafficking by heterodimerization. *Mol. Pharmacol.* **2008**, *74*, 59−69. b) Hounsou, C.; Margathe, J. F.; Oueslati, N.; Belhocine, A.; Dupuis, E.; Thomas, C.; Mann, A.; Ilien, B.; Rognan, D.; Trinquet, E.; Hibert, M.; Pin, J. P.; Bonnet, D.; Durroux, T. Time-resolved FRET binding assay to investigate hetero-

oligomer binding properties: proof of concept with dopamine D1/D3 heterodimer. *ACS Chem. Biol.* **2015**, *10*, 466-74.

[64] a) Han, Y.; Moreira, I. S.; Urizar, E.; Weinstein, H.; Javitch, J. A. Allosteric communication between protomers of dopamine class A GPCR dimers modulates activation. *Nat. Chem. Biol.* **2009**, *5*, 688−695. b) Carli, M.; Kolachalam, S.; Aringhieri, S.; Rossi, M.; Giovannini, L.; Maggio, R.; Scarselli, M. Dopamine D2 receptors dimers: how can we pharmacologically target them? *Curr. Neuropharmacol.* **2018**, *16*, 222-230.

[65] Scarselli, M.; Novi, F.; Schallmach, E.; Lin, R.; Baragli, A.; Colzi, A.; Griffon, N.; Corsini, G. U.; Sokoloff, P.; Levenson, R.; Vogel, Z.; Maggio, R. D2/D3 dopamine receptor heterodimers exhibit unique functional properties. *J. Biol. Chem.* **2001**, *276*, 30308−30314.

[66] Maggio, R.; Scarselli, M.; Novi, F.; Millan, M. J.; Corsini, G. U. Potent activation of dopamine D3/D2 heterodimers by the antiparkinsonian agents, S32504, pramipexole and ropinirole. *J. Neurochem.* **2003**, *87*, 631−641.

[67] Rocheville, M.; Lange, D. C.; Kumar, U.; Patel, S. C.; Patel, R. C.; Patel, Y. C. Receptors for dopamine and somatostatin: formation of hetero-oligomers with enhanced functional activity. *Science* **2000**, *288*, 154−157.

[68] a) Ferrada, C.; Ferre, S.; Casado, V.; Cortes, A.; Justinova, Z.; Barnes, C.; Canela, E. I.; Goldberg, S. R.; Leurs, R.; Lluis, C.; Franco, R. Interactions between histamine H3 and dopamine D2 receptors and the implications for striatal function. *Neuropharmacology* **2008**, *55*, 190−197. b) Kononoff Vanhanen, J.; Nuutinen, S.; Tuominen, M.; Panula, P. Histamine H3 receptor regulates sensorimotor gating and dopaminergic signaling in the striatum. *J. Pharmacol. Exp. Ther.* **2016**, *357*, 264-72.

[69] Romero-Fernandez, W.; Borroto-Escuela, D. O.; Agnati, L. F.; Fuxe, K. Evidence for the existence of dopamine d2-oxytocin receptor heteromers in the ventral and dorsal striatum with facilitatory receptor-receptor interactions. *Mol. Psychiatry* **2012**, *18*, 849-850.

[70] Gingrich, B.; Liu, Y.; Cascio, C.; Wang, Z.; Insel, T. R. Dopamine D2 receptors in the nucleus accumbens are important for social attachment in female prairie voles (Microtus ochrogaster). *Behav. Neurosci.* **2000**, *114*, 173-183.

[71] Kern, A.; Albarran-Zeckler, R.; Walsh, H. E.; Smith, R. G. Apo-ghrelin receptor forms heteromers with DRD2 in hypothalamic neurons and is essential for anorexigenic effects of DRD2 agonism. *Neuron* **2012**, *73*, 317-332.

[72] Schellekens, H.; van Oeffelen, W. E.; Dinan, T. G.; Cryan, J. F. Promiscuous dimerization of the growth hormone secretagogue receptor (GHS-R1a) attenuates ghrelin-mediated signaling. *J. Biol. Chem.* **2013**, *288*, 181-191.

[73] Jiang, H.; Betancourt, L.; Smith, R. G. Ghrelin amplifies dopamine signaling by cross talk involving formation of growth hormone secretagogue receptor/dopamine receptor subtype 1 heterodimers. *Mol. Endocrinol.* **2006**, *20*, 1772-1785.

[74] Lukasiewicz, S.; Polit, A.; Kedracka-Krok, S.; Wedzony, K.; Mackowiak, M.; Dziedzicka-Wasylewska, M. Hetero-dimerization of serotonin 5-HT(2A) and dopamine D(2) receptors. *Biochim. Biophys. Acta* **2010**, *1803*, 1347−1358.

[75] Albizu, L.; Holloway, T.; Gonzalez-Maeso, J.; Sealfon, S. C. Functional crosstalk and heteromerization of serotonin 5-HT2A and dopamine D2 receptors. *Neuropharmacology* **2011**, *61*, 770−777.

[76] Koschatzky, S.; Tschammer, N.; Gmeiner, P. Cross-receptor interactions between dopamine D2L and neurotensin NTS1 receptors modulate binding affinities of dopaminergics. *ACS Chem. Neurosci.* **2011**, *2*, 308−316.

[77] Marcellino, D.; Carriba, P.; Filip, M.; Borgkvist, A.; Frankowska, M.; Bellido, I.; Tanganelli, S.; Muller, C. E.; Fisone, G.; Lluis, C.; Agnati, L. F.; Franco, R.; Fuxe, K. Antagonistic cannabinoid CB1/ dopamine D2 receptor interactions in striatal CB1/D2 heteromers. A combined neurochemical and behavioral analysis. *Neuropharmacology* **2008**, *54*, 815−823.

[78] a) Kearn, C. S.; Blake-Palmer, K.; Daniel, E.; Mackie, K.; Glass, M. Concurrent stimulation of cannabinoid CB1 and dopamine D2 receptors enhances heterodimer formation: a mechanism for receptor cross-talk? *Mol. Pharmacol.* **2005**, *67*, 1697−1704. b) Bagher, A. M.; Laprairie, R. B.; Toguri, J. T.; Kelly, M. E. M.; Denovan-Wright, E. M. Bidirectional allosteric interactions between cannabinoid receptor 1 (CB1) and dopamine receptor 2 long (D2L) heterotetramers. *Eur. J. Pharmacol.* **2017**, *813*, 66-83.

[79] Gonzalez, S.; Rangel-Barajas, C.; Peper, M.; Lorenzo, R.; Moreno, E.; et al. Dopamine D4 receptor, but not the ADHD-associated D4.7 variant, forms functional heteromers with the dopamine D2S receptor in the brain. *Mol. Psychiatry* **2012**, *17*, 650-662.

[80] Gonzalez, S.; Moreno-Delgado, D.; Moreno, E.; Perez-Capote, K.; Franco, R.; et al. Circadian- related heteromerization of adrenergic and dopamine D(4) receptors modulates melatonin synthesis and release in the pineal gland. *PLoS Biol.* **2012**, *10*, e1001347.

[81] Baragli, A.; Alturaihi, H.; Watt, H. L.; Abdallah, A.; Kumar, U. Heterooligomerization of human dopamine receptor 2 and somatostatin receptor 2 Co-immunoprecipitation and fluorescence resonance energy transfer analysis. *Cell. Signal.* **2007**, *19*, 2304-2316.

[82] Zitzmann, K.; Andersen, S.; Vlotides, G.; Spottl, G.; Zhang, S.; et al. The novel somatostatin receptor 2/dopamine type 2 receptor chimeric compound BIM-23A758 decreases the viability of human GOT1 midgut carcinoid cells. *Neuroendocrinology* **2013**, *98*, 128-136.

[83] Gines, S.; Hillion, J.; Torvinen, M.; Le Crom, S.; Casado, V.; Canela, E. I.; Rondin, S.; Lew, J. Y.; Watson, S.; Zoli, M.; Agnati, L. F.; Verniera, P.; Lluis, C.; Ferre, S.; Fuxe, K.; Franco, R. Dopamine D1 and adenosine A1 receptors form functionally interacting heteromeric complexes. *Proc. Natl. Acad. Sci. U.S.A.* **2000**, *97*, 8606−8611. b) Rivera-Oliver, M.; Moreno, E.; Álvarez-Bagnarol, Y.; Ayala-Santiago, C.; Cruz-Reyes, N.; Molina-Castro, G. C.; Clemens, S.; Canela, E. I.; Ferré, S.; Casadó, V.; Díaz-Ríos, M. Adenosine A1-dopamine D1 receptor heteromers control the excitability of the spinal motoneuron. *Mol. Neurobiol.* **2018** May 24. DOI: 10.1007/s12035-018-1120-y.

[84] Hillion, J.; Canals, M.; Torvinen, M.; Casado, V.; Scott, R.; Terasmaa, A.; Hansson, A.; Watson, S.; Olah, M. E.; Mallol, J.; Canela, E. I.; Zoli, M.; Agnati, L. F.; Ibanez, C. F.; Lluis, C.; Franco, R.; Ferre, S.; Fuxe, K. Coaggregation, cointernalization, and codesensitization of adenosine A2A receptors and dopamine D2 receptors. *J. Biol. Chem.* **2002**, *277*, 18091−18097.

[85] a) Canals, M.; Marcellino, D.; Fanelli, F.; Ciruela, F.; de Benedetti, P.; Goldberg, S. R.; Neve, K.; Fuxe, K.; Agnati, L. F.; Woods, A. S.; Ferré, S.; Lluis, C.; Bouvier, M.; Franco, R. Adenosine A2A-dopamine D2 receptor-receptor heteromerization: qualitative and quantitative assessment by fluorescence and bioluminescence energy transfer. *J. Biol. Chem.* **2003**, *278*, 46741−46749. b) Borroto-Escuela, D. O.; Rodriguez, D.; Romero-Fernandez, W.; Kapla, J.; Jaiteh, M.; Ranganathan, A.; Lazarova, T.; Fuxe, K.; Carlsson, J. Mapping the Interface of a GPCR Dimer: A structural model of the A2A adenosine and D2 dopamine receptor heteromer. *Front Pharmacol.* **2018**, *9*, 829.

[86] a) Ciruela, F.; Escriche, M.; Burgueno, J.; Angulo, E.; Casado, V.; et al. Metabotropic glutamate 1alpha and adenosine A1 receptors assemble into functionally interacting complexes. *J. Biol. Chem.* **2001**, *276*, 18345-18351. b) Kamikubo, Y.; Tabata, T.; Sakairi, H.; Hashimoto, Y.; Sakurai, T. Complex formation and functional interaction between adenosine A1 receptor and type-1 metabotropic glutamate receptor. *J. Pharmacol. Sci.* **2015**, *128*, 125-30.

[87] González-Maeso, J.; Ang, R. L.; Yuen, T.; Chan, P.; Weisstaub, N. V.; López-Giménez, J. F.; Zhou, M.; Okawa, Y.; Callado, L. F.; Milligan, G.; Gingrich, J. A.; Filizola, M.; Meana, J. J.; Sealfon, S. C. Identification of a serotonin/glutamate receptor complex implicated in psychosis. *Nature.* **2008**, *452*, 93–97.

[88] Cabello, N.; Gandía, J.; Bertarelli, D. C.; Watanabe, M.; Lluís, C.; Franco, R.; Ferré, S.; Luján, R.; Ciruela, F. Metabotropic glutamate type 5, dopamine D2 and adenosine A2a receptors form higher-order oligomers in living cells. *J. Neurochem.* **2009**, *109*, 1497-1507.

[89] a) Ferré, S.; Karcz-Kubicha, M.; Hope, B. T.; Popoli, P.; Burgueño, J.; Gutiérrez, M. A.; Casadó, V.; Fuxe, K.; Goldberg, S. R.; Lluis, C.; Franco, R.; Ciruela, F. Synergistic interaction between adenosine A2A and glutamate mGlu5 receptors: implications for striatal neuronal function. *Proc. Natl. Acad. Sci. USA.* **2002**, *99*, 11940-11945. b) Wright S. R.; Zanos, P.; Georgiou, P.; Yoo, J. H.; Ledent, C.; Hourani, S. M.; Kitchen, I.; Winsky-Sommerer, R.; Bailey A. A critical role of striatal A_{2A}R-mGlu5R interactions in modulating the psychomotor and drug-seeking effects of methamphetamine. *Addict. Biol.* **2016**, *21*, 811-25.

[90] Gomes, I.; Ayoub, M. A.; Fujita, W.; Jaeger, W. C.; Pfleger, K. D.; Devi, L. A. G Protein-Coupled Receptor Heteromers. *Annu. Rev. Pharmacol. Toxicol.* **2016**, *56*, 403–425.

[91] Luttrell, L. M.; Gesty-Palmer, D. Beyond desensitization: physiological relevance of arrestin-dependent signaling. *Pharmacol. Rev.* **2010**, *62*, 305-330.

[92] Goddard, A. D.; Watts, A. Contributions of fluorescence techniques to understanding G protein-coupled receptor dimerisation. *Biophys. Rev.* **2012**, *4*, 291−298.

[93] Daniels, D. J.; Lenard, N. R.; Etienne, C. L.; Law, P. Y.; Roerig, S. C.; Portoghese, P. S. Opioid-induced tolerance and dependence in mice is modulated by the distance between pharmacophores in a bivalent ligand series. *Proc. Natl. Acad. Sci. U S A.* **2005**, *102*, 19208-19213.

[94] Daniels, D. J.; Kulkarni, A.; Xie, Z.; Bhushan, R. G.; Portoghese, P. S. A bivalent ligand (KDAN-18) containing delta-antagonist and kappa-agonist pharmacophores bridges delta2 and kappa1 opioid receptor phenotypes. *J. Med. Chem.* **2005**, *48*, 1713-1716.

[95] Lenard, N.R.; Daniels, D. J.; Portoghese, P. S.; Roerig, S. C. Absence of conditioned place preference or reinstatement with bivalent ligands containing mu-opioid receptor agonist and delta-opioid receptor antagonist pharmacophores. *Eur. J. Pharmacol.* **2007**, *566*, 75-82.

[96] Milligan, G.; Bouvier, M. Methods to monitor the quaternary structure of G protein-coupled receptors, *FEBS J.* **2005**, *272*, 2914-25.

[97] Yekkirala, A. S.; Lunzer, M. M.; McCurdy, C. R.; Powers, M. D.; Kalyuzhny, A. E.; Roerig, S. C.; Portoghese, P. S. N-naphthoyl-beta-naltrexamine (NNTA), a highly selective and potent activator of μ/kappa-opioid heteromers, *Proc. Natl. Acad. Sci. U S A.* **2011**, *108*, 5098-103.

[98] Soriano, A.; Ventura, R.; Molero, A.; Hoen, R.; Casadó, V.; Cortés, A.; Fanelli, F.; Albericio, F.; Lluís, C.; Franco, R.; Royo, M. Adenosine A2A receptor-antagonist/dopamine D2 receptor-agonist bivalent ligands as pharmacological tools to detect A2A-D2 receptor heteromers. *J. Med. Chem.* **2009**, *52*, 5590-602.

[99] Jacobson, K. A.; Xie, R.; Young, L.; Chang, L.; Liang, B. T. A novel pharmacological approach to treating cardiac ischemia. Binary conjugates of A1 and A3 adenosine receptor agonists. *J. Biol. Chem.* **2000**, *275*, 30272-9.

[100] Portoghese, P. S. From models to molecules: opioid receptor dimers, bivalent ligands, and selective opioid receptor probes. *J. Med. Chem.* **2001**, *44*, 2259-69.

[101] Decker, M.; Fulton, B. S.; Zhang, B.; Knapp, B. I.; Bidlack, J.M.; Neumeyer, J. L. Univalent and bivalent ligands of butorphan: characteristics of the linking chain determine the affinity and potency of such opioid ligands. *J. Med. Chem.* **2009**, *52*, 7389−7396.

[102] Zhang, B.; Zhang, T.; Sromek, A. W.; Scrimale, T.; Bidlack, J.M.; Neumeyer, J. L. Synthesis and binding affinity of novel mono- and bivalent morphinan ligands for kappa, mu, and delta opioid receptors. *Bioorg. Med. Chem.* **2011**, *19*, 2808−2816.

[103] Huber, D.; Hubner, H.; Gmeiner, P. 1,1′-Disubstituted ferrocenes as molecular hinges in mono- and bivalent dopamine receptor ligands. *J. Med. Chem.* **2009**, *52*, 6860−6870.

[104] Bonger, K. M.; van den Berg, R. J.; Knijnenburg, A. D.; Heitman, L. H.; Ijzerman, A. P.; Oosterom, J.; Timmers, C. M.; Overkleeft, H. S.; van der Marel, G. A. Synthesis and evaluation of homodimeric GnRHR antagonists having a rigid bis-propargylated benzene core. *Bioorg. Med. Chem.* **2008**, *16*, 3744−3758.

[105] Weiss, S.; Keller, M.; Bernhardt, G.; Buschauer, A.; Konig, B. Modular synthesis of non-peptidic bivalent NPY Y1 receptor antagonists. *Bioorg. Med. Chem.* **2008**, *16*, 9858−9866.

[106] Rajeswaran, W. G.; Cao, Y.; Huang, X .P.; Wroblewski, M. E.; Colclough, T.; Lee, S.; Liu, F.; Nagy, P. I.; et al.: Design, synthesis, and biological characterization of bivalent 1-methyl-1,2,5,6-tetrahydropyridyl-1,2,5-thiadiazole derivatives as selective muscarinic agonists. *J. Med. Chem.* **2001**, *44*, 4563-4576.

[107] Berque-Bestel, I.; Lezoualc'h, F.; Jockers, R. Bivalent ligands as specific pharmacological tools for G protein-coupled receptor dimers. *Curr. Drug Discov. Technol.* **2008**, *5*, 312-318.

[108] Neumeyer, J. L.; Zhang, A.; Xiong, W.; Gu, X. H.; Hilbert, J. E.; Knapp, B. I.; Negus, S. S.; Mello, N. K.; Bidlack, J. M. Design and synthesis of novel dimeric morphinan ligands for κ and μ opioid receptors. *J. Med. Chem.* **2003**, *46*, 5162-5170.

[109] Peng, X.; Knapp, B. I.; Bidlack, J. M.; Neumeyer, J. L. Synthesis and preliminary in vitro investigation of bivalent ligands containing homo- and heterodimeric pharmacophores at mu, delta, and kappa opioid receptors. *J. Med. Chem.* **2006**, *49*, 256-262.

[110] Bhushan, R. G.; Sharma, S. K.; Xie, Z.; Daniels, D. J.; Portoghese, P. S. A bivalent ligand (KDN-21) reveals spinal delta and kappa opioid receptors are organized as heterodimers that give rise to delta(1) and kappa(2) phenotypes. Selective targeting of delta-kappa heterodimers. *J. Med. Chem.* **2004**, *47*, 2969-2972.

[111] Rajeswaran, W. G.; Murphy, W. A.; Taylor, J. E.; Coy, D. H. Exploration of the DTrp-NMeLys motif in the search for potent somatostatin antagonists. *Bioorg. Med. Chem.* **2002**, *10*, 2023-2029.

[112] Yano, K.; Kimura, S.; Imanishi, Y. Simultaneous activation of two different receptor systems by enkephalin/neurotensin conjugates having spacer chains of various lengths. *Eur. J. Pharm. Sci.* **1998**, *7*, 41-48.

[113] Daniels, D. J.; Kulkarni, A.; Xie, Z.; Bushan, R. G.; Portoghese, P. S. A bivalent ligand (KDN-18) containing delta antagonist and kappa-agonist pharmacophores bridges delta2 and kappa1 opioid receptor phenotypes. *J. Med. Chem.* **2005**, *48*, 1713-1716.

[114] Li, T.; Fujita, Y.; Shiotani, K.; Miyazaki, A.; Tsuda, Y.; Ambo, A.; Sasaki, Y.; Jinsmaa, Y.; et al. Potent Dmt-Tic pharmacophoric delta- and mu-opioid receptor antagonists. *J. Med. Chem.* **2005**, *48*, 8035-8044.

[115] Zheng, Y.; Akgün, E.; Harikumar, K. G.; Hopson, J.; Powers, M. D.; Lunzer, M. M.; Miller, L. J.; Portoghese, P. S. Induced association of mu opioid (MOP) and type 2 cholecystokinin (CCK2) receptors by novel bivalent ligands. *J. Med. Chem.* **2009**, *52*, 247–258.

[116] Yekkirala, A. S.; Kalyuzhny, A. E.; Portoghese, P. S. An immunocytochemical-derived correlate for evaluating the bridging of heteromeric mu-delta opioid protomers by bivalent ligands. *ACS Chem. Biol.* **2013**, *8*, 1412−1416.

[117] Le Naour, M.; Akgün, E.; Yekkirala, A.; Lunzer, M. M.; Powers, M. D.; Kalyuzhny, A. E.; Portoghese, P. S. Bivalent ligands that target μ opioid (MOP) and cannabinoid1 (CB1) receptors are potent analgesics devoid of tolerance. *J. Med. Chem.* **2013**, *56*, 5505−5513.

[118] Akgün, E.; Javed, M. I.; Lunzer, M. M.; Smeester, B. A.; Beitz, A. J.; Portoghese, P. S. Ligands that interact with putative MOR-mGluR5 heteromer in mice with inflammatory pain produce potent antinociception. *Proc. Natl. Acad. Sci. USA.* **2013**, *110*, 11595-11599.

[119] Akgün, E.; Javed, M. I.; Lunzer, M. M.; Powers, M. D.; Sham, Y. Y.; Watanabe, Y.; Portoghese, P. S. Inhibition of Inflammatory and Neuropathic Pain by Targeting a Mu Opioid Receptor/Chemokine Receptor5 Heteromer (MOR-CCR5). *J. Med. Chem.* **2015**, *58*, 8647−8657.

[120] McRobb, F. M.; Crosby, I. T.; Yuriev, E.; Lane, J. R.; Capuano, B. Homobivalent ligands of the atypical antipsychotic clozapine: design, synthesis, and pharmacological evaluation. *J. Med. Chem.* **2012**, *55*, 1622−1634.

[121] Bhushan, R. G.; Sharma, S. K.; Xie, Z.; Daniels, D. J.; Portoghese, P. S. A bivalent ligand (KDN-21) reveals spinal delta and kappa opioid receptors are organized as heterodimers that give rise to delta(1) and kappa(2) phenotypes. Selective targeting of delta-kappa heterodimers. *J. Med. Chem.* **2004**, *47*, 2969−2972.

[122] Kuhhorn, J.; Gotz, A.; Hubner, H.; Thompson, D.; Whistler, J.; Gmeiner, P. Development of a bivalent dopamine D2 receptor agonist. *J. Med. Chem.* **2011**, *54*, 7911−7919.

[123] Huber, D.; Lober, S.; Hubner, H.; Gmeiner, P. Bivalent molecular probes for dopamine D2-like receptors. *Bioorg. Med. Chem.* **2012**, *20*, 455−466.

[124] Soulier, J. L.; Russo, O.; Giner, M.; Rivail, L.; Berthouze, M.; Ongeri, S.; Maigret, B.; Fischmeister, R.; Lezoualc'h, F.; Sicsic, S.; Berque-Bestel, I. Design and synthesis of specific probes for human 5-HT4 receptor dimerization studies. *J. Med. Chem.* **2005**, *48*, 6220−6228.

[125] Russo, O.; Berthouze, M.; Giner, M.; Soulier, J. L.; Rivail, L.; Sicsic, S.; Lezoualc'h, F.; Jockers, R.; Berque-Bestel, I. Synthesis of specific bivalent probes that functionally interact with 5-HT(4) receptor dimers. *J. Med. Chem.* **2007**, *50*, 4482−4492.

[126] Zhang, Y.; Gilliam, A.; Maitra, R.; Damaj, M. I.; Tajuba, J. M.; Seltzman, H. H.; Thomas, B. F. Synthesis and biological evaluation of bivalent ligands for the cannabinoid 1 receptor. *J. Med. Chem.* **2010**, *53*, 7048–7060.

[127] Perrey, D. A.; Gilmour, B. P.; Thomas, B. F.; Zhang, Y. Toward the Development of Bivalent Ligand Probes of Cannabinoid CB1 and Orexin OX1 Receptor Heterodimers. *ACS Med. Chem. Lett.* **2014**, *5*, 634−638.

[128] Portoghese, P. S.; Larson, D. L.; Sayre, L. M.; Yim, C. B.; Ronsisvalle, G.; Tam, S. W.; Takemori, A. E. Opioid agonist and antagonist bivalent ligands. The relationship between spacer length and selectivity at multiple opioid receptors. *J. Med. Chem.* **1986**, *29*, 1855−1861.

[129] Manglik, A.; Kruse, A. C.; Kobilka, T. S.; Thian, F. S.; Mathiesen, J. M.; Sunahara, R. K.; Pardo, L.; Weis, W. I.; Kobilka, B. K.; Granier, S. Crystal structure of the μ-opioid receptor bound to a morphinan antagonist. *Nature* **2012**, *485*, 321−326.

[130] Hiller, C.; Kühhorn, J.; Gmeiner, P. Class A G-protein-coupled receptor (GPCR) dimers and bivalent ligands. *J. Med. Chem.* **2013**, *56*, 6542−6559.

[131] Nimczick, M.; Decker, M. New approaches in the design and development of cannabinoid receptor ligands: multifunctional and bivalent compounds. *ChemMedChem* **2015**, *10*, 773 – 786.

[132] Tanaka, T.; Nomura, W.; Narumi, T.; Masuda, A.; Tamamura, H. Bivalent ligands of CXCR4 with rigid linkers for elucidation of the dimerization state in cells. *J. Am. Chem. Soc.* **2010**; *132*, 15899–15901.

[133] Soriano, A.; Ventura, R.; Molero, A.; Hoen, R.; Casadó, V.; Cortés, A.; Fanelli, F.; Albericio, F.; Lluís, C.; Franco, R.; Royo, M. Adenosine A2A receptor-antagonist/dopamine D2 receptor-agonist bivalent ligands as pharmacological tools to detect A2A-D2 receptor heteromers. *J. Med. Chem.* **2009**, *52*, 5590–5602.

[134] Portoghese, P. S.; Ronsisvalle, G.; Larson, D. L.; Takemori, A. E. Synthesis and opioid antagonist potencies of naltrexamine bivalent ligands with conformationally restricted spacers. *J. Med. Chem.* **1986**, *29*, 1650−1653.

[135] Shonberg, J.; Scammells, P. J.; Capuano, B. Design strategies for bivalent ligands targeting GPCRs. *ChemMedChem* **2011**, *6*, 963 – 974.

[136] Russo, O.; Berthouze, M.; Giner, M.; Soulier, J. L.; Rivail, L.; Sicsic, S.; Lezoualc'h, F.; Jockers, R.; Berque-Bestel, I. Synthesis of specific bivalent probes that functionally interact with 5-HT(4) receptor dimers. *J. Med. Chem.* **2007**, *50*, 4482–4492.

[137] Bobrovnik, S. A. The influence of rigid or flexible linkage between two ligands on the effective affinity and avidity for reversible interactions with bivalent receptors. *J. Mol. Recognit.* **2007**, *20*, 253 –262.

[138] Bonger, K. M.; Kapoerchan, V. V.; Grotenbreg, G. M.; van Koppen, C. J.; Timmers, C. M.; van der Marel, G. A.; Overkleeft, H. S. Oligoproline helices as structurally defined scaffolds for oligomeric G protein-coupled receptor ligands. *Org. Biomol. Chem.* **2010**, *8*, 1881 – 1884.

[139] Bonger, K. M.; van den Berg, R. J. B. H. N.; Knijnenburg, A. D.; Heitman, L. H.; Ijzerman, A. P.; Oosterom, J.; Timmers, C. M.; Overkleeft, H. S.; van der Marel, G. A. Synthesis and evaluation of homodimeric GnRHR antagonists having a rigid bis-propargylated benzene core. *Bioorg. Med. Chem.* **2008**, *16*, 3744 –3758.

[140] Bonger, K. M.; van den Berg, R. J. B. H. N.; Knijnenburg, A. D.; Heitman, L. H.; van Koppen, C. J.; Timmers, C. M.; Overkleeft, H. S.; van der Marel, G. A. Discovery of selective luteinizing hormone receptor agonists using the bivalent ligand method. *ChemMedChem* **2009**, *4*, 1189–1195.

[141] Rajeswaran, W. G.; Cao, Y.; Huang, X. P.; Wroblewski, M. E.; Colclough, T.; Lee, S.; Liu, F.; Nagy, P. I.; Ellis, J.; Levine, B. A.; Nocka, K. H.; Messer, W. S., Jr. Design, synthesis, and biological characterization of bivalent 1-methyl-1,2,5,6-tetrahydropyridyl-1,2,5-thiadiazole derivatives as selective muscarinic agonists. *J. Med. Chem.* **2001**, *44*, 4563−4576.

[142] Cao, Y.; Zhang, M.; Wu, C.; Lee, S.; Wroblewski, M. E.; Whipple, T.; Nagy, P. I.; Takacs-Novak, K.; Balazs, A.; Toros, S.; Messer, W. S., Jr. Synthesis and biological characterization of 1-methyl-1,2,5,6-tetrahydropyridyl-1,2,5-thiadiazole derivatives as muscarinic agonists for the treatment of neurological disorders. *J. Med. Chem.* **2003**, *46*, 4273−4286.

[143] Bhushan, R. G.; Sharma, S. K.; Xie, Z.; Daniels, D. J.; Portoghese, P. S. A bivalent ligand (KDN-21) reveals spinal delta and kappa opioid receptors are organized as heterodimers that give rise to delta(1) and kappa(2) phenotypes. Selective targeting of delta-kappa heterodimers. *J. Med. Chem.* **2004**, *47*, 2969−2972.

[144] Daniels, D. J.; Kulkarni, A.; Xie, Z. H.; Bhushan, R. G.; Portoghese, P. S. A bivalent ligand (KDAN-18) containing deltaantagonist and kappa-agonist pharmacophores bridges delta2 and kappa1 opioid receptor phenotypes. *J. Med. Chem.* **2005**, *48*, 1713−1716.

[145] Yuan, Y.; Arnatt, C. K.; Li, G.; Haney, K. M.; Ding, D.; Jacob, J.C.; Selley, D. E.; Zhang, Y. Design and synthesis of a bivalent ligand to explore the putative heterodimerization of the mu opioid receptor and the chemokine receptor CCR5. *Org. Biomol. Chem.* **2012**, *10*, 2633−2646.

[146] a) Fernandes, S. M.; Lee, Y. S.; Gillies, R. J.; Hruby, V. J. Synthesis and evaluation of bivalent ligands for binding to the human melanocortin-4 receptor. *Bioorg. Med. Chem.* **2014**, *22*, 6360–6365. b) Kiessling, L. L.; Gestwicki, J. E.; Strong, L. E. Synthetic multivalent ligands in the exploration of cell-surface interactions. *Curr. Opin. Chem. Biol.* **2000**, *4*, 696–703. c) Kiessling, L. L.; Gestwicki, J. E.; Strong, L. E. Synthetic multivalent ligands as probes of signal transduction. *Angew. Chem. Int. Ed.* **2006**, *45*, 2348 – 2368.

[147] Andersen, J.; Ladefoged, L. K.; Kristensen, T. N. B.; Munro, L.; Grouleff, J.; Stuhr-Hansen, N.; Kristensen, A. S.; Schiøtt, B.; Strømgaard. K. Interrogating the molecular basis for substrate recognition in serotonin and dopamine transporters with high-affinity substrate-based bivalent ligands. *ACS Chem. Neurosci.* **2016**, *7*, 1406−1417.

[148] She, X.; Pegoli, A.; Mayr, J.; Hübner, H.; Bernhardt, G.; Gmeiner, P.; Keller, M. Heterodimerization of dibenzodiazepinone-type muscarinic acetylcholine receptor ligands leads to increased M_2R affinity and selectivity. *ACS Omega* **2017**, *2*, 6741−6754.

[149] Pockes, S.; Wifling, D.; Keller, M.; Buschauer, A.; Elz, S. Highly potent, stable, and selective dimeric hetarylpropylguanidine-type histamine H_2 receptor agonists. *ACS Omega* **2018**, *3*, 2865−2882.

[150] Kuhhorn, J.; Hubner, H.; Gmeiner, P. Bivalent dopamine D2 receptor ligands: synthesis and binding properties. *J. Med. Chem.* **2011**, *54*, 4896−4903.

[151] Gogoi, S.; Biswas, S.; Modi, G.; Antonio, T.; Reith, M. E.; Dutta, A. K. Novel bivalent ligands for D2/D3 dopamine receptors: significant co-operative gain in D2 affinity and potency. *ACS Med. Chem. Lett.* **2012**, *3*, 991−996.

[152] Portoghese, P. S.; Akgün, E.; Lunzer, M. M. Heteromer Induction: An Approach to Unique Pharmacology? *ACS Chem. Neurosci.* **2017**, *8*, 426−428.

[153] Hübner, H.; Schellhorn, T.; Gienger, M.; Schaab, C.; Kaindl, J.; Leeb, L.; Clark, T.; Möller, D.; Gmeiner, P. Structure-guided development of heterodimer-selective GPCR ligands. *Nat Commun.* **2016**, *7*, 12298.

[154] Akgün, E.; Lunzer, M. M.; Portoghese, P. S. Combined glia inhibition and opioid receptor agonism afford highly potent analgesics without tolerance. *ACS Chem. Neurosci.* DOI: 10.1021/acschemneuro.8b00323. Publication Date: 15 Aug **2018**.

[155] Olson, K. M.; Keresztes, A.; Tashiro, J. K.; Daconta, L. V.; Hruby, V. J.; Streicher, J. M. Synthesis and Evaluation of a novel bivalent selective antagonist for the Mu-Delta opioid receptor heterodimer that reduces morphine withdrawal in mice. *J. Med. Chem.* **2018**, *61*, 6075−6086.

[156] Busnelli, M.; Kleinau, G.; Muttenthaler, M.; Stoev, S.; Manning, M.; Bibic, L.; Howell, L. A.; McCormick, P. J.; Di Lascio, S.; Braida, D.; Sala, M.; Rovati, G. E.; Bellini, T.; Chini, B. Design and characterization of superpotent bivalent ligands targeting oxytocin receptor dimers via a channel-like structure. *J. Med. Chem.* **2016**, *59*, 7152−7166.

CHAPTER II

OBJECTIVES

II. OBJECTIVES

Bivalent ligands possess great potential as pharmacological tools to investigate GPCR dimerization both in vitro and in vivo, and may evolve to promising drug candidates for diverse diseases.

The main goal of this PhD study is to design and synthesize bivalent GPCR ligands to study new receptor-receptor interactions. In a first study (Chapter III), we aim to synthesize a series of heterobivalent µOR -D_2-likeR ligands as pharmacological tools to study µOR-D_2-likeR heteromers. D_2-likeR agonist/antagonist and µOR agonist/antagonist will be linked through PEG spacers of variable length to probe the best interaction with the µOR-D_2-likeR heteromer. The binding properties of these compounds will be determined by radioligand binding studies in membrane preparations and intact cells. Furthermore, MAPK phosphorylation and β-arrestin2 recruitment assays will be performed to assess the pharmacological response of the ligands for D_2-likeR and µOR, respectively. This study will involve cells expressing the µOR and D_2-likeR, separately, as well as cells co-expressing both receptors.

As depicted in Figure 1, the bivalent ligands will be derived from a 6-hydromorphamine (to which we will gain access from hydromorphone) and the structurally related µOR antagonist 6-naltrexamine (NTA). As D_2-likeR ligands we plan to use 1,4-disubstituted aromatic piperazines (1,4-DAPs) and 5-hydroxy-2-(dipropylamino)tetralin (5-OH-DPAT) that will be equipped with an appropriate alkyne ligation handle.

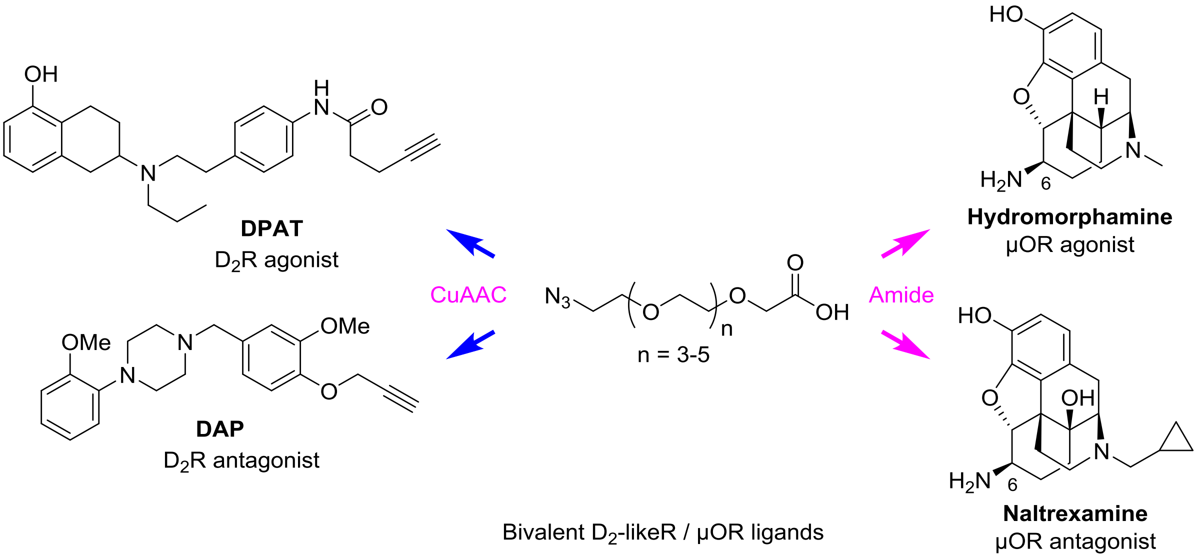

Figure 1. Designed heterobivalent ligands of D_2-likeR and µOR

In a next study (Chapter IV), we plan to design and synthesize bivalent D_2-likeR agonist/antagonist and mGluR5 antagonist ligands to study the mGluR5-D_2-likeR heteromers. For this study, we will explore different types of spacers including PEG linkers, alkyl linker, and tertiary amine spacers of varying length to investigate the effect of the length and nature of the spacers on binding affinity and functional activity. The binding properties of these compounds will be determined by radioligand binding assays. Moreover, cAMP and MAPK phosphorylation will be measured to assess the signal transduction for both D_2-likeR and mGluR5. Experiments to evaluate the behaviour of the heterobivalent ligands to dimeric receptors will be performed in cells coexpressing mGluR5 and D_2-likeR. The target bivalent ligands of mGluR5-D_2-likeR are shown in Figure 2.

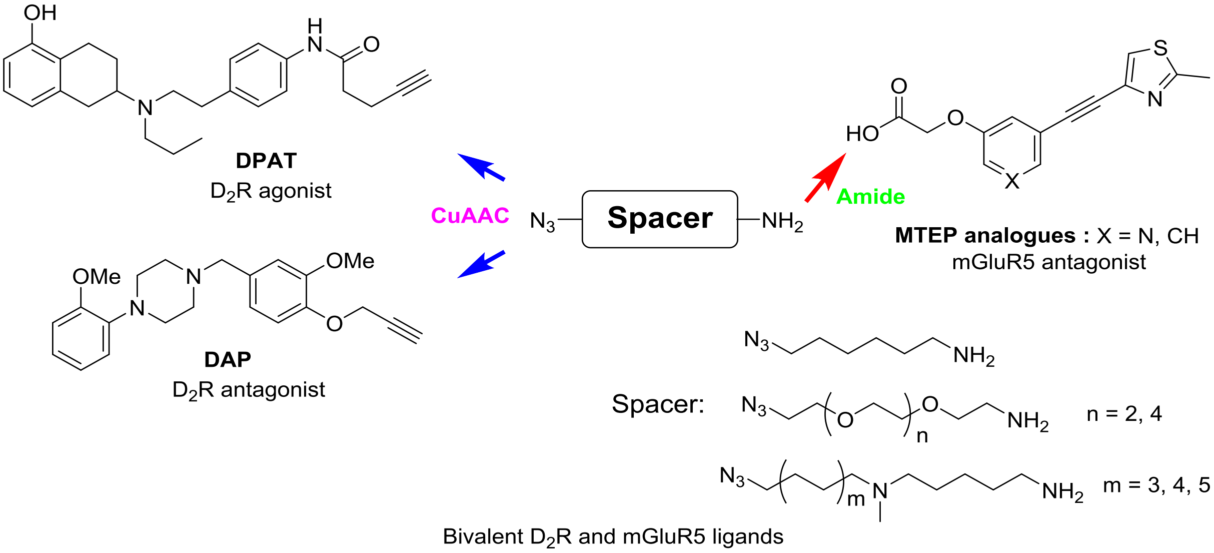
OH
H
N
O
N
DPAT
D2R agonist
CuAAC
N3
Spacer
NH2
Amide
O
HO
O
S
N
X
MTEP analogues : X = N, CH
mGluR5 antagonist
OMe
N
N
OMe
O
DAP
D2R antagonist
N3
NH2
Spacer:
N3
O
n
O
NH2
n = 2, 4
N3
m
N
NH2
m = 3, 4, 5
Bivalent D2R and mGluR5 ligands

Figure 2. Designed bivalent ligands of D_2-likeR and mGluR5

Fluorescently labeled ligands have been developed to study receptor localization, trafficking, and signaling processes via fluorescence imaging. They are also employed in fluorescent binding assays, where they offer advantages over radioligands which suffer from possible health risks and legal and disposal costs.

In Chapter IV, we will use alkyne functionalized boron dipyrromethene (BODIPY) dyes to construct possible fluorescent mGluR5 ligands (Figure 3). These ligands will be assessed by NanoBRET.

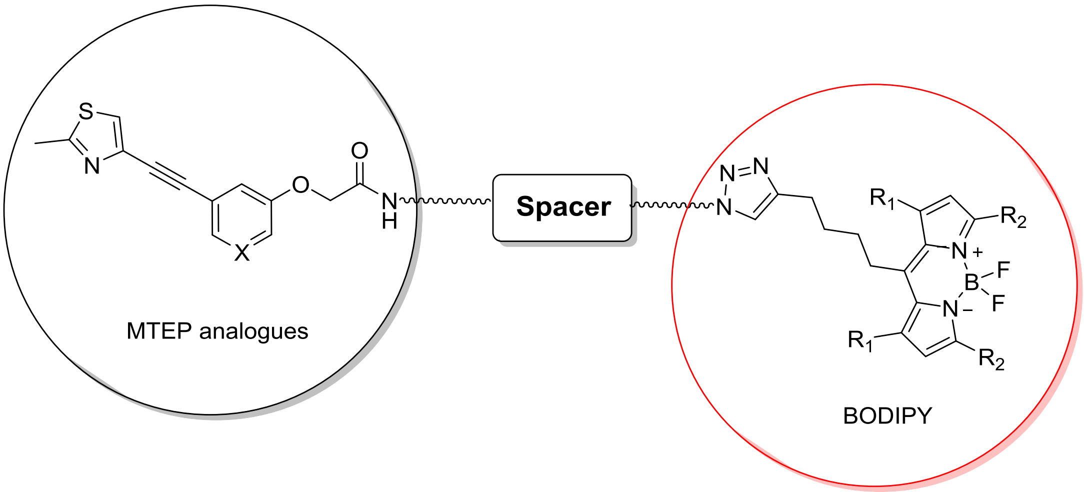
S
N
O
O
N
H
X
MTEP analogues
Spacer
N=N
N
R1
R2
N+
B
F
F
N−
R1
R2
BODIPY

Figure 3. Designed fluorescent mGluR5 ligands equipped with BODIPY dyes.

CHAPTER III

Design, synthesis and biological evaluation of bivalent ligands targeting Dopamine D_2-like receptors and the μ-opioid receptor

The content of this chapter was partially derived from:

Qian, M.; Vasudevan, L.; Huysentruyt, J.; Risseeuw, M. D. P.; Stove, C.; Vanderheyden, P. M. L.; Van Craenenbroeck, K.; Van Calenbergh, S. *ChemMedChem* **2018**, *13*, 944 – 956.

β-arrestin2 recruitment to μOR was partially asessed by Lakshmi Vasudevan. Ligand binding assay for D_2R using [^{3}H]raclopride was carried out with the help of Jelle Huysentruyt.

III. DESIGN, SYNTHESIS AND BIOLOGICAL EVALUATION OF BIVALENT LIGANDS TARGETING DOPAMINE D$_2$-LIKE RECEPTORS AND THE μ-OPIOID RECEPTOR

III.1. Abstract

Currently, there is mounting evidence that intermolecular receptor-receptor interactions may result in altered receptor recognition, pharmacology and signaling. Heterobivalent ligands have been proven useful molecular probes for confirming and targeting heteromeric receptors. This paper describes the design and synthesis of novel heterobivalent ligands for dopamine D$_2$-like receptors (D$_2$-likeR) and the μ opioid receptor (μOR) and their evaluation using ligand binding and functional assays. Interestingly, we identified a potent bivalent ligand that contains a short 18-atom linker and combines good potency with high efficacy both in β-arrestin2 recruitment for μOR and MAPK-P for D$_4$R. Furthermore, this compound was characterized by a biphasic competition binding curve for the D$_4$R-μOR heterodimer, indicative of a bivalent binding mode. As this compound possibly bridges the D$_4$R-μOR heterodimer, it could be used as a pharmacological tool to further investigate the interactions of D$_4$R and μOR.

III.2. Introduction

G protein-coupled receptors (GPCRs) represent the largest family of membrane proteins. About half of the clinically used drugs today recognize GPCRs. It is now widely accepted that different GPCRs can interact with each other and form complexes, so called heteromers. The first hypothesis on GPCR heteromers was already raised in the early eighties after observations of neuropeptide-monoamine receptor-receptor interactions.[1,2] The existence of heteromers was confirmed almost twenty years later for two non-functional GPCR monomers, gamma amino butyric acid (GABA) receptors, GABAB1 and GABAB2, which assemble at the cell surface in a signaling heterodimer, the GABAB receptor.[3] Now, dimerization has been described for many GPCRs in *in vitro* settings although evidence in native tissue is still sparse.[4,5]

In classical pharmacology allosteric mechanisms were only discussed in terms of intramolecular interactions within a receptor between orthosteric and allosteric sites. Nowadays, there is mounting evidence that also intermolecular receptor-receptor interactions may result in altered receptor recognition, pharmacology and signaling. Heterobivalent ligands have been proven useful molecular probes for confirming and targeting heteromeric receptors,[6,7,8] such as κ- and δ-opioid receptor heteromers.[7]

There are five dopamine receptor subtypes that can be divided into two distinct subfamilies: D$_1$-like (D$_1$R and D$_5$R) and D$_2$-like (D$_2$R, D$_3$R and D$_4$R). In this study we focus on the heterodimerization of the dopamine D$_2$-like receptors (D$_2$-likeR) and the μ opioid receptor (μOR). D$_2$-likeR and μOR are GPCRs, expressed in the brain, which play a major role in schizophrenia, Parkinson's disease, addiction and pain. Heterobivalent ligands are valuable tools to demonstrate the existence of receptor heteromers even in native tissue and can be used to study a specific GPCR dimer behavior without any receptor modification.[9,10,11] Such compounds may eventually also evolve to useful pharmacological agents.[10] Heterobivalent ligands with a spacer of optimal length are envisaged to exhibit a potency that is different from that derived from its two monovalent pharmacophores and may allow the targeting of certain heteromeric subtypes, increasing the selectivity of drug action.[11,12,13]

The dopaminergic and opioid peptide system are pharmacological targets for the treatment of addiction and chronic pain. They show an impressive co-distribution in many nuclei of the brain, which enables intermolecular receptor-receptor interactions[14,15] that may be relevant for the treatment of addiction and chronic pain. *In vivo* studies indicate that there exists a cross-regulation between the D_2-likeR and the µOR. Activation of dopaminergic receptors causes a transient reduction of the µOR immunoreactivity. Additionally, D_2-likeR/µOR interactions also modulate morphine-induced upregulation of certain transcription factors c-Fos, δFosB and P-CREB. [16,17,18,19] These results can be explained by the existence of direct D_2-like-R-µOR interactions. Furthermore, we have identified heterodimerization of D_2R-µOR and D_4R-µOR by co-immunoprecipitation (co-IP) and bioluminescence resonance energy transfer (BRET) studies in mammalian transfected cells (unpublished results). Therefore, all results discussed above indicate that D_2-likeR (especially D_2R and D_4R) and µOR heterodimers could be potentially therapeutic targets for the treatment of addiction and chronic pain.

Here we report the design and synthesis of a series of heterobivalent µOR agonist/antagonist-D_2-likeR agonist/antagonist ligands as pharmacological tools to further study µOR-D_2-likeR (µOR-D_2R and µOR-D_4R) heteromers. In these compounds, the D_2-likeR agonist/antagonist and the µOR agonist/antagonist were linked through a spacer of variable length. The spacers were based on PEG unit repeats, and their size was varied (from 18 to 24 atoms) to obtain the best interaction with the µOR-D_2-likeR heteromers. The binding properties of these compounds were determined by radioligand binding studies in membrane preparations and intact cells. Furthermore, MAPK phosphorylation and β-arrestin2 recruitment assays were performed to test the pharmacological response of the ligands for D_2-likeR and µOR, respectively. Experiments to evaluate the binding of the heterobivalent ligands to µOR and D_2-likeR were performed in cells expressing both µOR and D_2-likeR.

III.3. Design of heterobivalent ligands based on structure of D_2-likeR ligands and µOR ligands

As depicted in Figure 1, the bivalent ligands were derived from the µOR specific agonist hydromorphone (HM) and the structurally related µOR antagonist naltrexone (NTX). As D_2-likeR ligands we used the antagonist 1,4-disubstituted aromatic piperazines (DAPs, **3.03**)[20] and the agonist 5-

hydroxy-2-(dipropylamino)tetralin (DPAT, **3.07**)[11] that were equipped with an appropriate ligation handle.

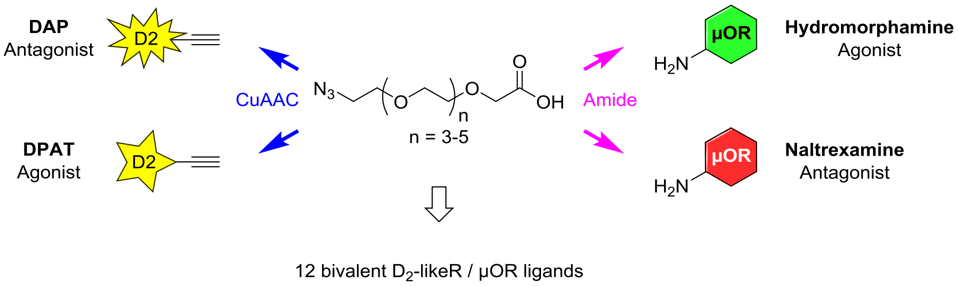
DAP
Antagonist
D2
DPAT
Agonist
D2
CuAAC
N_3
O
O
O
OH
n
n = 3-5
Amide
H_2N
μOR
Hydromorphamine
Agonist
H_2N
μOR
Naltrexamine
Antagonist
12 bivalent D_2-likeR / μOR ligands

Figure 1. Designed heterobivalent ligands.

The dimeric ligands were constructed around PEG spacers of variable length that were equipped with a carboxylic acid on one and an azide on the other end (Figure 2). The use of PEG linkers precludes cumulative incremental increases in hydrophobicity that would occur upon homologation if an alkyl chain were employed. Using existing procedures both opioid ligands **3.01a** and **3.01b** were converted to their corresponding 6'-*R*-amino derivatives **3.02a** and **3.02b**. The introduced amine groups allow coupling to the PEG spacers via an amide bond, whereas the azido group on the PEG linker allows facile connection to the alkyne derived dopamine ligands via a copper-catalyzed azide–alkyne cycloaddition (CuAAC) reaction. The choice of the position and nature of the attachment points for linking the two pharmacophore units to the spacer relies on two criteria: the feasibility of the chemical modification and the compatibility of the modification with the biological activity (SAR data) of the pharmacophore.

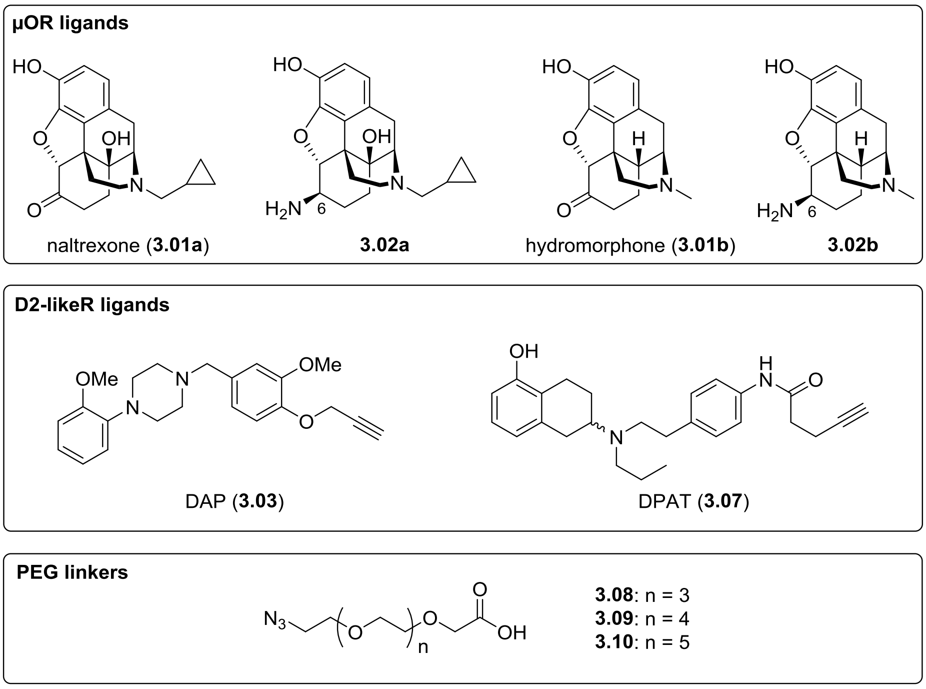
μOR ligands
HO
O
OH
N
O
naltrexone (3.01a)
HO
O
OH
N
H_2N
6
3.02a
HO
O
H
N
O
hydromorphone (3.01b)
HO
O
H
N
H_2N
6
3.02b
D2-likeR ligands
OMe
N
N
OMe
O
DAP (3.03)
OH
N
H
N
O
DPAT (3.07)
PEG linkers
N_3
O
O
O
OH
n
3.08: n = 3
3.09: n = 4
3.10: n = 5

Figure 2. Overview of used monovalent ligands and spacer molecules with appropriate ligation handles.

As indicated above, the selected D_2-likeR ligands need to be functionalized with an alkyne moiety to allow conjugation to the azide group of the PEG linkers. The intrinsic activity of DAPs for D_2-likeR is determined by an aromatic headgroup and an amine moiety, which forms a strong hydrogen bond to the crucial Asp3.32 residue in the transmembrane helix 3 (TM3) of D_2R.[20] A lipophilic appendage is necessary for enhancing ligand affinity. Because proper elongation of this appendage is expected to lead to the “entrance region” of the receptor and from there to the binding pocket of a neighboring protomer, the para-position of an aromatic moiety terminating this appendage is considered an appropriate point of attachment for a linker unit.[20] Vanilline allows for easy introduction of an alkyne group in para-position, while reductive amination permits coupling to the phenylpiperazine moiety.

DPAT is a prototypical D_2R/D_3R agonist suitable for constructing bivalent ligands.[21] Site-directed mutagenesis has demonstrated that the 2-amino tetralin moiety interacts with an agonist binding domain involving TM3 and TM5 for activation of either D_2R or D_3R. The basic nitrogen and the 5-OH group are critically important for binding affinity. A known aniline derivative of DPAT[11] was coupled with 4-pentynoic acid to afford compound **7** with an alkyne group for click reaction.

III.4. Results and Discussion

III.4.1. Chemistry

III.4.1.1 Individual components of the bivalent ligands

As µOR ligands the known *R*-amines **3.02a** and **3.02b** were prepared from NTX (**3.01a**) and HM (**3.01b**) respectively according to published procedures.[22] Briefly, compounds **3.01a** and **3.01b** were converted to the corresponding oximes, which were reduced to 6*R*-amines **3.02a** and **3.02b** in the presence of $ZrCl_4$ and $NaBH_4$. Although previous studies showed little stereoselectivity in opioid binding for 6*R* versus 6*S* amine diastereomers,[23] the predominant *R*-diastereomers were separated from their *S*-epimers by silica gel chromatography, to facilitate further characterization.

For the synthesis of the first alkyne functionalized D_2-likeR ligand, DPAT (**3.07**), commercially available 5-methoxyl-2-tetralone (**3.04**) was converted to the 1,2,3,4-tetrahydronaphthalen-2-amine derivative **3.05** in 4 steps following existing procedures.[11] Arylamine **3.05** was coupled with 4-pentynoic acid to give amide **3.06**. Deprotection of the methyl ether with Me_2SBF_3 in CH_2Cl_2 gave the desired compound **3.07** (Scheme 1). The alkyne functionalized D_2-likeR ligand DAP (**3.03**) was synthesized starting from vanillin as described earlier by Kühhorn et al.[20] The bifunctional PEG linkers were prepared as described earlier. [24,25,26]

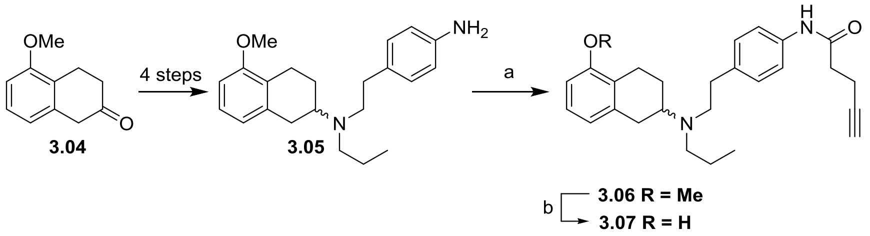
OMe
3.04
4 steps
OMe
NH2
N
3.05
a
OR
H
N
O
N
b
3.06 R = Me
3.07 R = H

Scheme 1. Reagents and conditions: a) 4-pentynoic acid, (3-dimethylaminopropyl)-N-ethylcarbodiimide hydrochloride, triethylamine, CH_2Cl_2, RT, overnight; b) Me_2SBF_3, CH_2Cl_2, RT, overnight.

III.4.1.2 Bivalent ligands synthesis.

The bivalent ligands were generated by first condensing each of the two µOR ligands with each of the three PEG linkers in the presence of the coupling agent EDC and triethylamine to yield the six intermediate azides **3.11a-f** (Scheme 2). The series of bivalent ligands was finalized by conjugating each of the six azides to both DPAT and DAP through CuAAC (Scheme 3). This yielded a concise series of 12 bivalent D_2-likeR-µOR ligands in which each of the sets of ligands and the three linkers are systematically represented.

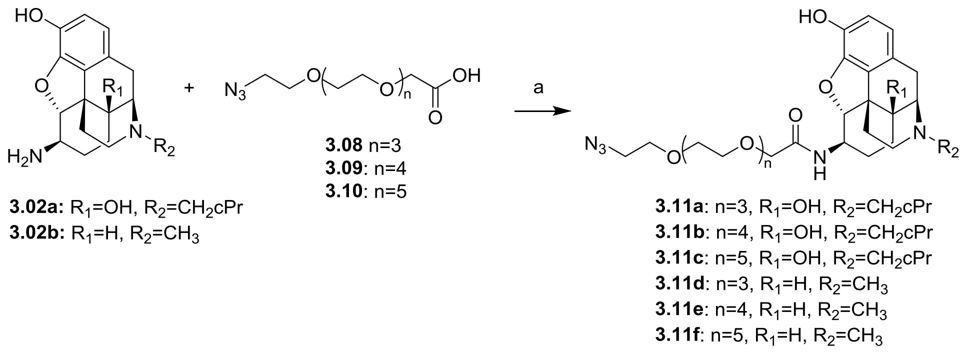
HO
O
R1
N
R2
H2N
+
N3
O
O
n
OH
O
3.08 n=3
3.09: n=4
3.10: n=5
3.02a: R1=OH, R2=CH2cPr
3.02b: R1=H, R2=CH3
a
HO
O
R1
N
R2
N3
O
O
n
O
N
H
3.11a: n=3, R1=OH, R2=CH2cPr
3.11b: n=4, R1=OH, R2=CH2cPr
3.11c: n=5, R1=OH, R2=CH2cPr
3.11d: n=3, R1=H, R2=CH3
3.11e: n=4, R1=H, R2=CH3
3.11f: n=5, R1=H, R2=CH3

Scheme 2. Reagents and conditions: a) (3-dimethylaminopropyl)-N-ethylcarbodiimide hydrochloride, 1-hydroxybenzotriazole, triethylamine, CH_2Cl_2.

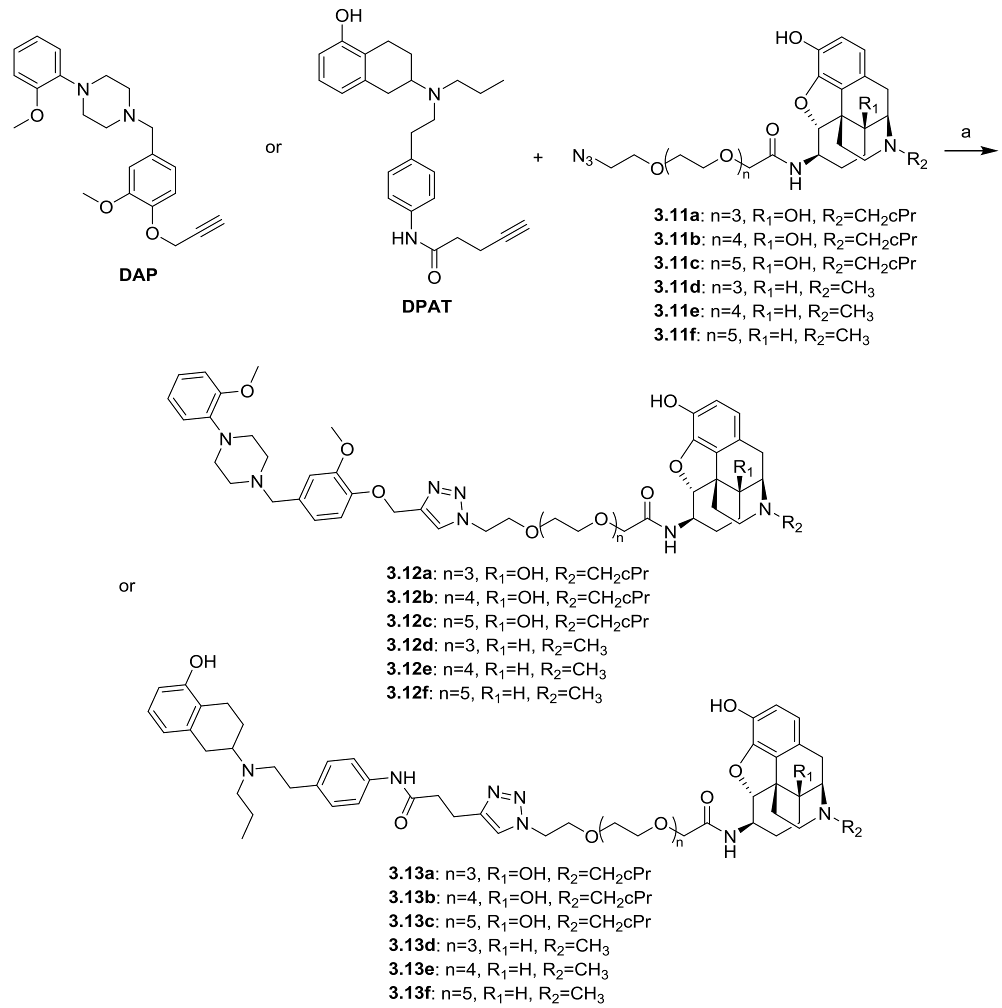
OH
HO
or
+
a
DAP
DPAT
3.11a: n=3, R1=OH, R2=CH2cPr
3.11b: n=4, R1=OH, R2=CH2cPr
3.11c: n=5, R1=OH, R2=CH2cPr
3.11d: n=3, R1=H, R2=CH3
3.11e: n=4, R1=H, R2=CH3
3.11f: n=5, R1=H, R2=CH3
3.12a: n=3, R1=OH, R2=CH2cPr
3.12b: n=4, R1=OH, R2=CH2cPr
3.12c: n=5, R1=OH, R2=CH2cPr
3.12d: n=3, R1=H, R2=CH3
3.12e: n=4, R1=H, R2=CH3
3.12f: n=5, R1=H, R2=CH3
3.13a: n=3, R1=OH, R2=CH2cPr
3.13b: n=4, R1=OH, R2=CH2cPr
3.13c: n=5, R1=OH, R2=CH2cPr
3.13d: n=3, R1=H, R2=CH3
3.13e: n=4, R1=H, R2=CH3
3.13f: n=5, R1=H, R2=CH3

Scheme 3. Reagents and conditions: a) sodium ascorbate, CuSO$_4$, triethylamine, tris[(1-benzyl-1,2,3-triazol-4-yl)methyl]amine, dimethylformamide.

III.4.2. Ligand binding assays

III.4.2.1 Evaluating the binding of the bivalent ligands to the D$_2$-likeR

A saturation binding assay for [^{3}H]spiperone, a non-selective antagonist of D$_2$-likeR, was described previously.[27,28] Here we performed a competition assay to evaluate the binding of the bivalent ligands to the D$_2$-likeR D$_2$R and D$_4$R. First the binding affinity of the bivalent ligands **3.12a-f** and **3.13a-f** along with their alkynylated DAP and DPAT precursors **3.03** and **3.07** was measured by displacement of [^{3}H]spiperone from the D$_4$R expressed in HEK 293T cells, indicating that all the bivalent ligands bind to the D$_4$R (Table 1). However, a clear reduction in the D$_4$R binding affinities of the bivalent ligands was detected when compared with the alkynes **3.03** and **3.07**. Compound **3.12d** with a short spacer length (18-atom) showed a slightly higher affinity for D$_4$R than **3.12e** and **3.12f**. This trend was also apparent for the other bivalent ligands (**3.12a**, **3.13a** and **3.13d**) possessing the same spacer as **3.12d**. In a next step we wanted to compare the affinity of the bivalent ligands for D$_4$R in the absence and presence of overexpressed µOR. Unexpectedly, no major differences in K_i values were found between both experimental set-ups, except for **3.12d**. Interestingly, a biphasic competition curve was observed for **3.12d** from which two individual affinity constants could be derived ($K_{i\ high}$ 1.2 ± 0.3 nM and $K_{i\ low}$ 207 ± 51 nM, Figure 3a). Such biphasic competition-binding curves are indicative of a bivalent binding mode.[11] Specifically, the high-affinity K_i value represents a bivalent receptor-bridging binding mode of **3.12d** to D_4R/µOR heterodimer, whereas the low-affinity K_i value reveals a monovalent-binding mode to D_4R. Bivalent ligand **3.12d** thus displays a 170-fold preference for the high-affinity bivalent interaction with the D_4R/µOR heterodimer over monovalent-binding mode to D_4R.

By following the same approach and still using [^{3}H]spiperone as the radioligand, we also tested the affinity of the bivalent ligand **3.12d** and its corresponding monovalent ligand **3** to the D_2R and D_2R-µOR receptors. The affinities of compound **3.12d** to D_2R and D_2R-µOR decreased 3-fold compared to the ligand **3.03** for both receptors (Table 2). Unfortunately, we only obtained a monophasic competition-binding curve for **3.12d** to D_2R-µOR and no major differences in binding affinity were observed between cells expressing only D_2R and cells expressing both D_2R and µOR (Figure 3b).

Next, following a similar protocol, we determined the affinity of monomeric ligand **3.03** and bivalent ligand **3.12d** on cells expressing D_2R and D_2R-µOR, utilizing an alternative radioligand, i.e. [^{3}H]raclopride. Raclopride that acts as a selective D_2R antagonist is more hydrophilic and has substantially less non-specific binding in intact cells as compared with spiperone. Furthermore it is not cell permeable, rendering the assay possibly more sensitive as binding of the radioligand to be displaced is restricted to receptors in the plasma membrane. In this experiment (Table 3) the affinities of **3.12d** to D_2R and D_2R-µOR were 32.4 ± 8.5 nM and 38.6 ± 3.2 nM, respectively, while the affinities of the monovalent alkyne **3.03** were 43.1 ± 9.0 nM and 49.9 ± 5.8 nM, respectively. Still, only one-site binding curves for **3.12d** were obtained from cells monoexpressing D_2R and cells coexpressing D_2R and µOR (Supporting information). The saturation binding data for [^{3}H]raclopride can be found in Supporting Information. Interestingly, we found that the affinity of **3.12d** for D_4R decreased 100-fold relative to the monovalent ligand **3**, while its K_i value for D_2R only decreased three-fold.

Table 1. Binding affinities (K_i) for D_4R and D_4R-µOR.[a]

Compd	R_1	R_2	n	D_4R K_i (nM)	D_4R-µOR K_i (nM)
3.03	-	-	-	1.6 ± 0.2	2.1 ± 0.3
3.12a	OH	CH_2cPr	3	117 ± 12	nd[b]

3.12b	OH	CH_2*c*Pr	4	214 ± 11	219 ± 10
3.12c	OH	CH_2*c*Pr	5	226 ± 18	nd
3.12d	H	CH_3	3	184 ± 35	-
3.12e	H	CH_3	4	369 ± 42	368 ± 10
3.12f	H	CH_3	5	339 ± 50	417 ± 8.8
3.07	-	-	-	15 ± 6.1	16 ± 2.5
3.13a	OH	CH_2*c*Pr	3	118 ± 12	101 ± 1.3
3.13b	OH	CH_2*c*Pr	4	157 ± 30	nd
3.13c	OH	CH_2*c*Pr	5	138 ± 25	nd
3.13d	H	CH_3	3	110 ± 9.3	nd
3.13e	H	CH_3	4	191 ± 9.5	394 ± 12
3.13f	H	CH_3	5	199 ± 16	493 ± 11

[a] Binding affinities (K_i) were obtained by competitive displacement of radiolabeled [^{3}H]spiperone binding to HEK293T D_4R and HEK293T D_4R-μOR membranes. All values are expressed as the mean ± SEM of three independent assays using 11 different concentrations of ligands, each performed in duplicate. [b] not determined.

Table 2. Binding affinities (K_i) for D_2R and D_2R-μOR.[a]

Compound	K_i (nM) for D_2R	K_i (nM) for D_2R-μOR
3.03	22 ± 5	32 ± 11
3.12d	62 ± 3	101 ± 10

[a] Binding affinities (K_i) were obtained by competitive displacement of radiolabeled [^{3}H]spiperone binding to HEK293T D_2R and HEK293T D_2R-μOR membranes. All values are expressed as the mean ± SEM of at least two independent assays.

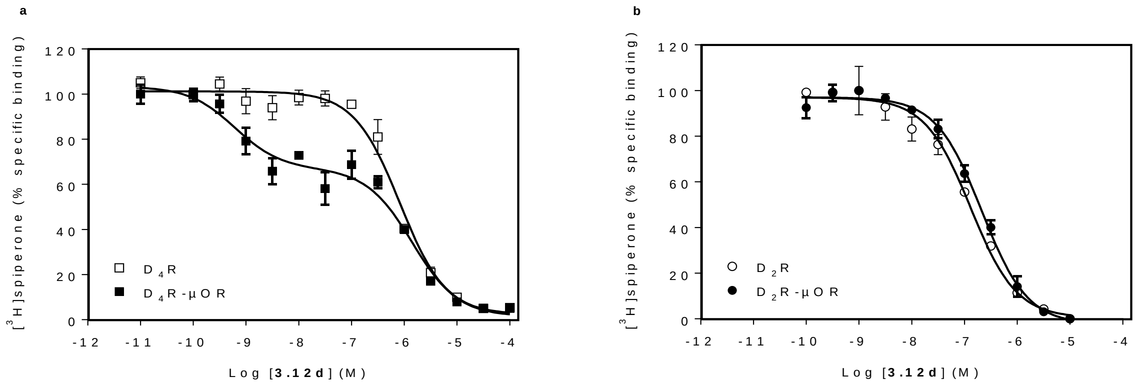

Figure 3. Representative competition curves for bivalent ligand **3.12d**. D_2-likeR binding of the bivalent ligand **3.12d** was measured by displacement of the radiolabeled [^{3}H]spiperone from membranes of HEK293T cells coexpressing D_4R/µOR (or D_2R/µOR) or monoexpressing D_4R (or D_2R) only. (**a**) D_4R binding of **3.12d** in the presence (filled squares, $K_{i\ high}$ 1.2 ± 0.3 nM, $K_{i\ low}$ 207 ± 51 nM) or absence (open squares, K_i 184 ± 35 nM) of µOR. (**b**) D_2R binding of **3.12d** in the presence (filled circles, K_i 101 ± 10 nM) or absence (open circles, K_i 62 ± 3 nM) of µOR. Data points represent the mean ± SEM of three independent assays, each performed in duplicate.

Table 3. Binding affinities (K_i) for D_2R and D_2R-µOR.[a]

Compound	K_i (nM) for D_2R	K_i (nM) for D_2R-µOR
3.03	43.1 ± 9.0	49.9 ± 5.8
3.12d	32.4 ± 8.5	38.6 ± 3.2

[a] Binding affinities (K_i) were obtained by competitive displacement of radiolabeled [^{3}H]raclopride binding to HEK293T D_2R and HEK293T D_2R-µOR intact cells. All values are expressed as the mean ± SEM of at least two independent experiments.

III.4.2.2 Evaluating the binding of the bivalent ligands to µOR

We performed competitive receptor binding assays in cell membranes expressing µOR to determine the binding affinity of bivalent ligands, using the tracer [^{3}H]diprenorphine, which is a nonselective opioid antagonist. Saturation binding assays showed that the Kd value and Bmax of [^{3}H]diprenorphine were 0.21 ± 0.064 nM and 489 ± 28 fmol/mg for µOR, respectively. In the competition assay the binding affinities for the monovalent ligands HM and NTX were 4.4 ± 0.21 nM and 7.8 ± 0.16 nM, respectively (Table 4). Compounds **3.12a-c** and **3.13a-c**, which were derived from NTX, exhibited a binding affinity for µOR comparable to NTX. Whereas, bivalent ligands **3.12b** and **3.13b** with a 21-atom spacer displayed relatively lower K_i values than the other NTX-based ligands. HM-based bivalent ligands

3.12d-f and **3.13d-f** showed a small reduction in the binding affinities for µOR compared to the corresponding monovalent compound HM, except for **3.12e** (3.7 ± 0.02 nM) and **3.13e** (7.2 ± 0.53 nM) with a medium spacer length (21 atoms). Therefore, the affinities of bivalent ligands with a medium length of spacer (21 atoms) to µOR were relatively higher than the other ligands with shorter (18 atoms) or longer linkers (24 atoms).

Table 4. Binding affinities (K_i) for µOR.[a]

Compd	R_1	R_2	n	K_i (nM)
Hydromorphone	H	CH_3	-	4.4 ± 0.21
Naltrexone	OH	CH_2cPr	-	7.8 ± 0.16
3.12a	OH	CH_2cPr	3	6.3 ± 1.1
3.12b	OH	CH_2cPr	4	4.6 ± 0.25
3.12c	OH	CH_2cPr	5	9.2 ± 0.41
3.13a	OH	CH_2cPr	3	7.5 ± 0.95
3.13b	OH	CH_2cPr	4	3.8 ± 0.84
3.13c	OH	CH_2cPr	5	7.6 ± 0.39
3.12d	H	CH_3	3	16 ± 0.87
3.12e	H	CH_3	4	3.7 ± 0.02
3.12f	H	CH_3	5	11 ± 0.57
3.13d	H	CH_3	3	13 ± 1.2
3.13e	H	CH_3	4	7.2 ± 0.53
3.13f	H	CH_3	5	17 ± 3.4

[a] Binding affinities (K_i) were obtained by competitive displacement of radiolabeled [^{3}H]diprenorphine binding to HEK293T µOR. All values are expressed as the mean ± SEM of three independent assays.

III.4.3. Functional assays

III.4.3.1 MAPK phosphorylation to study D_2-likeR activation by the newly developed bivalent ligands

The mitogen-activated protein kinase (MAPK) phosphorylation assay was used to define the functional activity of the bivalent ligands. The MAPK pathway, which includes the extracellular-signal regulated kinase (ERK) pathway, consists of an intracellular chain of proteins that transfer the signal from the cell surface receptor to the nuclear DNA or other subcellular targets causing cellular responses. Signaling molecules in this pathway communicate with each other by adding a phosphate group to the neighboring protein. This phosphorylation event functions as an "on/off" switch, leading to the activation or inhibition of the next signaling molecule in the chain.[29] The most commonly studied element of the MAPK pathway, initiated by GPCR activation, is the phosphorylation of p44/42 MAPK (ERK1/2).

In order to assess functional activation of the D_2R and D_4R by the above described bivalent ligands, we used a HEK293 cell line stably expressing the D_2R and D_4R, respectively.[30] Unexpectedly, the signal band of MAPK-P for D_2R was quite weak (see supporting information). Nevertheless, we found a strong immunoreactive band (Figure 4) for MAPK-P upon activation of D_4R with the agonist dopamine (DA), and with the alkynylated DAP (**3.03**) and DPAT (**3.07**). Next, all bivalent ligands were tested in this cell system (Figure 5 and Table 5). We can conclude that all bivalent ligands activate the MAPK signaling pathway. Interestingly, compound **3.12d** with an 18-atom linker (shown in Table 5) displayed modestly high potency ($EC_{50} = 0.12 \pm 0.04$ µM) and relatively high efficacy (92 ± 1%) as compared with the monovalent ligand **3.03** ($EC_{50} = 0.21 \pm 0.12$ µM, $E_{max} = 75 \pm 2\%$), while the potency of compounds **3.12a-c** decreased 8-16 fold compared to **3.03**. In addition, all the DAP-bond ligands, except for **3.12d**, showed a comparable efficacy (E_{max} = 72-85%) relative to compound **3.03**. On the other hand, DPAT-based bivalent ligands had a potency (EC_{50} = 0.45-0.95 µM) and efficacy (E_{max} = 86-108%) comparably to that of **7** ($EC_{50} = 0.37 \pm 0.17$ µM, $E_{max} = 100 \pm 3\%$). Overall, bivalent ligand **3.12d** with a short linker length (18 atoms) was the most potent compound to activate the MAPK phosphorylation of D_4R.

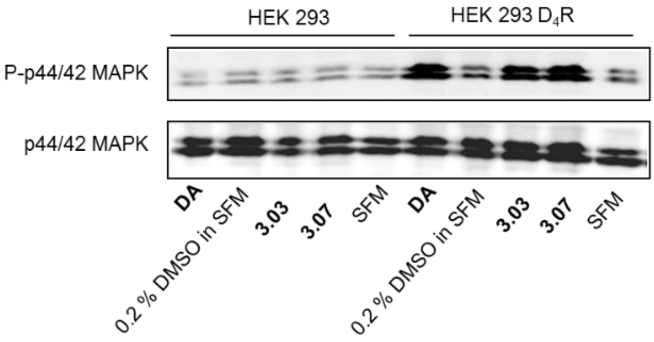

Figure 4. Stimulation of MAPK phosphorylation upon D$_4$R agonist treatment, as determined by immunoblotting assays. Cells were treated with serum-free media (SFM) for 12 h. Next, D$_2$-likeR agonists (10 µM), SFM or vehicle control were added for 5 min. Cells were washed and lysed as explained in the Experimental section. Phosphorylated MAPK was detected by immunoblotting using rabbit anti-phospho-p44/42 MAPK antibody and mouse anti-p44/42 MAPK antibody was used for demonstrating equal protein loading. The results shown are representative of three independent experiments. DA=dopamine.

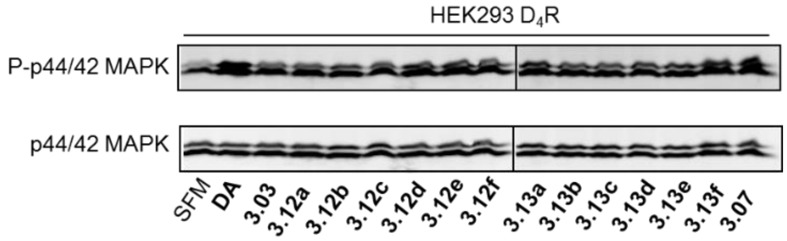

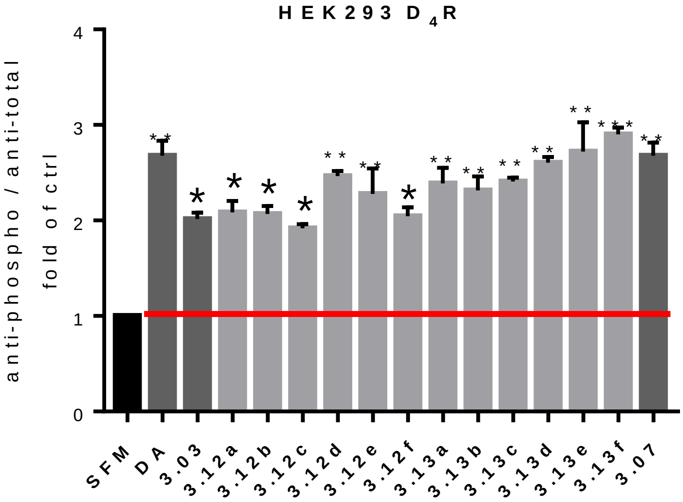

Figure 5. Efficacy of bivalent ligands to phosphorylate MAPK in HEK293 D$_4$R cells. Cells were treated with serum-free media (SFM) for 12 h. Next, D$_2$-likeR agonists (10 µM) and SFM were added for 5 min. Cells were washed and lysed as explained in the Experimental section. Phosphorylated MAPK was detected by immunoblotting using rabbit anti-phospho-p44/42 MAPK antibody and mouse anti-p44/42 MAPK antibody was used for demonstrating equal protein loading. The top panel shows a representative result from three independent experiments; the bottom panel is given as mean ± SD. DA=dopamine. Bivalent ligands were significantly different (**p*< 0.05, ***p* < 0.01, ****p* < 0.001) compared to the control SFM by One-way ANOVA.

Table 5. Potency (EC_{50}) of D_2-likeR agonists induced MAPK-P in HEK293 D_4R cells

Compd	R_1	R_2	n	EC_{50} µM[a]	E_{max} %[b]
Dopamine	-	-	-	0.037 ± 0.012	100 ± 4
3.03	-	-	-	0.21 ± 0.12	75 ± 2
3.12a	OH	CH_2*c*Pr	3	3.4 ± 0.2	78 ± 3
3.12b	OH	CH_2*c*Pr	4	1.9 ± 0.3	77 ± 2
3.12c	OH	CH_2*c*Pr	5	1.6 ± 0.1	72 ± 1
3.12d	H	CH_3	3	0.12 ± 0.04	92 ± 1
3.12e	H	CH_3	4	0.31 ± 0.02	85 ± 5
3.12f	H	CH_3	5	0.80 ± 0.06	76 ± 2
3.07	-	-	-	0.37 ± 0.17	100 ± 3
3.13a	OH	CH_2*c*Pr	3	0.55 ± 0.24	89 ± 4
3.13b	OH	CH_2*c*Pr	4	0.48 ± 0.06	86 ± 4
3.13c	OH	CH_2*c*Pr	5	0.88 ± 0.01	90 ± 1
3.13d	H	CH_3	3	0.95 ± 0.03	97 ± 1
3.13e	H	CH_3	4	0.57 ± 0.14	101 ± 6
3.13f	H	CH_3	5	0.45 ± 0.01	108 ± 2

[a] Data shown represent the mean ± SEM of three independent experiments. [b] E_{max} relative to the effect of the reference agonist dopamine at 10 µM.

III.4.3.2 β-arrestin2 recruitment to µOR

To assess activation of the µOR, HEK 293 cell line was used to stably express the µOR. Unfortunately, we did not obtain any good results from MAPK-P for µOR (data not shown). Then we performed a β-arrestin2 recruitment assay based on the NanoLuc Binary Technology (NanoBiT).[31] Our research group recently reported on the application of this assay for the monitoring of GPCR activation, via ligand induced interaction of βarr2 with CB1 and CB2 cannabinoid receptors.[32] Here, we optimized this assay for ligand induced interaction of βarr2 with µOR. Agonists of µOR, such as DAMGO, have previously been shown to induce robust receptor phosphorylation, β-arrestin2 recruitment and µOR trafficking.[33,34] On the other hand, morphine is a poor inducer of receptor phosphorylation, β-arrestin2 recruitment and internalization of µOR. However, upon overexpression of G protein-coupled receptor kinase (GRK2) in cell culture, morphine gained the capacity to induce µOR phosphorylation, accompanied by the rescue of β-arrestin2 recruitment.[34,35]

To assess the ligand induced interaction of β-arrestin2 with µOR, overexpression of GRK2 in cell culture was performed. Our results show that DAMGO induces a robust β-arrestin2 recruitment even in the absence of GRK2. On the other hand, HM could promote β-arrestin2 recruitment only when GRK2 was overexpressed in HEK 293 cells. Both results are in line with those found in the literature (see supporting information Figure 2).

Upon stimulation with a known agonist of µOR, HM, µOR-SmBiT showed a concentration dependent interaction with LgBiT-βarr2 in the presence of GRK2 (Figure 6). Also, for the bivalent ligands containing the agonistic HM-based monomer, concentration-dependence was obtained and EC_{50} values were determined as a measure of relative potency (Table 6 and Figure 6). Ranging from 12.73 nM to 57.06 nM, all the EC_{50} values of the bivalent ligands were comparable to that of the parent HM (EC_{50} = 30.09 nM). Amongst the DAP-based ligands, compound **3.12d**, having the shortest linker (18-atom), showed excellent potency (EC_{50} = 12.73 nM) and high efficacy (85 ± 3%). Remarkably, all DPAT-based ligands showed lower efficacies than DAP-bond ligands, with compound **3.13d**, having the same spacer as **3.12d**, displaying the lowest efficacy (24 ± 1%) amongst the DPAT-based ligands.

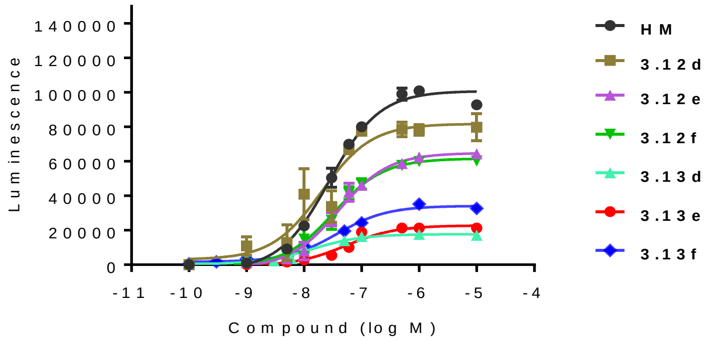

Figure 6. Concentration-dependent interaction of µOR with β-arrestin2 upon stimulation with agonists of µOR. Data are given as mean ± SEM of at least two independent experiments.

Table 6. Potency (EC_{50}) and maximal effect of µOR agonists on β-arrestin2 recruitment for µOR.

Compd	R_1	R_2	n	EC_{50} (95% C.I.) nM[a]	% HM[b]
HM	H	CH_3	-	30.09 (24.51-36.94)	100
3.12d	H	CH_3	3	12.73 (7.612-21.28)	85 ± 3
3.12e	H	CH_3	4	40.38 (30.41-53.61)	68 ± 1
3.12f	H	CH_3	5	34.86 (25.76-47.18)	64 ± 1
3.13d	H	CH_3	3	13.41 (8.286-23.15)	24 ± 1
3.13e	H	CH_3	4	57.06 (38.49-84.58)	28 ± 1
3.13f	H	CH_3	5	14.09 (10.14-21.08)	38 ± 1

[a] EC_{50} values are presented as a measure of potency for β-arrestin2 recruitment. Data are given as EC_{50} values (95% CI profile likelihood). [b] Percent maximal stimulation relative to the agonist HM at 10 μM.

III.5. Conclusions

In summary, we have designed and synthesized a series of novel heterobivalent ligands based on the chemical structure of two distinct D_2-likeR ligands and a μOR agonist and antagonist. Ligation of μOR ligands does not perturb the affinity for μOR. μOR bivalent ligands derived from the HM agonist are still capable of activating the μOR signaling pathway as demonstrated by β-arrestin2 recruitment. Furthermore, bivalent ligand **3.12d** containing the shortest linker (18-atom) showed excellent potency and high efficacy both in β-arrestin2 recruitment for μOR and MAPK-P for D_4R. On the other hand, ligation of D_2-likeR ligands negatively influences the affinity for D_2R and D_4R when using [^{3}H]spiperone as the radioligand. However, a biphasic competition-binding curve was observed for **3.12d** to D_4R-μOR, which indicates a bivalent binding mode.[11,43] Hence, compound **3.12d** could bridge the D_4R-μOR heterodimer.

Unexpectedly, we were unable to identify bivalent ligands that show a biphasic binding mode or a significant increase in affinity for cells expressing both the D_2R and the μOR, compared to cells that only express D_2R. This indicates that none of the bivalent ligands is capable of binding both receptors simultaneously, possibly owing to a suboptimal length or nature of the selected linkers, which, however, were based on the spacers of class A GPCR bivalent ligands.[20,36] On the other hand it cannot be excluded that subtle differences such as differences in the dissociation rate of the ligands remain undetected by comparing equilibrium dissociation constants. In a study investigating adenosine A_3 receptors, ligand binding kinetics were found to be influenced in membrane microdomains as a consequence of receptor dimerization.[37]

While future studies will try to address these shortcomings, the current study already gives access to the monomeric ligands that are equipped with appropriate ligation handles to construct second-generation bivalent ligands with alternative spacers. In conclusion, the present results provide useful insights into development of new bivalent ligands as tools to investigate the µOR-D_4R heterodimer.

III.6. Experimental Section

III.6.1. Chemistry

All reactions described were performed under an N_2 atmosphere and at ambient temperature unless stated otherwise. All regents and solvents were purchased from Sigma-Aldrich (Diegem, Belgium), Fisher Scientific (Merelbeke, Belgium), TCI Europe (Zwijndrecht, Belgium) or Apollo Scientific (Bredbury, Stockport, United Kingdom) and used as received. NMR solvents were acquired from Eurisotop (Saint-Aubin, France). Reactions were monitored by TLC analysis using TLC aluminium sheets (Macherey-Nagel, Alugram Sil G/UV254) with detection by spraying with a solution of $(NH_4)_6Mo_7O_{24}\cdot 4H_2O$ (25 gL^{-1}) and $(NH_4)_4Ce(SO_4)_4\cdot 2H_2O$ (10 gL^{-1}) in H_2SO_4 (10 % aq.) followed by charring or an aqueous solution of $KMnO_7$ (20 gL^{-1}) and K_2CO_3 (10 gL^{-1}) or an ethanolic solution of ninhydrin (2 gL^{-1}) and acetic acid (1% v/v) followed by charring. Solution pH values were estimated using universal indicator paper (Merck). Silica gel column chromatography was performed using a Grace Reveleris X2 system and the corresponding silica gel cartridges. ESI-HRMS spectra were measured with a Waters LCT Premier XE Mass spectrometer calibrated using leucine enkephalin as an external standard. ^{1}H- and ^{13}C-APT-NMR spectra were recorded with a Varian Mercury-300BB (300/75 MHz) spectrometer. Chemical shifts are given in ppm (δ) relative to tetramethylsilane as an internal standard (^{1}H NMR) or the NMR solvent (^{13}C NMR). Coupling constants are given in Hertz (Hz). Weak signals in ^{13}C NMR are indicated as (w). LC-MS analyses were carried out on a Waters AutoPurification System equipped with PDA and ESI-MS detection and using a Waters CORTECS C18 Column (4.6×100 mm, 2.7µm) and a water/acetonitrile/formic acid linear gradient system at a flow rate of 1.44 $mLmin^{-1}$.

General procedure 1: Carbodiimide-mediated amide formation.

To a solution of (3-Dimethylaminopropyl)-N-ethylcarbodiimide hydrochloride (1.5 eq.) and 1-hydroxybenzotriazole (1.4 eq.) in CH_2Cl_2 was added a solution of the PEG spacer (1.2 eq.) in CH_2Cl_2 (0.2 M) and cooled to 0°C under an argon atmosphere. After 15 min at 0°C, amines **3.02a-b** (1.0 eq.) were added and triethylamine (2 eq.) was added dropwise; the reaction was slowly warmed to room temperature and stirred overnight. The reaction was diluted with CH_2Cl_2, washed successively with water, HCl (5% aq.), $NaHCO_3$ (sat. aq.), NaCl (sat. aq.), dried over Na_2SO_4, filtered and solvent was evaporated under reduced pressure. The crude product was purified by silica gel chromatography (NH_4OH/MeOH/CH_2Cl_2, 1:5:94 v/v/v) to yield the amides **3.11a-f**.

General procedure 2: Copper mediated azide-alkyne cycloaddition.

To a solution of the intermediate azide (1.0 eq.) in dimethylformamide (0.1 M) was added the alkyne (1.5 eq.), sodium ascorbate (1.0 eq., 0.5 M), $CuSO_4$ (0.2 eq., 0.05 M), triethylamine (3.0 eq.) and a catalytic amount of tris[(1-benzyl-1,2,3-triazol-4-yl)methyl]amine. The reaction mixture was stirred overnight at room temperature in the dark under an argon atmosphere. The solvent was evaporated under reduced pressure and the residue was redissolved in water and extracted with CH_2Cl_2. Then combined organic fractions were pooled, washed with brine and dried over Na_2SO_4. The crude compound was purified by silica gel chromatography (NH_4OH/MeOH/CH_2Cl_2, 1:5:94 v/v/v) to give the final compound as a white solid (yield, 40-57%).

N-(4-(2-((5-methoxy-1,2,3,4-tetrahydronaphthalen-2-yl)(propyl)amino)ethyl)phenyl)pent-4-ynamide (**3.06**)

To a solution of (3-Dimethylaminopropyl)-N-ethylcarbodiimide hydrochloride (1.1 g, 4.92 mmol) in CH_2Cl_2 (20 mL) was added a solution of 4-pentynoic acid (0.39 g, 3.93 mmol) in CH_2Cl_2 (5 mL) followed by a solution of **3.05** (1.1 g, 3.28 mmol) in CH_2Cl_2 (5 mL). The mixture was cooled to 0 ºC and triethylamine (0.68 mL, 4.92 mmol) was added dropwise; the reaction was slowly warmed to room temperature and stirred overnight. The reaction was diluted with CH_2Cl_2, washed successively with water, HCl (5% aq.), $NaHCO_3$ (sat. aq.), NaCl (sat. aq.), dried over Na_2SO_4, filtered and solvent was evaporated under reduced pressure. The crude product was purified by silica gel chromatography (Hexane/EtOAc, 3:2 v/v) to give **3.06** as a pale yellow solid (1.32 g, 95%). ^1H NMR (300 MHz, $CDCl_3$) δ ppm 7.42 (d, J = 8.4 Hz, 2H), 7.15 (d, J = 8.4 Hz, 2H), 7.07 (t, J = 7.9 Hz, 1H), 6.69 (d, J = 7.8 Hz, 1H), 6.62 (d, J = 8.1, 1H), 3.78 (s, 3H), 3.04-2.91 (m, 2H), 2.91-2.80 (m, 1H), 2.79-2.63 (m, 6H), 2.63-2.53 (m, 7H), 2.05 (d, J = 3.2 Hz, 2H), 1.61-1.41 (m, 3H), 0.88 (t, J = 7.3 Hz, 3H). ^{13}C NMR (75 MHz, $CDCl_3$) δ 169.4, 157.2, 137.9, 137.0, 135.7, 129.2, 126.1, 125.2, 121.6, 120.1, 106.9, 82.9, 69.5, 56.7, 55.2, 52.9, 52.6, 36.1, 35.4, 32.3, 25.7, 23.8, 22.2, 14.8, 11.9. HRMS (ESI) m/z: calculated for $C_{27}H_{35}N_2O_2$ $[M+H]^+$ 419.2699; found 419.2705.

N-(4-(2-((5-hydroxy-1,2,3,4-tetrahydronaphthalen-2-yl)(propyl)amino)ethyl)phenyl)pent-4-ynamide (**3.07**)

To a solution of **3.06** (1.05 g, 2.51 mmol) in CH_2Cl_2 (20 mL) was added boron trifluoride methyl sulfide complex (4.77 mL, 45.21 mmol). The reaction was stirred overnight under nitrogen at room temperature. The mixture was treated with a saturated aqueous $NaHCO_3$ solution, extracted with CH_2Cl_2, dried over

Na_2SO_4 and the solvent was evaporated under reduced pressure. The crude product was purified by silica gel chromatography (Hexane/EtOAc, 1:1 v/v) to yield **3.07** as a white foam (750 mg, 74%). ^{1}H NMR (300 MHz, $CDCl_3$) δ ppm 7.41 (d, *J* = 8.4 Hz, 2H), 7.14 (d, *J* = 8.4 Hz, 2H), 6.97 (t, *J* = 7.8 Hz, 1H), 6.66 (d, *J* = 7.5 Hz, 1H), 6.59 (d, *J* = 7.8 Hz, 1H), 3.02-2.94 (m, 2H), 2.90-2.82 (m, 1H), 2.79 -2.66 (m, 6H), 2.62-2.53 (m, 7H), 2.05 (d, *J* = 3.2 Hz, 2H), 1.66-1.56 (m, 1H), 1.53-1.46 (m, 2H), 0.89 (t, *J* = 7.3 Hz, 3H). ^{13}C NMR (75 MHz, $CDCl_3$) δ ppm 169.1, 153.5, 138.3, 137.1, 135.4, 129.2, 126.3, 123.0, 121.6, 120.0, 111.9, 82.8, 69.7, 56.6, 52.7, 52.6, 36.2, 35.2, 32.2, 25.7, 23.5, 22.0, 14.8, 11.9. HRMS (ESI) m/z: calculated for $C_{26}H_{33}N_2O_2$ $[M+H]^+$ 405.2542; found 405.2545.

14-azido-N-((4R,4aS,7R,7aR,12bS)-3-(cyclopropylmethyl)-4a,9-dihydroxy-2,3,4,4a,5,6,7,7a-octahydro-1H-4,12-methanobenzofuro[3,2-e]isoquinolin-7-yl)-3,6,9,12-tetraoxatetradecanamide (**3.11a**)

Compound **3.11a** was subjected to general procedure 1. Pale yellow solid, 68%. ^{1}H NMR (300 MHz, $CDCl_3$) δ 6.71 (d, *J* = 8.1 Hz, 1H), 6.56 (dd, *J* = 8.2 Hz, 1H), 4.45 (d, *J* = 7.5 Hz, 1H), 4.01 (s, 2H), 3.74-3.66 (m, 14H), 3.39 (t, *J* = 5.6 Hz, 2H), 3.10-3.04 (m, 2H), 2.99 (s, 1H), 2.67-2.54 (m, 2H), 2.40-2.34 (m, 4H), 2.24-2.13 (m, 2H), 1.89 (dd, *J* = 12.8, 3.1 Hz, 2H), 1.70-1.40 (m, 4H), 0.90-0.77 (m, 1H), 0.57-0.48 (m, 2H). ^{13}C NMR (75 MHz, $CDCl_3$) δ 169.9, 142.4, 140.0, 131.0, 129.0, 128.2, 125.2, 119.1, 117.7, 93.5, 70.9, 70.6, 70.5, 70.5, 70.4, 70.3, 70.0, 62.3, 59.2, 50.7, 50.6, 47.7, 44.0, 30.6, 30.1, 24.4, 22.6, 9.4, 3.9, 3.7. HRMS (ESI) m/z: calculated for $C_{30}H_{44}N_5O_8$ $[M+H]^+$ 602.3190; found 602.3205.

17-azido-N-((4R,4aS,7R,7aR,12bS)-3-(cyclopropylmethyl)-4a,9-dihydroxy-2,3,4,4a,5,6,7,7a-octahydro-1H-4,12-methanobenzofuro[3,2-e]isoquinolin-7-yl)-3,6,9,12,15-pentaoxaheptadecanamide (**3.11b**)

Compound **3.11b** was subjected to general procedure 1. Pale yellow solid, 62%. ^{1}H NMR (300 MHz, $CDCl_3$) δ 6.70 (d, *J* = 8.1 Hz, 1H), 6.54 (d, *J* = 8.2 Hz, 1H), 4.45 (d, *J* = 7.5 Hz, 1H), 3.99 (s, 2H), 3.73 – 3.60 (m, 18H), 3.37 (t, *J* = 5.6 Hz, 2H), 3.11 (br s, 1H), 3.01 (d, *J* = 18.4 Hz, 1H), 2.70 – 2.55 (m, 2H), 2.38 (d, *J* = 6.6 Hz, 2H), 2.26 – 2.10 (m, 2H), 1.87 (td, *J* = 12.5, 2.9 Hz, 1H), 1.72 – 1.54 (m, 2H), 1.46 (dt, *J* = 11.3, 2.8 Hz, 2H), 0.91 – 0.79 (m, 2H), 0.58 – 0.49 (m, 2H), 0.17 – 0.09 (m, 2H). ^{13}C NMR (75 MHz, $CDCl_3$) δ 170.0, 142.5, 140.1, 130.9, 124.1, 119.0, 117.8, 93.2, 70.9, 70.6, 70.6, 70.5, 70.5, 70.4, 70.30, 70.0, 70.0, 62.3, 59.1, 50.8, 50.6, 47.6, 44.1, 30.5, 30.1, 24.3, 22.6, 9.3, 3.9, 3.8. HRMS (ESI) m/z: calculated for $C_{32}H_{48}N_5O_9$ $[M+H]^+$ 646.3452; found 646.3458.

20-azido-N-((4R,4aS,7R,7aR,12bS)-3-(cyclopropylmethyl)-4a,9-dihydroxy-2,3,4,4a,5,6,7,7a-octahydro-1H-4,12-methanobenzofuro[3,2-e]isoquinolin-7-yl)-3,6,9,12,15,18-hexaoxaicosanamide (**3.11c**)

Compound **3.11c** was subjected to general procedure 1. Pale yellow solid, 56%. ^{1}H NMR (300 MHz, $CDCl_3$) δ 6.71 (d, *J* = 8.1 Hz, 1H), 6.56 (d, *J* = 8.1 Hz, 1H), 4.45 (d, *J* = 7.5 Hz, 1H), 4.00 (s, 2H), 3.75 – 3.60 (m, 22H), 3.38 (t, *J* = 5.1 Hz, 2H), 3.10 – 2.98 (m, 2H), 2.59 (dd, *J* = 19.1, 6.3 Hz, 2H), 2.36 (d, *J* = 6.5 Hz, 2H), 2.24 – 2.08 (m, 2H), 1.90 (qd, *J* = 12.7, 3.2 Hz, 1H), 1.72 – 1.53 (m, 2H), 1.46 (dd, *J* = 9.0, 4.4 Hz, 2H), 0.83 (dp, *J* = 13.0, 6.3 Hz, 2H), 0.56 – 0.49 (m, 2H), 0.12 (d, *J* = 4.7 Hz, 2H). ^{13}C NMR (75 MHz, $CDCl_3$) δ 169.9, 142.4, 140.0, 131.0, 124.3, 119.0, 117.7, 93.3, 70.9, 70.6, 70.6, 70.6, 70.5, 70.5, 70.4, 70.4, 70.3, 70.0, 70.0, 62.3, 59.2, 50.8, 50.6, 47.7, 44.0, 30.6, 30.1, 24.4, 22.6, 9.4, 3.9, 3.7. HRMS (ESI) m/z: calculated for $C_{34}H_{52}N_5O_{10}$ [M+H]$^+$ 690.3714; found 690.3744.

14-azido-N-((4R,4aR,7R,7aR,12bS)-9-hydroxy-3-methyl-2,3,4,4a,5,6,7,7a-octahydro-1H-4,12-methanobenzofuro[3,2-e]isoquinolin-7-yl)-3,6,9,12-tetraoxatetradecanamide (**3.11d**)

Compound **3.11d** was subjected to general procedure 1. Offwhite solid, 62%. ^{1}H NMR (300 MHz, $CDCl_3$) δ 6.66 (d, *J* = 8.1 Hz, 1H), 6.56 (d, *J* = 8.1 Hz, 1H), 4.41 (d, *J* = 7.9 Hz, 1H), 3.96 (s, 2H), 3.72-3.57 (m, 14H), 3.37 (t, *J* = 5.6 Hz, 2H), 3.11 (br s, 1H), 2.98 (d, *J* = 18.4 Hz, 1H), 2.54 (dd, *J* = 11.9, 4.4 Hz, 1H), 2.39 (s, 3H), 2.34-2.14 (m, 2H), 1.92-1.75 (m, 2H), 1.71-1.48 (m, 3H), 1.42-1.23 (m, 2H), 1.14-1.00 (m, 1H). ^{13}C NMR (75 MHz, $CDCl_3$) δ 169.9, 142.8, 140.3, 129.3, 125.2, 119.4, 117.5, 93.2, 70.8, 70.6, 70.5, 70.4, 70.4, 70.4, 70.2, 70.0, 59.4, 51.5, 50.6, 47.2, 44.9, 43.4, 42.6, 35.2, 28.8, 24.1, 20.1. HRMS (ESI) m/z: calculated for $C_{27}H_{40}N_5O_7$ [M+H]$^+$ 546.2928; found 546.2923.

17-azido-N-((4R,4aR,7R,7aR,12bS)-9-hydroxy-3-methyl-2,3,4,4a,5,6,7,7a-octahydro-1H-4,12-methanobenzofuro[3,2-e]isoquinolin-7-yl)-3,6,9,12,15-pentaoxaheptadecanamide (**3.11e**)

Compound **3.11e** was subjected to general procedure 1. Offwhite solid, 53%. ^{1}H NMR (300 MHz, $CDCl_3$) δ 6.59 (d, *J* = 8.1 Hz, 1H), 6.51 (d, *J* = 8.1 Hz, 1H), 4.36 (d, *J* = 7.9 Hz, 1H), 3.92 (s, 2H), 3.73 – 3.54 (m, 18H), 3.34 (t, *J* = 5.6 Hz, 2H), 2.95 (d, *J* = 19.1 Hz, 1H), 2.49 (dd, *J* = 12.5, 4.2 Hz, 1H), 2.39 – 2.29 (m, 2H), 2.20 (s, 3H), 1.79 (dd, *J* = 12.4, 4.6 Hz, 2H), 1.68 – 1.55 (m, 2H), 1.33 – 1.20 (m, 2H), 1.07 (t, *J* = 7.2 Hz, 1H). ^{13}C NMR (75 MHz, $CDCl_3$) δ 169.8, 143.0, 140.7, 129.3, 124.8, 119.2, 117.5, 92.8, 70.8, 70.6, 70.5, 70.4, 70.4, 70.3, 70.3, 70.2, 69.9, 59.3, 51.6, 47, 45.0, 43.4, 42.7(d, *J* = 5.2 Hz), 38.9, 35.3, 28.9, 24.1, 20.0, 15.49. HRMS (ESI) m/z: calculated for $C_{29}H_{44}N_5O_8$ [M+H]$^+$ 590.3190; found 590.3192.

20-azido-N-((4R,4aR,7R,7aR,12bS)-9-hydroxy-3-methyl-2,3,4,4a,5,6,7,7a-octahydro-1H-4,12-methanobenzofuro[3,2-e]isoquinolin-7-yl)-3,6,9,12,15,18-hexaoxaicosanamide (**3.11f**)

Compound **3.11f** was subjected to general procedure 1. Offwhite solid, 51%. ^{1}H NMR (300 MHz, $CDCl_3$) δ 6.64 (d, *J* = 8.1 Hz, 1H), 6.54 (d, *J* = 8.1 Hz, 1H), 4.42 (d, *J* = 8.0 Hz, 1H), 3.95 (s, 2H), 3.76-3.49 (m, 22H), 3.36 (t, *J* = 5.6 Hz, 2H), 3.10 (br s, 1H), 2.93 (s, 2H), 2.86 (d, *J* = 0.6 Hz, 1H), 2.58-2.46 (m, 1H), 2.37 (s, 3H), 2.26-2.10 (m, 2H), 1.85 (dt, *J* = 12.0, 6.0 Hz, 1H), 1.70-1.59 (m, 1H), 1.51 (dd, *J* = 13.4, 3.5 Hz, 1H), 1.45-1.20 (m, 2H), 1.06 (ddd, *J* = 15.3, 10.5, 2.4 Hz, 1H). ^{13}C NMR (75 MHz, $CDCl_3$) δ 169.9, 142.8, 140.3, 129.4, 125.2, 119.3, 117.4, 93.1, 70.8, 70.6, 70.6, 70.5, 70.5, 70.4, 70.4, 70.4, 70.3, 70.2, 69.9, 59.3, 51.7, 50.6, 47.2, 43.4, 42.7, 35.2, 28.7, 24.1, 20.0. HRMS (ESI) m/z: calculated for $C_{31}H_{48}N_5O_9$ [M+H]$^+$ 634.3452; found 634.3444.

N-((4R,4aS,7R,7aR,12bS)-3-(cyclopropylmethyl)-4a,9-dihydroxy-2,3,4,4a,5,6,7,7a-octahydro-1H-4,12-methanobenzofuro[3,2-e]isoquinolin-7-yl)-14-(4-((2-methoxy-4-((4-(2-methoxyphenyl)piperazin-1-yl)methyl)phenoxy)methyl)-1H-1,2,3-triazol-1-yl)-3,6,9,12-tetraoxatetradecanamide (**3.12a**)

Compound **3.12a** was subjected to general procedure 2. Offwhite solid, 55%. LC-HRMS: t_R=5.43 min (10–100% MeCN, 15 min run), 96.49 %. ^{1}H NMR (300 MHz, $CDCl_3$) δ 7.85 (s, 1H), 7.20 (d, *J* = 8.7 Hz, 1H), 7.00 – 6.79 (m, 6H), 6.68 (d, *J* = 8.1 Hz, 1H), 6.53 (d, *J* = 8.1 Hz, 1H), 5.28 (d, *J* = 7.1 Hz, 2H), 4.53 (t, *J* = 5.6 Hz, 2H), 4.42 (d, *J* = 7.5 Hz, 1H), 3.93 (s, 2H), 3.87 (t, *J* = 5.2 Hz, 2H), 3.84 (s, 3H), 3.82 (s, 3H), 3.68 – 3.56 (m, 14H), 3.53 (s, 2H), 3.09-3.03 (m, 5H), 2.95 (d, *J* = 6.4 Hz, 1H), 2.72 – 2.53 (m, 6H), 2.35 (d, *J* = 6.5 Hz, 2H), 2.21 – 2.11 (m, 2H), 1.86 (qd, *J* = 12.6, 3.3 Hz, 1H), 1.74 – 1.62 (m, 1H), 1.61 – 1.37 (m, 3H), 0.90 – 0.75 (m, 1H), 0.55 – 0.47 (m, 2H), 0.15 – 0.07 (m, 2H). ^{13}C NMR (75 MHz, $CDCl_3$) δ 169.8, 152.2, 149.4, 146.8, 144.1, 142.5, 141.2, 140.2, 131.1, 130.9, 124.2, 124.08, 122.8, 121.7, 120.9, 119.0, 118.2, 118.0, 113.7, 112.9, 111.1, 92.8, 70.8, 70.5, 70.4, 70.4, 70.3, 70.3, 70.0, 69.4, 63.1, 62.7, 62.3, 59.1, 55.8, 55.3, 53.1, 51.0, 50.3, 50.2, 47.6, 44.0, 30.7, 30.0, 24.4, 22.6, 9.4, 3.9, 3.7. HRMS (ESI) m/z: calculated for $C_{52}H_{71}N_7O_{11}$ [M+2H]$^{2+}$ 484.7600; found 484.7572.

N-((4R,4aS,7R,7aR,12bS)-3-(cyclopropylmethyl)-4a,9-dihydroxy-2,3,4,4a,5,6,7,7a-octahydro-1H-4,12-methanobenzofuro[3,2-e]isoquinolin-7-yl)-17-(4-((2-methoxy-4-((4-(2-methoxyphenyl)piperazin-1-yl)methyl)phenoxy)methyl)-1H-1,2,3-triazol-1-yl)-3,6,9,12,15-pentaoxaheptadecanamide (**3.12b**)

Compound **3.12b** was subjected to general procedure 2. Offwhite solid, 52%. LC-HRMS: t_R=5.44 min (10–100% MeCN, 15 min run), 92.62%. HRMS (ESI) m/z: calculated for $C_{54}H_{75}N_7O_{12}$ [M+2H]$^{2+}$ 506.7731; found 506.7713.

N-((4R,4aS,7R,7aR,12bS)-3-(cyclopropylmethyl)-4a,9-dihydroxy-2,3,4,4a,5,6,7,7a-octahydro-1H-4,12-methanobenzofuro[3,2-e]isoquinolin-7-yl)-20-(4-((2-methoxy-4-((4-(2-methoxyphenyl)piperazin-1-yl)methyl)phenoxy)methyl)-1H-1,2,3-triazol-1-yl)-3,6,9,12,15,18-hexaoxaicosanamide (**3.12c**)

Compound **3.12c** was subjected to general procedure 2. Offwhite solid, 50%. LC-HRMS: t_R=5.63 min (10–100% MeCN, 15 min run), 95.23 %. HRMS (ESI) m/z: calculated for $C_{56}H_{79}N_7O_{13}$ [M+2H]$^{2+}$ 528.7862; found 528.7854.

N-((4R,4aR,7R,7aR,12bS)-9-hydroxy-3-methyl-2,3,4,4a,5,6,7,7a-octahydro-1H-4,12-methanobenzofuro[3,2-e]isoquinolin-7-yl)-14-(4-((2-methoxy-4-((4-(2-methoxyphenyl)piperazin-1-yl)methyl)phenoxy)methyl)-1H-1,2,3-triazol-1-yl)-3,6,9,12-tetraoxatetradecanamide (**3.12d**)

Compound **3.12d** was subjected to general procedure 2. Offwhite solid, 42%. LC-HRMS: t_R=5.23 min (10–100% MeCN, 15 min run), 96.94 %. ^{1}H NMR (300 MHz, $CDCl_3$) δ 7.85 (s, 1H), 7.11 (d, *J* = 8.2 Hz, 1H), 7.01 – 6.94 (m, 2H), 6.94 – 6.88 (m, 2H), 6.83 (ddd, *J* = 8.1, 5.5, 1.7 Hz, 2H), 6.68 (d, *J* = 8.1 Hz, 1H), 6.56 (d, *J* = 8.1 Hz, 1H), 5.28 (d, *J* = 6.7 Hz, 2H), 4.53 (t, *J* = 5.7 Hz, 2H), 4.42 (d, *J* = 8.0 Hz, 1H), 3.91 (d, *J* = 1.4 Hz, 2H), 3.87 (t, *J* = 5.5 Hz, 2H), 3.84 (s, 3H), 3.82 (s, 3H), 3.66 – 3.51 (m, 14H), 3.09 (br s, 4H), 2.98 – 2.85 (m, 1H), 2.66 (br s, 3H), 2.52 (dd, *J* = 12.1, 4.6 Hz, 1H), 2.39 (s, 3H), 2.19 (dt, *J* = 9.8, 5.3 Hz, 2H), 1.82 (td, *J* = 12.2, 5.1 Hz, 1H), 1.58 (ddd, *J* = 33.7, 12.6, 3.5 Hz, 2H), 1.45 – 1.21 (m, 1H), 1.17 – 0.98 (m, 1H). ^{13}C NMR (75 MHz, $CDCl_3$) δ 169.8, 152.2, 149.4, 146.7, 144.1, 142.7, 141.2, 140.1, 131.2, 129.3, 125.3, 124.25, 122.8, 121.7, 120.9, 119.5, 118.2, 117.7, 113.7, 112.9, 111.1, 93.0, 70.8, 70.5, 70.4, 70.3, 70.3, 70.2, 69.4, 63.1, 62.8, 59.4, 55.8, 55.3, 53.2, 51.3, 50.3, 50.2, 47.2, 43.4, 42.8, 42.7, 35.3, 28.7, 24.1, 20.0. HRMS (ESI) m/z: calculated for $C_{49}H_{67}N_7O_{10}$ $[M+2H]^{2+}$ 456.7469; found 456.7434.

N-((4R,4aR,7R,7aR,12bS)-9-hydroxy-3-methyl-2,3,4,4a,5,6,7,7a-octahydro-1H-4,12-methanobenzofuro[3,2-e]isoquinolin-7-yl)-17-(4-((2-methoxy-4-((4-(2-methoxyphenyl)piperazin-1-yl)methyl)phenoxy)methyl)-1H-1,2,3-triazol-1-yl)-3,6,9,12,15-pentaoxaheptadecanamide (**3.12e**)

Compound **3.12e** was subjected to general procedure 2. Offwhite solid, 46%. LC-HRMS: t_R=5.30 min (10–100% MeCN, 15 min run), 88.20 %. HRMS (ESI) m/z: calculated for $C_{51}H_{71}N_7O_{11}$ $[M+2H]^{2+}$ 478.7600; found 478.7562.

N-((4R,4aR,7R,7aR,12bS)-9-hydroxy-3-methyl-2,3,4,4a,5,6,7,7a-octahydro-1H-4,12-methanobenzofuro[3,2-e]isoquinolin-7-yl)-20-(4-((2-methoxy-4-((4-(2-methoxyphenyl)piperazin-1-yl)methyl)phenoxy)methyl)-1H-1,2,3-triazol-1-yl)-3,6,9,12,15,18-hexaoxaicosanamide (**3.12f**)

Compound **3.12f** was subjected to general procedure 2. Offwhite solid, 40%. LC-HRMS: t_R=5.37 min (10–100% MeCN, 15 min run), 92.86 %. ^{1}H NMR (300 MHz, $CDCl_3$) δ 7.84 (s, 1H), 7.22 (d, *J* = 9.7 Hz, 1H), 7.02 – 6.88 (m, 4H), 6.82 (t, *J* = 8.0 Hz, 2H), 6.66 (d, *J* = 8.0 Hz, 1H), 6.55 (d, *J* = 8.1 Hz, 1H), 5.26 (s, 2H), 4.71 (s, 0H), 4.52 (t, *J* = 5.1 Hz, 2H), 4.43 (dd, *J* = 8.0, 3.6 Hz, 1H), 3.92 (s, 2H), 3.85 (d, *J* = 4.3 Hz, 5H), 3.81 (d, *J* = 3.0 Hz, 3H), 3.77 – 3.45 (m, 29H), 3.19 – 2.98 (m, 6H), 2.98 – 2.92 (m, 1H), 2.65 (t, *J* = 4.8 Hz, 4H), 2.51 (dd, *J* = 11.9, 4.4 Hz, 1H), 2.38 (s, 3H), 2.18 (dt, *J* = 15.9, 5.0 Hz, 2H), 1.82 (dt, *J* = 11.6, 5.3 Hz, 2H), 1.71 – 1.47 (m, 2H), 1.44 – 1.23 (m, 1H), 1.15 – 0.99 (m, 1H). ^{13}C NMR (75 MHz, $CDCl_3$) δ 169.9, 152.2, 149.4, 146.8, 144.1, 142.7, 141.3, 140.2, 131.3 (d, *J* = 4.5 Hz), 129.3, 125.3, 124.2, 122.8, 121.6, 120.9, 119.4, 118.2, 117.5, 113.7, 112.8, 111.1, 93.1, 70.8, 70.5, 70.4, 70.3, 70.2, 69.4, 63.1, 62.8, 59.4, 55.8, 55.3, 53.2, 51.8, 50.3 (d, *J* = 14.4 Hz), 47.2, 43.4, 42.8 (d, *J* = 8.3 Hz), 35.3, 28.7, 24.2, 20.1. HRMS (ESI) m/z: calculated for $C_{53}H_{75}N_7O_{12}$ $[M+2H]^{2+}$ 500.7731; found 500.7742.

N-((4R,4aS,7R,7aR,12bS)-3-(cyclopropylmethyl)-4a,9-dihydroxy-2,3,4,4a,5,6,7,7a-octahydro-1H-4,12-methanobenzofuro[3,2-e]isoquinolin-7-yl)-14-(4-(3-((4-(2-((5-hydroxy-1,2,3,4-tetrahydronaphthalen-2-yl)(propyl)amino)ethyl)phenyl)amino)-3-oxopropyl)-1H-1,2,3-triazol-1-yl)-3,6,9,12-tetraoxatetradecanamide (**3.13a**)

Compound **3.13a** was subjected to general procedure 2. Offwhite solid, 60%. LC-HRMS: t_R=5.43 min (10–100% MeCN, 15 min run), 99.45%. ^1H NMR (300 MHz, $CDCl_3$) δ 7.40 (d, *J* = 8.2 Hz, 2H), 7.22 (d, *J* = 8.9 Hz, 1H), 7.08 (d, *J* = 8.4 Hz, 2H), 6.94 (t, *J* = 7.8 Hz, 1H), 6.72 (d, *J* = 8.1 Hz, 1H), 6.62 (d, *J* = 7.9 Hz, 2H), 6.53 (d, *J* = 8.2 Hz, 1H), 4.47 (t, *J* = 5.1 Hz, 2H), 4.41 (d, *J* = 7.5 Hz, 1H), 3.92 (s, 2H), 3.83 (t, *J* = 5.2 Hz, 2H), 3.64-3.56 (m, 14H), 3.07 (dt, *J* = 15.4, 6.3 Hz, 3H), 2.99 – 2.85 (m, 2H), 2.76 (dt, *J* = 14.2, 7.4 Hz, 6H), 2.56 (dt, *J* = 17.0, 7.8 Hz, 4H), 2.35 (d, *J* = 6.5 Hz, 2H), 2.20 – 1.99 (m, 3H), 1.85 (q, *J* = 12.8 Hz, 1H), 1.71 – 1.36 (m, 6H), 1.25 (s, 1H), 0.89 (t, *J* = 7.3 Hz, 3H), 0.56 – 0.48 (m, 2H), 0.11 (q, *J* = 5.0 Hz, 2H). ^{13}C NMR (75 MHz, $CDCl_3$) δ 170.6, 170.1, 153.8, 146.2, 142.5, 140.3, 137.9, 136.2 (d, *J* = 9.1 Hz), 130.3, 129.1, 126.3, 124.0, 123.1, 122.9, 121.3, 119.9, 119.1, 118.0, 112.1, 92.6, 77.2, 74.6, 70.8, 70.5, 70.4, 70.4, 70.3, 70.3, 70.1, 69.4, 62.3, 59.1, 56.8, 53.4, 52.7 (d, *J* = 18.9 Hz), 51.0, 50.2, 47.6, 44.1, 36.5, 34.9, 32.0, 30.6, 30.0, 25.6, 24.5, 23.5, 22.6, 21.7, 21.3, 11.9, 9.4, 3.9, 3.7. HRMS (ESI) m/z: calculated for $C_{56}H_{77}N_7O_{10}$ $[M+2H]^{2+}$ 503.7860; found 503.7833.

N-((4R,4aS,7R,7aR,12bS)-3-(cyclopropylmethyl)-4a,9-dihydroxy-2,3,4,4a,5,6,7,7a-octahydro-1H-4,12-methanobenzofuro[3,2-e]isoquinolin-7-yl)-17-(4-(3-((4-(2-((5-hydroxy-1,2,3,4-tetrahydronaphthalen-2-yl)(propyl)amino)ethyl)phenyl)amino)-3-oxopropyl)-1H-1,2,3-triazol-1-yl)-3,6,9,12,15-pentaoxaheptadecanamide (**3.13b**)

Compound **3.13b** was subjected to general procedure 2. Offwhite solid, 47%. LC-HRMS: t_R=5.48 min (10–100% MeCN, 15 min run), 95.65%. ^1H NMR (300 MHz, $CDCl_3$) δ 7.59 (s, 1H), 7.40 (d, *J* = 8.4 Hz, 2H), 7.08 (d, *J* = 8.3 Hz, 2H), 6.95 (t, *J* = 7.8 Hz, 1H), 6.72 (d, *J* = 8.1 Hz, 1H), 6.62 (t, *J* = 7.8 Hz, 2H), 6.54 (d, *J* = 8.1 Hz, 1H), 3.92 (s, 2H), 3.81 (t, *J* = 5.0 Hz, 2H), 3.72 – 3.48 (m, 18H), 3.17 – 3.02 (m, 3H), 3.02 – 2.85 (m, 2H), 2.85 – 2.65 (m, 5H), 2.63 – 2.49 (m, 4H), 2.35 (d, *J* = 6.5 Hz, 2H), 2.15 (s, 1H), 1.61 – 1.38 (m, 3H), 0.89 (t, *J* = 7.3 Hz, 3H), 0.55 – 0.47 (m, 2H), 0.14 – 0.09 (m, 2H). ^{13}C NMR (75 MHz, $CDCl_3$) δ 170.6, 170.0, 153.6, 146.2, 142.5, 140.2, 138.2, 136.5, 136.1, 130.9, 129.0, 126.2, 124.1, 123.1, 122.8, 121.4, 119.8, 119.0, 118.0, 112.0, 92.7, 77.2, 70.8, 70.5, 70.5, 70.4, 70.3, 70.3, 70.1, 69.4, 62.3, 59.1, 56.6, 52.8, 52.5, 51.0, 50.2, 47.7, 44.0, 36.5, 35.2, 32.1, 30.6, 30.0, 25.7, 24.4, 23.5, 22.6, 21.9, 21.3, 11.9, 9.4, 3.9, 3.7. HRMS (ESI) m/z: calculated for $C_{58}H_{81}N_7O_{11}$ $[M+2H]^{2+}$ 525.7991; found 525.8002.

N-((4R,4aS,7R,7aR,12bS)-3-(cyclopropylmethyl)-4a,9-dihydroxy-2,3,4,4a,5,6,7,7a-octahydro-1H-4,12-methanobenzofuro[3,2-e]isoquinolin-7-yl)-20-(4-(3-((4-(2-((5-hydroxy-1,2,3,4-tetrahydronaphthalen-2-yl)(propyl)amino)ethyl)phenyl)amino)-3-oxopropyl)-1H-1,2,3-triazol-1-yl)-3,6,9,12,15,18-hexaoxaicosanamide (**3.13c**)

Compound **3.13c** was subjected to general procedure 2. Offwhite solid, 43%. LC-HRMS: t_R=5.53 min (10–100% MeCN, 15 min run), 98.35 %. HRMS (ESI) m/z: calculated for $C_{60}H_{85}N_7O_{12}$ $[M+2H]^{2+}$ 547.8122; found 547.8098.

14-(4-(3-((4-(2-((5-hydroxy-1,2,3,4-tetrahydronaphthalen-2-yl)(propyl)amino)ethyl)phenyl)amino)-3-oxopropyl)-1H-1,2,3-triazol-1-yl)-N-((4R,4aR,7R,7aR,12bS)-9-hydroxy-3-methyl-2,3,4,4a,5,6,7,7a-octahydro-1H-4,12-methanobenzofuro[3,2-e]isoquinolin-7-yl)-3,6,9,12-tetraoxatetradecanamide (**3.13d**)

Compound **3.13d** was subjected to general procedure 2. Offwhite solid, 52%. LC-HRMS: t_R=5.26 min (10–100% MeCN, 15 min run), 98.63 %. ^{1}H NMR (300 MHz, $CDCl_3$) δ 8.23 (s, 1H), 7.59 (s, 1H), 7.39 (d, *J* = 8.3 Hz, 2H), 7.09 (d, *J* = 8.1 Hz, 2H), 6.96 (t, *J* = 7.7 Hz, 1H), 6.72 (d, *J* = 8.1 Hz, 1H), 6.64 (d, *J* = 7.6 Hz, 1H), 6.58 (dd, *J* = 8.0, 4.2 Hz, 2H), 4.47 (t, *J* = 5.0 Hz, 2H), 4.37 (d, *J* = 7.9 Hz, 1H), 3.92 (s, 2H), 3.82 (t, *J* = 5.0 Hz, 2H), 3.69 – 3.50 (m, 14H), 3.11 (d, *J* = 6.9 Hz, 3H), 2.98 – 2.85 (m, 3H), 2.83 – 2.66 (m, 6H), 2.55 (dd, *J* = 8.6, 6.5 Hz, 3H), 2.41 (s, 3H), 2.19 (d, *J* = 12.6 Hz, 2H), 2.02 (d, *J* = 12.6 Hz, 1H), 1.81 (td, *J* = 12.2, 11.3, 7.1 Hz, 2H), 1.69 – 1.57 (m, 1H), 1.50 (q, *J* = 7.1 Hz, 3H), 1.25 (s, 3H), 0.89 (t, *J* = 7.3 Hz, 3H). ^{13}C NMR (75 MHz, $CDCl_3$) δ 170.6, 169.9, 146.2, 153.8, 142.8, 140.2, 136.6, 136.0, 129.1, 126.3, 123.2, 122.8, 121.3, 119.8, 119.5, 117.8, 112.0, 93.0, 70.7, 70.5, 70.4, 70.4, 70.2, 70.2, 69.4, 59.5, 56.7, 53.4, 51.6, 50.1, 47.2, 43.3, 42.5, 36.6, 35.2, 32.1, 29.6, 28.7, 25.7, 24.0, 23.5, 21.9, 21.4, 20.1, 11.9. HRMS (ESI) m/z: calculated for $C_{53}H_{73}N_7O_9$ $[M+2H]^{2+}$ 475.7729; found 475.7702.

17-(4-(3-((4-(2-((5-hydroxy-1,2,3,4-tetrahydronaphthalen-2-yl)(propyl)amino)ethyl)phenyl)amino)-3-oxopropyl)-1H-1,2,3-triazol-1-yl)-N-((4R,4aR,7R,7aR,12bS)-9-hydroxy-3-methyl-2,3,4,4a,5,6,7,7a-octahydro-1H-4,12-methanobenzofuro[3,2-e]isoquinolin-7-yl)-3,6,9,12,15-pentaoxaheptadecanamide (**3.13e**)

Compound **3.13e** was subjected to general procedure 2. Offwhite solid, 48%. LC-HRMS: t_R=5.33 min (10–100% MeCN, 15 min run), 95.43 %. HRMS (ESI) m/z: calculated for $C_{55}H_{77}N_7O_{10}$ $[M+2H]^{2+}$ 497.7860; found 497.7826.

20-(4-(3-((4-(2-((5-hydroxy-1,2,3,4-tetrahydronaphthalen-2-yl)(propyl)amino)ethyl)phenyl)amino)-3-oxopropyl)-1H-1,2,3-triazol-1-yl)-N-((4R,4aR,7R,7aR,12bS)-9-hydroxy-3-methyl-2,3,4,4a,5,6,7,7a-octahydro-1H-4,12-methanobenzofuro[3,2-e]isoquinolin-7-yl)-3,6,9,12,15,18-hexaoxaicosanamide (**3.13f**)

Compound **3.13f** was subjected to general procedure 2. Offwhite solid, 44%. LC-HRMS: t_R=5.37 min (10–100% MeCN, 15 min run), 97.02 %. ^{1}H NMR (300 MHz, $CDCl_3$) δ 8.48 (d, *J* = 7.4 Hz, 1H), 7.59 (s, 1H), 7.40 (d, *J* = 7.9 Hz, 2H), 7.07 (d, *J* = 8.0 Hz, 2H), 6.93 (t, *J* = 7.7 Hz, 1H), 6.69 (d, *J* = 8.1 Hz, 1H), 6.58 (q, *J* = 8.6 Hz, 3H), 5.29 (s, 1H), 4.52 – 4.35 (m, 3H), 3.90 (s, 2H), 3.79 (t, *J* = 5.0 Hz, 2H), 3.71 – 3.42 (m, 22H), 3.10 (t, *J* = 6.7 Hz, 3H), 2.94 (td, *J* = 13.9, 13.5, 7.0 Hz, 2H), 2.83 – 2.62 (m, 6H), 2.62 – 2.44 (m, 4H), 2.38 (s, 3H), 2.18 (dt, *J* = 12.5, 4.2 Hz, 2H), 2.02 (d, *J* = 11.2 Hz, 1H), 1.80 (t, *J* = 11.9 Hz, 1H), 1.69 – 1.40 (m, 4H), 1.27 (d, *J* = 12.9 Hz, 1H), 1.03 (t, *J* = 12.9 Hz, 1H), 0.88 (t, *J* = 7.3 Hz, 3H). ^{13}C NMR (75 MHz, $CDCl_3$) δ 170.6, 170.1, 154.1, 146.3, 142.8, 140.3, 138.1, 136.4, 136.2, 129.2, 129.0, 126.2, 125.0, 123.4, 122.9, 121.0, 119.8, 119.4, 117.7, 111.9, 92.9, 70.7, 70.5, 70.4, 70.3, 70.3, 70.2, 69.3, 59.4, 56.7, 52.8, 52.6, 51.6, 50.2, 47.2, 43.3, 42.5 (d, *J* = 11.1 Hz), 36.4, 35.1 (d, *J* = 8.9 Hz), 32.2, 28.7, 25.8, 24.1, 23.7, 22.0, 21.3, 20.1. HRMS (ESI) m/z: calculated for $C_{57}H_{81}N_7O_{11}$ $[M+2H]^{2+}$ 519.7991; found 519.7953.

III.6.2. Plasmids and receptor fusion constructs

The plasmids HA $D_{4.2}$ and HA D_2 were described previously.[38] The NanoBiT constructs (NB MCS1) and (NB MCS2) were procured from Promega. These plasmids encode for the split fragments of Nanoluciferase: LargeBiT (LgBiT) and SmallBiT (SmBiT). The human µOR was PCR amplified and SmBiT was cloned at the C-terminus of the receptor. A flexible linker (GSSGGGGSGGGGSSG) is present in between µOR and SmBiT.

In order to clone µOR-SmBiT, specific primers were generated with a *Hind*III restriction site at the 5’ terminus and a *Xho*I site at the 3’ terminus of the µOR coding sequence by removing the stop codon. PCR was performed with 20 ng of plasmid with *Pfu* DNA Polymerase (2.5 U/µL, Thermo Fisher Scientific) according to the manufacturer’s protocol. The reactions were performed in a Mastercycler™ Nexus Thermal Cycler (Eppendorf, Hamburg, Germany) and then purified using QIAquick Gel Extraction Kit (QIAGEN, Germany). The resultant amplicon and the vector (NB MCS2) were digested with *Hind*III and *Xho*I for 3 h at 37°C. The digested PCR product was cleaned using “High Pure PCR Product Purification Kit” (Roche, Germany) and then ligated into the corresponding digested NB MCS2. After transformation of the ligated product into competent MC 1061 “E. *coli*” strain, the ampicillin resistant clones were screened by performing PCR with primers against µOR. Furthermore, a digestion was performed with *Hind*III and *Xba*I, which are the restriction sites flanking µOR-SmBiT. The constructs were verified by sequencing. LgBiT-Barr2 has been previously described.[32]

III.6.3. Cell culture and transfection

Human embryonic kidney (HEK) 293T cells were cultured in Dulbecco's modified Eagle's medium (DMEM; Invitrogen), supplemented with 10% fetal bovine serum, penicillin (100 U/ml), and streptomycin (100 µg/ml) in a controlled environment (37 °C, 98% humidity, 5% CO_2). For ligand binding experiments and β-arrestin2 recruitment assay, HEK293T cells were transiently transfected using the Polyethylenimine (PEI) method as described before.[30] A total amount of 10 µg of DNA was used for transfection of cells in one 10-cm dish. HEK293S cells stably expressing HA $D_{4.2}R$[30] were grown in DMEM/F12 (Gibco, Invitrogen) supplemented with 10% fetal bovine serum, penicillin (100 U/ml), streptomycin (100 µg/ml), and 0.5 mg/ml G418 (Geneticin, Gibco) in a controlled environment (37 °C, 98% humidity, 5% CO_2).

III.6.4. Membrane Preparation and Protein Determination.

Membrane suspensions from HEK293T cells transiently transfected with the receptors of interest were prepared as described previously.[27,28] Cells were disrupted with a Polytron homogenizer for two 10 s periods in 10 volumes of ice-cold Tris-HCl buffer (50 mM, pH 7.4). Membranes were obtained by centrifugation at 16500g for 20 min at 4 °C, and the pellet was resuspended and centrifuged under the same conditions. The resulting pellet was stored at –80 °C and was washed once more as described above and resuspended in Tris-HCl buffer (50 mM, pH 7.4) for immediate use. Protein was quantified by the BCA method using bovine serum albumin dilutions as the standard.

III.6.5. [^{3}H]Spiperone Binding.

Saturation binding assay for [^{3}H]spiperone was performed as previously described.[27,28] For competition binding assays, membranes (20 µg) were incubated in binding buffer (50 mM Tris-HCl containing 5 mM KCl, 1 mM EDTA, 1.5 mM $CaCl_2$ and 4 mM $MgCl_2$, pH 7.4) with 0.2 nM [^{3}H] spiperone (specific activity = 76 Ci/mmol, PerkinElmer, USA) in the absence or presence of 11 different concentrations (0.1 nM-10 µM) of unlabeled ligands for 1 h at 22 °C. Nonspecific binding was determined in the presence of 1 µM haloperidol. Incubation was terminated by rapid filtration through GF/C glass-fiber filters (Whatman Schleicher and Schuell, Keene, NH) embedded in 0.1% polyethylenimine and mounted on a Brandel cell harvester. Filters were washed three times with cold 50 mM Tris-HCl, pH 7.4 buffer and transferred to vials containing 3 mL of scintillation cocktail to soak the filter overnight. The radioactivity counts were measured with a Tri-Carb 2800TR liquid scintillation analyzer (PerkinElmer).

III.6.6. [^{3}H]Raclopride Binding.

[^{3}H]raclopride saturation binding assay was performed as described before.[39] Briefly, a suspension of whole cells (corresponding to a total protein amount of 20 µg) were incubated with different concentrations (0–20 nM) of [^{3}H]raclopride in 50 mM Tris-HCl, pH 7.4 buffer (containing 5 mM KCl, 100 mM NaCl, 1.5 mM $CaCl_2$, 4 mM $MgCl_2$ and 1 mM EDTA) at 37°C for 1 h. For competitive binding experiments, 2.0 nM [^{3}H]raclopride (specific activity = 73.8 Ci/mmol, PerkinElmer, USA) was incubated with 20 µg of whole cells in the absence or presence of varying concentrations (0.1 nM-10 µM) of unlabeled ligands at 37°C for 1 h. Nonspecific binding was determined in the presence of 1 µM haloperidol. Free and cell-bound ligand were separated by rapid filtration through GF/C glass-fiber filters (Whatman Schleicher and Schuell, Keene, NH) embedded in 0.1% polyethylenimine and mounted on a Brandel cell harvester. Filtration and measuring were as described above.

III.6.7. [^{3}H]Diprenorphine Binding.

[^{3}H]diprenorphine saturation binding assay was adapted from a published protocol.[40] Membranes (10 µg) were incubated with different concentrations (0–6 nM) of [^{3}H]diprenorphine in 50 mM Tris-HCl, pH 7.4 buffer at 25°C for 1 h. For competitive binding experiments, 0.5 nM [^{3}H]diprenorphine (specific activity = 25.8 Ci/mmol, PerkinElmer, USA) was incubated with 10 µg of membranes in the absence or presence of varying concentrations (0.1 nM-10 µM) of unlabeled ligands at 25°C for 1 h. Nonspecific binding was determined in the presence of 10 µM naloxone. Filtration and measuring were as described above.

III.6.8. Data Analysis.

Results are expressed as means ± SEM for at least three experiments, each performed in duplicate. Statistical analysis and curve fits of dose-response curves were performed using GraphPad Prism 7. Ki values were calculated by using the Cheng-Prusoff equation.[41]

III.6.9. MAPK phosphorylation

HEK293S cells stably expressing HA $D_{4.2}$R were seeded in 6-well plates at 400,000 cells per well. When the cells were 70% confluent, cells were starved overnight with serum free medium. The ligands (1 nM-10µM) were added sequentially to the cells at the concentrations indicated in the legend for 5 min. To stop the reaction, medium was aspirated, the cells were placed on ice and washed with ice-cold PBS. RIPA buffer [150 mM NaCl; 50 mM Tris/HCl pH 7.5; 1 % NP-40; 0.1 % SDS; and 0.5 % deoxycholic acid sodium salt (Acros Organics: 218591000). protease inhibitors: aprotinin (2.5 µg/ml, Sigma-Aldrich: A6279), pefablock (1 mM, Sigma-Aldrich: 76307), leupeptin (10 µg/ml, Acros Organics: 328350050), and phosphatase inhibitor β-glycerol phosphate disodium salt pentahydrate (10 mM, Fluka BioChemika: 50020) was used to prepare the cell lysate for western blotting according to the protocol described before.[42] After western blotting, the membrane was incubated with blocking buffer (LI-COR Biosciences) for 1h at RT. Then, primary antibody rabbit polyclonal phospho-p44/42 MAPK (1/2000) (Cell Signaling, cat. no. 9101L) or mouse monoclonal p44/42 MAPK (1/2000) (clone L34F12; Cell

Signaling, cat. no. 4696S) was added to develop the blot overnight at 4 °C. Next, the blot was washed with washing buffer (PBS + 0.05% Tween 20 from Sigma-Aldrich) for three times and then secondary antibodies goat anti-rabbit IRDye680 LT (1/10000) (cat. no. 926–68021, LI-COR Biosciences) or goat anti-mouse IRDye800 (1/10000) (cat. no.926–32210, LI-COR Biosciences) were added for 1h at RT in the dark. The blot was washed three times with washing buffer and the fluorescent signal was detected with the Odyssey Infrared Imaging system. In the analysis, the phospho-p44/42 MAPK signal is normalized against the total p44/42 MAPK signal after quantification by Image J.

III.6.10. β-arrestin2 recruitment

HEK293T cells were seeded in 10-cm dishes with 2.5 x 10^6 cells/dish and transiently transfected with pμOR-SmBiT (4 μg), pLgBiT-βarr2 (1 μg), pGRK2 (1 μg) and pcDNA3 (4 μg) per 10-cm dish. Forty-eight hours after transfection, the cells were washed with warm PBS, a cell suspension was prepared with warm HBSS and proteins were estimated by the bicinchoninic acid method (BCA, Thermo Scientific™) using bovine serum albumin dilutions as the standard. The cell suspension was added to a 96-well plate (100 µl cell suspension in each well corresponding to 800 ng protein). The Nano-Glo Live Cell reagent, a nonlytic detection reagent containing the cell permeable furimazine substrate, was prepared by diluting the Nano-Glo Live Cell substrate 20× using Nano-Glo LCS Dilution buffer, and 25 µl was added to each well. Subsequently, the plate was placed in the luminodetecter (CLARIOstar) for measurement. Luminescence was monitored during the equilibration period until the signal was stabilized before adding the agonists of µOR (0.1 nM-10µM, 14 µl). After adding the test compounds, luminescence was continuously detected for 20-22 cycles. Solvent controls were run in all experiments.

Keywords: Dopamine D_2-like receptors • µ opioid receptor • Bivalent ligands • Ligand binding • Signal transduction

References:

[1] Agnati, L. F.; Fuxe, K.; Zini, I.; Lenzi, P.; Hökfelt, T. Aspects on receptor regulation and isoreceptor identification. *Med. Biol.* **1980**, *58*, 182–187.

[2] Fuxe, K.; Agnati, L. F.; Benfenati, F.; Cimmino, M.; Algeri, S.; Hökfelt, T.; Mutt, V. Modulation by cholecystokinins of 3H-spiroperidol binding in rat striatum: evidence for increased affinity and reduction in the number of binding sites. *Acta Physiol. Scand.* **1981**, *113*, 567–569.

[3] White, J. H.; Wise, A.; Main, M. J.; Green, A.; Fraser, N. J.; Disney, G.H.; Barnes, A. A.; Emson, P.; Foord, S. M.; Marshall, F. H. Heterodimerization is required for the formation of a functional GABA(B) receptor. *Nature*. **1998**, *396*, 679–682.

[4] Fuxe, K.; Marcellino, D.; Woods, A. S.; Giuseppina, L.; Antonelli, T.; Ferraro, L.; Tanganelli, S.; Agnati, L. F. Integrated signaling in heterodimers and receptor mosaics of different types of GPCRs of the forebrain: relevance for schizophrenia. *J. Neural. Transm. (Vienna)*. **2009**, *116*, 923–939.

[5] Milligan, G. The role of dimerisation in the cellular trafficking of G-protein-coupled receptors. *Curr. Opin. Pharmacol.* **2010**, *10*, 23–29.

[6] Daniels, D. J.; Lenard, N. R.; Etienne, C. L.; Law, P. Y.; Roerig, S. C.; Portoghese, P. S. Opioid-induced tolerance and dependence in mice is modulated by the distance between pharmacophores in a bivalent ligand series. *Proc. Natl. Acad. Sci. U S A.* **2005**, *102*, 19208–19213.

[7] Daniels, D. J.; Kulkarni, A.; Xie, Z.; Bhushan, R. G.; Portoghese, P. S. A bivalent ligand (KDAN-18) containing delta-antagonist and kappa-agonist pharmacophores bridges delta2 and kappa1 opioid receptor phenotypes. *J. Med. Chem.* **2005**, *48*, 1713–1716.

[8] Lenard, N. R.; Daniels, D. J.; Portoghese, P. S.; Roerig, S. C. Absence of conditioned place preference or reinstatement with bivalent ligands containing mu-opioid receptor agonist and delta-opioid receptor antagonist pharmacophores. *Eur. J. Pharmacol.* **2007**, *566*, 75–82.

[9] Milligan, G.; Bouvier, M. Methods to monitor the quaternary structure of G protein-coupled receptors. *FEBS J.* **2005**, *272*, 2914–2925.

[10] Yekkirala, A. S.; Lunzer, M. M.; McCurdy, C. R.; Powers, M. D.; Kalyuzhny, A. E.; Roerig, S. C.; Portoghese, P. S. N-naphthoyl-beta-naltrexamine (NNTA), a highly selective and potent activator of μ/kappa-opioid heteromers. *Proc. Natl. Acad. Sci. U S A.* **2011**, *108*, 5098–5103.

[11] Soriano, A.; Ventura, R.; Molero, A.; Hoen, R.; Casadó, V.; Cortés, A.; Fanelli, F.; Albericio, F.; Lluís, C.; Franco, R.; Royo, M. Adenosine A2A receptor-antagonist/dopamine D2 receptor-agonist

bivalent ligands as pharmacological tools to detect A2A-D2 receptor heteromers. *J. Med. Chem.* **2009**, *52*, 5590–5602.

[12] Jacobson, K. A.; Xie, R.; Young, L.; Chang, L.; Liang, B. T. A novel pharmacological approach to treating cardiac ischemia. Binary conjugates of A1 and A3 adenosine receptor agonists. *J. Biol. Chem.* **2000**, *275*, 30272–30279.

[13] Portoghese, P. S. From models to molecules: opioid receptor dimers, bivalent ligands, and selective opioid receptor probes. *J. Med. Chem.* **2001**, *44*, 2259–2269.

[14] Ambrose, L. M.; Unterwald, E. M.; Van Bockstaele, E. J. Ultrastructural evidence for co-localization of dopamine D2 and micro-opioid receptors in the rat dorsolateral striatum. *Anat. Rec. A Discov. Mol. Cell Evol. Biol.* **2004**, *279*, 583–591.

[15] Rivera, A.; Cuéllar, B.; Girón, F. J.; Grandy, D. K.; de la Calle, A.; Moratalla, R. Dopamine D4 receptors are heterogeneously distributed in the striosomes/matrix compartments of the striatum. *J. Neurochem.* **2002**, *80*, 219–229.

[16] Gago, B.; Suárez-Boomgaard, D.; Fuxe, K.; Brené, S.; Reina-Sánchez, M. D.; Rodríguez-Pérez, L. M.; Agnati, L. F.; de la Calle, A.; Rivera, A. Effect of acute and continuous morphine treatment on transcription factor expression in subregions of the rat caudate putamen. Marked modulation by D4 receptor activation. *Brain Res.* **2011**, *1407*, 47–61.

[17] Gago, B.; Fuxe, K.; Agnati, L.; Peñafiel, A.; De La Calle, A.; Rivera, A. Dopamine D(4) receptor activation decreases the expression of mu-opioid receptors in the rat striatum. *J. Comp. Neurol.* **2007**, *502*, 358–366.

[18] Hagelberg, N.; Kajander, J. K.; Någren, K.; Hinkka, S.; Hietala, J.; Scheinin, H. Mu-receptor agonism with alfentanil increases striatal dopamine D2 receptor binding in man. *Synapse*. **2002**, *45*, 25–30.

[19] Park, Y.; Ho, I. K.; Fan, L. W.; Loh, H. H.; Ko, K. H. Region specific increase of dopamine receptor D1/D2 mRNA expression in the brain of mu-opioid receptor knockout mice. *Brain Res.* **2001**, *894*, 311–315.

[20] Kühhorn, J.; Hübner, H.; Gmeiner, P. Bivalent dopamine D2 receptor ligands: synthesis and binding properties. *J. Med. Chem.* **2011**, *54*, 4896–4903.

[21] Gogoi, S.; Biswas, S.; Modi, G.; Antonio, T.; Reith, M. E.; Dutta, A. K. Novel bivalent ligands for D2/D3 dopamine receptors: Significant co-operative gain in D2 affinity and potency. *ACS Med. Chem. Lett.* **2012**, *3*, 991–996.

[22] Cami-Kobeci, G.; Neal, A. P.; Bradbury, F. A.; Purington, L. C.; Aceto, M. D.; Harris, L. S.; Lewis, J. W.; Traynor, J. R.; Husbands, S. M. Mixed kappa/mu opioid receptor agonists: the 6 beta-naltrexamines. *J. Med. Chem.* **2009**, *52*, 1546–1552.

[23] Ghirmai, S.; Azar, M. R.; Polgar, W. E.; Berzetei-Gurske, I.; Cashman, J. R. Synthesis and biological evaluation of alpha- and beta-6-amido derivatives of 17-cyclopropylmethyl-3, 14beta-dihydroxy-4, 5alpha-epoxymorphinan: potential alcohol-cessation agents. *J. Med. Chem.* **2008**, *51*, 1913-1924.

[24] Wan, Z.; Li , Y.; Bo, S.; Gao, M.; Wang, X.; Zeng, K.; Tao, X.; Li, X.; Yang, Z.; Jiang, Z. X. Amide bond-containing monodisperse polyethylene glycols beyond 10 000 Da. *Org. Biomol. Chem.* **2016**, *14*, 7912-7919.

[25] Bondia, A. M.; Larcher, N.; Garrelly, L.; Rossi, J. C.; Pascal, R. Synthesis and ligation ability of mono-aminooxy-functionalized dendrigraft poly-l-lysine (DGL). *Tetrahedron Lett.* **2010**, *51*, 3330-3333.

[26] Abronina, P. I.; Zinin, A. I.; Orlova, A. V.; Sedinkin, S. L.; Kononov, L. O. An easy access to asymmetrically substituted oligoethylene glycols from 18-crown-6. *Tetrahedron Lett.* **2013**, *54*, 4533-4535.

[27] Van Wieringen, J. P.; Michel, M. C. [^{3}H]-Spiperone Competition Binding to Dopamine D_2, D_3 and D_4 Receptors. **2013**. Available at: DOI: https://doi.org/10.21769/BioProtoc.944.

[28] Van Craenenbroeck, K.; Clark, S. D.; Cox, M. J.; Oak, J. N.; Liu, F.; Van Tol, H. H. Folding efficiency is rate-limiting in dopamine D4 receptor biogenesis. *J. Biol. Chem.* **2005**, *280*, 19350-19357.

[29] Pearson, G.; Robinson, F.; Beers Gibson, T.; Xu, B. E.; Karandikar, M.; Berman, K.; Cobb, M. H. Mitogen-activated protein (MAP) kinase pathways: regulation and physiological functions. *Endocr. Rev.* **2001**, *22*, 153-183.

[30] Skieterska, K.; Rondou, P.; Lintermans, B.; Van Craenenbroeck, K. KLHL12 Promotes Non-Lysine Ubiquitination of the Dopamine Receptors D4.2 and D4.4, but Not of the ADHD-Associated D4.7 Variant. *PLoS One*. **2015**, *10*, e0145654.

[31] Dixon, A. S.; Schwinn, M. K.; Hall, M. P.; Zimmerman, K.; Otto, P.; Lubben, T. H.; Butler, B. L.; Binkowski, B. F.; Machleidt, T.; Kirkland, T. A.; Wood, M. G.; Eggers, C. T.; Encell, L. P.; Wood, K. V. NanoLuc Complementation Reporter Optimized for Accurate Measurement of Protein Interactions in Cells. *ACS Chem. Biol.* **2016**, *11*, 400-408.

[32] Cannaert, A.; Storme, J.; Franz, F.; Auwärter, V.; Stove, C. P. Detection and Activity Profiling of Synthetic Cannabinoids and Their Metabolites with a Newly Developed Bioassay. *Anal. Chem.* **2016**, *88*, 11476-11485.

[33] Groer, C. E.; Tidgewell, K.; Moyer, R. A.; Harding, W. W.; Rothman, R. B.; Prisinzano, T. E.; Bohn, L. M. An opioid agonist that does not induce mu-opioid receptor--arrestin interactions or receptor internalization. *Mol. Pharmacol.* **2007**, *71*, 549-557.

[34] Groer, C. E.; Schmid, C. L.; Jaeger, A. M.; Bohn, L. M. Agonist-directed interactions with specific beta-arrestins determine mu-opioid receptor trafficking, ubiquitination, and dephosphorylation. *J. Biol. Chem.* **2011**, *286*, 31731-31741.

[35] Zhang, J.; Ferguson, S. S. ; Barak, L. S.; Bodduluri, S. R.; Laporte, S. A.; Law, P. Y.; Caron, M. G. Role for G protein-coupled receptor kinase in agonist-specific regulation of mu-opioid receptor responsiveness. *Proc. Natl. Acad. Sci. U S A.* **1998**, *95*, 7157-7162.

[36] Le Naour, M.; Akgün, E.; Yekkirala, A.; Lunzer, M. M.; Powers, M. D.; Kalyuzhny, A. E.; Portoghese, P. S. Bivalent ligands that target μ opioid (MOP) and cannabinoid1 (CB1) receptors are potent analgesics devoid of tolerance. *J. Med. Chem.* **2013**, *56*, 5505-5513.

[37] Corriden, R.; Kilpatrick, L. E.; Kellam, B.; Briddon, S. J.; Hill, S. J. Kinetic analysis of antagonist-occupied adenosine-A3 receptors within membrane microdomains of individual cells provides evidence of receptor dimerization and allosterism. *FASEB J.* **2014**, *28*, 4211-4222.

[38] Rondou, P.; Haegeman, G.; Vanhoenacker, P.; Van Craenenbroeck, K. BTB Protein KLHL12 targets the dopamine D4 receptor for ubiquitination by a Cul3-based E3 ligase. *J. Biol. Chem.* **2008**, *283*, 11083-11096.

[39] Kiss, B.; Horti, F.; Bobok, A. In vitro and in vivo comparison of [^{3}H](+)-PHNO and [^{3}H]raclopride binding to rat striatum and lobes 9 and 10 of the cerebellum: a method to distinguish dopamine D_3 from D_2 receptor sites. *Synapse.* **2011**, *65*, 467-478.

[40] Wang, D.; Sun, X.; Sadee, W. Different effects of opioid antagonists on mu-, delta-, and kappa-opioid receptors with and without agonist pretreatment. *J. Pharmacol. Exp. Ther.* **2007**, *321*, 544-552.

[41] Cheng, Y.; Prusoff, W. H. Relationship between the inhibition constant (K1) and the concentration of inhibitor which causes 50 per cent inhibition (I50) of an enzymatic reaction. *Biochem. Pharmacol.* **1973**, *22*, 3099-3108.

[42] Skieterska, K.; Duchou, J.; Lintermans, B.; Van Craenenbroeck, K. Detection of G protein-coupled receptor (GPCR) dimerization by coimmunoprecipitation. *Methods Cell Biol.* **2013**, *117*, 323-340.

[43] Hübner, H.; Schellhorn, T.; Gienger, M.; Schaab, C.; Kaindl, J.; Leeb, T. Clark, L.; Möller, D.; Gmeiner, P. Structure-guided development of heterodimer-selective GPCR ligands. *Nat. Commun.* **2016**, *7*, 12298.

III.7. Supporting information (SI)

Table of contents

MAPK-P for D_2R S1

Interaction of μOR with β-arrestin2 S2

Ligand binding with [^{3}H]raclopride S3

Ligand binding with [^{3}H]DAMGO S4

Immunoflurescence microscopy for μOR-D_2R S5

Immunoflurescence microscopy for μOR-D_4R S6

Chromatographic analyses for bivalent ligands S7

NMR spectra S8

S1

MAPK-P for D_2R

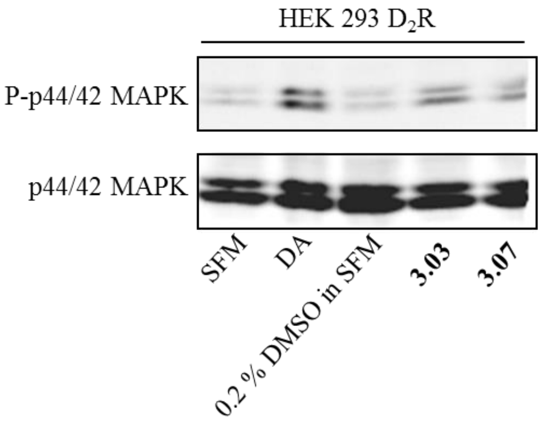

Figure 1. Stimulation of MAPK phosphorylation upon D_2R agonist treatment, as determined by immunoblotting assays. Cells were treated with serum-free media (SFM) for 12 h. Next, D_2-likeR agonists (10 µM), SFM or vehicle control were added for 5 min. Cells were washed and lysed as explained in the Experimental section. Phosphorylated MAPK was detected by immunoblotting using rabbit anti-phospho-p44/42 MAPK antibody and mouse anti-p44/42 MAPK antibody was used for demonstrating equal protein loading. The results shown are representative of three independent experiments. DA=dopamine.

S2

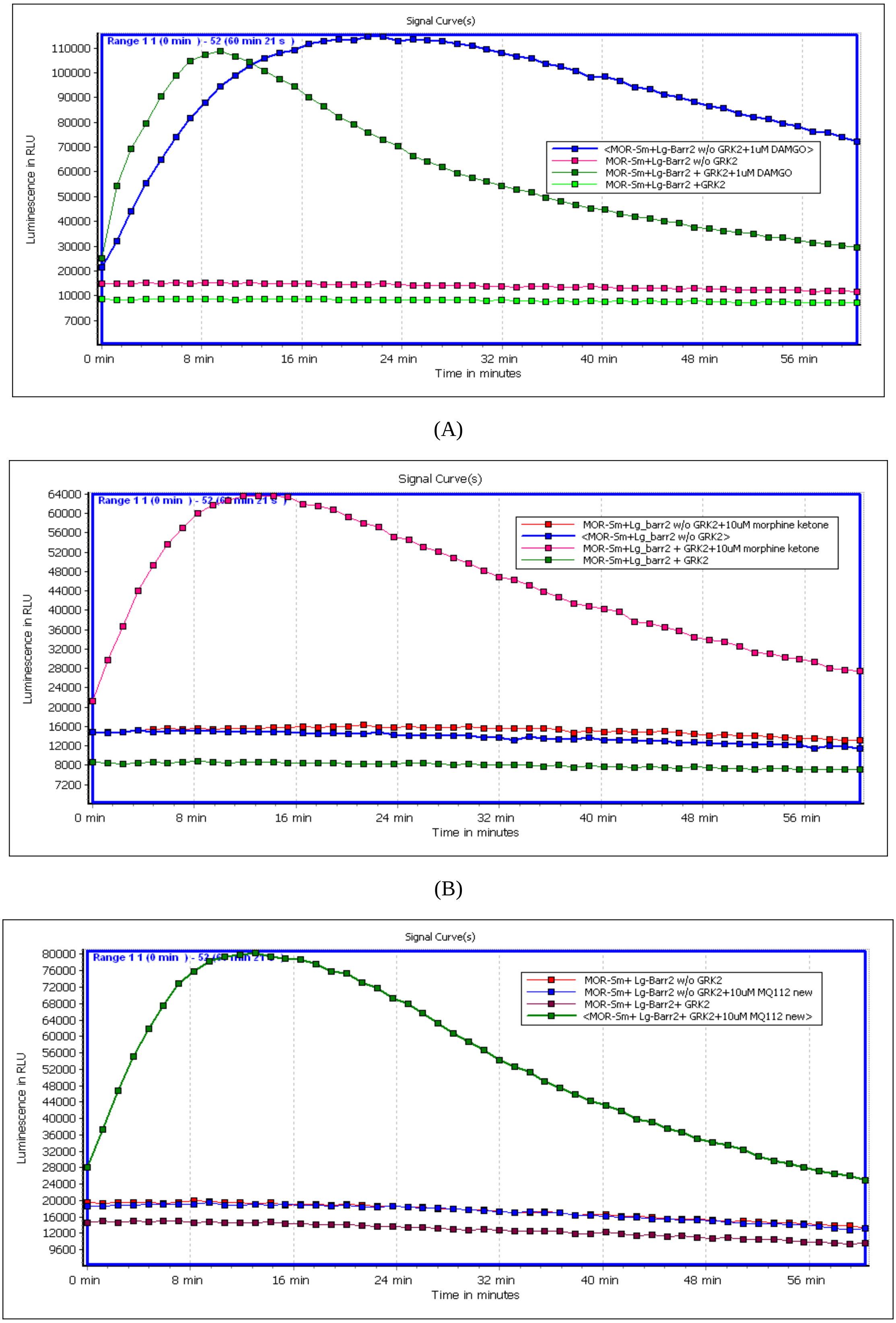

(A)

(B)

(C)

Figure 2. Interaction of μOR with β-arrestin2 upon stimulation with DAMGO (A), Hydromorphone (morphine ketone, B) or **3.13f** (MQ112, C) with or without overexpression of GRK2.

S3

Saturation assay for [^{3}H]raclopride

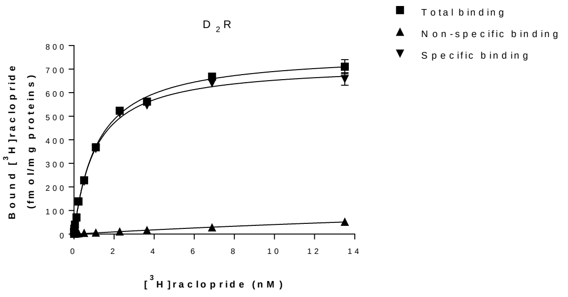

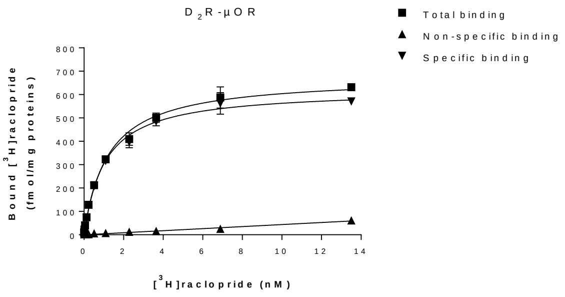

Entry	Bmax fmol/mg	Kd nM
D$_2$R	722.7 ± 9.7	1.07 ± 0.05
D$_2$R-μOR	621.9 ± 14.1	1.05 ± 0.08

All values are expressed as the mean ± SEM of three independent assays performed in duplicate.

Binding affinities for D$_2$R and D$_2$R-μOR

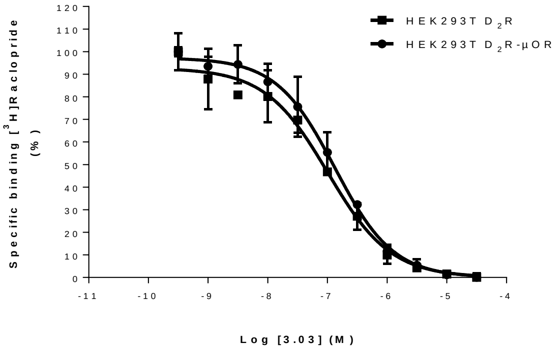

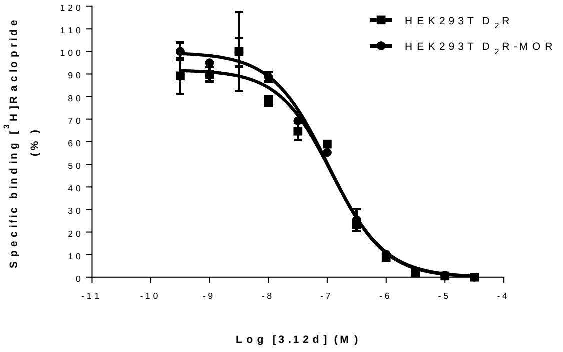

Binding curves were obtained by competitive displacement of radiolabeled [^{3}H]raclopride binding to HEK293T D$_2$R and HEK293T D$_2$R-μOR intact cells. Data are expressed as the mean ± SEM of at least two independent assays.

S4

Saturation assay for µOR with [^{3}H]DAMGO

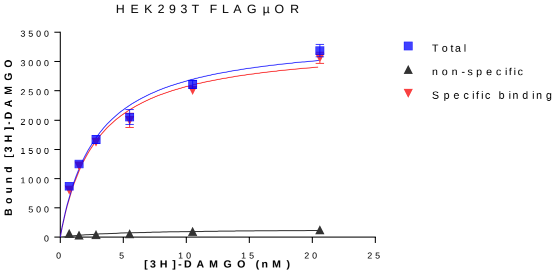

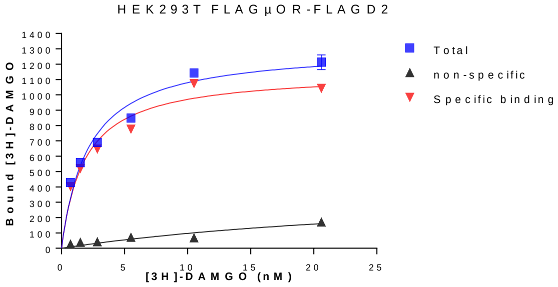

Entry	Bmax fmol/mg	K_d nM
µOR	3315 ± 139	2.6 ± 0.3
µOR-D_2R	1148 ± 54	1.8 ± 0.2

Binding affinities (K_i) for µOR and D_2R-µOR

Compound	K_i (nM) for µOR	K_i (nM) for D_2R-µOR
diprenorphine	0.16 ± 0.15	0.21 ± 0.11
3.13e	4.5 ± 1.7	4.8 ± 2.9

Binding affinities (K_i) were obtained by competitive displacement of radiolabeled [^{3}H]DAMGO binding to HEK293T µOR and HEK293T D_2R-µOR cells membrane. All values are expressed as the mean ± SEM of two independent assays performed in duplicate.

S5

Immunoflurescence microscopy

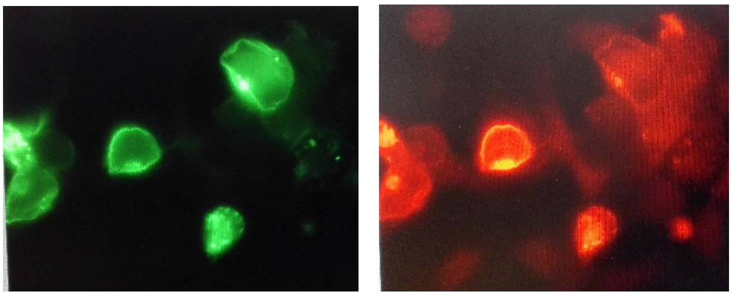

μOR D$_2$R

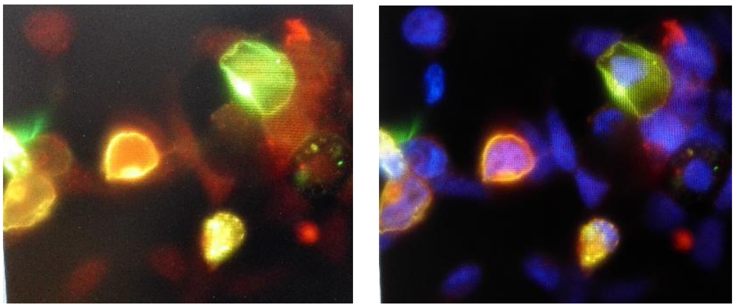

μOR-D$_2$R DAPI

Figure 3. Expression of D$_2$R and μOR on cell membrane. HEK293T cells were seeded in 6-well plate with coverslips and transfected with FLAG-μOR and HAD$_2$R in a 2:1 ratio. After 48 h post-transfection, cells were fixed, permeabilized and labeled with rabbit anti-HA and mouse anti-FLAG. Finally, cells were incubated with fluorescent secondary antibodies, anti-mouse Alexa Fluor 488 and anti-rabbit Alexa Fluor 594. μOR and D$_2$R are visualized in green and red, respectively and μOR-D$_2$R in the overlay picture. The results shown are representative of three independent experiments.

S6

HEK293T transiently transfected HA D$_4$R and FLAG-µOR (1:2)

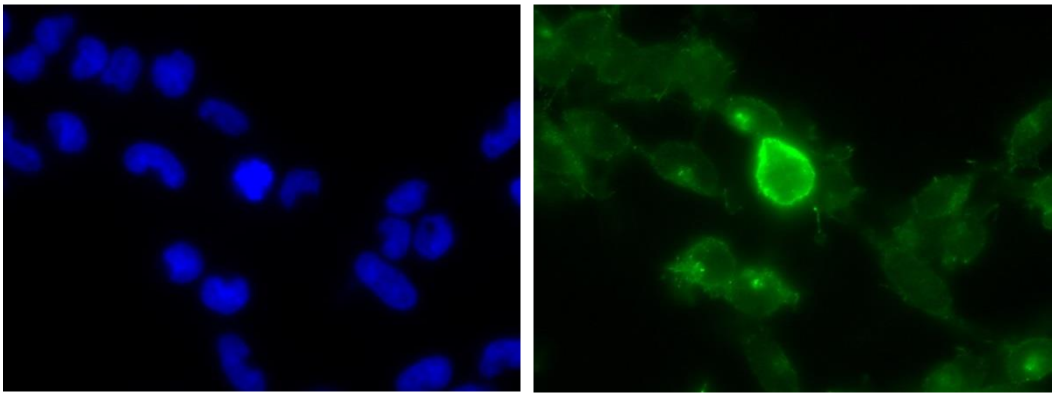

DAPI µOR

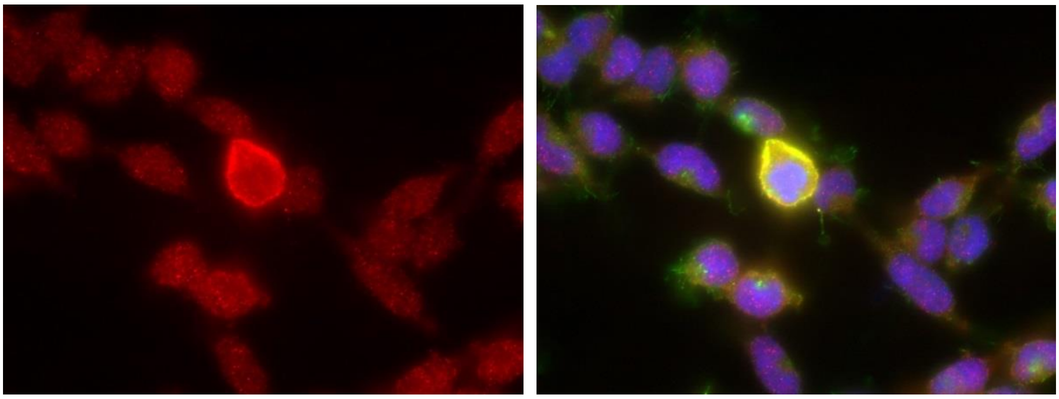

D$_4$R µOR-D$_4$R

Figure 4. Expression of D$_4$R and µOR on cell membrane. HEK293T cells were seeded in 6-well plate with coverslips and transfected with FLAG-µOR and HAD$_4$R in a 2:1 ratio. After 48 h post-transfection, cells were fixed, permeabilized and labeled with rabbit anti-HA and mouse anti-FLAG. Finally, cells were incubated with fluorescent secondary antibodies, anti-mouse Alexa Fluor 488 and anti-rabbit Alexa Fluor 594. µOR and D$_4$R are visualized in green and red, respectively and µOR-D$_4$R in the overlay picture. The results shown are representative of three independent experiments.

S7

Chromatographic analyses

Chromatographic analysis of representative bivalent ligands.[1] LC-MS analyses were carried out on a Waters Alliance 2695 XE separation Module by using a Phenomenex Kinetex EVO C18, 5μm 100x2.1mm and a gradient system of HCOOH in H_2O (0.1 %, v/v)/HCOOH in MeCN (0.1%, v/v) at a flow rate of 0.6 mLmin^{-1}, 100:0 to 0:100 (0 to 100 % MeCN) in 15 minutes. High-resolution spectra were recorded on a Waters LCT Premier XE Mass spectrometer and a 2996 Photodiode Array Detector, range 220 nm-400 nm.

Blank

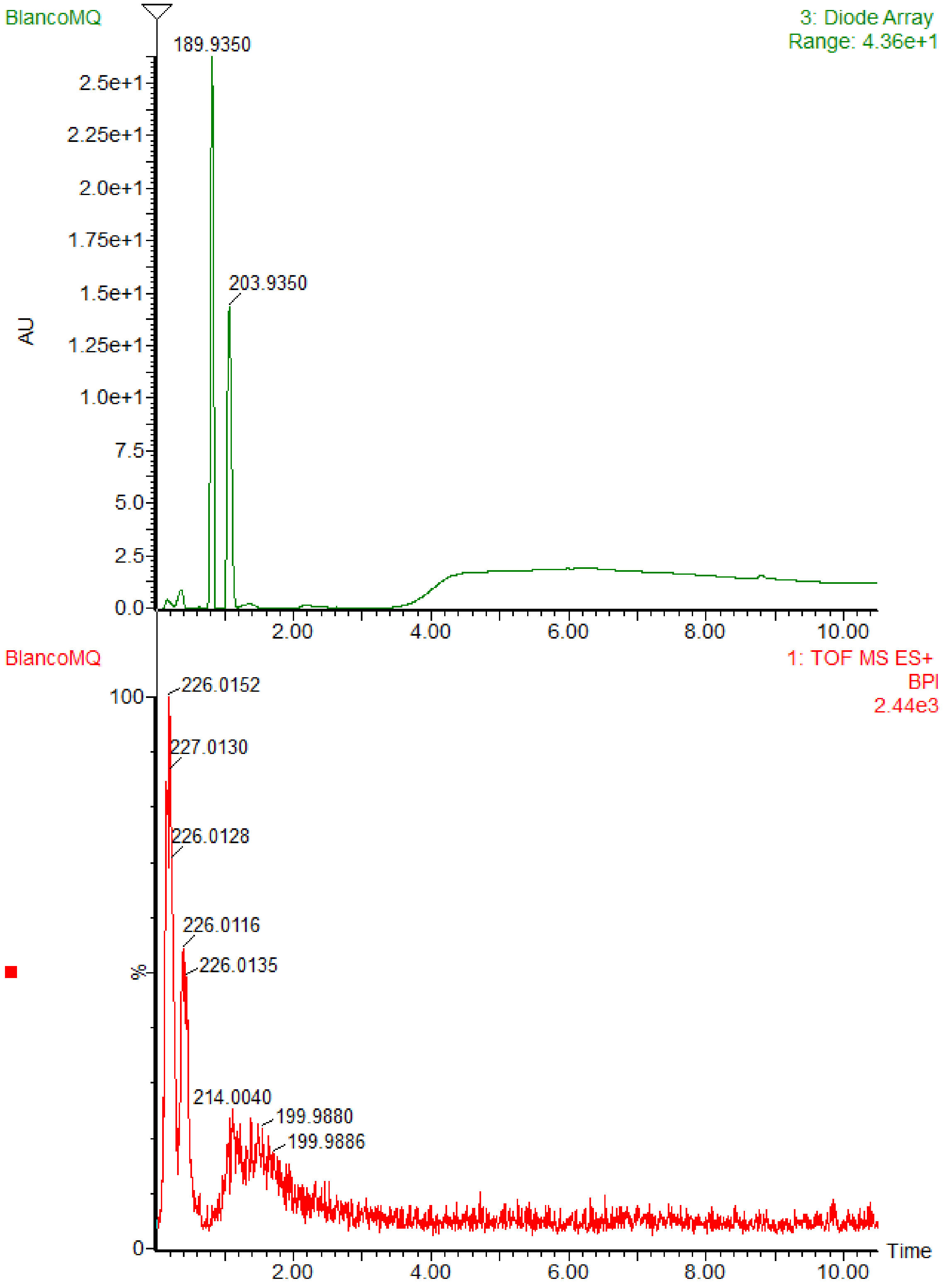
BlancoMQ
3: Diode Array
Range: 4.36e+1
189.9350
203.9350
AU
2.5e+1
2.25e+1
2.0e+1
1.75e+1
1.5e+1
1.25e+1
1.0e+1
7.5
5.0
2.5
0.0
2.00
4.00
6.00
8.00
10.00
BlancoMQ
1: TOF MS ES+
BPI
2.44e3
100
226.0152
227.0130
226.0128
226.0116
226.0135
%
214.0040
199.9880
199.9886
0
2.00
4.00
6.00
8.00
10.00
Time

Compound **3.12a**

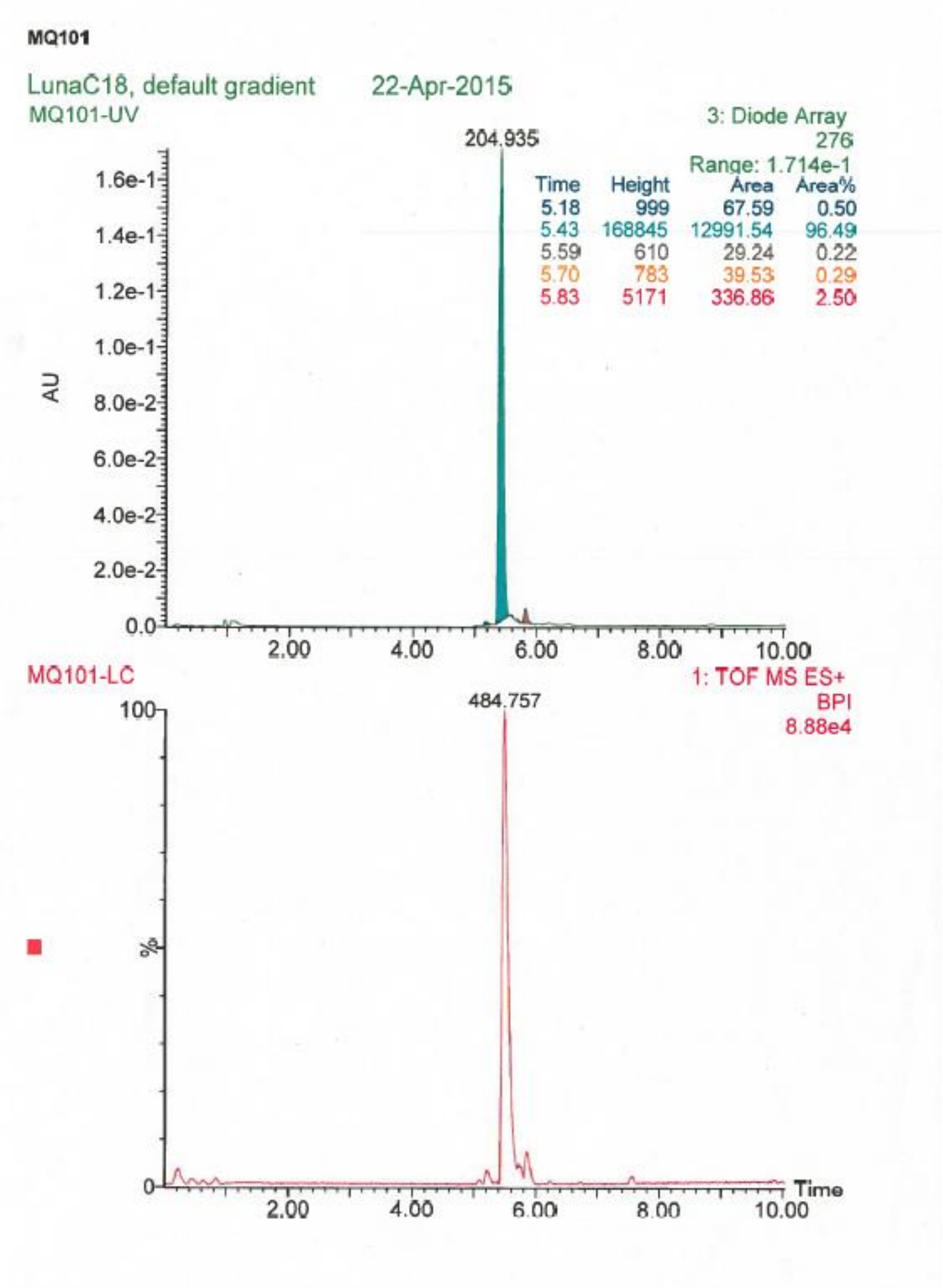

MQ101

LunaC18, default gradient 22-Apr-2015

MQ101-UV

3: Diode Array
276
Range: 1.714e-1

Time	Height	Area	Area%
5.18	999	67.59	0.50
5.43	168845	12991.54	96.49
5.59	610	29.24	0.22
5.70	783	39.53	0.29
5.83	5171	336.86	2.50

MQ101-LC

1: TOF MS ES+
BPI
8.88e4

Compound **3.12d**

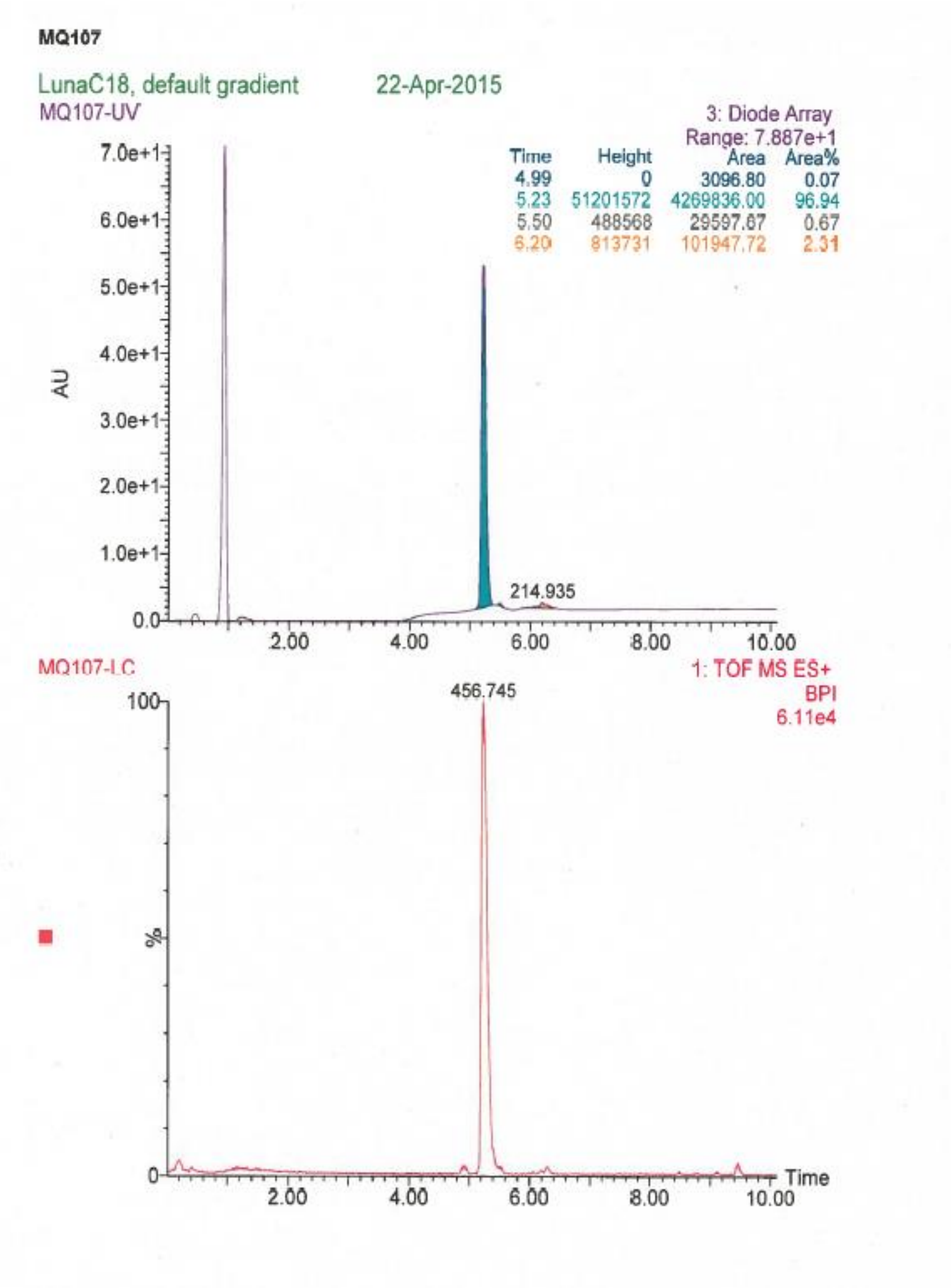

MQ107

LunaC18, default gradient 22-Apr-2015

MQ107-UV

3: Diode Array
Range: 7.887e+1

Time	Height	Area	Area%
4.99	0	3096.80	0.07
5.23	51201572	4269836.00	96.94
5.50	488568	29597.67	0.67
6.20	813731	101947.72	2.31

Compound **3.13a**

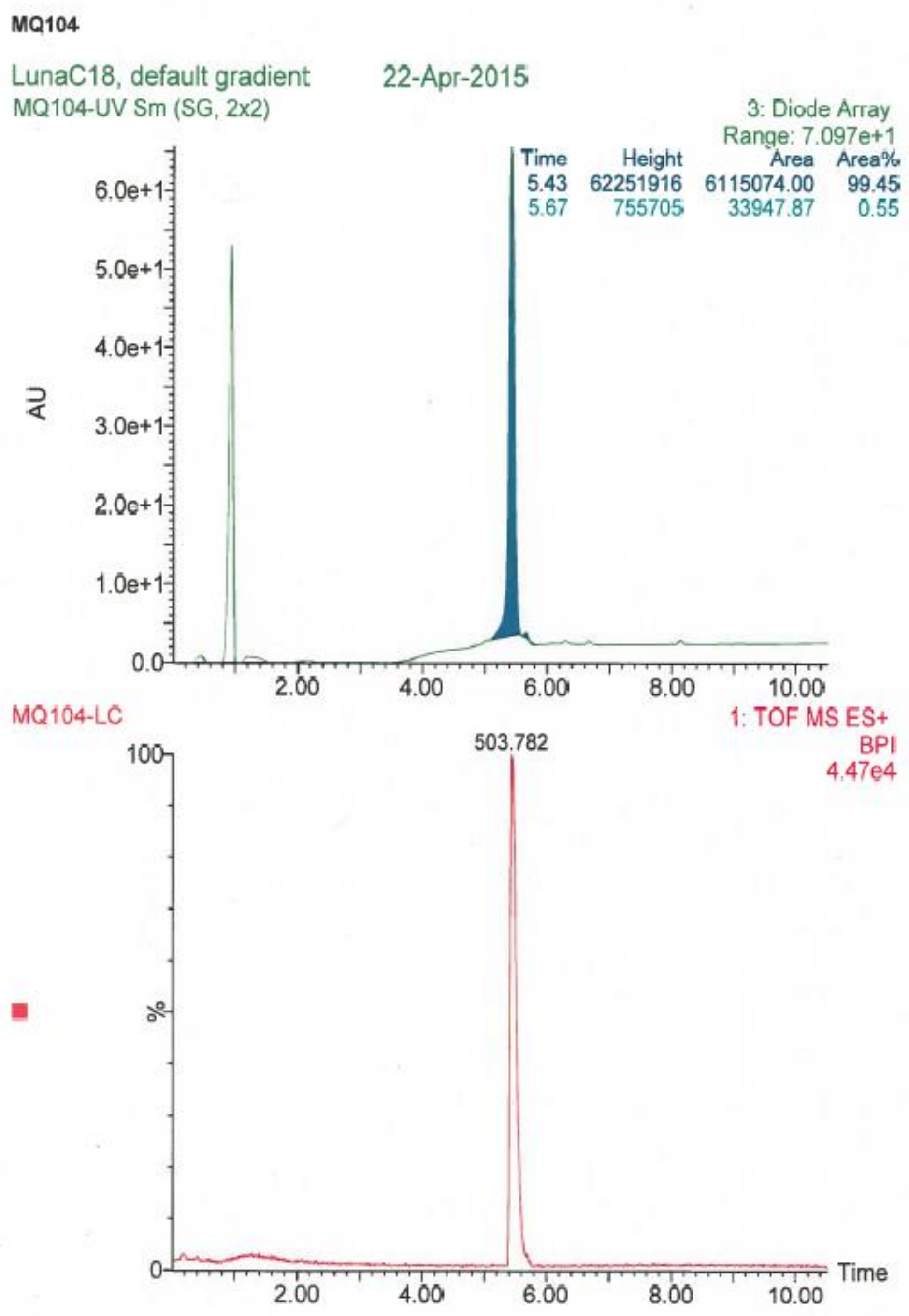

Time	Height	Area	Area%
5.43	62251916	6115074.00	99.45
5.67	755705	33947.87	0.55

Compound **3.13d**

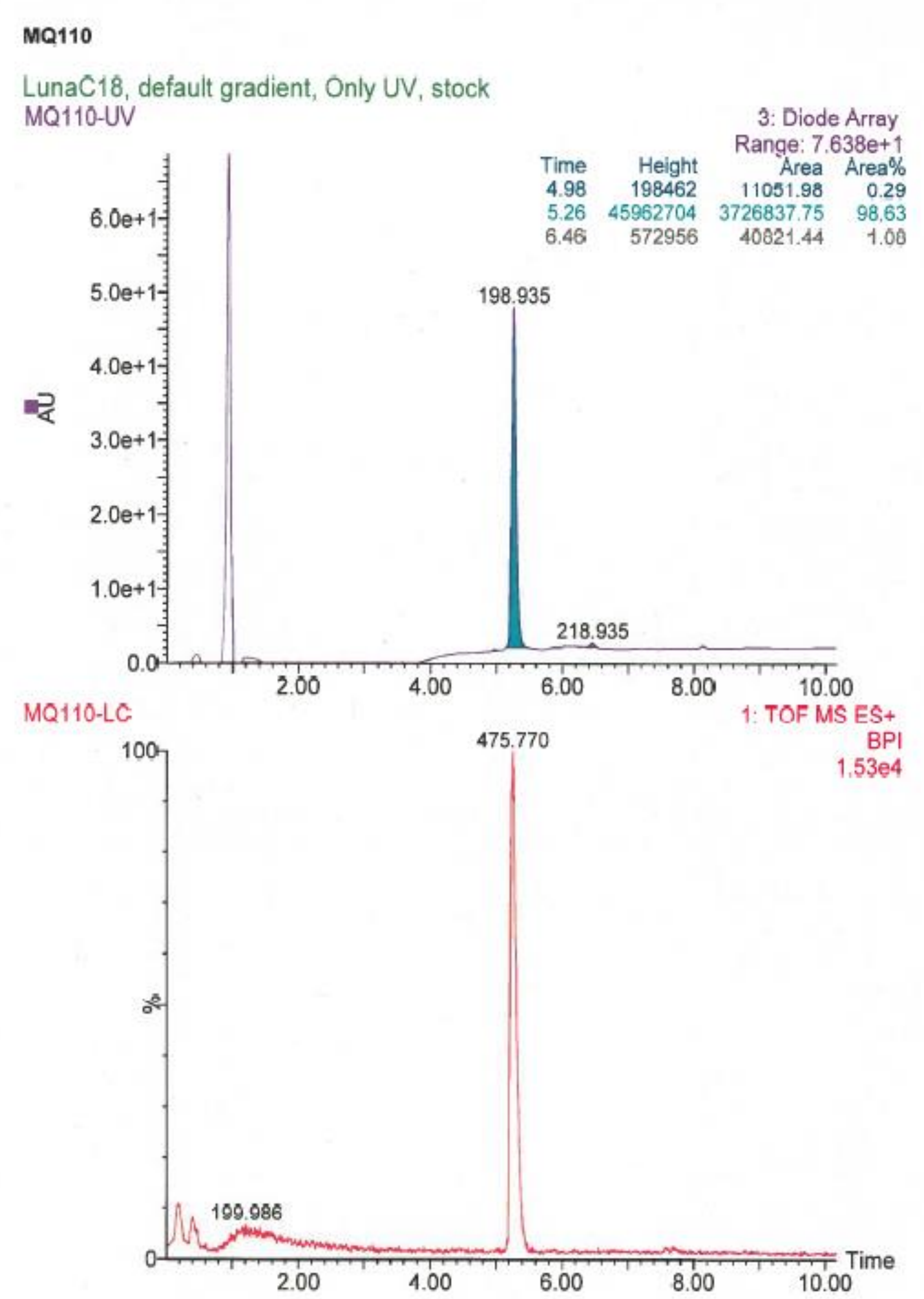

Time	Height	Area	Area%
4.98	198462	11051.98	0.29
5.26	45962704	3726837.75	98.63
6.46	572956	40821.44	1.08

S8

NMR spectra

For a representative selection of compounds described in this paper (**3.12a**, **3.12d**, **3.13a**, **3.13d**), the ^{1}H NMR and ^{13}C NMR spectra are given below.[1]

Compound **3.12a**

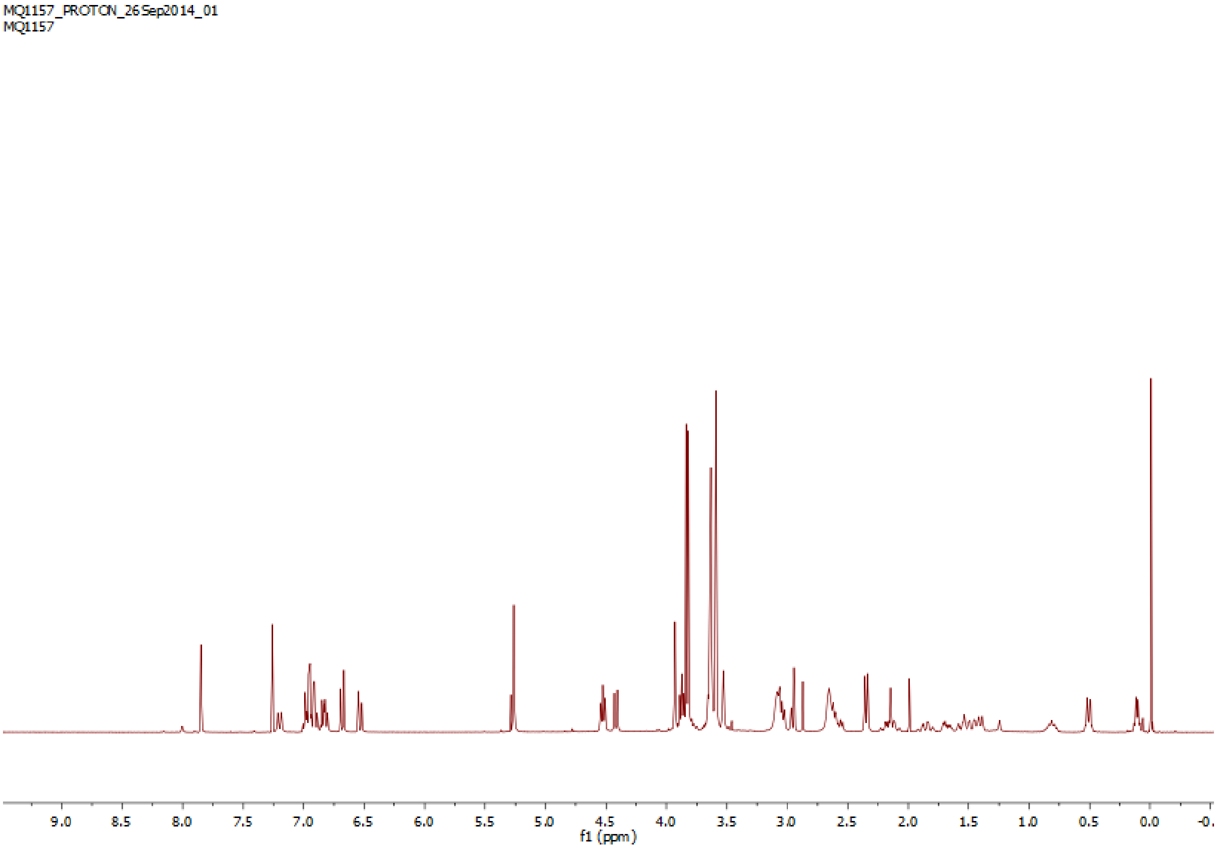

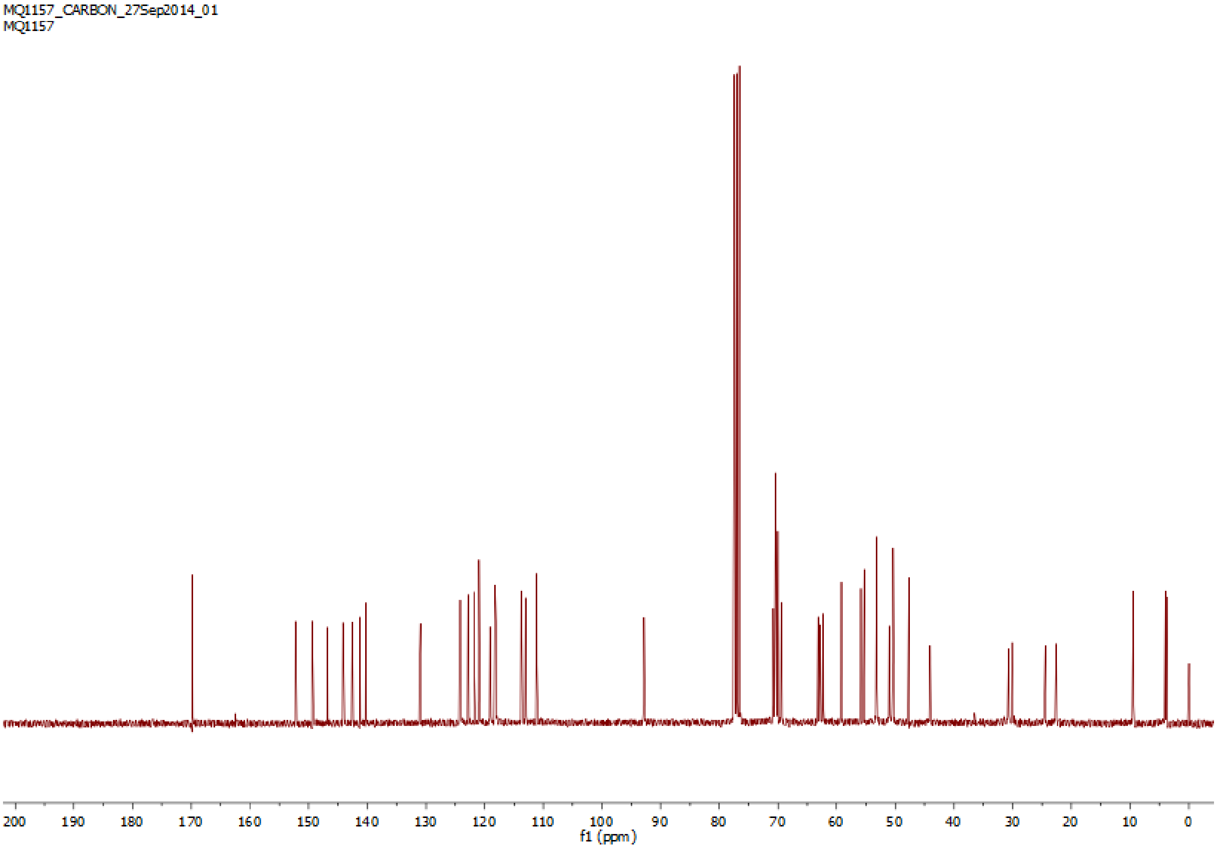

Compound **3.12d**

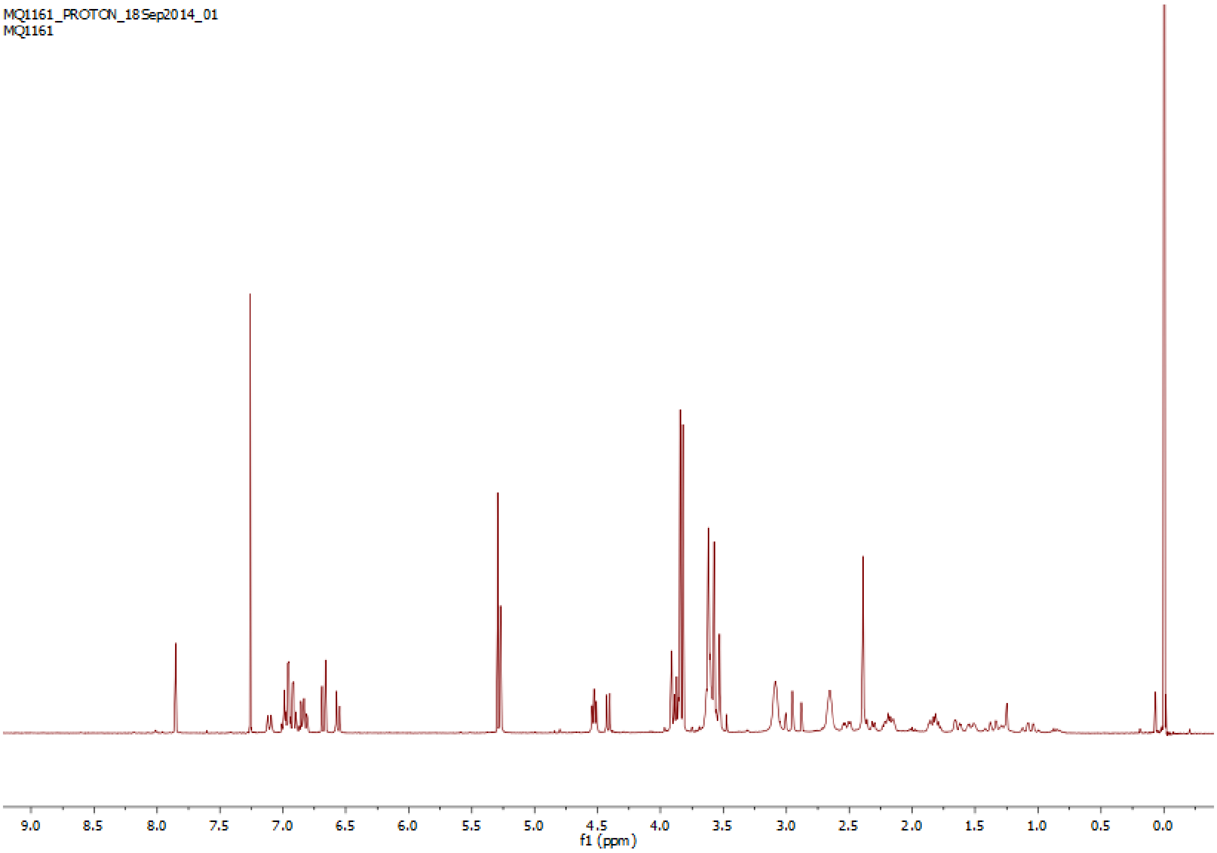

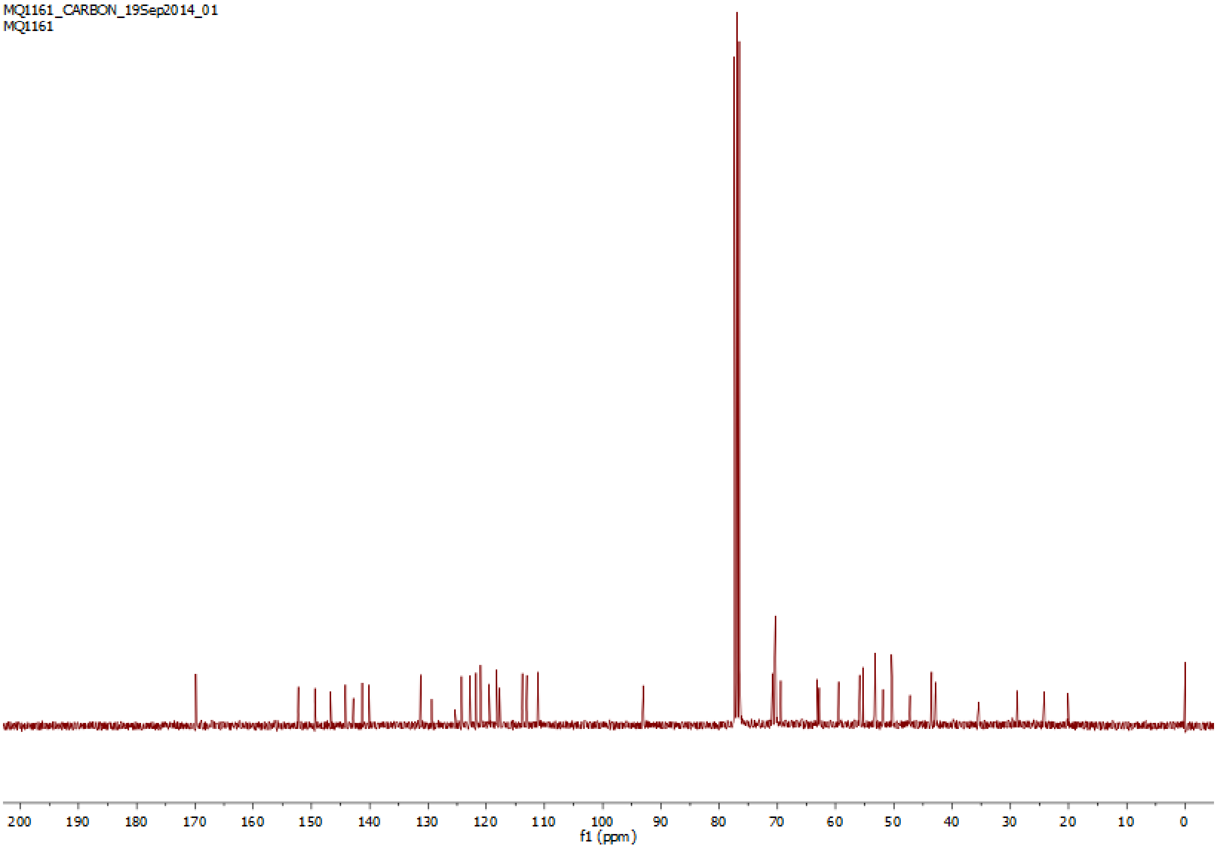

Compound **3.13a**

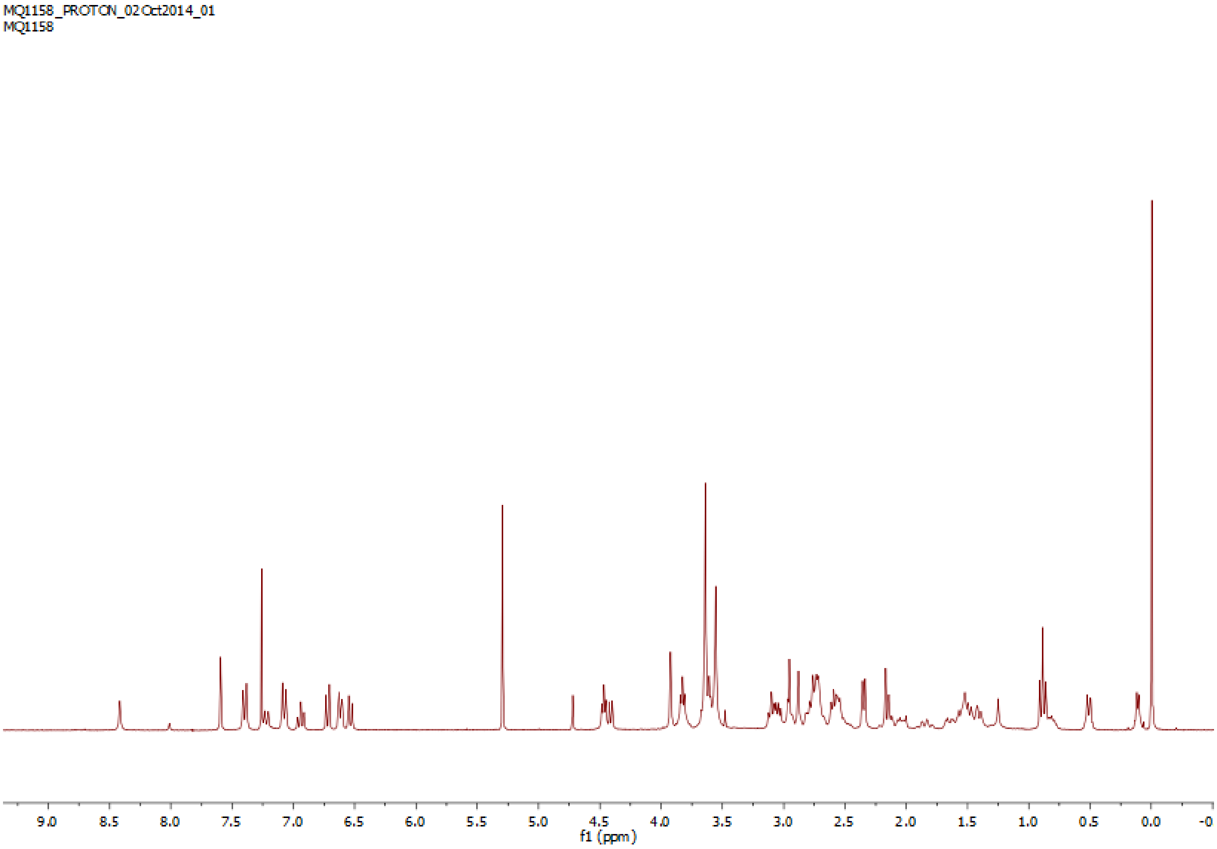

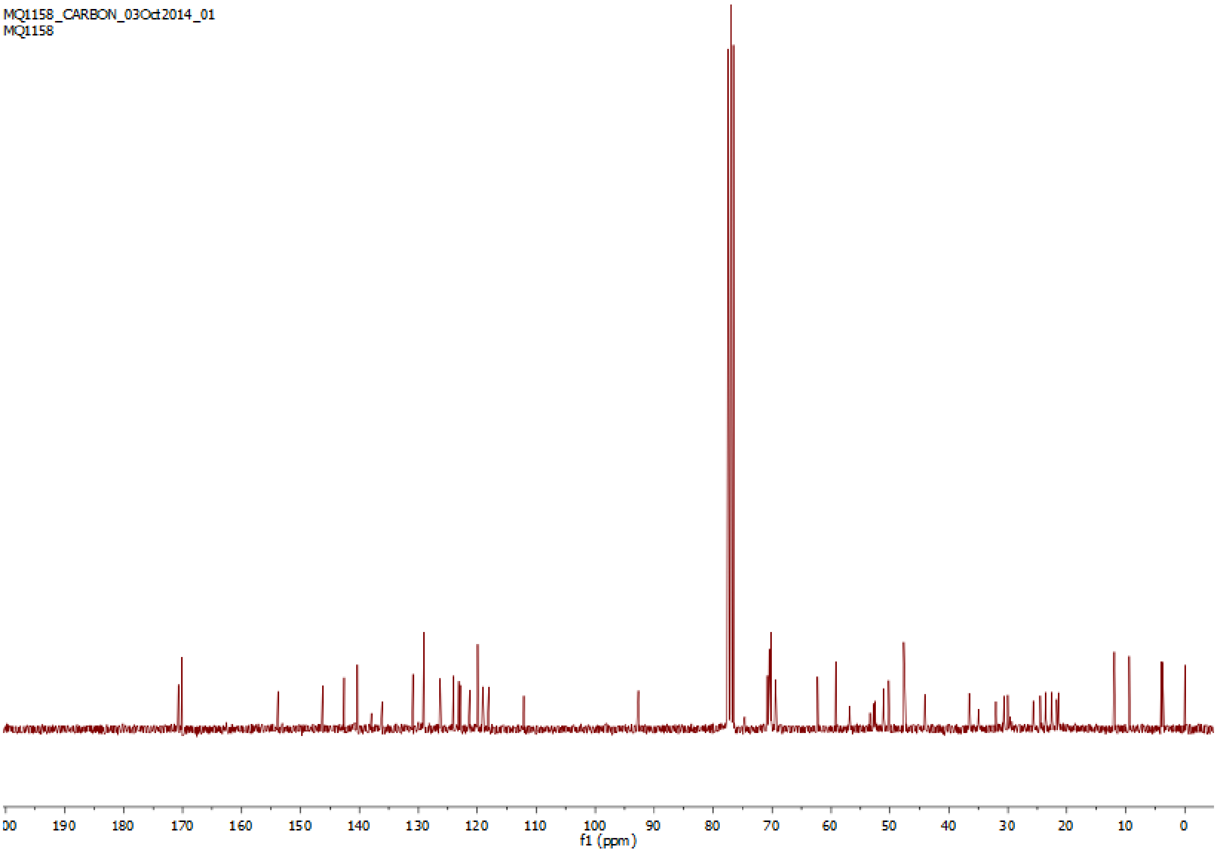

Compound **3.13d**

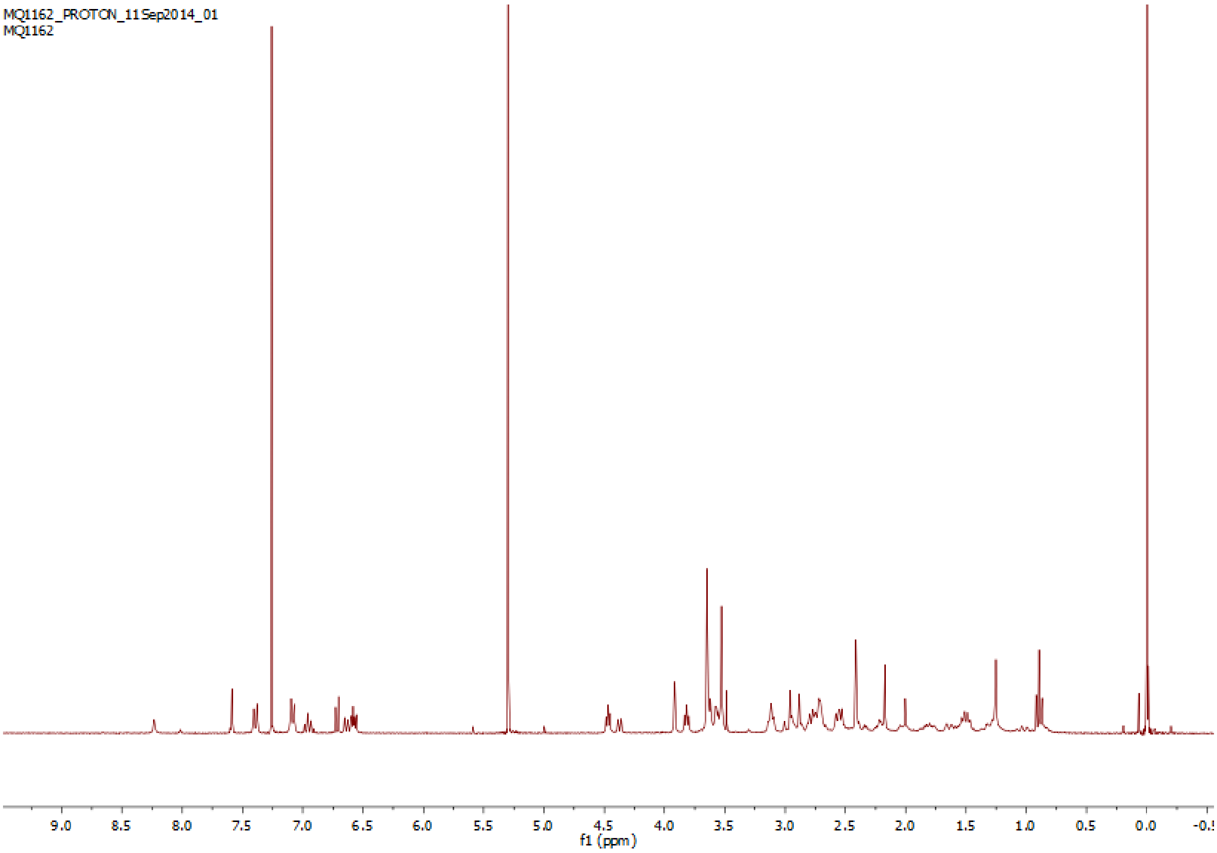

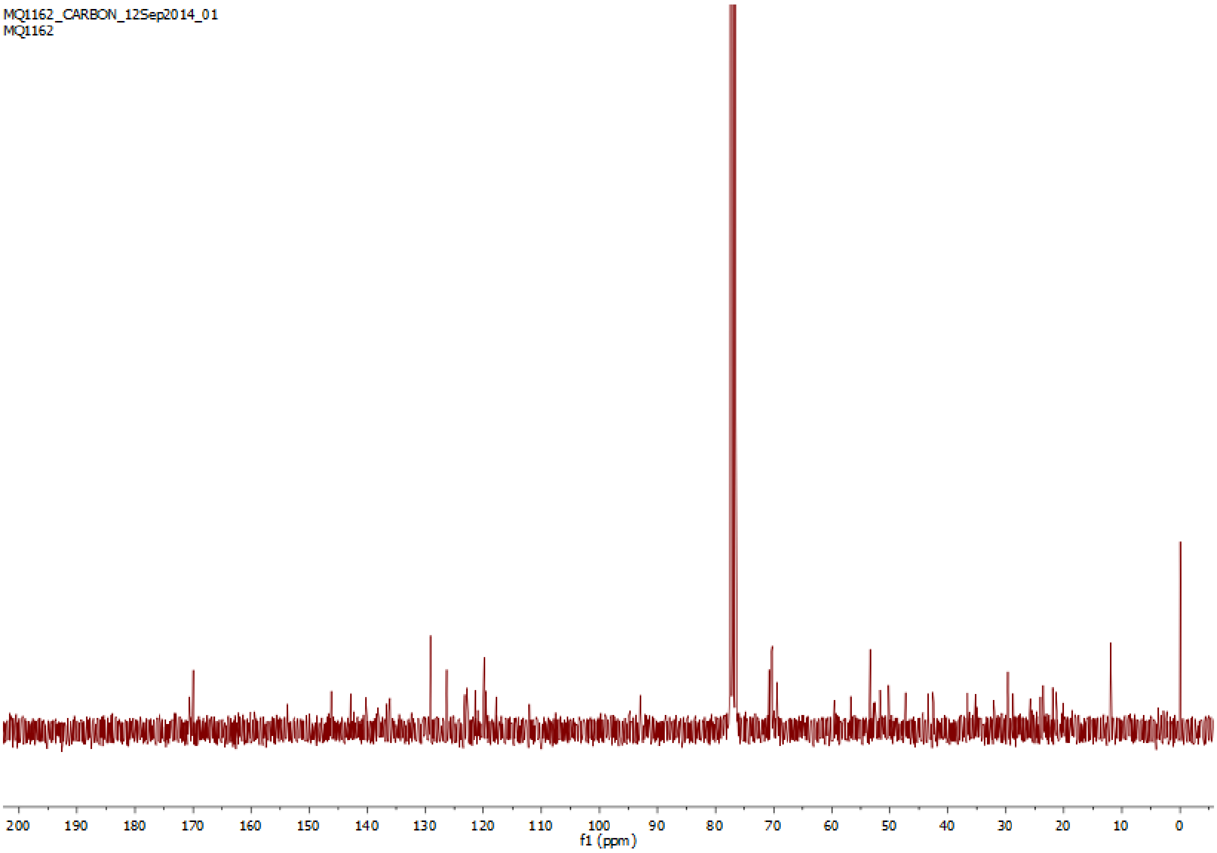

References

[1] Qian, M.; Vasudevan, L.; Huysentruyt, J.; Risseeuw, M. D. P.; Stove, C.; Vanderheyden, P. M. L.; Van Craenenbroeck, K.; Van Calenbergh, S. Design, synthesis and biological evaluation of bivalent ligands targeting dopamine D_2-like receptors and the μ-opioid receptor. *ChemMedChem* **2018**, *13*, 944 – 956.

CHAPTER IV

Synthesis toward bivalent ligands for the dopamine D_2 and metabotropic glutamate 5 receptors

The content of this chapter was partially derived from:

Qian, M.; Wouters, E.; Dalton, J. A. R.; Risseeuw, M. D. P.; Crans, R. A. J.; Stove, C.; Giraldo, J.; Van Craenenbroeck, K.; Van Calenbergh, S. *J. Med. Chem.* **2018**, *61*, 8212−8225.

Ligand binding assays for D_2R were performed with the help of Elise Wouters. The cAMP assays were performed by Elise Wouters. Molecular docking study was carried out by James Dalton under supervision of Jésus Giraldo (Universitat Autònoma de Barcelona).

IV. SYNTHESIS TOWARD BIVALENT LIGANDS FOR THE DOPAMINE D2 AND METABOTROPIC GLUTAMATE 5 RECEPTORS

IV.1. ABSTRACT

Recently, the existence of heteromers consisting of the metabotropic glutamate 5 receptor (mGluR5) and the dopamine D_2 receptor (D_2R) has been demonstrated in living cells and native tissue. This study describes the design and synthesis of heterobivalent ligands targeting this heterodimer and their evaluation via ligand binding and functional assays. Bivalent ligand **4.20a** with a linker consisting of 20 atoms showed 4-fold increase in affinity for cells coexpressing D_2R and mGluR5 compared to cells solely expressing D_2R. Likewise, the affinity of **4.20a** for mGluR5 increased 2-fold in cells in which both receptors were coexpressed. Additionally, **4.20a** exhibited a 5-fold higher mGluR5 affinity than its monovalent precursor **4.19a** in cells coexpressing D_2R and mGluR5. These binding results indicate that **4.20a** is able to bridge binding sites on both receptors constituting the heterodimer. Furthermore, **4.20a** showed about 4-fold and 7-fold higher potency in MAPK phosphorylation in stable cell lines coexpressing D_2R and mGluR5 compared to monovalent ligands **3.07** and **4.19a**, respectively. Likewise, cAMP assays revealed that **4.20a** had a 4-fold higher potency than **3.07** in the coexpressing cells. Furthermore, molecular modeling reveals that **4.20a** is able to simultaneously bind both receptors by passing between the TM5-TM6 interface and establishing six protein-ligand H-bonds. The above mentioned affinity, functional data and docking study suggest that **4.20a** holds promise to further study the interactions between D_2R and mGluR5.

IV.2. Introduction

The metabotropic glutamate receptors (mGluRs) constitute a family of G protein-coupled receptors (GPCR) characterized by the presence of large, extracellular, N-terminal orthosteric binding domains, which are activated by L-glutamate.[1],[2],[3] Based on sequence homology, receptor pharmacology and signal transduction pathways the eight mGluR subtypes are divided into three groups (Group I, II, and III).

Group I mGluRs (mGluR1 and mGluR5) are mainly localized postsynaptically and are extensively distributed in many brain regions, including the hippocampus, thalamic nuclei, and spinal cord. Stimulation of Gq protein coupled mGluR1 and mGluR5 leads to phosphoinositide (PI) hydrolysis and formation of the intracellular second messengers inositol triphosphate (IP3), which induces intracellular Ca^{2+} release, and diacylglycerol (DAG), which stimulates protein kinase C activity (PKC).[3],[4],[5] In contrast, Group II (mGluR2 and mGluR3) and group III (mGluR4, mGluR6, mGluR7, and mGluR8) are primarily located presynaptically and negatively coupled to adenylyl cyclase to reduce intracellular cAMP levels upon stimulation.[6],[7],[8] Excessive activation of mGluR5 has been shown to be involved in the development of neurodegenerative diseases like Alzheimer's,[9],[10] Parkinson's disease,[11],[12] or numerous CNS disorders including neuropathic pain,[13] anxiety and depression,[14] drug addiction[15] and fragile X syndrome.[16],[17]

Five dopamine receptor subtypes can be divided into two distinct subfamilies: D_1-like (D_1R and D_5R) and D_2-like (D_2R, D_3R, and D_4R). There is mounting evidence that GPCRs may form homo- and heteromers at the plasma membrane. Cabello *et al.* first suggested the existence of heterodimers of mGluR5 and D_2R in living cells using a fluorescence complementation assay. Additionally, bioluminescence resonance energy transfer, and sequential resonance energy transfer assays also allowed detecting receptor oligomers containing more than two protomers, in which the mGluR5 and D_2R also assembled with the adenosine A_{2A} receptor ($A_{2A}R$). Co-immunoprecipitation in native tissue confirmed the association of mGluR5, D_2R and $A_{2A}R$ in rat striatum homogenates. Overall, these results indicate the occurrence of mGluR5-D_2R-$A_{2A}R$ heteromers in living cells and support their presence in the GABAergic striatopallidal neurons, where they may represent important targets for the treatment of locomotion, neuropsychiatric disorders and drug addiction.[18],[19]

A recent study by Beggiato *et al.*[20] revealed a functional role for $A_{2A}R$, D_2R and the mGluR5 in regulating rat basal ganglia activity using dual-probe microdialysis in freely moving rats. The results suggested that $A_{2A}R$ and mGluR5 interact synergistically in modulating the D_2R-mediated control of striatopallidal GABA neurons. D_2R appears to suppress synaptic delivery of mGluR5 by limiting Src family kinase (SFK)-mediated tyrosine phosphorylation of mGluR5 in rat striatum.[21] In the basal ganglia, mGluR5 negative allosteric modulators regulate the L-3,4-dihydroxyphenylalanine (L-DOPA) induced changes of D_2R, the associated signaling proteins ERK1/2 and Akt/GSK3β and neuropeptides preproenkephalin and preprodynorphin, as well as the $A_{2A}R$ expression.[22] It is well known that cocaine increases both extracellular dopamine (DA) and glutamate levels in the nucleus accumbens (NAc) and that these effects are enhanced with repeated administration.[23]

Nowadays, heterobivalent ligands have emerged as valuable tools to demonstrate the existence of receptor heteromers without the need for receptor modification.[24],[25],[26] Heterobivalent ligands with a spacer of optimal length are envisaged to exhibit a potency that is different from that derived from its two monovalent pharmacophores.[26],[27],[28] Compounds able to modulate two GPCR dimers may eventually also evolve to useful pharmacological agents that target selected heteromeric subtypes, thereby potentially increasing selectivity.[25]

Here we report the design and synthesis of a series of mGluR5 negative allosteric modulators (NAMs)-D_2R agonist/antagonist heterobivalent ligands as pharmacological tools to study mGluR5-D_2R

heteromers. Towards this end ligands for the protomeric D_2R and the mGluR5 were conjugated through a spacer of variable length.

These bivalent ligands were evaluated in radioligand binding and functional assays both in cells in which the mGluR5 and D_2R were expressed separately and in cells co-expressing both target receptors.

IV.3. Results and Discussion

IV.3.1. Design of heterobivalent ligands

The dimeric ligands were constructed around spacers that were equipped with a primary amine on one and an azide on the other end to allow orthogonal coupling to the appropriately derivatized dopamine and mGluR5 ligands, respectively (Figure 1).

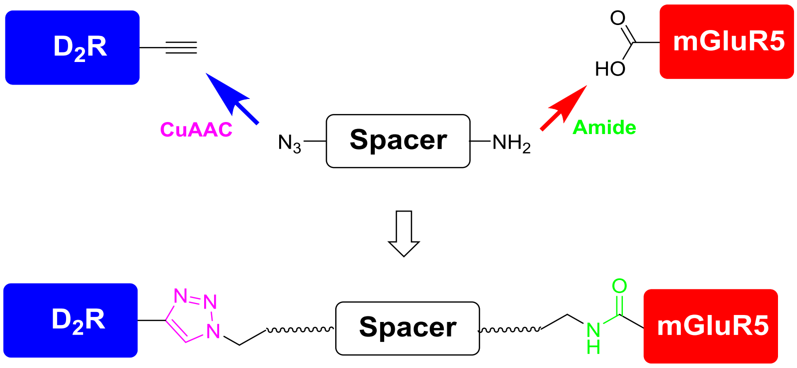

Figure 1. Construction of the heterobivalent ligands.

As D_2R ligands we selected the 5-hydroxy-2-(dipropylamino)tetralin (5-OH-DPAT)[29] and the 1,4-disubstituted aromatic piperazine (1,4-DAPs)[30] that were equipped with an alkyne ligation handle to afford **3.07** and **3.03**, which may be swiftly connected to the azide group of the spacer via a copper-catalyzed azide–alkyne cycloaddition (CuAAC) reaction (Figure 2).

5-OH-DPAT is a prototypical D_2R/D_3R agonist suitable for constructing bivalent ligands.[31] Site directed mutagenesis has demonstrated that the 2-aminotetralin moiety interacts with an agonist binding domain involving TM3 and TM5 for activation of either D_2R or D_3R. The basic nitrogen and the 5-OH group are critical for binding affinity.

The intrinsic activity of 1,4-DAPs for D_2R originates from the aromatic head group and the amine moiety that forms a strong hydrogen bond with $Asp^{3.32}$. A lipophilic appendage enhances affinity. Because proper elongation of this appendage is expected to lead to the “entrance region” of the receptor and from there reaching out to the binding pocket of the neighboring protomer, the para-position of the benzylic appendage is considered an appropriate attachment point for a linker unit.[30]

As mGluR5 ligand we opted for the selective and potent mGluR5 NAM 3-[(2-methyl-4-thiazolyl)ethynyl]pyridine (MTEP).[5] MTEP analogues substituted at the 5-position of the 3-pyridyl moiety have been demonstrated to be more potent mGluR5 NAMs than those modified at the 2- or 6-positions.[23] Hence, we introduced a carboxylic acid at the 5-position of the 3-pyridyl moiety to afford two carboxylic acid analogues of MTEP **4.01a-b** which are amenable for coupling to the amine group of the bifunctional spacers.

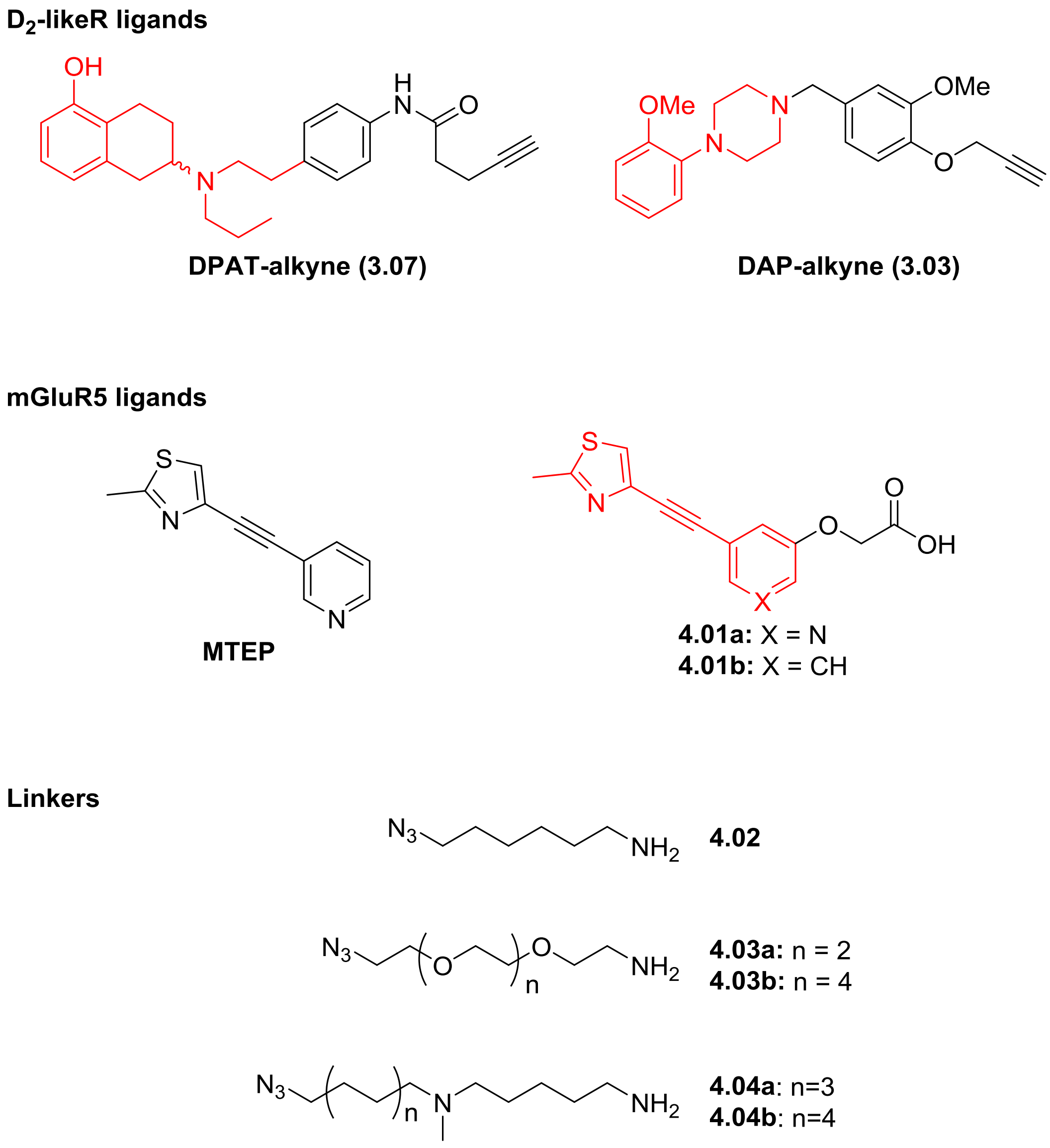
D2-likeR ligands
OH
H
N
O
N
OMe
N
N
OMe
O
DPAT-alkyne (3.07)
DAP-alkyne (3.03)
mGluR5 ligands
S
N
N
MTEP
S
N
O
O
OH
X
4.01a: X = N
4.01b: X = CH
Linkers
N3
NH2
4.02
N3
O
O
n
NH2
4.03a: n = 2
4.03b: n = 4
N3
n
N
NH2
4.04a: n=3
4.04b: n=4

Figure 2. Overview of appropriately modified monovalent ligands (parent ligands in red) and linkers used in this study. Parent ligands are indicated in red.

To construct the desired bivalent ligands, we considered three types of linkers with an azido group on one and an amino group on the other end, as to allow swift conjugation to alkyne modified dopamine ligands **3.07** and **3.03**, and the carboxylic acid containing MTEP analogues **4.01a-b**, respectively (Figure 2).

The first linker **4.02** is composed of a simple bifunctional hexamethylene chain. The polyethylene glycol (PEG) linkers **4.03a-b** were previously used to construct bivalent D_2R-μOR ligands.[29] These two classes of linkers have been frequently employed to compose bivalent ligands.[28],[30],[31],[32] They allow to gradually increase spacer length. However, bivalent ligands involving such linkers resulted in a significant drop in binding affinity for D_4R. In a third type of linkers **4.04a-b**, we decided to introduce a protonatable nitrogen atom near the middle of the bifunctional polymethylene chain to reduce incremental increase in hydrophobicity upon elongation, which may result in aggregation in aqueous media.

IV.3.2. Synthesis

The alkyne functionalized D_2R ligands **3.07** and **3.03** were prepared as described earlier.[26],[29],[30] The synthesis of the MTEP derivatives equipped with a carboxylic acid handle started from thiazole **4.06**, which was obtained from 2-chloro acetyl chloride (**4.05**) in 2 steps following published procedures.[5],[23] Esters **4.08a-b** were obtained upon treatment of phenols **4.07a-b** with ethyl bromoacetate,[33],[34] and coupled with thiazole **4.06** in the presence of $Pd(PPh_3)_2Cl_2$ to furnish **4.09a-b**, respectively. Saponification of **4.09a-b** yielded carboxylic acids **4.01a-b**.

Scheme 1. Synthesis of Carboxylic Acid Modified MTEP Analogues **4.01a** and **4.01b**.

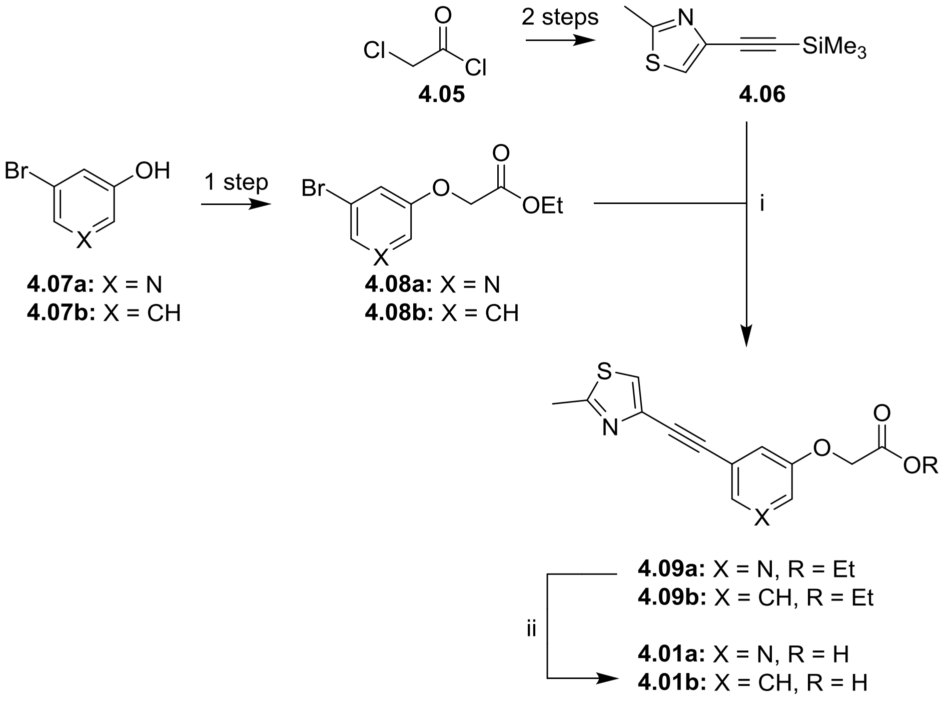

Reagents and conditions: i) $Pd(PPh_3)_2Cl_2$, CuI, TBAF, Et_3N, DMF, 85 °C, 2 h; ii) aq. NaOH.

Earlier procedures were followed for the preparation of the bifunctional polymethylene linker **4.02**,[35],[36] and the PEG linkers **4.03a-b**.[37]

Scheme 2. Synthesis of Orthogonally Functionalized Linkers **4.04a** and **4.04b**.

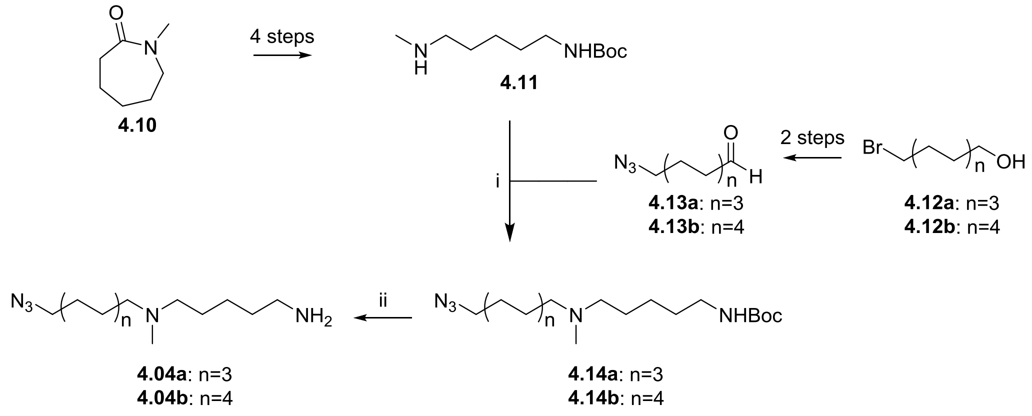
4 steps
NHBoc
4.10
4.11
i
2 steps
N3
Br
OH
H
n
4.13a: n=3
4.13b: n=4
4.12a: n=3
4.12b: n=4
ii
NH2
4.04a: n=3
4.04b: n=4
4.14a: n=3
4.14b: n=4

Reagents and conditions: i) NaBH(OAc)$_3$, CH$_2$Cl$_2$; ii) TFA, CH$_2$Cl$_2$.

Compound **4.11** was synthesized from the commercially available *N*-methylcaprolactam (**4.10**) in 4 steps.[38],[39],[40] Aldehydes **4.13a-b** were obtained from **4.12a-b** in 2 steps following the existing protocols.[41] Reductive amination **4.13a-b** with **4.11** using NaBH(OAc)$_3$ yielded **4.14a-b**, which, after Boc-deprotection with TFA, afforded the desired linkers **4.04a-b**.

The bivalent ligands were generated by first coupling the mGluR5 ligands with the different spacers using EDC and triethylamine to yield the seven intermediate azides **4.15**, **4.17a-b** and **4.19a-d**, which were subsequently conjugated with the DPAT- and DAP-alkynes through CuAAC (Scheme 3), leading to a series of nine bivalent D$_2$R-mGluR5 ligands.

Scheme 3. Synthesis of the Target Bivalent Ligands **4.16**, **4.18a-b**, **4.20a-b** and **4.21a-d**.

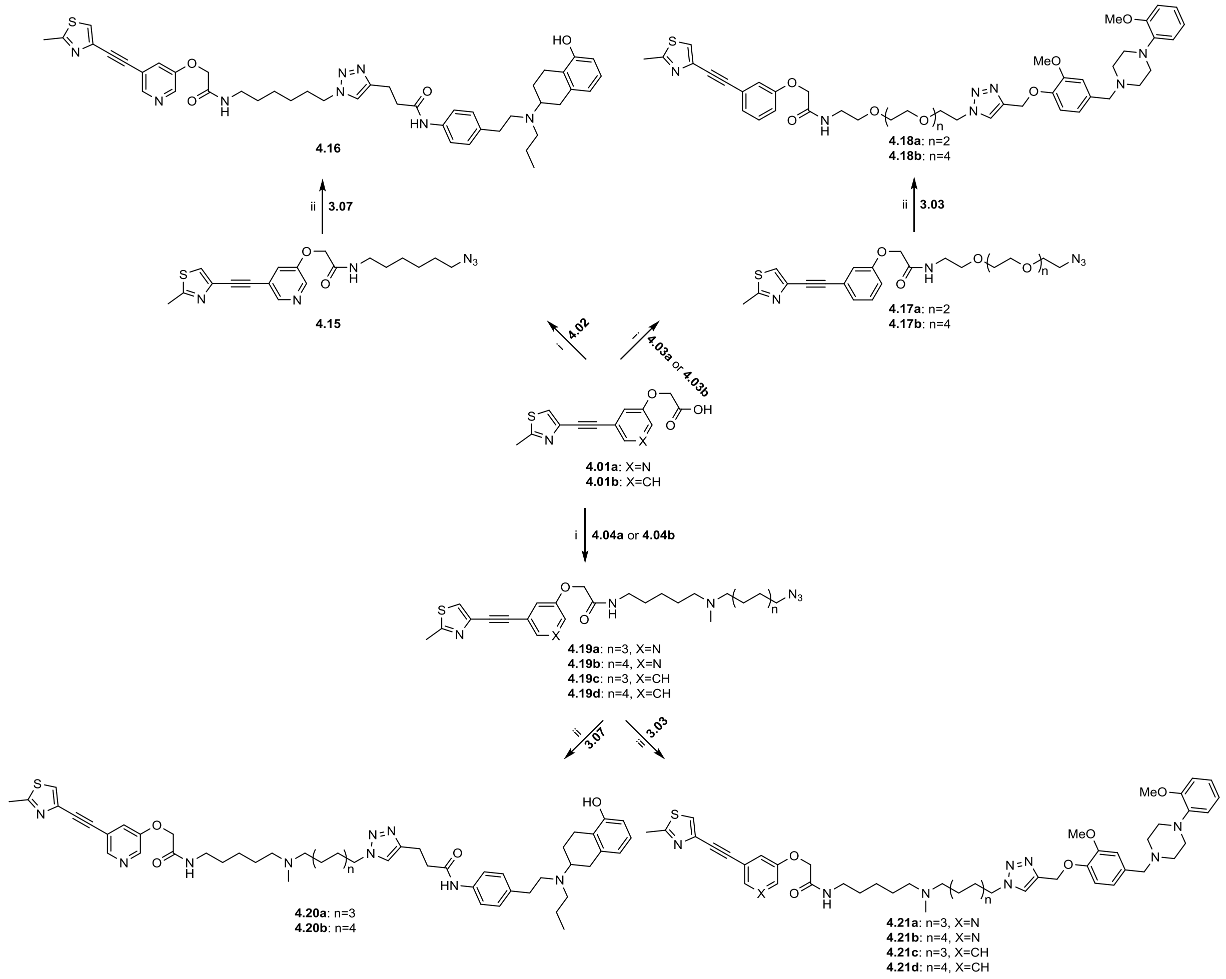
4.16
ii
3.07
4.15
4.18a: n=2
4.18b: n=4
ii
3.03
4.17a: n=2
4.17b: n=4
i
4.02
i
4.03a or 4.03b
4.01a: X=N
4.01b: X=CH
i
4.04a or 4.04b
4.19a: n=3, X=N
4.19b: n=4, X=N
4.19c: n=3, X=CH
4.19d: n=4, X=CH
ii
3.07
ii
3.03
4.20a: n=3
4.20b: n=4
4.21a: n=3, X=N
4.21b: n=4, X=N
4.21c: n=3, X=CH
4.21d: n=4, X=CH

Reagents and conditions: i) (3-dimethylaminopropyl)-N-ethylcarbodiimide hydrochloride, 1-hydroxybenzotriazole, triethylamine, CH_2Cl_2; ii) sodium ascorbate, $CuSO_4$, triethylamine, tris[(1-benzyl-1,2,3-triazol-4-yl)methyl]amine, dimethylformamide.

IV.3.3. Pharmacological evaluation

IV.3.3.1 Affinity of the bivalent ligands for the D_2R

A competition assay was performed to evaluate the binding affinity of the bivalent ligands for the D_2R (Table 1). First, the affinity of nine bivalent ligands along with the alkynylated precursors of DPAT (**3.07**) and DAP (**3.03**) was measured by displacement of $[^3H]$raclopride from the D_2R expressed in HEK 293T cells. Raclopride is a selective D_2R antagonist that due to its more pronounced hydrophilic character shows substantially less non-specific binding than spiperone.[29] All bivalent ligands retained good to moderate affinity for the D_2R (Table 1). Similar observations were made in stably D_4R expressing HEK293 cells (supporting information). The DPAT-based ligand **4.20a**, featuring a type 3 linker consisting of 20 atoms showed the best affinity (50 ± 6.4 nM) for D_2R. Interestingly, amongst the

DAP-based ligands compound **4.21a** and **4.21c**, featuring the same spacer as **4.20a**, displayed the lowest K_i value (132 nM and 147 nM, respectively). A significant reduction (5- to 17-fold) in D_2R binding affinities was observed for the bivalent ligands with hexamethylene and PEG linkers.

Table 1. Binding affinities (K_i) for D_2R and D_2R-mGluR5.

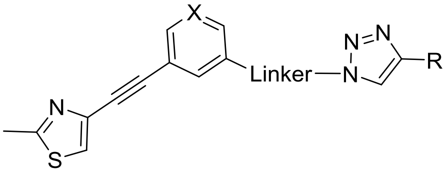

Compd	X	R	Linker	K_i (nM) for D_2R	K_i (nM) for D_2R-mGluR5
3.07	-	-	-	17 ± 2.6	19 ± 1.8
3.03	-	-	-	77 ± 6.8	69 ± 22
4.16	N	DPAT	$-OCH_2CONH\,(CH_2)_6-$	295 ± 99	142 ± 10
4.20a	N	DPAT	$-OCH_2CONH(CH_2)_5NCH_3(CH_2)_8-$	50 ± 6.4	13 ± 3.6*
4.20b	N	DPAT	$-OCH_2CONH\,(CH_2)_5NCH_3(CH_2)_{10}-$	79 ± 16	171 ± 12
4.21a	N	DAP	$-OCH_2CONH\,(CH_2)_5NCH_3(CH_2)_8-$	132 ± 44	45 ± 5.3*
4.21b	N	DAP	$-OCH_2CONH\,(CH_2)_5NCH_3(CH_2)_{10}-$	303 ± 43	115 ± 32
4.21c	CH	DAP	$-OCH_2CONH\,(CH_2)_5NCH_3(CH_2)_8-$	147 ± 24	94 ± 21
4.21d	CH	DAP	$-OCH_2CONH\,(CH_2)_5NCH_3(CH_2)_{10}-$	398 ± 100	252 ± 54
4.18a	CH	DAP	$-OCH_2CONH-PEG_4-$	438 ± 89	251 ± 42
4.18b	CH	DAP	$-OCH_2CONH-PEG_6-$	352 ± 94	186 ± 75

Binding affinities (K_i) obtained by competitive displacement of [^{3}H]raclopride from HEK293T D_2R and HEK293T D_2R-mGluR5 cell membranes. All values are expressed as the mean ± SEM of three independent assays. The affinity of bivalent ligands in the cells coexpressing D_2R and mGluR5 is significantly different (*$p<0.05$) compared to the cells monoexpressing D_2R.

Next, we determined the affinity of nine bivalent ligands and their corresponding alkyne precursors **3.07** and **3.03** for D_2R in the presence of overexpressed mGluR5. Interestingly, the affinity of **4.20a** to cells expressing both D_2R and mGluR5 (13 ± 3.6 nM) increased 4-fold compared to cells expressing only D_2R (50 ± 6.4 nM). Likewise, the D_2R affinity of the DAP-containing bivalent ligand **4.21a** was 3-fold higher in cells co-expressing the mGluR5 (45 ± 5.3 nM versus 132 ± 44 nM). Furthermore, **4.20a** showed moderately higher affinity than **3.07** (19 ± 1.8 nM) and 10-fold higher affinity compared to the two other DPAT-based bivalent ligands **4.16** and **4.20b** in D_2R and mGluR5 co-expressing cells. All these data indicate that bivalent ligands **4.20a** and **4.21a** possibly bridge the binding sites of the D_2R and mGluR5 heterodimers. Furthermore, DPAT-based compound **4.16** containing a short hexamethylene linker showed a lower affinity for D_2R-mGluR5 relative to **4.20a** probably because its linker is too short to bridge the binding sites of the heterodimer. The preference for a tertiary amine linker as deduced from the superior affinities of **4.20a** and **4.21a** in the coexpressing cells may be partly due the H-bond that is formed between the tertiary amine group and D400 located on extracellular loop 3 (ECL3) of D_2R (see Computational modeling part below), which may compensate for the entropic penalty of the flexible linker. Based on the above results, a type 3 linker of appropriate length is preferred in this study.

These data indicate that bivalent ligands **4.20a** and **4.21a** possibly bridge the binding sites of the D_2R and mGluR5 heterodimers.

IV.3.3.2 Affinity of the bivalent ligands for the mGluR5

Competitive receptor binding assays in cell membranes from mGluR5 expressing cells allowed to determine the affinity for said receptor using [^{3}H]MPEP, a nonselective mGluR5 antagonist. Results of saturation binding assays for [^{3}H]MPEP can be found in supporting information. The binding affinities of the azido precursor **4.19a** for mGluR5 and D_2R-mGluR5 were 5.8 ± 0.9 µM and 5.7 ± 0.8 µM, respectively (Table 2). In addition, the affinity of **4.01a** for mGluR5 was 6.5 ± 0.6 µM, which is comparable to that of **4.19a**. This led us to use **4.19a** as control in ligand binding and further functional assays for mGluR5.

Bivalent ligand **4.20a** showed a 2-fold gain in binding affinity in cells expressing both D_2R and mGluR5 compared to cells solely expressing mGluR5. Interestingly, **4.20a** exhibited a 5-fold higher affinity (1.1 ± 0.2 µM) for D_2R-mGluR5 compared to its azido precursor **4.19a** lacking a D_2R ligand (5.7 ± 0.8 µM). Likewise, **4.21a** displayed 4-fold higher affinity (1.3 ± 0.2 µM) for D_2R-mGluR5 relative to **4.19a**. All these results indicate that bivalent ligands **4.20a** and **4.21a** bridge the orthosteric and allosteric binding sites of the D_2R and mGluR5 heteromer, respectively.

Table 2. Binding affinities (K_i) for mGluR5 and mGluR5-D_2R.

Entry	X	R	Linker	K_i (µM) for mGluR5	K_i (µM) for D_2R-mGluR5

4.19a	N	-	$-OCH_2CONH(CH_2)_5NCH_3(CH_2)_8-$	5.8 ± 0.9	5.7 ± 0.8
4.20a	N	DPAT	$-OCH_2CONH(CH_2)_5NCH_3(CH_2)_8-$	2.3 ± 0.5	1.1 ± 0.2*
4.21a	N	DAP	$-OCH_2CONH\ (CH_2)_5NCH_3(CH_2)_8-$	1.0 ± 0.3	1.3 ± 0.2*

Binding affinities (K_i) obtained by competitive displacement of [^{3}H]MPEP from HEK293T cell membranes expressing mGluR5 and D_2R-mGluR5. All values are expressed as the mean ± SEM of three independent assays performed in duplicate. The affinity of bivalent ligands is significantly different (*$p<0.05$) compared to that of monovalent ligand in the cells coexpressing D_2R and mGluR5.

IV.3.3.3 D_2-likeR activation (MAPK phosphorylation) by the bivalent ligands

The mitogen-activated protein kinase (MAPK) phosphorylation assay was used to assess the efficiency of the bivalent ligands. The MAPK pathway, also known as the extracellular-signal regulated kinase (ERK) pathway, consists of an intracellular chain of proteins that transfer the signal from the transmembrane receptor to the nuclear DNA or other subcellular targets via transfer of phosphate groups and functions as an “on/off” switch.[42] The most commonly studied step of the MAPK pathway, initiated by GPCR activation, is the phosphorylation of p44/42 MAPK (ERK1/2).

In a previous study we demonstrated that D_2-likeR ligands based on DAP-alkyne and DPAT-alkyne caused stronger MAPK phosphorylation in D_4R-expressing than in D_2R-expressing cells.[29] To assess functional activation of the D_2-likeR by our bivalent ligands, we therefore used HEK293 cell lines stably expressing either D_4R or D_2R and mGluR5 (Figure 3 and Table 3).[43] All bivalent ligands were found to activate the MAPK signaling pathway in cells expressing the D_4R (Figure 3), with a potency that is comparable or slightly weaker than that of alkyne precursors **3.07** and **3.03** (Table 3). Interestingly, compound **4.20a** was slightly more potent ($EC_{50} = 0.28 \pm 0.03$ μM) than alkyne derived DPAT (**1**) ($EC_{50} = 0.37 \pm 0.17$ μM), while the potency of the DPAT derivatives with shorter (**4.16**) and longer linkers (**4.20b**) decreases 3- and 5-fold. Similarly, ligand **4.21a** was slightly more potent (0.8 ± 0.1 μM) than the other DAP-based bivalent ligands (EC_{50} = 1.1-2.7 μM).

Next, we performed MAPK phosphorylation to test bivalent ligands **4.20a**, **4.21a** and their corresponding alkyne precursors **3.07** and **3.03** in a stable cell line coexpressing D_2R and mGluR5 (Table 3 and supporting information). Unexpectedly, only bivalent ligand **4.20a** gave a stronger MAPK-P band than the control serum-free media (SFM). It displayed 4-fold higher potency (0.021 ± 0.009 μM) than **3.07** (0.078 ± 0.007 μM). On the other hand, **4.21a** and **3.03** gave weaker MAPK-P signal bands than SFM, indicative for D_2R antagonist properties for DAP-alkyne based ligands (supporting information).

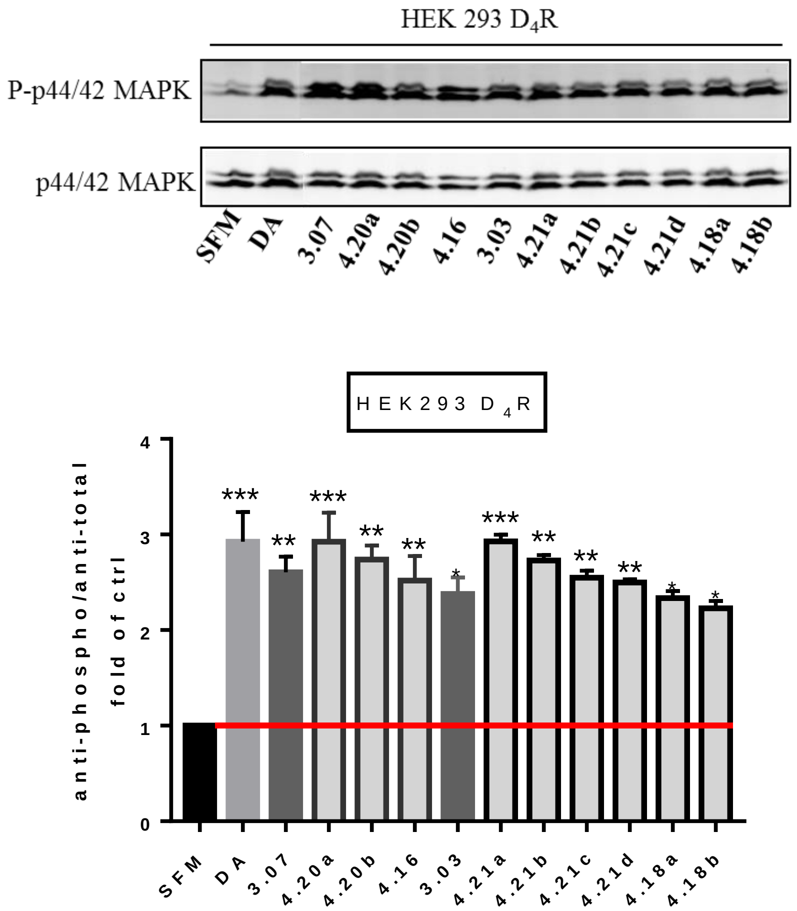

Figure 3. Efficacy of bivalent ligands to phosphorylate MAPK in HEK293 D_4R cells. Cells were treated with serum-free media (SFM) for 12 h. Next, D_2R agonists (10 µM) and SFM were added for 5 min. Cells were washed and lysed as explained in the Experimental section. Phosphorylated MAPK was detected by immunoblotting using rabbit anti-phospho-p44/42 MAPK antibody and mouse anti-p44/42 MAPK antibody was used for demonstrating equal protein loading. Cells treated with SFM served as control. The top panel shows a representative result from three independent experiments; the bottom panel is given as mean ± SD. DA=dopamine. Bivalent ligands were significantly different (*$p< 0.05$, **$p < 0.01$, ***$p < 0.001$) compared to the control SFM by One-way ANOVA.

Table 3. Potency (EC_{50}) of D_2R agonists induced MAPK-P in HEK293 D_4R and HEK293 D_2R-mGluR5 stable cell lines.

Compd	X	R	Linker	MAPK EC_{50} µM D_4R	MAPK EC_{50} µM D_2R-mGluR5
3.07	-	-	-	0.37 ± 0.17	0.078 ± 0.007

3.03	-	-	-	0.21 ± 0.12	nd
4.16	N	DPAT	$-OCH_2CONH\ (CH_2)_6-$	0.97 ± 0.42	nd
4.20a	N	DPAT	$-OCH_2CONH(CH_2)_5NCH_3(CH_2)_8-$	0.28 ± 0.03	0.021 ± 0.009
4.20b	N	DPAT	$-OCH_2CONH(CH_2)_5NCH_3(CH_2)_{10}-$	2.0 ± 0.1	nd
4.21a	N	DAP	$-OCH_2CONH(CH_2)_5NCH_3(CH_2)_8-$	0.8 ± 0.1	nd
4.21b	N	DAP	$-OCH_2CONH(CH_2)_5NCH_3(CH_2)_{10}-$	1.9 ± 0.4	nd
4.21c	CH	DAP	$-OCH_2CONH(CH_2)_5NCH_3(CH_2)_8-$	1.7 ± 0.1	nd
4.21d	CH	DAP	$-OCH_2CONH(CH_2)_5NCH_3(CH_2)_{10}-$	1.8 ± 0.5	nd
4.18a	CH	DAP	$-OCH_2CONH-PEG_4-$	2.7 ± 0.4	nd
4.18b	CH	DAP	$-OCH_2CONH-PEG_6-$	1.1 ± 0.5	nd

Data shown represent the mean ± SEM of three independent experiments. nd, not determined.

IV.3.3.4 cAMP assay to study intrinsic activities of the selected D_2R ligands.

To further understand the intrinsic activities of the selected bivalent ligands **4.20a** and **4.21a** and their corresponding monovalent ligands **3.07** and **3.03** comprising the pharmacophore of a D_2R agonist and a D_2R antagonist, respectively, we performed a bioluminescence based cAMP accumulation assay (Figure 4 and Table 4).[44] Coupled to inhibitory $G\alpha_{i/o}$ proteins, activation of the D_2R decreases cAMP production.

Similar to the reference D_2R agonist quinpirole, bivalent ligands **4.16**, **4.20a**, **4.20b** and its alkyne precursor **3.07** inhibited forskolin-induced cAMP accumulation both in cells monoexpressing D_2R or in cells coexpressing D_2R and mGluR5. Interestingly, in the latter cells a significantly lower EC_{50} value was observed for bivalent ligand **4.20a** ($EC_{50} = 1.5 \pm 0.5$ nM) compared to **3.07** ($EC_{50} = 6.5 \pm 0.6$ nM), indicating that the bivalent binding requires a lower receptor occupation to exert signaling. However, **4.16** and **4.20b** exhibited 3- and 5-fold lower potencies (20 nM and 32 nM, respectively) in the coexpressing cell line relative to **3.07**, revealing weak D_2R agonism. In D_2R/mGluR5-coexpressing cells, quinpirole and the monovalent D_2R agonist **3.07** inhibited cAMP formation with similar potencies as in cells monoexpressing D_2R, while **4.20a** decreased cAMP production with a 2-fold higher potency in the coexpressing cells than in monoexpressing D_2R cells. Nevertheless, **4.16** and **4.20b** displayed 2- and 6-fold lower potencies in the coexpressing cells than in the monoexpressing cells.

Consistent with the MAPK-P results, bivalent ligand **4.21a** and its alkyne precursor **3.03** failed to inhibit cAMP accumulation (Figure 4) both in the D_2R solely expressed cells and in the D_2R/mGluR5 coexpressed cells, suggesting that DAP-based bivalent ligands show D_2R antagonist behavior, which is in line with the reported results.[30]

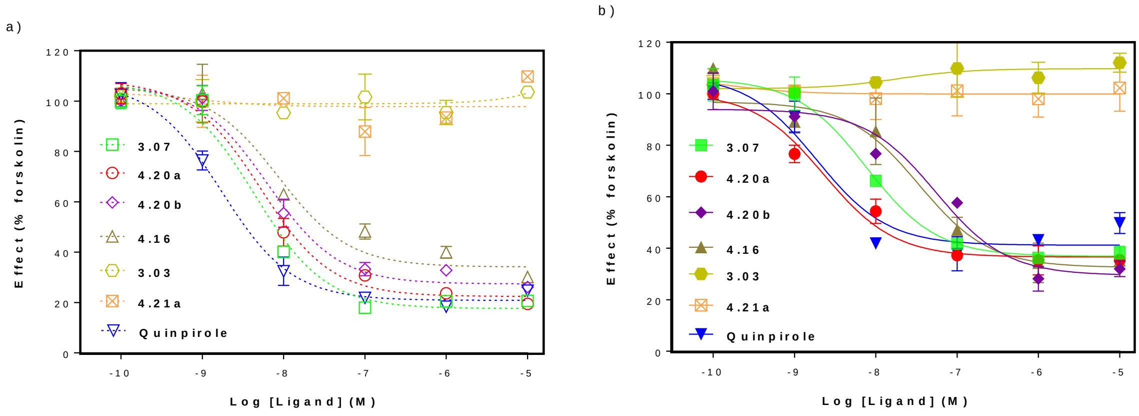

Figure 4. Dose-response curves of cAMP accumulation for representative ligands. Functional activity of selected bivalent ligands and its precursor **3.03** and **3.07** determined in HEK 293T cells stably expressing the D_2R (a) or both D_2R and mGluR5 (b) and coexpressing the pGloSensor-22F cAMP plasmid via transient transfection. Cells were stimulated with increasing amounts of the ligands (0.1 nM–10 µM) in the presence of 10 µM forskolin. cAMP production was normalized to the percentage of forskolin-induced cAMP concentration (100%). Data represent mean ± SD of three independent experiments each performed in duplicate.

Table 4. Potency of inhibition of forskolin mediated cAMP accumulation for bivalent ligands based on D_2R agonist DPAT-alkyne.

Compd	cAMP EC_{50} (nM) D_2R	cAMP EC_{50} (nM) D_2R-mGluR5
Quinpirole	1.8 ± 0.4	1.9 ± 0.3
3.07	3.0 ± 0.8	6.5 ± 0.6
4.16	7.6 ± 0.7	20 ± 9.8
4.20a	3.3 ± 0.7	1.5 ± 0.5
4.20b	5.5 ± 0.6	32 ± 15

Data shown represent the mean ± SEM of three independent experiments.

IV.3.3.5 MAPK phosphorylation to study the potency of the newly developed bivalent ligands for mGluR5

It is well known that activation of mGluR5 by its agonist (*S*)-3,5-dihydroxyphenylglycine (DHPG) leads to phosphorylation of MAPK in HepG2 cells.[45] Here, we examined the MAPK-P in response to L-glutamic acid (L-Glu) and (*R,S*)-2-chloro-5-hydroxyphenylglycine (CHPG) treatment in HEK293 mGluR5 and HEK293 mGluR5-D_2R stable cell lines (supporting information). The results showed that MAPK-P peaked at approximately 10 min for mGluR5 and 7-10 min for mGluR5-D_2R after 10 µM L-Glu treatment. To assess the inhibition of MAPK phosphorylation by the bivalent ligands, cells were pretreated with **4.19a** and all bivalent ligands for 30 min before incubation of the cells for 10 min with L-Glu (10 µM). All bivalent ligands proved capable of inhibiting MAPK-P activated by L-Glu (supporting information).

To assess their potency we tested all bivalent ligands and azido precursor **4.19a** (1 nM-10 µM) in HEK 293 mGluR5 cells (Table 5) and selected compounds **4.19a**, **4.20a** and **4.21a** in HEK 293 mGluR5-D_2R cells (Table 5). Compound **4.20a** was more potent (0.17 ± 0.02 µM) than the other DPAT-based bivalent ligands in blocking MAPK-P for mGluR5. DAP-based bivalent ligand **4.21a** featuring an identical linker as **4.20a** displayed a higher potency (0.11 ± 0.05 µM) than the other DAP-bond ligands in the cells monoexpressing the mGluR5. In addition, DAP-based bivalent ligands with PEG linkers showed lower antagonistic activity compared to DAP-based ligands with a tertiary amine linker.

Interestingly, bivalent ligands **4.20a** and **4.21a** exhibited 7- and 2-fold higher potency (IC_{50} = 0.62 µM and 1.8 µM) in mGluR5-D_2R compared with their monovalent precursor **4.19a** (IC_{50} = 4.5 µM).

Table 5. Potency (IC_{50}) of mGluR5 antagonists blocking MAPK-P activated by L-Glu (10 µM) in HEK293 mGluR5 and HEK293 mGluR5-D_2R stable cell lines.

Compd	X	R	Linker	MAPK IC_{50} µM mGluR5	MAPK IC_{50} µM mGluR5-D_2R
4.19a	N	-	$-OCH_2CONH(CH_2)_5NCH_3(CH_2)_8-$	2.6 ± 0.8	4.5 ± 1.1
4.16	N	DPAT	$-OCH_2CONH\ (CH_2)_6-$	1.6 ± 0.7	nd
4.20a	N	DPAT	$-OCH_2CONH(CH_2)_5NCH_3(CH_2)_8-$	0.17 ± 0.02	0.62 ± 0.15
4.20b	N	DPAT	$-OCH_2CONH\ (CH_2)_5NCH_3(CH_2)_{10}-$	0.32 ± 0.06	nd
4.21a	N	DAP	$-OCH_2CONH\ (CH_2)_5NCH_3(CH_2)_8-$	0.11 ± 0.05	1.8 ± 0.5

4.21b	N	DAP	$-OCH_2CONH\ (CH_2)_5NCH_3(CH_2)_{10}-$	0.45 ± 0.15	nd
4.21c	CH	DAP	$-OCH_2CONH\ (CH_2)_5NCH_3(CH_2)_8-$	0.24 ± 0.08	nd
4.21d	CH	DAP	$-OCH_2CONH\ (CH_2)_5NCH_3(CH_2)_{10}-$	0.31 ± 0.11	nd
4.18a	CH	DAP	$-OCH_2CONH\text{-}PEG_4-$	1.2 ± 0.3	nd
4.18b	CH	DAP	$-OCH_2CONH\text{-}PEG_6-$	0.90 ± 0.32	nd

Data shown represent the mean ± SEM of three independent experiments. nd, not determined.

IV.3.3.6 Computational modeling of a bivalent ligand bound to an mGluR5-D$_2$R heterodimer

The binding pose of compound **4.20a** was investigated *in silico* through protein-protein docking of crystal structures: transmembrane domains (TMD) of mGluR5 and D$_2$R, followed by docking of the bivalent ligand into the modeled heterodimer (see Experimental Section). As both receptors are co-crystallized with either negative allosteric modulator (NAM)[46] or antagonist,[47] they can be considered to be in their respective inactive states. As the bivalent ligand **4.20a** is a fusion of mGluR5 NAM and D$_2$R agonist, this means mGluR5 is in an ideal conformation but not D$_2$R, which would theoretically be active in such a heterodimer-ligand complex. Furthermore, as the original crystal structure of mGluR5 has no clear entrance or exit for NAMs because of its tightly closed extracellular loops and TMD,[46] a modified conformation of the receptor was deemed necessary to correctly bind a bivalent compound. Such a conformation has been observed previously, firstly with a Monte Carlo sampling technique employed for the purposes of docking photo-sensitive[48] and long linear[49] mGluR5 NAMs, and secondly during molecular dynamics (MD) simulations of mGluR5 with bound NAM.[50] In summary, this alternative mGluR5 conformation is in an inactive state and similar to the original mGluR5 crystal structure[46] but undergoes a partial separation of the extracellular ends of TM5 and TM6, which are highly flexible.[50] This potentially allows NAMs to enter or leave and is conducive for the linker of a bivalent ligand to pass outside of the receptor. As such, we utilized this MD-generated mGluR5 conformation[50] for modeling interactions with D$_2$R, whose crystal structure has no such limitations regarding the binding of a bivalent ligand.

In terms of modeling an mGluR5-D$_2$R heterodimer, referring to experimental information is important as these proteins can potentially interact in a number of ways. Interestingly, TM5 and TM6 have been experimentally observed to dynamically participate in the interface(s) of an mGluR2 homodimer,[51] as well as TM5 involved in cross-talk between mGluR2 and the Class A GPCR, 5-HT$_{2A}$ receptor.[52],[53],[54] Based on homology between mGluR2 and mGluR5 TMDs (sequence identity of 51%), physical interaction between mGluR5 and D$_2$R may follow a similar pattern. In addition, participation of mGluR5 TM5 and/or TM6 in a direct interaction with D_2R would provide a means of passing a bivalent ligand between receptors. Likewise for D2R, TM5 and TM6 have been observed to participate in its experimentally characterized homodimeric and heteromeric receptor interactions.[55],[56],[57],[58] As such, we modeled an mGluR5-D_2R heterodimer via its respective TM5-TM6 helices by using the mu-opioid homodimer crystal structure as a template,[59]which contains an analogous interface. This initial mGluR5-D_2R model was refined with protein-protein docking to identify an optimal interaction between the receptors (see Experimental Section). The best docked mGluR5-D_2R conformation results in close packing of residues at the TM5-TM6 interface (Figure 5B). However, as D_2R is in an inactive state with its TM6 in an inward rather than outward orientation,[47] the contact surface between receptors is possibly not as extensive as it could be. Nevertheless, the reported docking score is respectable, suggesting a favorable interaction (I_sc of -6.6 on a scale of 0 to -10, where better than -5 is considered satisfactory[60]).

Compound **4.20a** was bound to the mGluR5-D_2R heterodimer model by first, automatically docking its separate mGluR5 NAM (MTEP) and D_2R agonist (DPAT-alkyne, 1) components, second, by manually connecting these with the appropriate linker, and third, energy minimizing the resulting complex (see Experimental Section). It was found that by following this process, **4.20a** is able to simultaneously bind both receptors, passing between TM5 and TM6 of each (Figure 5A) with the linker residing at the membrane surface or just beneath (Figure 5B). In the modeled complex, compound 22a is able to make six protein-ligand H-bonds: two with mGluR5 and four with D2R (Figure 4C). In mGluR5, these H-bonds involve residues S805 and S809 on TM7, both of which interact with the MTEP component of **4.20a** (Figure 5C). These observed protein-ligand H-bonds are consistent with known mGluR5 NAM binding modes previously identified in mGluR5 crystal structures,[46],[61] and published mGluR5 MD simulations.[48],[50] In D_2R, the DPAT component of **4.20a** makes an H-bond with D114 on TM3 in the same manner as co-crystallized risperidone in the original D_2R crystal structure.[47] However, in line with its potential D_2R agonism and unlike risperidone, **4.20a** makes additional H-bonds with the backbone oxygen of S193 on TM5 and Y408 hydroxyl group on TM7 (Figure 5C). The importance of S193 for the binding of D2R agonists has been noted before,[62] along with neighboring residues, S194 and S197. Due to the closeness of these three particular serine residues in the D_2R crystal structure, only moderate conformational changes in TM5 (due to receptor activation, for example) would be required for **4.20a** to make H-bonds with the sidechain hydroxyl groups of either S193, S194 or S197. Finally, the tertiary amine on the linker of **4.20a** makes an H-bond with D400 located on extracellular loop 3 (ECL3) of D_2R (Figure 5C). This interaction is likely conducive to the conformational stability of this particular linker, which might otherwise (e.g. PEG-linkers) become a destabilizing factor.

Overall, due to the number of observed protein-ligand H-bonds with both receptors, as well as consistency with known mGluR5 and D_2R ligand binding modes, the modeled heterodimer-ligand complex appears to be compatible with the reported biological activity of compound **4.20a**.

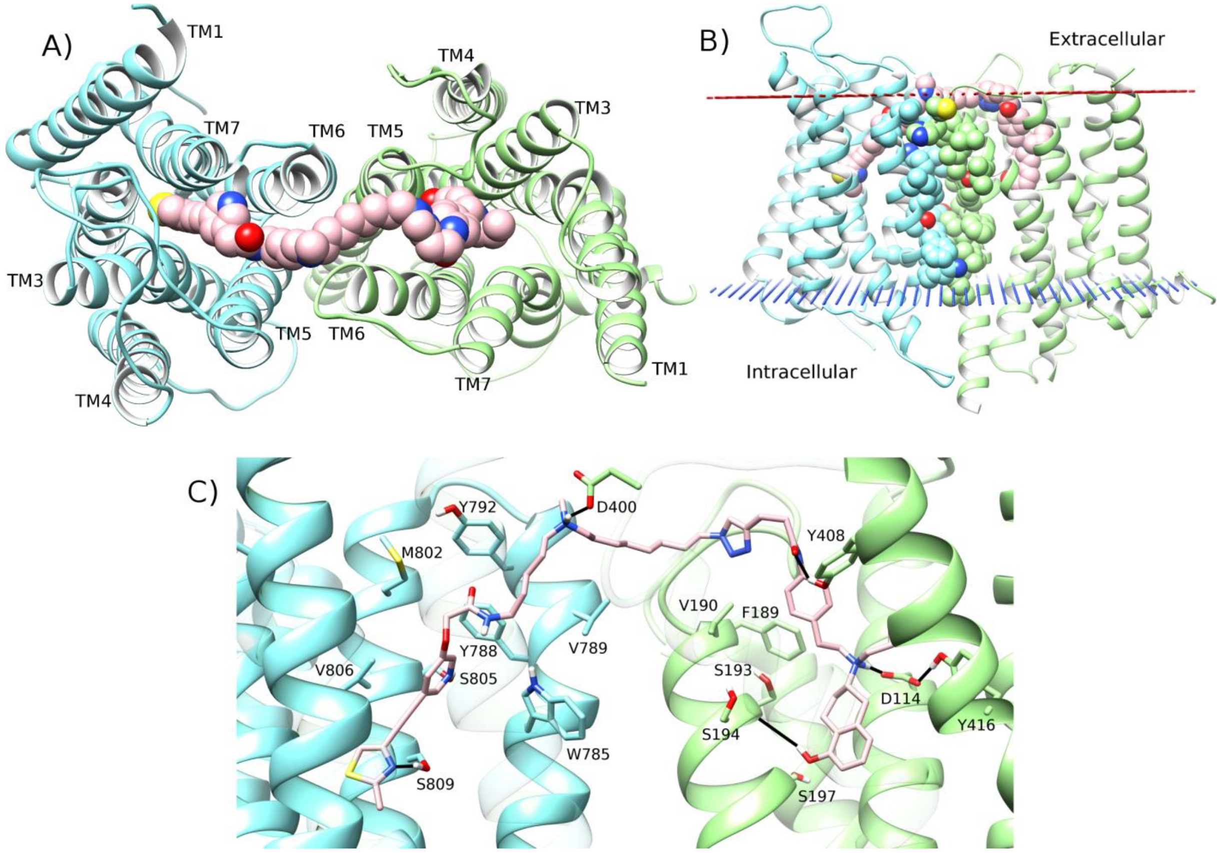

Figure 5. The modeled mGluR5-D_2R-compound 4.20a complex. A) Extracellular top-view of the interaction between mGluR5 (blue ribbon, derived from PDB id: 4009) and D_2R (green ribbon, PDB id: 6CM4) via symmetrical TM5-TM6 interface, including bound compound **4.20a** (carbons as pink spheres). B) Side-view of mGluR5-D_2R heterodimer with bound **4.20a** (carbon, nitrogen, oxygen and sulphur atoms as pink, dark blue, red and yellow spheres, respectively), showing contact interface (carbons as blue and green spheres, respectively) within a model membrane (red dots and blue lines, representing upper and lower leaflets, respectively). C) Modeled binding mode of compound **4.20a** (pink) within respective allosteric and orthosteric pockets of mGluR5-D_2R heterodimer (blue and green ribbons, respectively). Protein-ligand H-bonds are displayed as solid black lines (S805 is partially obscured by the ligand). Selected residues on mGluR5: TM6, TM7 and D2R: TM3, TM5, TM7 and ECL3 are displayed (mGluR5: TM3, TM5 and D2R: TM6 are transparent for visualization purposes).

IV.4. Conclusion

In summary, we have designed and synthesized nine potential heterobivalent ligands based on the chemical structure of two distinct D_2-likeR agonist/antagonist and two mGluR5 NAMs. Ligation of D_2-likeR ligands shows that bivalent ligands with PEG (PEG_4 and PEG_6) and hexamethylene linkers exhibit relatively low affinity for D_2R and D_4R, contrary to bivalent ligands with alkylamine spacers, while all can still activate MAPK phosphorylation in D_4R cells. Interestingly, bivalent ligand **4.20a**, with a 20-atom alkylamine spacer, showed a 4-fold affinity increase for the D_2R in cells expressing both the D_2R and the mGluR5, compared to cells only expressing D_2R, suggesting that **4.20a** may bridge the binding sites of the D_2R and mGluR5 receptors. Moreover, **4.20a** shows a 5-fold higher affinity for the mGluR5 than its MTEP azido precursor **4.19a** in D_2R-mGluR5 cells, also pointing towards its capacity to simultaneously occupy both binding sites of the heteromer. From a functional point of view, **4.20a** displays 4- and 7-fold higher potency compared to the monomeric precursors **3.07** and **4.19a** in MAPK phosphorylation, respectively, in cell lines stably expressing D_2R and mGluR5 receptors. Moreover, **4.20a** inhibits forskolin stimulated cAMP formation with a 4-fold higher potency compared to alkyne **3.07** in the coexpressing cells, indicating that the bivalent binding requires a lower receptor occupation to exert signaling. In addition, a docking study reveals that **4.20a** is indeed able to simultaneously bind both receptors by passing between the heterodimeric interface, comprised of TM5 and TM6 of both receptors, and establishing six protein-ligand H-bonds.

Overall, we demonstrated that the length and composition of the linker between the two receptor pharmacophores strongly affect binding affinity and functional potency both from a D_2R and from a mGluR5 viewpoint. Most importantly, this study allowed to identify bivalent ligand **4.20a**, which emerges as a promising molecular probe to further investigate D_2R and mGluR5 heterodimerization.

IV.5. Experimental Section

IV.5.1. Chemistry

IV.5.1.1 General

All reactions described were performed under an N_2 atmosphere and at ambient temperature unless stated otherwise. All reagents and solvents were purchased from Sigma-Aldrich (Diegem, Belgium), Fisher Scientific (Merelbeke, Belgium), TCI Europe (Zwijndrecht, Belgium) or Apollo Scientific (Bredbury, Stockport, United Kingdom) and used as received. NMR solvents were acquired from Eurisotop (Saint-Aubin, France). Reactions were monitored by TLC analysis using TLC aluminium sheets (Macherey-Nagel, Alugram Sil G/UV254) with detection by spraying with a solution of $(NH_4)_6Mo_7O_{24}\cdot4H_2O$ (25 gL^{-1}) and $(NH_4)_4Ce(SO_4)_4\cdot2H_2O$ (10 gL^{-1}) in H_2SO_4 (10 % aq.) followed by charring or an aqueous solution of $KMnO_7$ (20 gL^{-1}) and K_2CO_3 (10 gL^{-1}) or an ethanolic solution of ninhydrin (2 gL^{-1}) and acetic acid (1% v/v) followed by charring. Solution pH values were estimated using universal indicator paper (Merck). Silica gel column chromatography was performed using a Grace Reveleris X2 system and the corresponding silica gel cartridges. ESI-HRMS spectra were measured with a Waters LCT Premier XE Mass spectrometer calibrated using leucine enkephalin as an external standard. ^1H- and ^{13}C-APT-NMR spectra were recorded with a Varian Mercury-300BB (300/75

MHz) spectrometer. Chemical shifts are given in ppm (δ) relative to tetramethylsilane as an internal standard (^{1}H NMR) or the NMR solvent (^{13}C NMR). Coupling constants are given in Hertz (Hz). Weak signals in ^{13}C NMR are indicated as (w). LC-MS analyses were carried out on a Waters AutoPurification System equipped with PDA and ESI-MS detection and using a Waters CORTECS C18 Column (4.6×100 mm, 2.7µm) and a water/acetonitrile/formic acid linear gradient system at a flow rate of 1.44 mLmin^{-1}.

IV.5.1.2 General Procedure for the Carbodiimide-Mediated Amide Formation.

To a solution of (3-Dimethylaminopropyl)-N-ethylcarbodiimide hydrochloride (1.5 eq.) and 1-hydroxybenzotriazole (1.4 eq.) in CH_2Cl_2 was added a solution of the PEG spacer (1.2 eq.) in CH_2Cl_2 (0.2 M) and cooled to 0 °C under an argon atmosphere. After 15 min at 0 °C, amines (1.0 eq.) were added and triethylamine (2 eq.) was added dropwise; the reaction was slowly warmed to room temperature and stirred overnight. The reaction was diluted with CH_2Cl_2, washed successively with water, HCl (5% aq.), $NaHCO_3$ (sat. aq.), NaCl (sat. aq.), dried over Na_2SO_4, filtered and solvent was evaporated under reduced pressure. The crude product was purified by silica gel chromatography (NH_4OH/MeOH/CH_2Cl_2, 1:5:94 v/v/v) to yield the amides.

IV.5.1.3 General Procedure for Copper Mediated Azide-Alkyne Cycloaddition.

To a solution of the intermediate azide (1.0 eq.) in dimethylformamide (0.1 M) was added the alkyne (1.5 eq.), sodium ascorbate (1.0 eq., 0.5 M), $CuSO_4$ (0.2 eq., 0.05 M), triethylamine (3.0 eq.) and a catalytic amount of tris[(1-benzyl-1,2,3-triazol-4-yl)methyl]amine. The reaction mixture was stirred overnight at room temperature in the dark under an argon atmosphere. The solvent was evaporated under reduced pressure and the residue was redissolved in water and extracted with CH_2Cl_2. Then combined organic fractions were pooled, washed with brine and dried over Na_2SO_4. The crude compound was purified by silica gel chromatography (NH_4OH/MeOH/CH_2Cl_2, 1:5:94 v/v/v) to give the final compound as a white solid.

Ethyl 2-((5-((2-methylthiazol-4-yl)ethynyl)pyridin-3-yl)oxy)acetate (4.09a). To a solution of compound **4.06** (1.95 g, 10 mmol) in DMF was added esters **4.08a** (2.8 g, 11 mmol), CuI (190 mg, 1 mmol) and triethylamine (2.1 ml, 15 mmol). $Pd(PPh_3)_2Cl_2$ (350 mg, 0.5 mmol) was added to the reaction solution and the argon flow was continued for 10 min to remove air. Then a solution of TBAF (11 mmol, 1.0 M in THF) was added dropwise over 30 min. The mixture was heated at 85 °C for 1 h. After reaction, the mixture was filtrated and concentrated under reduced pressure. The residue was purified by silica gel chromatography (Hexane/EtOAc, 3:1-1:1 v/v) to yield compound **4.09a** as a brown solid (1.82 g, 60.2%). ^{1}H NMR (300 MHz, $CDCl_3$) δ ppm 8.43 (d, J = 1.6, 1H), 8.30 (d, J = 2.9 Hz, 1H), 7.42 (s, 1H), 7.30 (dd, J = 2.9, 1.6 Hz, 1H), 4.65 (s, 2H), 4.28 (q, J = 7.1 Hz, 2H), 2.74 (s, 3H), 1.30 (t, J = 7.1 Hz, 3H). ^{13}C NMR (75 MHz, $CDCl_3$) δ 167.8, 166.0, 153.4, 145.6, 138.2, 136.1, 123.2 (d, J = 4.5 Hz), 119.9, 86.7, 85.0, 65.4, 61.7, 19.2, 14.1. HRMS (ESI) m/z: calculated for $C_{15}H_{15}N_2O_3S$ $[M+H]^+$ 303.0803; found 303.0807.

Ethyl 2-(3-((2-methylthiazol-4-yl)ethynyl)phenoxy)acetate (4.09b). Compound **4.09b** was prepared using the procedure described as **4.09a**. Yellow oil (3.88 g, 64%). ^{1}H NMR (300 MHz, $CDCl_3$) δ ppm 7.36 (s, 1H), 7.28 – 7.22 (m, 1H), 7.18 (dt, J = 7.6, 1.3, 1H), 7.07 – 7.04 (m, 1H), 6.95 – 6.90 (m, 1H), 4.61 (s, 2H), 4.27 (q, J = 7.1 Hz, 2H), 2.73 (s, 3H), 1.29 (t, J = 7.2 Hz, 3H). ^{13}C NMR (75 MHz, $CDCl_3$) δ ppm 168.5, 165.6, 157.5, 136.7, 129.5, 125.3, 123.6, 122.3, 117.0, 116.0, 88.3, 83.4, 65.3, 61.4, 19.2, 14.1. HRMS (ESI) m/z: calculated for $C_{16}H_{16}NO_3S$ $[M+H]^+$ 302.0851; found 302.0850.

2-((5-((2-Methylthiazol-4-yl)ethynyl)pyridin-3-yl)oxy)acetic acid (**4.01a**). To a solution of ester **4.09a** (2.3 g, 7.6 mmol) in methanol was added 4 M NaOH (38 mmol, aq.) and then stirred at room temperature for 2 h. Then 1 M HCl (aq.) was added to the solution to acidify it till pH=2. Next the solvent was removed under reduced pressure and the residue was purified by silica gel chromatography (AcOH/Hexane/EtOAc 1:49:50 v/v/v) to yield acid **4.01a** as a pale yellow solid (1.8 g, 86%). ^{1}H NMR (300 MHz, DMSO-d_6) δ ppm 12.37 (br s., 1H), 8.29 (br s, 2H), 7.90 (s, 1H), 7.52 (s, 1H), 4.82 (s, 2H), 2.63 (s, 3H). ^{13}C NMR (75 MHz, DMSO-d_6) δ ppm 172.4, 166.3, 151.6, 144.4, 138.8, 135.2, 125.6, 123.1, 119.1, 87.4, 85.1, 65.1, 19.0. HRMS (ESI) m/z: calculated for $C_{13}H_{11}N_2O_3S$ $[M+H]^+$ 275.0490; found 275.0478.

2-(3-((2-Methylthiazol-4-yl)ethynyl)phenoxy)acetic acid (**4.01b**). Compound **4.01b** was prepared using the procedure described as **4.01a**. Pale yellow solid (2.5 g, 82%). ^{1}H NMR (300 MHz, DMSO-d_6) δ ppm 12.88 (br s., 1H), 7.88 (s, 1H), 7.32 (t, J = 8.4 Hz, 1H), 7.14 – 7.09 (m, 1H), 7.03 (dt, J = 2.5, 0.9 Hz, 1H), 6.98 (ddd, J = 8.3, 2.7, 1.0 Hz, 1H), 4.71 (s, 2H), 2.64 (s, 3H). ^{13}C NMR (75 MHz, DMSO-d_6) δ 170.4, 166.1, 158.1, 135.7, 130.4, 124.9, 124.6, 123.0, 117.0, 116.5, 88.2, 84.4, 64.9, 19.1. HRMS (ESI) m/z: calculated for $C_{14}H_{12}NO_3S$ $[M+H]^+$ 274.0538; found 274.0544.

***tert*-Butyl (5-((8-azidooctyl)(methyl)amino)pentyl)carbamate** (**4.14a**). To a solution of **4.13a** (1.7 g, 10 mmol) in CH_2Cl_2 (50 ml) was added the compound **4.11** (2.4 g, 11 mmol) and $Na(OAc)_3BH$ (4.2 g, 20 mmol) and stirred at room temperature for 6 h. The mixture was quenched by $NaHCO_3$ (sat.) and extracted with CH_2Cl_2 (3x 50 ml), washed with brine and dried over Na_2SO_4. The mixture was filtered and concentrated under reduced pressure. The crude was purified by silica gel chromatography ($MeOH/CH_2Cl_2$ 5:95 v/v) to yield **4.14a** as a colorless oil (2.3 g, 62%). ^{1}H NMR (300 MHz, $CDCl_3$) δ 4.65 (s, 1H), 3.22 (t, J = 6.9, 2H), 3.08 (q, J = 6.4 Hz, 2H), 2.74 – 2.63 (m, 4H), 2.50 (s, 3H), 1.73 – 1.43 (m, 6H), 1.40 (s, 9H), 1.36 – 1.23 (m, 12H). ^{13}C NMR (75 MHz, $CDCl_3$) δ 156.1, 80.6, 56.2, 51.3, 45.6, 40.3, 29.6, 29.0, 28.9, 28.7, 28.3, 26.9, 26.5, 24.6, 24.3, 24.1. HRMS (ESI) m/z: calculated for $C_{19}H_{40}N_5O_2$ $[M+H]^+$ 370.3182; found 370.3175.

***tert*-Butyl (5-((10-azidodecyl)(methyl)amino)pentyl)carbamate** (**4.14b**). Compound **4.14b** was obtained according to the procedure described for compound **4.14a**. Colorless oil (3.3 g, 83%). ^{1}H NMR (300 MHz, $CDCl_3$) δ 4.62 (s, 1H), 3.23 (t, *J* = 6.9 Hz, 2H), 3.08 (q, *J* = 6.6 Hz, 2H), 2.64 – 2.52 (m, 4H), 2.41 (s, 3H), 1.68 – 1.43 (m, 6H), 1.41 (s, 9H), 1.38 – 1.20 (m, 16H). ^{13}C NMR (75 MHz, $CDCl_3$) δ 156.0, 79.4, 56.5 (d, *J* = 16.0 Hz), 51.4, 45.6, 40.8, 40.2, 29.6, 29.2 (d, *J* = 5.1 Hz), 29.1, 28.7, 28.3, 27.1, 26.6, 25.1 (d, *J* = 25.6 Hz), 24.3. HRMS (ESI) m/z: calculated for $C_{21}H_{44}N_5O_2$ $[M+H]^+$ 398.3495; found 398.3427.

***N*^{1}-(8-Azidooctyl)-*N*^{1}-methylpentane-1,5-diamine** (**4.04a**). To a solution of **4.14a** (2.3 g, 6.2 mmol) in CH_2Cl_2 (20 ml) was added TFA (10 ml) and stirred at RT for 6 h. After reaction, the solution was basified with 4 M NaOH (aq.) till pH=8. The mixture was filtered and concentrated under reduced pressure to give the amine liner **4.04a** as a colorless oil (1.6 g, 96%). ^{1}H NMR (300 MHz, $CDCl_3$) δ 5.81 (br s., 2H), 3.24 (t, *J* = 6.9 Hz, 2H), 2.78 (t, *J* = 7.1 Hz, 2H), 2.58 – 2.45 (m, 4H), 2.37 (s, 3H), 1.56 (dt, *J* = 13.9, 7.0 Hz, 6H), 1.37-1.24 (m, 12H). ^{13}C NMR (75 MHz, $CDCl_3$) δ 55.1, 51.0, 45.6, 40.7, 38.9, 29.6, 29.0, 28.7, 26.4, 26.2, 24.6, 24.1, 23.2, 23.1. HRMS (ESI) m/z: calculated for $C_{14}H_{32}N_5$ $[M+H]^+$ 270.2658; found 270.2648.

***N*^{1}-(10-Azidodecyl)-*N*^{1}-methylpentane-1,5-diamine** (**4.04b**). Compound **4.04b** was obtained according to the procedure described for compound **4.04a**. Colorless oil (2.3 g, 93%). ^{1}H NMR (300 MHz, DMSO-*d*$_6$) δ 3.25 (t, *J* = 6.9 Hz, 2H), 3.83 (t, *J* = 6.9 Hz, 2H), 2.61 – 2.52 (m, 4H), 2.43 (s, 3H), 1.69 – 1.42 (m, 6H), 1.38 – 1.21 (m, 16H). ^{13}C NMR (75 MHz, DMSO-*d*$_6$) δ 56.5, 51.4, 45.6, 40.8, 40.2, 29.7, 29.3, 28.7, 28.4, 27.2, 26.6, 25.1, 23.5, 23.1. HRMS (ESI) m/z: calculated for $C_{16}H_{36}N_5$ $[M+H]^+$ 298.2971; found 298.2966.

***N*-(6-Azidohexyl)-2-((5-((2-methylthiazol-4-yl)ethynyl)pyridin-3-yl)oxy)acetamide** (**4.15**). Compound **4.15** was subjected to general procedure 1. Offwhite solid, 72%. ^{1}H NMR (300 MHz, $CDCl_3$) δ 8.32 (br s., 2H), 7.71-7.68 (m, 1H), 7.35 (s, 1H), 6.78 (t, *J* = 5.9 Hz, 1H), 4.43 (s, 2H), 3.23 (td, *J* = 7.2, 6.1 Hz, 2H), 3.17 – 3.10 (m, 2H), 2.62 (s, 3H), 1.53 – 1.41 (m, 4H), 1.31-1.24 (m, 4H). ^{13}C NMR (75 MHz, $CDCl_3$) δ 166.8, 166.0, 137.8, 135.8, 132.6, 123.1, 87.0, 84.6, 67.4, 51.2, 45.8, 43.1, 38.9, 29.3, 28.6, 26.3, 26.2, 19.2, 8.6. HRMS (ESI) m/z: calculated for $C_{19}H_{23}N_6O_2S$ $[M+H]^+$ 399.1603; found 399.1613.

***N*-(5-((8-Azidooctyl)(methyl)amino)pentyl)-2-((5-((2-methylthiazol-4-yl)ethynyl)pyridin-3-yl)oxy)acetamide** (**4.19a**). Compound **4.19a** was subjected to general procedure 1. Offwhite solid, 65%. ^{1}H NMR (300 MHz, $CDCl_3$) δ 8.44 (d, *J* = 1.6 Hz, 1H), 8.30 (dd, *J* = 2.9, 0.4 Hz, 1H), 7.44 (s, 1H), 7.33 (dd, *J* = 2.9, 1.6 Hz, 1H), 6.54 (t, *J* = 6.0 Hz, 1H), 4.50 (s, 2H), 3.35 (td, *J* = 7.1, 5.9 Hz, 2H), 3.23 (t, *J* = 6.9 Hz, 2H), 2.73 (s, 3H), 2.33 – 2.23 (m, 6H), 2.17 (s, 3H), 1.57 (p, *J* = 7.2 Hz, 6H), 1.50 – 1.38 (m, 2H), 1.38 – 1.15 (m, 12H), 0.92 – 0.67 (m, 3H). ^{13}C NMR (75 MHz, $CDCl_3$) δ 166.7, 152.7, 145.9, 137.9, 135.9, 123.5, 123.1, 120.2, 87.1, 84.6, 67.4, 57.8, 57.6, 51.4, 42.3, 39.1, 29.6, 29.5, 29.4, 29.1, 28.7, 27.4, 27.2, 26.9, 26.6, 24.8, 19.2. HRMS (ESI) m/z: calculated for $C_{27}H_{40}N_7O_2S$ $[M+H]^+$ 526.2964; found 526.2967.

***N*-(5-((10-Azidodecyl)(methyl)amino)pentyl)-2-((5-((2-methylthiazol-4-yl)ethynyl)pyridin-3-yl)oxy)acetamide** (**4.19b**). Compound **4.19b** was subjected to general procedure 1. Offwhite solid, 51%. ^{1}H NMR (300 MHz, $CDCl_3$) δ 8.40 (s, 1H), 8.29 (s, 1H), 7.42 (s, 1H), 7.33 (dd, *J* = 2.9, 1.4 Hz, 1H), 6.95 – 6.87 (m, 1H), 5.26 (s, 1H), 4.49 (s, 2H), 3.37 – 3.27 (m, 2H), 3.21 (t, *J* = 6.9 Hz, 2H), 2.94 – 2.85 (m, 5H), 2.71 (s, 3H), 1.75-1.64 (m, 4H), 1.55 (dt, *J* = 14.7, 7.4 Hz, 3H), 1.38-1.16 (m, 16H). HRMS (ESI) m/z: calculated for $C_{29}H_{44}N_7O_2S$ $[M+H]^+$ 554.3277; found 554.3276.

***N*-(5-((8-Azidooctyl)(methyl)amino)pentyl)-2-(3-((2-methylthiazol-4-yl)ethynyl)phenoxy)acetamide** (**4.19c**). Compound **4.19c** was subjected to general procedure 1. Offwhite solid, 76%. ^{1}H NMR (300 MHz, $CDCl_3$) δ 7.37 (s, 1H), 7.30 – 7.24 (m, 1H), 7.20 (dt, *J* = 7.6, 1.3 Hz, 1H), 7.08 (ddd, *J* = 2.7, 1.4, 0.5 Hz, 1H), 6.90 (ddd, *J* = 8.1, 2.7, 1.2 Hz, 1H), 6.61 – 6.51 (m, 1H), 4.46 (s, 2H), 3.33 (td, *J* = 7.1, 5.9 Hz, 2H), 3.22 (t, *J* = 6.9 Hz, 2H), 2.72 (s, 3H), 2.33 – 2.24 (m, 6H), 2.17 (s, 3H), 1.62 – 1.39 (m, 4H), 1.28 (td, *J* = 13.0, 11.3, 7.1 Hz, 12H). ^{13}C NMR (75 MHz, $CDCl_3$) δ 167.6, 156.9, 129.7, 125.6, 123.9, 122.5, 117.5, 115.4, 88.1, 83.8, 67.3, 57.8, 57.6, 51.4, 42.2, 39.0, 29.5, 29.4, 29.1, 28.8, 27.4, 27.2, 26.8, 26.6, 24.8, 19.2. HRMS (ESI) m/z: calculated for $C_{28}H_{41}N_6O_2S$ $[M+H]^+$ 525.3012; found 525.3027.

***N*-(5-((10-Azidodecyl)(methyl)amino)pentyl)-2-(3-((2-methylthiazol-4-yl)ethynyl)phenoxy)acetamide** (**4.19d**). Compound **4.19d** was subjected to general procedure 1. Offwhite solid, 55%. ^{1}H NMR (300 MHz, $CDCl_3$) δ 7.37 (s, 1H), 7.30 – 7.24 (m, 1H), 7.20 (dt, *J* = 7.6, 1.3 Hz, 1H), 7.08 (dd, *J* = 2.7, 1.3 Hz, 1H), 6.89 (ddd, *J* = 8.1, 2.7, 1.3 Hz, 1H), 6.55 (t, *J* = 6.0 Hz, 1H), 4.46 (s, 2H), 3.33 (td, *J* = 7.1, 6.0 Hz, 2H), 3.22 (t, *J* = 6.9 Hz, 2H), 2.72 (s, 3H), 2.34 – 2.23 (m, 6H), 2.17 (s, 3H), 1.62 – 1.40 (m, 4H), 1.35 – 1.20 (m, 16H). ^{13}C NMR (75 MHz, $CDCl_3$) δ 167.6, 165.7, 156.9, 136.6, 129.8, 125.6, 123.9, 122.5, 117.6, 115.4, 88.1, 83.9, 67.4, 57.8, 57.6, 51.4, 42.2, 39.0, 29.5, 29.5, 29.4, 29.4, 29.1, 28.8, 27.5, 27.2, 26.9, 26.6, 24.8, 19.2. HRMS (ESI) m/z: calculated for $C_{30}H_{45}N_6O_2S$ $[M+H]^+$ 553.3325; found 553.3311.

***N*-(2-(2-(2-(2-Azidoethoxy)ethoxy)ethoxy)ethyl)-2-(3-((2-methylthiazol-4-yl)ethynyl)phenoxy)acetamide** (**4.17a**). Compound **4.17a** was subjected to general procedure 1. Offwhite solid, 87%. ^{1}H NMR (300 MHz, $CDCl_3$) δ 7.35 (s, 1H), 7.27 – 7.21 (m, 1H), 7.17 (dt, *J* = 7.6, 1.3 Hz, 1H), 7.05 (ddd, *J* = 2.7, 1.4, 0.5 Hz, 1H), 6.96 (wide peak, 1H), 6.88 (ddd, *J* = 8.1, 2.7, 1.2 Hz, 1H), 4.45 (s, 2H), 3.62 – 3.47 (m, 14H), 3.31 (t, *J* = 5.6 Hz, 2H), 2.69 (s, 3H). ^{13}C NMR (75 MHz, $CDCl_3$) δ 167.8, 165.8, 157.0, 136.5, 129.7, 125.6, 123.9, 122.5, 117.5, 115.5, 88.1, 83.8, 70.6, 70.5, 70.3, 69.9, 69.6, 67.4, 50.6, 38.76, 19.2. HRMS (ESI) m/z: calculated for $C_{22}H_{28}N_5O_5S$ $[M+H]^+$ 474.1811; found 474.1817.

***N*-(17-Azido-3,6,9,12,15-pentaoxaheptadecyl)-2-(3-((2-methylthiazol-4-yl)ethynyl)phenoxy)acetamide** (**4.17b**). Compound **4.17b** was subjected to general procedure 1. Offwhite solid, 94%. ^{1}H NMR (300 MHz, $CDCl_3$) δ 7.35 (s, 1H), 7.27 – 7.21 (m, 1H), 7.17 (dtd, *J* = 7.6, 1.3, 0.5 Hz, 1H), 7.06 (dd, *J* = 2.7, 1.4 Hz, 1H), 6.89 (dddd, *J* = 8.1, 2.7, 1.2, 0.5 Hz, 1H), 4.46 (s, 2H), 3.65 – 3.46 (m, 22H), 3.32 (t, *J* = 5.1 Hz, 2H), 2.69 (s, 3H). ^{13}C NMR (75 MHz, $CDCl_3$) δ 167.8, 165.7, 157.0, 136.5, 129.7, 125.5, 123.8, 122.6, 117.4, 115.6, 88.1, 83.7, 70.6, 70.6, 70.5, 70.5, 70.4, 70.30, 69.9, 69.6, 67.4, 50.6, 38.7. HRMS (ESI) m/z: calculated for $C_{26}H_{36}N_5O_7S$ $[M+H]^+$ 562.2335; found 562.2363.

***N*-(4-(2-((5-Hydroxy-1,2,3,4-tetrahydronaphthalen-2-yl)(propyl)amino)ethyl)phenyl)-3-(1-(6-(2-((5-((2-methylthiazol-4-yl)ethynyl)pyridin-3-yl)oxy)acetamido)hexyl)-1H-1,2,3-triazol-4-yl)propanamide** (**4.16**). Compound **4.16** was subjected to general procedure 2. White solid, 51%. LC-HRMS: t_R=7.09 min (10–100% MeCN, 15 min run), purity 95.09 %.HRMS (ESI) m/z: calculated for $C_{45}H_{56}N_8O_4S$ $[M+2H]^{2+}$ 402.2067; found 402.2058.

***N*-(4-(2-((5-Hydroxy-1,2,3,4-tetrahydronaphthalen-2-yl)(propyl)amino)ethyl)phenyl)-3-(1-(8-(methyl(5-(2-((5-((2-methylthiazol-4-yl)ethynyl)pyridin-3-yl)oxy)acetamido)pentyl)amino)octyl)-1H-1,2,3-triazol-4-yl)propanamide** (**4.20a**). Compound **4.20a** was subjected to general procedure 2. White solid, 38%. LC-HRMS: t_R=6.21 min (10–100% MeCN, 15 min run), purity 96.64 %. ^{1}H NMR (300 MHz, DMSO-*d*$_6$) δ 9.82 (s, 1H), 8.35 (br s, 2H), 8.21 (br s, 1H), 8.17 – 8.09 (m, 1H), 7.95 (s, 1H), 7.78 (s, 1H), 7.51 (dd, *J* = 2.8, 1.7 Hz, 1H), 7.47 – 7.40 (m, 2H), 7.10 (d, *J* = 8.4 Hz, 2H), 6.84 (t, *J* = 7.7 Hz, 1H), 6.53 (dd, *J* = 8.0, 1.1 Hz, 1H), 6.48 (dd, *J* = 7.6, 1.1 Hz, 1H), 4.61 (s, 2H), 4.24 (t, *J* = 6.8 Hz, 2H), 3.10 (q, *J*=6.54 Hz, 2H), 2.96 – 2.69 (m, 6H), 2.68 – 2.55 (m, 10H), 2.43 – 2.31 (m, 5H), 2.20 (s, 3H), 1.91 (br d, *J* = 11.6 Hz, 1H), 1.77 – 1.66 (m, 2H), 1.51 – 1.25 (m, 10H), 1.17 (br s, 10H), 0.81 (t, *J* = 7.3 Hz, 3H). ^{13}C NMR (75 MHz, DMSO-*d*$_6$) δ 170.4, 167.2, 166.5, 155.2, 154.0, 146.2, 144.6, 139.1, 138.0, 137.5, 135.7, 135.2, 129.3, 126.3, 125.8, 123.4, 123.3, 122.3, 120.2, 119.4, 111.9, 87.4, 85.1, 67.5, 56.8, 56.6, 52.8, 52.2, 49.6, 41.4, 38.6, 36.3, 35.0, 32.4, 30.2, 29.3, 29.1, 28.8, 27.0, 26.2, 26.1, 25.8, 24.4, 23.9, 22.1, 21.5, 19.2, 12.2. HRMS (ESI) m/z: calculated for $C_{53}H_{73}N_9O_4S$ $[M+2H]^{2+}$ 465.7747; found 465.7756.

***N*-(4-(2-((5-Hydroxy-1,2,3,4-tetrahydronaphthalen-2-yl)(propyl)amino)ethyl)phenyl)-3-(1-(10-(methyl(5-(2-((5-((2-methylthiazol-4-yl)ethynyl)pyridin-3-yl)oxy)acetamido)pentyl)amino)decyl)-1H-1,2,3-triazol-4-yl)propanamide** (**4.20b**). Compound **4.20b** was subjected to general procedure 2. White solid, 45%. LC-HRMS: t_R=6.47 min (10–100% MeCN, 15 min run), purity 96.97 %. HRMS (ESI) m/z: calculated for $C_{55}H_{77}N_9O_4S$ $[M+2H]^{2+}$ 479.7904; found 479.7895.

***N*-(5-((8-(4-((2-Methoxy-4-((4-(2-methoxyphenyl)piperazin-1-yl)methyl)phenoxy)methyl)-1H-1,2,3-triazol-1-yl)octyl)(methyl)amino)pentyl)-2-((5-((2-methylthiazol-4-yl)ethynyl)pyridin-3-yl)oxy)acetamide** (**4.21a**). Compound **4.21a** was subjected to general procedure 2. White solid, 47%. LC-HRMS: t_R=6.25 min (10–100% MeCN, 15 min run), purity 96.54 %. HRMS (ESI) m/z: calculated for $C_{49}H_{67}N_9O_5S$ $[M+2H]^{2+}$ 446.7487; found 446.7470.

***N*-(5-((10-(4-((2-Methoxy-4-((4-(2-methoxyphenyl)piperazin-1-yl)methyl)phenoxy)methyl)-1H-1,2,3-triazol-1-yl)decyl)(methyl)amino)pentyl)-2-((5-((2-methylthiazol-4-yl)ethynyl)pyridin-3-yl)oxy)acetamide** (**4.21b**). Compound **4.21b** was subjected to general procedure 2. White solid, 49%. LC-HRMS: t_R=6.92 min (10–100% MeCN, 15 min run), purity 96.47 %. HRMS (ESI) m/z: calculated for $C_{51}H_{71}N_9O_5S$ $[M+2H]^{2+}$ 460.7643; found 460.7631.

***N*-(5-((8-(4-((2-Methoxy-4-((4-(2-methoxyphenyl)piperazin-1-yl)methyl)phenoxy)methyl)-1H-1,2,3-triazol-1-yl)octyl)(methyl)amino)pentyl)-2-(3-((2-methylthiazol-4-yl)ethynyl)phenoxy)acetamide** (**4.21c**). Compound **4.21c** was subjected to general procedure 2. White solid, 52%. LC-HRMS: t_R=6.96 min (10–100% MeCN, 15 min run), purity 97.07 %. HRMS (ESI) m/z: calculated for $C_{50}H_{68}N_8O_5S$ $[M+2H]^{2+}$ 446.2511; found 446.2488.

***N*-(5-((10-(4-((2-Methoxy-4-((4-(2-methoxyphenyl)piperazin-1-yl)methyl)phenoxy)methyl)-1H-1,2,3-triazol-1-yl)decyl)(methyl)amino)pentyl)-2-(3-((2-methylthiazol-4-yl)ethynyl)phenoxy)acetamide** (**4.21d**). Compound **4.21d** was subjected to general procedure 2. White solid, 54%. LC-HRMS: t_R=6.87 min (10–100% MeCN, 15 min run), purity 92.29 %. HRMS (ESI) m/z: calculated for $C_{52}H_{72}N_8O_5S$ $[M+2H]^{2+}$ 460.2667; found 460.2644.

***N*-(2-(2-(2-(2-(4-((2-Methoxy-4-((4-(2-methoxyphenyl)piperazin-1-yl)methyl)phenoxy)methyl)-1H-1,2,3-triazol-1-yl)ethoxy)ethoxy)ethoxy)ethyl)-2-(3-((2-methylthiazol-4-yl)ethynyl)phenoxy)acetamide** (**4.18a**). Compound **4.18a** was subjected to general procedure 2. White solid, 51%. LC-HRMS: t_R=7.37 min (10–100% MeCN, 15 min run), purity 97.82 %. HRMS (ESI) m/z: calculated for $C_{44}H_{55}N_7O_8S$ $[M+2H]^{2+}$ 420.6911; found 420.6891.

***N*-(17-(4-((2-Methoxy-4-((4-(2-methoxyphenyl)piperazin-1-yl)methyl)phenoxy)methyl)-1H-1,2,3-triazol-1-yl)-3,6,9,12,15-pentaoxaheptadecyl)-2-(3-((2-methylthiazol-4-yl)ethynyl)phenoxy)acetamide** (**4.18b**). Compound **4.18b** was subjected to general procedure 2. White solid, 58%. LC-HRMS: t_R=7.24 min (10–100% MeCN, 15 min run), purity 97.78 %. HRMS (ESI) m/z: calculated for $C_{48}H_{63}N_7O_{10}S$ $[M+2H]^{2+}$ 464.7173; found 464.7140.

IV.5.2. Generation of the stable D2s-mGluR5 co-expressing cell line

Production of the stable D2s-mGluR5 co-expressing cell line was conducted by a retroviral transduction of D2s (human) into the *mGluR5a-HEK293-TREx* stable cell line (a kind gift of Janssen Pharmaceutical Companies of Johnson & Johnson), stably transfected with the mGluR5a/pcDNA4-TO construct (RefSeq NM_000842; RefSeqP NP_000833).

The retroviral construct of D2s was generated by PCR-amplifying the D2s sequence (RefSeq NM_016574.3) flanked by the *Sna*BI/*Not*I restriction enzyme sites and cloned into the digested retroviral vector pLZRS-IRES-EGFP. The integrity of the insert was confirmed by DNA sequencing. The pLZRS-D2s-IRES-EGFP plasmid leads to co-expression of the D2s and eGFP, the latter can be used as a marker for cell sorting and to check the stability of the cell lines by flow cytometry.

For the production of retrovirus and retroviral transduction the Phoenix-Amphotropic packaging cell line[33] was used (a kind gift from prof. Bruno Verhasselt, Department of Clinical Chemistry, Microbiology, and Immunology, Ghent University, Belgium). The cells were transfected with LZRS-D2s-IRES-EGFP, by calcium phosphate precipitation (Invitrogen, San Diego, CA, USA). After puromycin selection of 2 weeks, the retroviral supernatant was harvested, spun down (10 min at 350 × g) and aliquots of the supernatant were stored at −80 °C until use. For transduction of human embryonic kidney (HEK) 293T cells, 10^4 cells/well were seeded in a transparent 96-well plate. After 24 h, the medium was refreshed with the retroviral supernatant, which had been preincubated for 10 min with Dotap (Roche Diagnostics). To increase transduction efficiency, the plates were spun down (90 min, 950 × g, 32 °C). Transduction efficiency was measured by flow cytometry 48 h after transduction, via assessment of expression of EGFP. Cell sorting was done on a BD FACSAria III, equipped with 405, 488, 561, and 640 nm lasers (BD Biosciences, Erembodegem, Belgium).

All cells were cultured at 37 °C, 5% CO_2, under humidified atmosphere in DMEM (high glucose) supplemented with 10% heat inactivated fetal bovine serum (FBS), 2 mM of glutamine, 100 IU/ml of penicillin, 100 µg/mL of streptomycin, and 0.25 µg/ mL of amphotericin B. Stability of the cell line was followed up by flow cytometric analysis.

IV.5.3. Cell culture and transfection

Human embryonic kidney (HEK) 293T cells and HEK 293 mGluR5 cells (Janssen Pharmaceutica, Belgium) were cultured in Dulbecco's modified Eagle's medium (DMEM; Invitrogen), supplemented with 10% fetal bovine serum, penicillin (100 U/ml), and streptomycin (100 µg/ml) in a controlled environment (37 °C, 98% humidity, 5% CO_2). For ligand binding experiments, HEK293T cells were transiently transfected using the Polyethylenimine (PEI) method as described before.[43],[63] A total amount of 10 µg of DNA was used for transfection of cells in one 10-cm dish. HEK293S cells stably expressing HA $D_{4.2}R$[43] were grown in DMEM/F12 (Gibco, Invitrogen) supplemented with 10% fetal bovine serum, penicillin (100 U/ml), streptomycin (100 μg/ml), and 0.5 mg/ml G418 (Geneticin, Gibco) in a controlled environment (37 °C, 98% humidity, 5% CO_2).

IV.5.4. Membrane Preparation and Protein Determination.

Membrane suspensions from HEK293T cells transiently transfected with the receptors of interest were prepared as described previously.[29] Cells were disrupted with a Polytron homogenizer for two 10 s periods in 10 volumes of ice-cold Tris-HCl buffer (50 mM, pH 7.4). Membranes were obtained by centrifugation at 16500g for 20 min at 4 °C, and the pellet was resuspended and centrifuged under the same conditions. The resulting pellet was stored at -80 °C and was washed once more as described above and resuspended in Tris-HCl buffer (50 mM, pH 7.4) for immediate use. Protein was quantified by the BCA method using bovine serum albumin dilutions as the standard.

IV.5.5. [^{3}H]Spiperone Binding.

Saturation binding assay for [^{3}H]spiperone was performed as previously described.[64],[65] For competition binding assays, membranes (20 μg) were incubated in binding buffer (50 mM Tris-HCl containing 5 mM KCl, 1 mM EDTA, 1.5 mM $CaCl_2$ and 4 mM $MgCl_2$, pH 7.4) with 0.2 nM [^{3}H]spiperone (specific activity = 76 Ci/mmol, PerkinElmer, USA) in the absence or presence of varying concentrations (0.1 nM-10 μM) of unlabeled ligands for 1 h at 22 °C. Nonspecific binding was determined in the presence of 1 μM haloperidol. Incubation was terminated by rapid filtration through GF/C glass-fiber filters (Whatman Schleicher and Schuell, Keene, NH) embedded in 0.1% polyethylenimine and mounted on a Brandel cell harvester. Filters were washed three times with cold 50 mM Tris-HCl, pH 7.4 buffer and transferred to vials containing 3 mL of scintillation cocktail to soak the filter overnight. The radioactivity counts were measured with a Tri-Carb 2800TR liquid scintillation analyzer (PerkinElmer).

IV.5.6. [^{3}H]Raclopride Binding.

[^{3}H]raclopride saturation binding assay was performed as described before.[66] Briefly, a suspension of whole cells or cell membranes (corresponding a total protein amount of 20 μg) were incubated with different concentrations (0–20 nM) of [^{3}H]raclopride in 50 mM Tris-HCl, pH 7.4 buffer (containing 5 mM KCl, 100 mM NaCl, 1.5 mM $CaCl_2$, 4 mM $MgCl_2$ and 1 mM EDTA) at 37 °C for 1 h. For competitive binding experiments, 2.0 nM [^{3}H]raclopride (specific activity = 73.8 Ci/mmol, PerkinElmer, USA) was incubated with 20 μg of cell membranes in the absence or presence of varying concentrations (0.1 nM-10 μM) of unlabeled ligands at 37 °C for 1 h. Nonspecific binding was determined in the presence of 1 μM haloperidol. Filtration and measuring were as described above.

IV.5.7. [^{3}H]MPEP Binding.

[^{3}H]MPEP saturation binding assay was adapted from a published protocol.[67] Membranes (20 µg) were incubated with different concentrations (0–10 nM) of [^{3}H]MPEP in 50 mM Tris-HCl and 2 mM $MgCl_2$, pH 7.4 buffer at 25 °C for 1 h. For competitive binding experiments, 3.0 nM [^{3}H]MPEP (specific activity = 60 Ci/mmol, American Radiolabeled Chemicals, Inc.) was incubated with 20 µg of membranes in the absence or presence of varying concentrations (0.1 nM-100 µM) of unlabeled ligands at 25 °C for 1 h. Nonspecific binding was determined in the presence of 10 µM MPEP. Filtration and measuring were as described above.

IV.5.8. Data Analysis.

Results are expressed as means ± SEM for at least three experiments, each performed in duplicate. Statistical analysis and curve fits of dose-response curves were performed using GraphPad Prism 7. Ki values were calculated by using the Cheng-Prusoff equation.[68]

IV.5.9. MAPK phosphorylation

HEK293S cells stably expressing HA D4.2R were seeded in 6-well plates with 400,000 cells per well. When the cells were 70% confluent, cells were starved overnight with serum free medium. The ligands (1 nM-10 µM) were added sequentially to the cells at the concentrations indicated in the legend for 5 min. To stop the reaction, medium was aspirated, the cells were placed on ice and washed with ice-cold PBS. RIPA buffer [150 mM NaCl; 50 mM Tris/HCl pH 7.5; 1 % NP-40; 0.1 % SDS; and 0.5 % deoxycholic acid sodium salt (Acros Organics: 218591000); protease inhibitors: aprotinin (2.5 µg/ml, Sigma-Aldrich: A6279), pefablock (1 mM, Sigma-Aldrich: 76307), leupeptin (10 µg/ml, Acros Organics: 328350050), and phosphatase inhibitor β-glycerol phosphate disodium salt pentahydrate (10 mM, Fluka BioChemika: 50020)] was used to prepare the cell lysate for western blotting according to the protocol described before.[69] After western blotting, the membrane was incubated with blocking buffer (LI-COR Biosciences) for 1h at RT. Then, primary antibody rabbit polyclonal phospho-p44/42 MAPK (1/2000) (Cell Signaling, cat. no. 9101L) or mouse monoclonal p44/42 MAPK (1/2000) (clone L34F12; Cell Signaling, cat. no. 4696S) was added to develop the blot overnight at 4 °C. Next, the blot was washed with washing buffer (PBS + 0.05% Tween 20 from Sigma-Aldrich) for three times and then secondary antibodies goat anti-rabbit IRDye680 LT (1/10000) (cat. no. 926–68021, LI-COR Biosciences) or goat anti-mouse IRDye800 (1/10000) (cat. no.926–32210, LI-COR Biosciences) were added for 1h at RT in the dark. The blot was washed with washing buffer for three times and the fluorescent signal was detected with the Odyssey Infrared Imaging system. In the analysis, the phospho-p44/42 MAPK signal is normalized against the total p44/42 MAPK signal after quantification by Image J.

IV.5.10. GloSensor cAMP protocol

HEK293T D2s-mGluR5 co-expressing cells and HEK293T D2s cells were seeded in 6-well plates at 500 000 cells/well. The day after, cells were transfected with the pGloSensor-22F cAMP plasmid, using the FuGene transfection reagent (as described previously).[44]

Cells were first washed with CO_2-independent medium and afterwards incubated with equilibration medium containing 2% v/v GloSensor cAMP reagent stock solution in 10% FBS CO_2-independent medium. After an incubation of 30 min at 37 °C, the luminescence signal was measured until a steady-state basal signal was obtained. Serial concentrations of monovalent agonist DPAT-alkyne (**3.07**) or bivalent ligand (**4.20a**) (0.1 nM-10 µM) were added. After 15 min, 10 µM Forskolin (FSK) was added. The agonist profile of the compounds was evaluated by assessing their ability to counteract the Forskolin-induced increase of cAMP accumulation. Therefore, the maximal luminescent responses were used for generating dose-response curves and EC_{50}-values.

IV.5.11. Computational modeling

IV.5.11.1 Receptor structure preparation

Crystallographic missing residues and/or atoms in the human D_2R crystal structure[47] (PDB id: 6CM4) were added using CHIMERA v1.11.2 software[70] by selecting the most probable rotamer at relevant positions with fewest possible steric clashes. Mutated residues: I122A, L375A, L379A were converted back to wild-type using the same procedure. The four-residue missing segment of intracellular loop 2 (ICL2) was *ab initio* modeled with MODELLER v9.18.[71] Co-crystallized risperidone and endolysin fusion protein were removed from the D_2R structure. Energy minimization was then performed on added residues/loops and any clashing atoms in the AMBER14SB force-field.[72]

From a previously published MD simulation of mGlu5 with bound NAM,[50] a conformation of mGlu5 was extracted which has a larger extracellular gap between TM5 and TM6 than the original crystal structure[46] (PDB id: 4009). The simulated NAM was removed from this structure.

IV.5.11.2 Protein-protein docking

For construction of an mGluR5-D2R heterodimer model, where D_2R and mGluR5 interact via a symmetrical TM5-TM6 interface, both receptors were systematically superimposed onto relevant monomers of the mu-opioid receptor homodimer crystal structure[59] (PDB id: 4DKL). The mGluR5-D_2R heterodimer model was then submitted to the ROSIE webserver[60] for protein-protein docking using default parameters. The best docked heterodimer structure was identified by two factors: best interface score (“I_sc”) and best membrane-compatible orientation.

IV.5.11.3 Bivalent ligand docking

Coordinates for MTEP and 5-OH-DPAT were downloaded from PubChem.[73] Autodock v4.2[74] was used to dock MTEP into mGluR5 and 5-OH-DPAT into D_2R in the heterodimer model. Grid points were extended to cover total allosteric and orthosteric pocket volumes, respectively. The selected docked conformation of each ligand in its receptor represents the top hit identified by best predicted affinity in the largest docking cluster. The linker between MTEP and 5-OH-DPAT components, corresponding to compound **4.20a**, was modeled with CHIMERA by manually extending the chain from both sides and connecting at the heterodimer interface between TM5 and TM6 of both receptors. The **4.20a** linker was modeled to follow the shortest path possible between receptors whilst avoiding steric clashes. The heterodimer-ligand complex was energy minimized without restraints with CHIMERA in the AMBER-14SB force-field[72] to relax the **4.20a** linker and optimize protein-ligand interactions.

REFERENCES

[1] Bräuner-Osborne, H.; Egebjerg, J.; Nielsen, E. O.; Madsen, U.; Krogsgaard-Larsen, P. Ligands for glutamate receptors: design and therapeutic prospects. *J. Med. Chem.* **2000**, *43*, 2609–2645.

[2] Roppe, J. R.; Wang, B.; Huang, D.; Tehrani, L.; Kamenecka, T.; Schweiger, E. J.; Anderson, J. J.; Brodkin, J.; Jiang, X.; Cramer, M.; Chung, J.; Reyes-Manalo, G.; Munoz, B.; Cosford, N. D. 5-[(2-Methyl-1,3-thiazol-4-yl)ethynyl]-2,3'-bipyridine: a highly potent, orally active metabotropic glutamate subtype 5 (mGlu5) receptor antagonist with anxiolytic activity. *Bioorg. Med. Chem. Lett.* **2004**, *14*, 3993–3996.

[3] Pin, J. P.; Acher, F. The metabotropic glutamate receptors: structure, activation mechanism and pharmacology. *Curr. Drug Targets CNS Neurol. Disord.* **2002**, *1*, 297–317.

[4] Conn, P. J.; Pin, J. P. Pharmacology and functions of metabotropic glutamate receptors. *Annu. Rev. Pharmacol. Toxicol.* **1997**, *37*, 205–237.

[5] Cosford, N. D.; Tehrani, L.; Roppe, J.; Schweiger, E.; Smith, N. D.; Anderson, J.; Bristow, L.; Brodkin, J.; Jiang, X.; McDonald, I.; Rao, S.; Washburn, M.; Varney, M. A. 3-[(2-Methyl-1,3-thiazol-4-yl)ethynyl]-pyridine: a potent and highly selective metabotropic glutamate subtype 5 receptor antagonist with anxiolytic activity. *J. Med. Chem.* **2003**, *46*, 204–206.

[6] Alagille, D.; Baldwin, R. M.; Roth, B. L.; Wroblewski, J. T.; Grajkowska, E.; Tamagnan, G. D. Synthesis and receptor assay of aromatic-ethynyl-aromatic derivatives with potent mGluR5 antagonist activity. *Bioorg. Med. Chem.* **2005**, *13*, 197–209.

[7] Kulkarni, S. S.; Zou, M. F.; Cao, J.; Deschamps, J. R.; Rodriguez, A. L.; Conn, P. J.; Newman, A. H. Structure-activity relationships comparing N-(6-methylpyridin-yl)-substituted aryl amides to 2-methyl-6-(substituted-arylethynyl)pyridines or 2-methyl-4-(substituted-arylethynyl)thiazoles as novel metabotropic glutamate receptor subtype 5 antagonists. *J. Med. Chem.* **2009**, *52*, 3563–3575.

[8] Baumann, C. A.; Mu, L.; Johannsen, S.; Honer, M.; Schubiger, P. A.; Ametamey, S. M. Structure-activity relationships of fluorinated (E)-3-((6-methylpyridin-2-yl)ethynyl)cyclohex-2-enone-O-methyloxime (ABP688) derivatives and the discovery of a high affinity analogue as a potential candidate for imaging metabotropic glutamate recepors subtype 5 (mGluR5) with positron emission tomography (PET). *J. Med. Chem.* **2010**, *53*, 4009–4017.

[9] Bruno, V.; Ksiazek, I.; Battaglia, G.; Lukic, S.; Leonhardt, T.; Sauer, D.; Gasparini, F.; Kuhn, R.; Nicoletti, F.; Flor, P. J. Selective blockade of metabotropic glutamate receptor subtype 5 is neuroprotective. *Neuropharmacology* **2000**, *39*, 2223–2230.

[10] Wang, Q.; Walsh, D. M.; Rowan, M. J.; Selkoe, D. J.; Anwyl, R. Block of long-term potentiation by naturally secreted and synthetic amyloid beta-peptide in hippocampal slices is mediated via activation of the kinases c-Jun N-terminal kinase, cyclin-dependent kinase 5, and p38 mitogen-activated protein kinase as well as metabotropic glutamate receptor type 5. *J. Neurosci.* **2004**, *24*, 3370–3378.

[11] Rouse, S. T.; Marino, M. J.; Bradley, S. R.; Awad, H.; Wittmann, M.; Conn, P. J. Distribution and roles of metabotropic glutamate receptors in the basal ganglia motor circuit: implications for treatment of Parkinson's disease and related disorders. *Pharmacol. Ther.* **2000**, *88*, 427–435.

[12] Ossowska, K.; Konieczny, J.; Wardas, J.; Pietraszek, M.; Kuter, K.; Wolfarth, S.; Pilc, A. An influence of ligands of metabotropic glutamate receptor subtypes on parkinsonian-like symptoms and the striatopallidal pathway in rats. *Amino Acids.* **2007**, *32*, 179–188.

[13] Varney, M. A.; Gereau, R. W. 4th. Metabotropic glutamate receptor involvement in models of acute and persistent pain: prospects for the development of novel analgesics. *Curr. Drug Targets CNS Neurol. Disord.* **2002**, *1*, 283–296.

[14] Pilc, A.; Kłodzińska, A.; Brański, P.; Nowak, G.; Pałucha, A.; Szewczyk, B.; Tatarczyńska, E.; Chojnacka-Wójcik, E.; Wierońska, J. M. Multiple MPEP administrations evoke anxiolytic- and antidepressant-like effects in rats. *Neuropharmacology* **2002**, *43*, 181–187.

[15] Chiamulera, C.; Epping-Jordan, M. P.; Zocchi, A.; Marcon, C.; Cottiny, C.; Tacconi, S.; Corsi, M.; Orzi, F.; Conquet, F. Reinforcing and locomotor stimulant effects of cocaine are absent in mGluR5 null mutant mice. *Nat. Neurosci.* **2001**, *4*, 873–874.

[16] Bear, M. F. Therapeutic Implications of the mGluR5 theory of fragile X mental retardation. *Genes Brain Behav.* **2005**, *4*, 393–398.

[17] Todd, P. K.; Mack, K. J.; Malter, J. S. The fragile X mental retardation protein is required for type-I metabotropic glutamate receptor-dependent translation of PSD-95. *Proc. Natl. Acad. Sci. U.S.A.* **2003**, *100*, 14374–14378.

[18] Cabello, N.; Gandía, J.; Bertarelli, D. C.; Watanabe, M.; Lluís, C.; Franco, R.; Ferré, S.; Luján, R.; Ciruela, F. Metabotropic glutamate type 5, dopamine D2 and adenosine A2a receptors form higher-order oligomers in living cells. *J. Neurochem.* **2009**, *109*, 1497–1507.

[19] Díaz-Cabiale, Z.; Vivó, M.; Del Arco, A.; O'Connor, W. T.; Harte, M. K.; Müller, C. E.; Martínez, E.; Popoli, P.; Fuxe, K.; Ferré, S. Metabotropic glutamate mGlu5 receptor-mediated modulation of the ventral striopallidal GABA pathway in rats. Interactions with adenosine A(2A) and dopamine D(2) receptors. *Neurosci. Lett.* **2002**, *324*, 154–158.

[20] Beggiato, S.; Tomasini, M. C.; Borelli, A. C.; Borroto-Escuela, D. O.; Fuxe, K.; Antonelli, T.; Tanganelli, S.; Ferraro, L. Functional role of striatal A2A, D2, and mGlu5 receptor interactions in regulating striatopallidal GABA neuronal transmission. *J. Neurochem.* **2016**, *138*, 254–264.

[21] Mao, L. M.; Wang, J. Q. Dopamine D2 receptors are involved in the regulation of Fyn and metabotropic glutamate receptor 5 phosphorylation in the rat striatum in vivo. *J. Neurosci. Res.* **2016**, *94*, 329–338.

[22] Morin, N.; Morissette, M.; Grégoire, L.; Di Paolo, T. mGlu5, Dopamine D2 and Adenosine A2A Receptors in L-DOPA-induced Dyskinesias. *Curr. Neuropharmacol.* **2016**, *14*, 481–493.

[23] Iso, Y.; Grajkowska, E.; Wroblewski, J. T.; Davis, J.; Goeders, N. E.; Johnson, K. M.; Sanker, S.; Roth, B. L.; Tueckmantel, W.; Kozikowski, A. P. Synthesis and structure-activity relationships of 3-[(2-methyl-1,3-thiazol-4-yl)ethynyl]pyridine analogues as potent, noncompetitive metabotropic glutamate receptor subtype 5 antagonists; search for cocaine medications. *J. Med. Chem.* **2006**, *49*, 1080–1100.

[24] Milligan, G,; Bouvier, M. Methods to monitor the quaternary structure of G protein-coupled receptors. *FEBS J.* **2005**, *272*, 2914–2925.

[25] Yekkirala, A. S.; Lunzer, M. M.; McCurdy, C. R.; Powers, M. D.; Kalyuzhny, A. E.; Roerig, S. C.; Portoghese, P. S. N-naphthoyl-beta-naltrexamine (NNTA), a highly selective and potent activator of μ/kappa-opioid heteromers. *Proc. Natl. Acad. Sci. U.S.A.* **2011**, *108*, 5098–5103.

[26] Soriano, A.; Ventura, R.; Molero, A.; Hoen, R.; Casadó, V.; Cortés, A.; Fanelli, F.; Albericio, F.; Lluís, C.; Franco, R.; Royo, M. Adenosine A2A receptor-antagonist/dopamine D2 receptor-agonist bivalent ligands as pharmacological tools to detect A2A-D2 receptor heteromers. *J. Med. Chem.* **2009**, *52*, 5590–5602.

[27] Jacobson, K. A.; Xie, R.; Young, L.; Chang, L.; Liang, B. T. A novel pharmacological approach to treating cardiac ischemia. Binary conjugates of A1 and A3 adenosine receptor agonists. *J. Biol. Chem.* **2000**, *275*, 30272–30279.

[28] Portoghese, P. S. From models to molecules: opioid receptor dimers, bivalent ligands, and selective opioid receptor probes. *J. Med. Chem.* **2001**, *44*, 2259–2269.

[29] Qian, M.; Vasudevan, L.; Huysentruyt, J.; Risseeuw, M. D. P.; Stove, C.; Vanderheyden, P. M. L.; Van Craenenbroeck, K.; Van Calenbergh, S. Design, Synthesis, and Biological Evaluation of Bivalent Ligands Targeting Dopamine D_2-Like Receptors and the μ-Opioid Receptor *ChemMedChem* **2018**, *13*, 944 – 956.

[30] Kühhorn, J.; Hübner, H.; Gmeiner, P. Bivalent dopamine D2 receptor ligands: synthesis and binding properties. *J. Med. Chem.* **2011**, *54*, 4896–4903.

[31] Gogoi, S.; Biswas, S.; Modi, G.; Antonio, T.; Reith, M. E.; Dutta, A. K. Novel bivalent ligands for D2/D3 dopamine receptors: Significant co-operative gain in D2 affinity and potency. *ACS Med. Chem. Lett.* **2012**, *3*, 991–996.

[32] Zhang, Y.; Gilliam, A.; Maitra, R.; Damaj, M. I.; Tajuba, J. M.; Seltzman, H. H.; Thomas, B. F. Synthesis and biological evaluation of bivalent ligands for the cannabinoid 1 receptor. *J Med. Chem.* **2010**, *53*, 7048–7060.

[33] Leung, J. C.; Chatalova-Sazepin, C.; West, J. G.; Rueda-Becerril, M.; Paquin, J. F.; Sammis, G. M. Photo-fluorodecarboxylation of 2-aryloxy and 2-aryl carboxylic acids. *Angew. Chem. Int. Ed Engl.* **2012**, *51*, 10804–10807.

[34] Sathisha, K. R.; Khanum, S. A.; Chandra, J. N.; Ayisha, F.; Balaji, S.; Marathe, G. K.; Gopal, S.; Rangappa, K. S. Synthesis and xanthine oxidase inhibitory activity of 7-methyl-2-(phenoxymethyl)-5H-[1,3,4]thiadiazolo[3,2-a]pyrimidin-5-one derivatives. *Bioorg. Med. Chem.* **2011**, *19*, 211–220.

[35] Junker, A.; Balasubramanian, R.; Ciancetta, A.; Uliassi, E.; Kiselev, E.; Martiriggiano, C.; Trujillo, K.; Mtchedlidze, G.; Birdwell, L.; Brown, K. A.; Harden, T. K.; Jacobson, K. A. Structure-Based Design of 3-(4-Aryl-1H-1,2,3-triazol-1-yl)-Biphenyl Derivatives as P2Y14 Receptor Antagonists. *J. Med. Chem.* **2016**, *59*, 6149–6168.

[36] Akiba, H.; Sumaoka, J.; Tsumoto, K.; Komiyama, M. Click conjugation of a binuclear terbium(III) complex for real-time detection of tyrosine phosphorylation. *Anal. Chem.* **2015**, *87*, 3834–3840.

[37] Risseeuw, M. D.; De Clercq, D. J.; Lievens, S.; Hillaert, U.; Sinnaeve, D.; Van den Broeck, F.; Martins, J. C.; Tavernier, J.; Van Calenbergh, S. A "clickable" MTX reagent as a practical tool for profiling small-molecule-intracellular target interactions via MASPIT. *ChemMedChem* **2013**, *8*, 521–526.

[38] Zhao, Y.; Zhang, Y.; Wang, C.; Chen, G.; Jiang, M. Role of Protecting Groups in Synthesis and Self-Assembly of Glycopolymers. *Biomacromolecules.* **2017**, *18*, 568–575.

[39] Díaz, L.; Casas, J.; Bujons, J.; Llebaria, A.; Delgado, A. New glucocerebrosidase inhibitors by exploration of chemical diversity of N-substituted aminocyclitols using click chemistry and in situ screening. *J. Med. Chem.* **2011**, *54*, 2069–2079.

[40] Fer, M. J.; Bouhss, A.; Patrão, M.; Le Corre, L.; Pietrancosta, N.; Amoroso, A.; Joris, B.; Mengin-Lecreulx, D.; Calvet-Vitale, S.; Gravier-Pelletier, C. 5'-Methylene-triazole-substituted-aminoribosyl uridines as MraY inhibitors: synthesis, biological evaluation and molecular modeling. *Org. Biomol. Chem.* **2015**, *13*, 7193–7222.

[41] Liang, P. H.; Cheng, W. C.; Lee, Y. L.; Yu, H. P.; Wu, Y. T.; Lin, Y. L.; Wong, C. H. Novel five-membered iminocyclitol derivatives as selective and potent glycosidase inhibitors: new structures for antivirals and osteoarthritis. *ChemBioChem* **2006**, *7*, 165–173.

[42] Pearson, G.; Robinson, F.; Beers Gibson, T.; Xu, B. E.; Karandikar, M.; Berman, K.; Cobb, M. H. Mitogen-activated protein (MAP) kinase pathways: regulation and physiological functions. *Endocr. Rev.* **2001**, *22*, 153–183.

[43] Skieterska, K.; Rondou, P.; Lintermans, B.; Van Craenenbroeck, K. KLHL12 Promotes Non-Lysine Ubiquitination of the Dopamine Receptors D4.2 and D4.4, but Not of the ADHD-Associated D4.7 Variant. *PLoS One* **2015**, *10*, e0145654.

[44] Buccioni, M.; Marucci, G.; Dal Ben, D.; Giacobbe, D.; Lambertucci, C.; Soverchia, L.; Thomas, A.; Volpini, R.; Cristalli, G. Innovative functional cAMP assay for studying G protein-coupled receptors: application to the pharmacological characterization of GPR17. *Purinergic Signal.* **2011**, *7*, 463–468.

[45] Wu, Y.L.; Wang, N. N.; Gu, L.; Yang, H. M.; Xia, N.; Zhang, H. The suppressive effect of metabotropic glutamate receptor 5 (mGlu5) inhibition on hepatocarcinogenesis. *Biochimie.* **2012**, *94*, 2366–2375.

[46] Dore, A. S.; Okrasa, K.; Patel, J. C.; Serrano-Vega, M.; Bennett, K.; Cooke, R. M.; Errey, J. C.; Jazayeri, A.; Khan, S.; Tehan, B.; Weir, M.; Wiggin, G. R.; Marshall, F. H. Structure of class C GPCR metabotropic glutamate receptor 5 transmembrane domain. *Nature* **2014**, *511*, 557–562.

[47] Wang, S.; Che, T.; Levit, A.; Shoichet, B. K.; Wacker, D.; Roth, B. L. Structure of the D2 dopamine receptor bound to the atypical antipsychotic drug risperidone. *Nature* **2018**, *555*, 269–273.

[48] Dalton, J. A.; Lans, I.; Rovira, X.; Malhaire, F.; Santacana, X. G.; Pittolo, S.; Gorostiza, P.; Llebaria, A.; Goudet, C.; Pin, J. P.; Giraldo, J. Shining light on an mGlu5 photoswitchable NAM: a theoretical perspective. *Curr. Neuropharmacol.* **2016**, *14*, 441–454.

[49] Gomez-Santacana, X.; Dalton, J. A.; Rovira, X.; Pin, J. P.; Goudet, C.; Gorostiza, P.; Giraldo, J.; Llebaria, A. Positional isomers of bispyridine benzene derivatives induce efficacy changes on mGlu5 negative allosteric modulation. *Eur. J. Med. Chem.* **2017**, *127*, 567–576.

[50] Dalton, J. A.; Pin, J. P.; Giraldo, J. Analysis of positive and negative allosteric modulation in metabotropic glutamate receptors 4 and 5 with a dual ligand. *Sci. Rep.* **2017**, *7*, 4944.

[51] Xue, L.; Rovira, X.; Scholler, P.; Zhao, H.; Liu, J.; Pin, J. P.; Rondard, P. Major ligand-induced rearrangement of the heptahelical domain interface in a GPCR dimer. *Nat. Chem. Biol.* **2015**, *11*, 134–140.

[52] Gonzalez-Maeso, J.; Ang, R. L.; Yuen, T.; Chan, P.; Weisstaub, N. V.; Lopez-Gimenez, J. F.; Zhou, M.; Okawa, Y.; Callado, L. F.; Milligan, G.; Gingrich, J. A.; Filizola, M.; Meana,

J. J.; Sealfon, S. C. Identification of a serotonin/glutamate receptor complex implicated in psychosis. *Nature* **2008**, *452*, 93–97.

[53] Fribourg, M.; Moreno, J. L.; Holloway, T.; Provasi, D.; Baki, L.; Mahajan, R.; Park, G.; Adney, S. K.; Hatcher, C.; Eltit, J. M.; Ruta, J. D.; Albizu, L.; Li, Z.; Umali, A.; Shim, J.; Fabiato, A.; MacKerell, A. D., Jr.; Brezina, V.; Sealfon, S. C.; Filizola, M.; Gonzalez-Maeso, J.; Logothetis, D. E. Decoding the signaling of a GPCR heteromeric complex reveals a unifying mechanism of action of antipsychotic drugs. *Cell* **2011**, *147*, 1011–1023.

[54] Moreno, J. L.; Miranda-Azpiazu, P.; Garcia-Bea, A.; Younkin, J.; Cui, M.; Kozlenkov, A.; Ben-Ezra, A.; Voloudakis, G.; Fakira, A. K.; Baki, L.; Ge, Y.; Georgakopoulos, A.; Moron, J. A.; Milligan, G.; Lopez-Gimenez, J. F.; Robakis, N. K.; Logothetis, D. E.; Meana, J. J.; Gonzalez-Maeso, J. Allosteric signaling through an mGlu2 and 5-HT2A heteromeric receptor complex and its potential contribution to schizophrenia. *Sci. Signal.* **2016**, *9*, ra5.

[55] Guo, W.; Shi, L.; Filizola, M.; Weinstein, H.; Javitch, J. A., Crosstalk in G protein-coupled receptors: changes at the transmembrane homodimer interface determine activation. *Proc. Natl. Acad. Sci. U. S. A.* **2005**, *102*, 17495–17500.

[56] Ferre, S.; Bonaventura, J.; Zhu, W.; Hatcher-Solis, C.; Taura, J.; Quiroz, C.; Cai, N. S.; Moreno, E.; Casado-Anguera, V.; Kravitz, A. V.; Thompson, K. R.; Tomasi, D. G.; Navarro, G.; Cordomi, A.; Pardo, L.; Lluis, C.; Dessauer, C. W.; Volkow, N. D.; Casado, V.; Ciruela, F.; Logothetis, D. E.; Zwilling, D. Essential control of the function of the striatopallidal neuron by pre-coupled complexes of adenosine A2A-dopamine D2 receptor heterotetramers and adenylyl cyclase. *Front. Pharmacol.* **2018**, *9*, 243.

[57] Navarro, G.; Cordomi, A.; Casado-Anguera, V.; Moreno, E.; Cai, N. S.; Cortes, A.; Canela, E. I.; Dessauer, C. W.; Casado, V.; Pardo, L.; Lluis, C.; Ferre, S. Evidence for functional pre-coupled complexes of receptor heteromers and adenylyl cyclase. *Nat. Commun.* **2018**, *9*, 1242.

[58] Bonaventura, J.; Navarro, G.; Casado-Anguera, V.; Azdad, K.; Rea, W.; Moreno, E.; Brugarolas, M.; Mallol, J.; Canela, E. I.; Lluis, C.; Cortes, A.; Volkow, N. D.; Schiffmann, S. N.; Ferre, S.; Casado, V. Allosteric interactions between agonists and antagonists within the adenosine A2A receptor-dopamine D2 receptor heterotetramer. *Proc. Natl. Acad. Sci. U. S. A.* **2015**, *112*, E3609–3618.

[59] Manglik, A.; Kruse, A. C.; Kobilka, T. S.; Thian, F. S.; Mathiesen, J. M.; Sunahara, R. K.; Pardo, L.; Weis, W. I.; Kobilka, B. K.; Granier, S. Crystal structure of the mu-opioid receptor bound to a morphinan antagonist. *Nature* **2012**, *485*, 321–326.

[60] Lyskov, S.; Chou, F. C.; Conchuir, S. O.; Der, B. S.; Drew, K.; Kuroda, D.; Xu, J.; Weitzner, B. D.; Renfrew, P. D.; Sripakdeevong, P.; Borgo, B.; Havranek, J. J.; Kuhlman, B.; Kortemme, T.; Bonneau, R.; Gray, J. J.; Das, R. Serverification of molecular modeling applications: the Rosetta Online Server that Includes Everyone (ROSIE). *PloS one* **2013**, *8*, e63906.

[61] Christopher, J. A.; Aves, S. J.; Bennett, K. A.; Dore, A. S.; Errey, J. C.; Jazayeri, A.; Marshall, F. H.; Okrasa, K.; Serrano-Vega, M. J.; Tehan, B. G.; Wiggin, G. R.; Congreve, M. Fragment and structure-based drug discovery for a class C GPCR: discovery of the mGlu5 negative allosteric modulator HTL14242 (3-Chloro-5-[6-(5-fluoropyridin-2-yl)pyrimidin-4-yl]benzonitrile). *J. Med. Chem.* **2015**, *58*, 6653–6664.

[62] Malo, M.; Brive, L.; Luthman, K.; Svensson, P. Investigation of D2 receptor-agonist interactions using a combination of pharmacophore and receptor homology modeling. *ChemMedChem* **2012**, *7*, 471–482.

[63] Rondou, P.; Skieterska, K.; Packeu, A.; Lintermans, B.; Vanhoenacker, P.; Vauquelin, G.; Haegeman, G.; Van Craenenbroeck, K. KLHL12-mediated ubiquitination of the dopamine D4 receptor does not target the receptor for degradation. *Cell. Signal.* **2010**, *22*, 900–913.

[64] Van Craenenbroeck, K.; Clark, S. D.; Cox, M. J.; Oak, J. N.; Liu, F.; Van Tol, H. H. Folding efficiency is rate-limiting in dopamine D4 receptor biogenesis. *J. Biol. Chem.* **2005**, *280*, 19350–19357.

[65] Van Wieringen, J. P.; Michel, M. C. [3H]-Spiperone Competition Binding to Dopamine D2, D3 and D4 Receptors. (**2013**). Available at: DOI: https://doi.org/10.21769/BioProtoc.944.

[66] Kiss, B.; Horti, F.; Bobok, A. In vitro and in vivo comparison of [^{3}H](+)-PHNO and [^{3}H]raclopride binding to rat striatum and lobes 9 and 10 of the cerebellum: a method to distinguish dopamine D_3 from D_2 receptor sites. *Synapse* **2011**, *65*, 467–478.

[67] Domenici, M. R.; Potenza, R. L.; Martire, A.; Coccurello, R.; Pèzzola, A.; Reggio, R.; Tebano, M. T.; Popoli, P. Chronic treatment with the mGlu5R antagonist MPEP reduces the functional effects of the mGlu5R agonist CHPG in the striatum of 6-hydroxydopamine-lesioned rats: possible relevance to the effects of mGlu5R blockade in Parkinson's disease. *J. Neurosci. Res.* **2005**, *80*, 646–654.

[68] Cheng, Y.; Prusoff, W. H. Relationship between the inhibition constant (K1) and the concentration of inhibitor which causes 50 per cent inhibition (I50) of an enzymatic reaction. *Biochem. Pharmacol.* **1973**, *22*, 3099–3108.

[69] Skieterska, K.; Duchou, J.; Lintermans, B.; Van Craenenbroeck, K. Detection of G protein-coupled receptor (GPCR) dimerization by coimmunoprecipitation. *Methods Cell. Biol.* **2013**, *117*, 323–340.

[70] Pettersen, E. F.; Goddard, T. D.; Huang, C. C.; Couch, G. S.; Greenblatt, D. M.; Meng, E. C.; Ferrin, T. E. UCSF Chimera--a visualization system for exploratory research and analysis. *J. Comput. Chem.* **2004**, *25*, 1605–1612.

[71] Sali, A. Comparative protein modeling by satisfaction of spatial restraints. *Mol. Med. Today* **1995**, *1*, 270–277.

[72] Case, D. A.; Cheatham, T. E., 3rd; Darden, T.; Gohlke, H.; Luo, R.; Merz, K. M., Jr.; Onufriev, A.; Simmerling, C.; Wang, B.; Woods, R. J. The amber biomolecular simulation programs. *J. Comput. Chem.* **2005**, *26*, 1668–1688.

[73] Kim, S.; Thiessen, P. A.; Bolton, E. E.; Chen, J.; Fu, G.; Gindulyte, A.; Han, L.; He, J.; He, S.; Shoemaker, B. A.; Wang, J.; Yu, B.; Zhang, J.; Bryant, S. H. PubChem substance and compound databases. *Nucleic Acids Res.* **2016**, *44*, D1202–1213.

[74] Morris, G. M.; Huey, R.; Lindstrom, W.; Sanner, M. F.; Belew, R. K.; Goodsell, D. S.; Olson, A. J. AutoDock4 and AutoDockTools4: Automated docking with selective receptor flexibility. *J. Comput. Chem.* **2009**, *30*, 2785–2791.

IV.6. Supporting information

Synthesis towards bivalent ligands for the dopamine D_2 and metabotropic glutamate 5 receptors

Table of contents

Synthesis of linker and bivalent ligands S1

Ligand binding assays S2

MAPK phosphorylation for D_4R, D_2R and mGluR5 S3

Experimental Section S4

Chromatographic analyses for bivalent ligands S5

NMR spectra S6

S1

Synthesis of tertiary amine linker

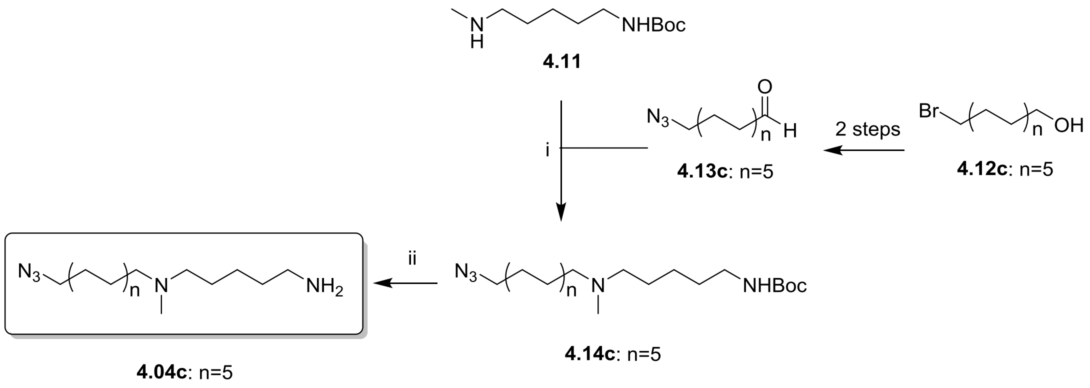
NHBoc
4.11
N3
n
H
2 steps
Br
OH
4.13c: n=5
4.12c: n=5
i
ii
NH2
4.04c: n=5
NHBoc
4.14c: n=5

Scheme 1. Reagents and conditions: i) **4.13c**, Na(OAc)$_3$BH, CH$_2$Cl$_2$; ii) TFA, CH$_2$Cl$_2$, 4 M NaOH

Synthesis of bivalent ligands

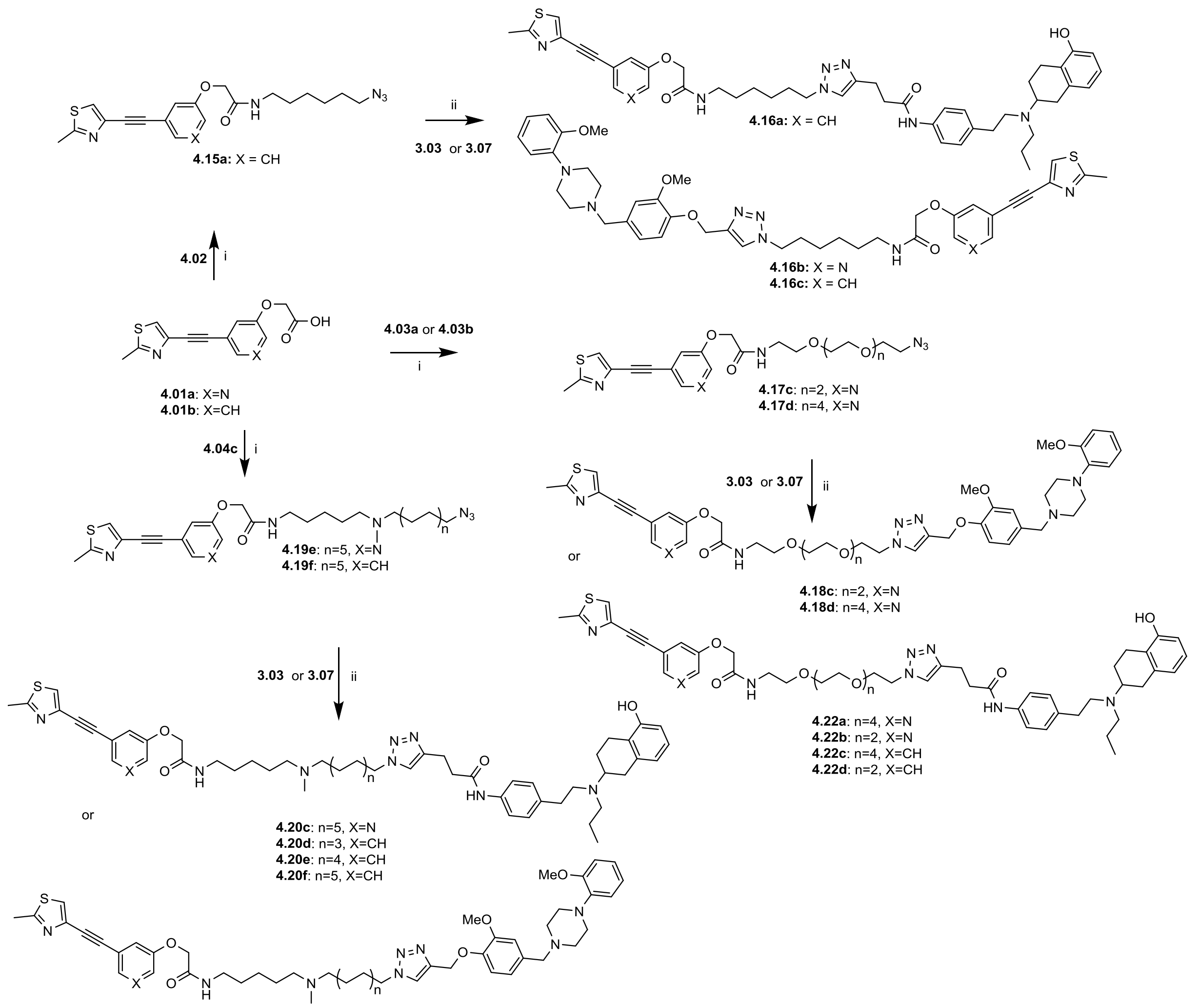
4.15a: X = CH
ii
3.03 or 3.07
4.16a: X = CH
OMe
OMe
4.16b: X = N
4.16c: X = CH
4.02
i
4.01a: X=N
4.01b: X=CH
4.03a or 4.03b
i
4.17c: n=2, X=N
4.17d: n=4, X=N
4.04c
i
4.19e: n=5, X=N
4.19f: n=5, X=CH
3.03 or 3.07
ii
or
MeO
MeO
4.18c: n=2, X=N
4.18d: n=4, X=N
4.22a: n=4, X=N
4.22b: n=2, X=N
4.22c: n=4, X=CH
4.22d: n=2, X=CH
3.03 or 3.07
ii
or
4.20c: n=5, X=N
4.20d: n=3, X=CH
4.20e: n=4, X=CH
4.20f: n=5, X=CH
MeO
MeO
4.21e: n=5, X=N
4.21f: n=5, X=CH

Scheme 2. Reagents and conditions: i) (3-dimethylaminopropyl)-N-ethylcarbodiimide hydrochloride, 1-hydroxybenzotriazole, triethylamine, CH$_2$Cl$_2$; ii) sodium ascorbate, CuSO$_4$, triethylamine, tris[(1-benzyl-1,2,3-triazol-4-yl)methyl]amine, dimethylformamide.

S2

Table 1 Binding affinities (K_i) for D_4R

Compound	X	R	Linker	K_i (nM) for D_4R
3.07	-	DPAT	-	15 ± 6.1
3.03	-	DAP	-	1.6 ± 0.2
4.16	N	DPAT	$-OCH_2CONH\ (CH_2)_6-$	62 ± 8.3
4.20a	N	DPAT	$-OCH_2CONH(CH_2)_5NCH_3(CH_2)_8-$	21 ± 2.4
4.20b	N	DPAT	$-OCH_2CONH\ (CH_2)_5NCH_3(CH_2)_{10}-$	64 ± 2.9
4.21a	N	DAP	$-OCH_2CONH\ (CH_2)_5NCH_3(CH_2)_8-$	4.3 ± 0.2
4.21b	N	DAP	$-OCH_2CONH\ (CH_2)_5NCH_3(CH_2)_{10}-$	9.4 ± 1.6
4.21c	CH	DAP	$-OCH_2CONH\ (CH_2)_5NCH_3(CH_2)_8-$	5.6 ± 1.8
4.21d	CH	DAP	$-OCH_2CONH\ (CH_2)_5NCH_3(CH_2)_{10}-$	7.3 ± 0.8
4.18a	CH	DAP	$-OCH_2CONH-PEG_4-$	189 ± 12
4.18b	CH	DAP	$-OCH_2CONH-PEG_6-$	23 ± 3.7

Binding affinities (K_i) were obtained by competitive displacement of radiolabeled [^{3}H]spiperone binding to HEK293T D_4R cell membranes. All values are expressed as the mean ± SEM of three independent assays performed in duplicate.

Saturation assay for mGluR5

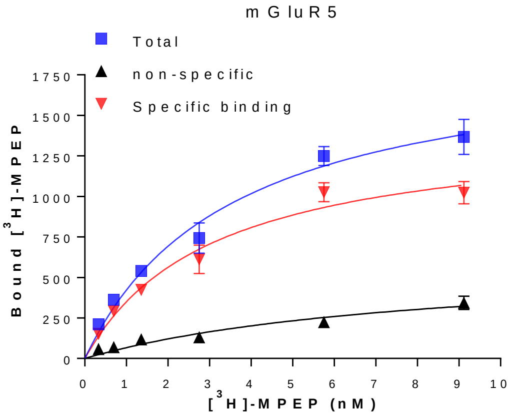

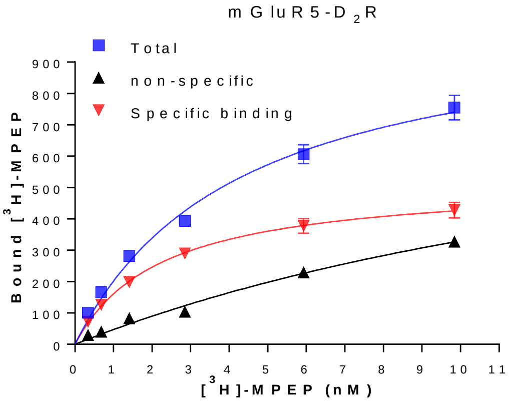

Entry	Bmax fmol/mg	Kd nM
mGluR5	1488 ± 153	2.2 ± 0.7
mGluR5-D$_2$R	522 ± 19	2.0 ± 0.2

All values are expressed as the mean ± SEM of two independent assays performed in duplicate.

S3

MAPK phosphorylation for D_4R

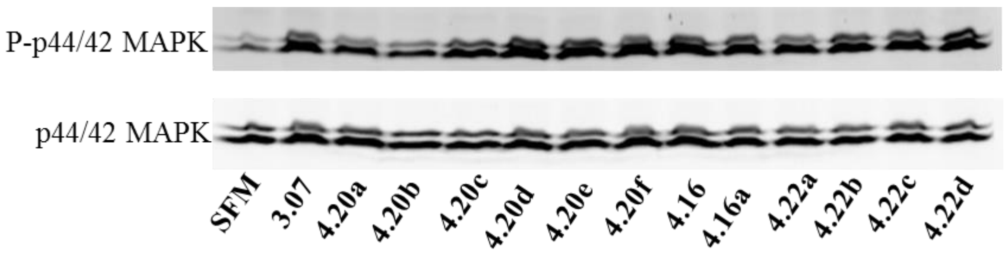
P-p44/42 MAPK
p44/42 MAPK
SFM
3.07
4.20a
4.20b
4.20c
4.20d
4.20e
4.20f
4.16
4.16a
4.22a
4.22b
4.22c
4.22d

(A)

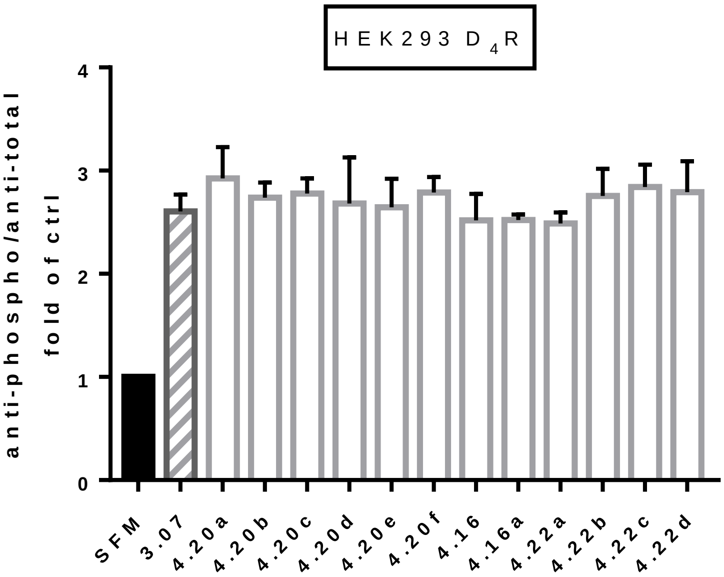

(B)

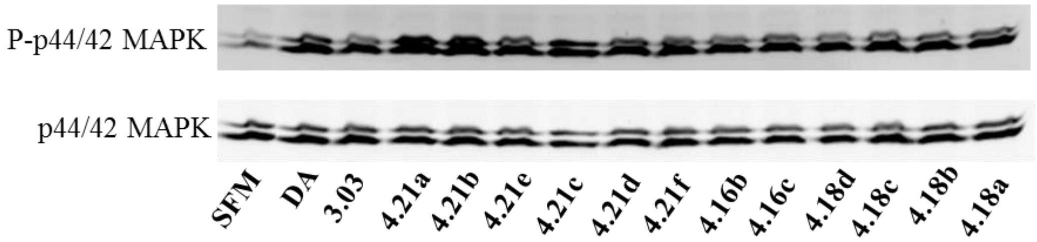
P-p44/42 MAPK
p44/42 MAPK
SFM
DA
3.03
4.21a
4.21b
4.21e
4.21c
4.21d
4.21f
4.16b
4.16c
4.18d
4.18c
4.18b
4.18a

(C)

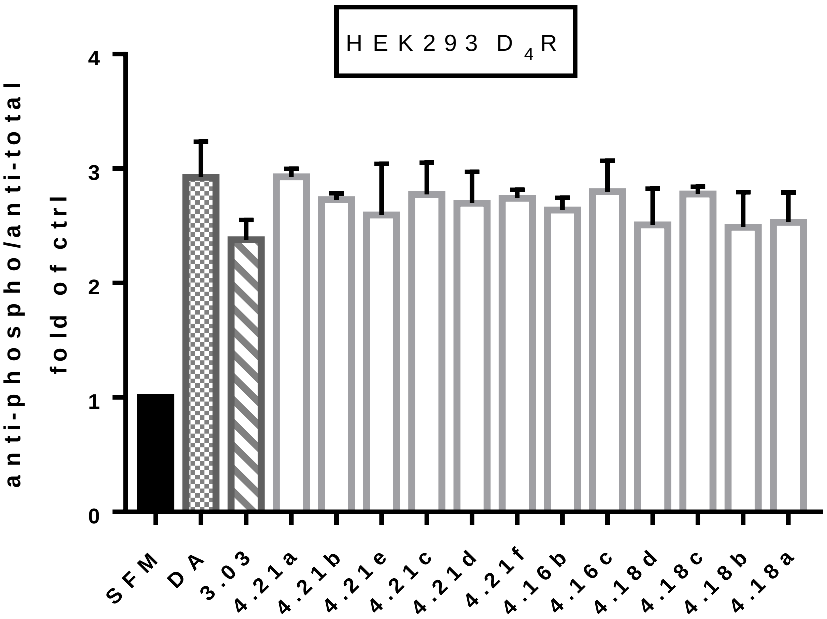

(D)

Figure 1. Efficacy of bivalent ligands to phosphorylate MAPK in HEK293 D_4R cells. Cells were treated with serum-free media (SFM) for 12 h. Next, D_2-likeR agonists and SFM were added for 5 min. Cells were washed and lysed as explained in the Experimental section. Phosphorylated MAPK was detected by immunoblotting using rabbit anti-phospho-p44/42 MAPK antibody and mouse anti-p44/42 MAPK antibody was used for demonstrating equal protein loading. Cells treatment with SFM served as control. The panels A and C show a representative result from three independent experiments; the panels B and D are given as mean ± SEM. DA=dopamine.

MAPK phosphorylation for D_2R-mGluR5

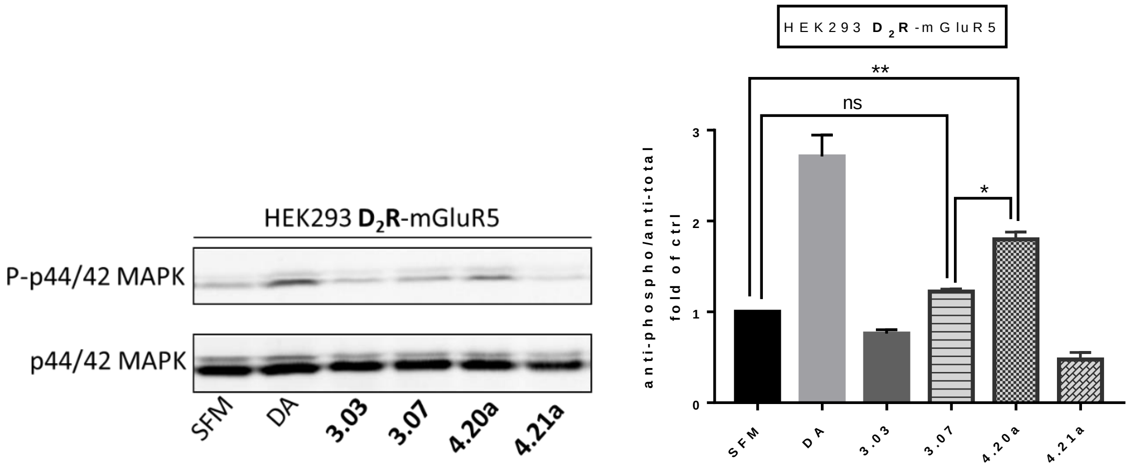

Figure 2. Efficacy of bivalent ligands to phosphorylate MAPK in HEK293 D_2R-mGluR5 cells. Cells were treated with serum-free media (SFM) for 12 h. Next, D_2-likeR agonists and SFM were added for 5 min. Cells were washed and lysed as explained in the Experimental section. Phosphorylated MAPK was detected by immunoblotting using rabbit anti-phospho-p44/42 MAPK antibody and mouse anti-p44/42 MAPK antibody was used for demonstrating equal protein loading. Cells treatment with SFM served as control. The left panel shows a representative result from three independent experiments; the right panel is given as mean ± SEM. DA=dopamine. *$p < 0.05$ and **$p < 0.01$. *ns*, not significant.

MAPK phosphorylation for mGluR5

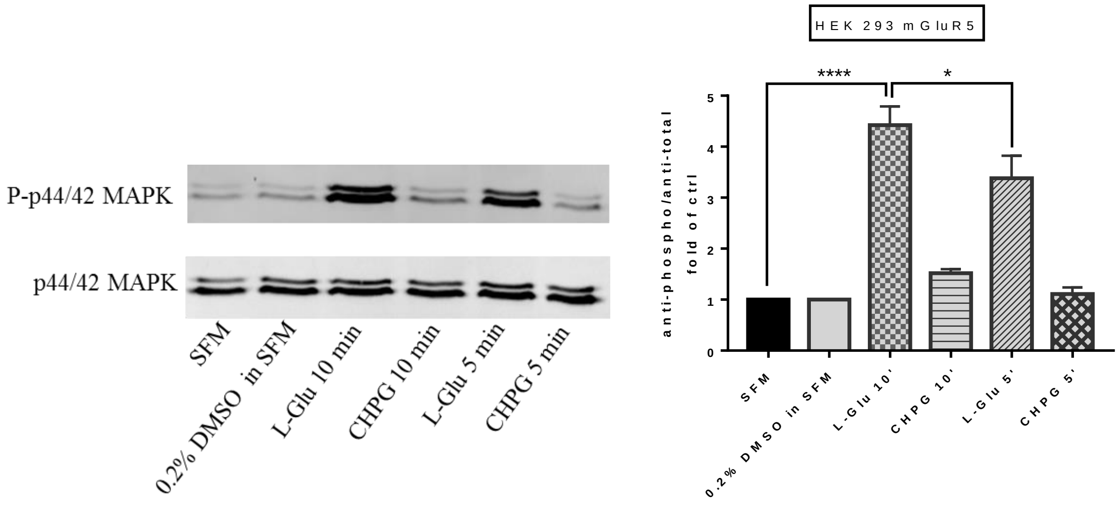

Figure 3. Time-dependent response on activity of MAPK-P by L-Glu and CHPG in HEK293 mGluR5 cells. Cells were treated with serum-free media (SFM) for 12 h. Next, mGluR5 agonists, SFM or vehicle control were added for 5 min or 10 min. Cells were washed and lysed as explained in the Experimental section. Phosphorylated MAPK was detected by immunoblotting using rabbit anti-phospho-p44/42 MAPK antibody and mouse anti-p44/42 MAPK antibody was used for demonstrating equal protein loading. Cells treatment with SFM served as control. The left panel shows a representative result from three independent experiments; the right panel is given as mean ± SEM. L-Glu = L-Glutamic acid. CHPG = (*RS*)-2-Chloro-5-hydroxyphenylglycine. *$p < 0.05$, ****$p < 0.0001$.

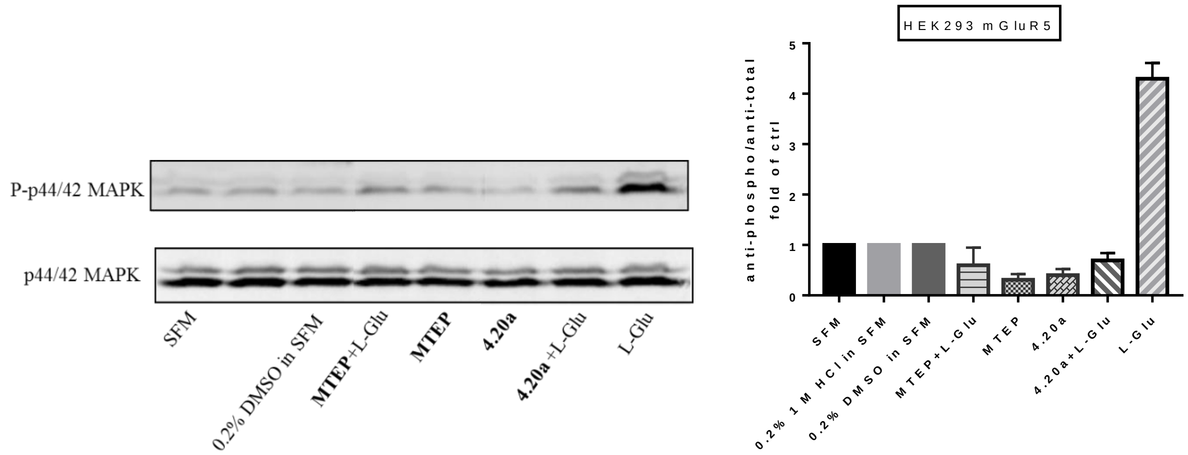

Figure 4. Efficacy of one bivalent ligand **4.20a** and MTEP to inhibit phosphorylation of MAPK activated by L-Glu in HEK293 mGluR5 cells. Cells were treated with serum-free media (SFM) for 12 h and then pretreated with or without MTEP and **4.20a** (10 µM) for 30 min before treatment with L-Glu (10 µM, 10 min). Cells were washed and lysed as explained in the Experimental section. Phosphorylated MAPK was detected by immunoblotting using rabbit anti-phospho-p44/42 MAPK antibody and mouse anti-p44/42 MAPK antibody was used for demonstrating equal protein loading. Results are expressed as the fold of control. Cells treatment with SFM served as control. The left panel shows a representative result from three independent experiments; the right panel is given as mean ± SEM. L-Glu = L-Glutamic acid.

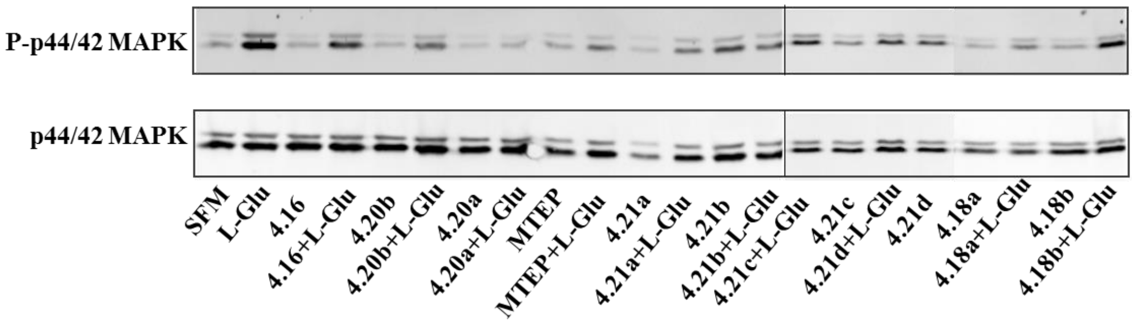
P-p44/42 MAPK
p44/42 MAPK
SFM
L-Glu
4.16
4.16+L-Glu
4.20b
4.20b+L-Glu
4.20a
4.20a+L-Glu
MTEP
MTEP+L-Glu
4.21a
4.21a+L-Glu
4.21b
4.21b+L-Glu
4.21c+L-Glu
4.21c
4.21d+L-Glu
4.21d
4.18a
4.18a+L-Glu
4.18b
4.18b+L-Glu

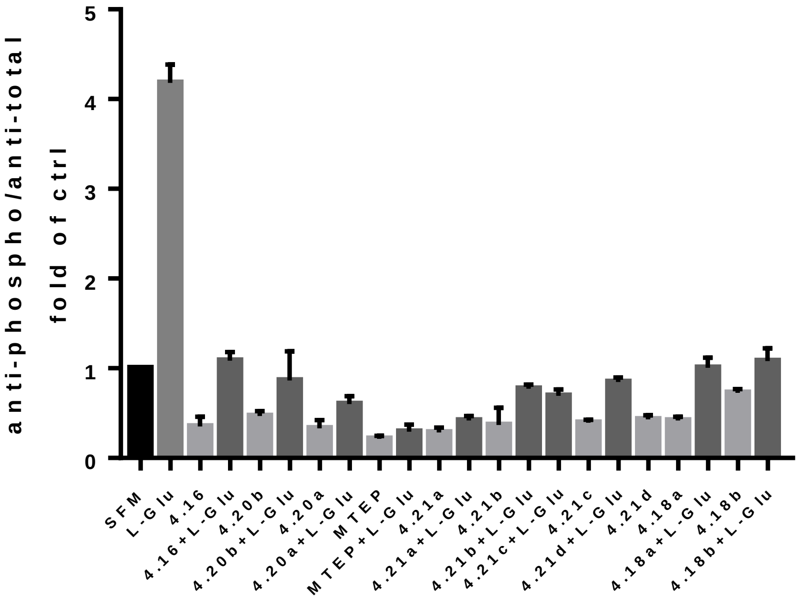

Figure 5. Efficacy of bivalent ligands to inhibit phosphorylation of MAPK activated by L-Glu in HEK293 mGluR5 cells. Cells were treated with serum-free media (SFM) for 12 h and then pretreated with or without MTEP and bivalent ligands (10 µM) for 30 min before treatment with L-Glu (10 µM, 10 min). Cells were washed and lysed as explained in the Experimental section. Phosphorylated MAPK was detected by immunoblotting using rabbit anti-phospho-p44/42 MAPK antibody and mouse anti-p44/42 MAPK antibody was used for demonstrating equal protein loading. Results are expressed as the fold of control. Cells treatment with SFM served as control. The top panel shows a representative result from three independent experiments; the bottom panel is given as mean ± SEM. L-Glu = L-Glutamic acid.

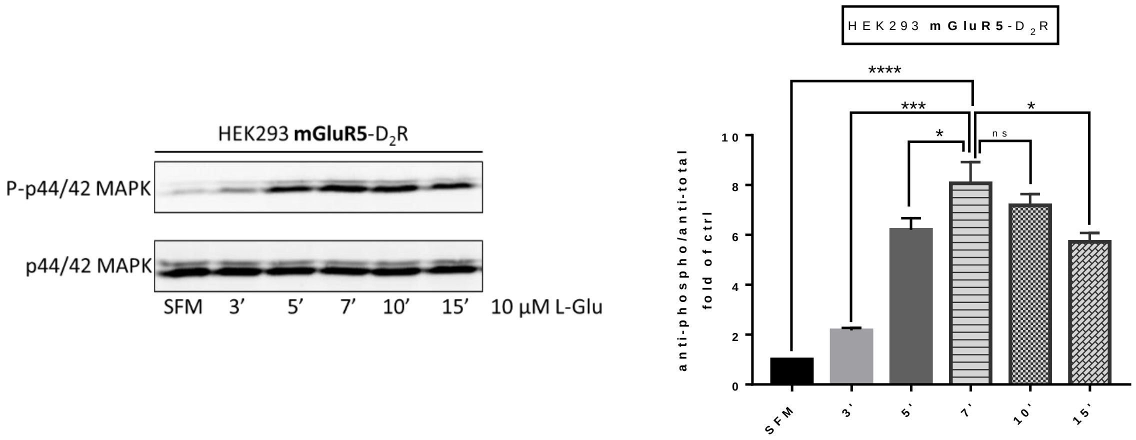

Figure 6. Time-dependent response on activity of MAPK-P by 10 µM L-Glu in HEK293 mGluR5-D$_2$R cells. Cells were treated with serum-free media (SFM) for 12 h. Next, SFM and mGluR5 agonist were added for 3 min, 5 min 7 min, 10 min or 15 min. Cells were washed and lysed as explained in the Experimental section. Phosphorylated MAPK was detected by immunoblotting using rabbit anti-phospho-p44/42 MAPK antibody and mouse anti-p44/42 MAPK antibody was used for demonstrating equal protein loading. Cells treatment with SFM served as control. The left panel shows a representative result from three independent experiments; the right panel is given as mean ± SEM. L-Glu = L-Glutamic acid. *$p < 0.05$, ***$p < 0.001$ and ****$p < 0.0001$. *ns*, not significant.

Table 2. Overview of MAPK-P for D$_4$R and mGluR5.

Entry	X	R	Linker	MAPK for D$_4$R	MAPK for mGluR5
3.03	-	-	-	+	-
3.07	-	-	-	+	-
MTEP	-	-	-	-	+
4.20a	N	DPAT	-OCH$_2$CONH(CH$_2$)$_5$NCH$_3$(CH$_2$)$_8$-	+	+
4.20b	N	DPAT	-OCH$_2$CONH (CH$_2$)$_5$NCH$_3$(CH$_2$)$_{10}$-	+	+
4.20c	N	DPAT	-OCH$_2$CONH (CH$_2$)$_5$NCH$_3$(CH$_2$)$_{12}$-	+	+
4.20d	CH	DPAT	-OCH$_2$CONH(CH$_2$)$_5$NCH$_3$(CH$_2$)$_8$-	+	+
4.20e	CH	DPAT	-OCH$_2$CONH (CH$_2$)$_5$NCH$_3$(CH$_2$)$_{10}$-	+	+
4.20f	CH	DPAT	-OCH$_2$CONH (CH$_2$)$_5$NCH$_3$(CH$_2$)$_{12}$-	+	+
4.21a	N	DAP	-OCH$_2$CONH (CH$_2$)$_5$NCH$_3$(CH$_2$)$_8$-	+	+
4.21b	N	DAP	-OCH$_2$CONH (CH$_2$)$_5$NCH$_3$(CH$_2$)$_{10}$-	+	+
4.21e	N	DAP	-OCH$_2$CONH (CH$_2$)$_5$NCH$_3$(CH$_2$)$_{12}$-	+	+
4.21c	CH	DAP	-OCH$_2$CONH (CH$_2$)$_5$NCH$_3$(CH$_2$)$_8$-	+	+
4.21d	CH	DAP	-OCH$_2$CONH (CH$_2$)$_5$NCH$_3$(CH$_2$)$_{10}$-	+	+
4.21f	CH	DAP	-OCH$_2$CONH (CH$_2$)$_5$NCH$_3$(CH$_2$)$_{12}$-	+	+
4.16	N	DPAT	-OCH$_2$CONH (CH$_2$)$_6$-	+	+
4.16b	N	DAP	-OCH$_2$CONH (CH$_2$)$_6$-	+	+
4.16a	CH	DPAT	-OCH$_2$CONH (CH$_2$)$_6$-	+	+
4.16c	CH	DAP	-OCH$_2$CONH (CH$_2$)$_6$-	+	+
4.18d	N	DAP	-OCH$_2$CONH-PEG$_6$-	+	+
4.22a	N	DPAT	-OCH$_2$CONH-PEG$_6$-	+	+
4.18c	N	DAP	-OCH$_2$CONH-PEG$_4$-	+	+
4.22b	N	DPAT	-OCH$_2$CONH-PEG$_4$-	+	+
4.18b	CH	DAP	-OCH$_2$CONH-PEG$_6$-	+	+
4.22c	CH	DPAT	-OCH$_2$CONH-PEG$_6$-	+	+
4.18a	CH	DAP	-OCH$_2$CONH-PEG$_4$-	+	+
4.22d	CH	DPAT	-OCH$_2$CONH-PEG$_4$-	+	+

"+" means MAPK works for D$_4$R or mGluR5.

S4

Experimental Section

General procedure 1: Carbodiimide-mediated amide formation.

To a solution of (3-Dimethylaminopropyl)-N-ethylcarbodiimide hydrochloride (1.5 eq.) and 1-hydroxybenzotriazole (1.4 eq.) in CH_2Cl_2 was added a solution of the PEG spacer (1.2 eq.) in CH_2Cl_2 (0.2 M) and cooled to 0°C under an argon atmosphere. After 15 min at 0°C, amines (1.0 eq.) were added and triethylamine (2 eq.) was added dropwise; the reaction was slowly warmed to room temperature and stirred overnight. The reaction was diluted with CH_2Cl_2, washed successively with water, HCl (5% aq.), $NaHCO_3$ (sat. aq.), NaCl (sat. aq.), dried over Na_2SO_4, filtered and solvent was evaporated under reduced pressure. The crude product was purified by silica gel chromatography (NH_4OH/MeOH/CH_2Cl_2, 1:5:94 v/v/v) to yield the amides.

General procedure 2: Copper mediated azide-alkyne cycloaddition.

To a solution of the intermediate azide (1.0 eq.) in dimethylformamide (0.1 M) was added the alkyne (1.5 eq.), sodium ascorbate (1.0 eq., 0.5 M), $CuSO_4$ (0.2 eq., 0.05 M), triethylamine (3.0 eq.) and a catalytic amount of tris[(1-benzyl-1,2,3-triazol-4-yl)methyl]amine. The reaction mixture was stirred overnight at room temperature in the dark under an argon atmosphere. The solvent was evaporated under reduced pressure and the residue was redissolved in water and extracted with CH_2Cl_2. Then combined organic fractions were pooled, washed with brine and dried over Na_2SO_4. The crude compound was purified by silica gel chromatography (NH_4OH/MeOH/CH_2Cl_2, 1:5:94 v/v/v) to give the final compound as a white solid.

12-azidododecanal (4.13c)

Compound **4.13c** was prepared using the procedure described as **4.13a**. Colorless oil (3.4 g, 89%). ^1H NMR (300 MHz, $CDCl_3$) δ 9.71 (s, 1H), 3.21 (t, *J* = 6.9 Hz, 2H), 2.37 (td, *J* = 7.4, 1.9 Hz, 2H), 1.68 – 1.48 (m, 4H), 1.37 – 1.16 (m, 14H). ^{13}C NMR (75 MHz, $CDCl_3$) δ 202.9, 51.4, 43.8, 29.4, 29.3, 29.3, 29.1, 29.1, 29.1, 28.8, 26.6, 22.0.

tert-butyl (5-((12-azidododecyl)(methyl)amino)pentyl)carbamate (4.14c)

Compound **4.14c** was obtained according to the procedure described for compound **4.14a**. Colorless oil (3.31 g, 78%). ^1H NMR (300 MHz, $CDCl_3$) δ 4.61 (s, 1H), 3.22 (t, *J* = 6.9 Hz, 2H), 3.08 (q, *J* = 6.6 Hz, 2H), 2.53 – 2.42 (m, 4H), 2.33 (s, 3H), 1.63 – 1.43 (m, 6H), 1.41 (s, 9H), 1.37 – 1.17 (m, 20H). ^{13}C NMR (75 MHz, $CDCl_3$) δ 155.9, 79.0, 56.8 (d, *J* = 17.9 Hz), 51.4, 41.2, 40.3, 29.7, 29.4, 29.4, 29.4, 29.3, 29.1, 28.7, 28.4, 27.3, 26.6, 25.7 (d, *J* = 26.6 Hz), 24.5. HRMS (ESI) m/z: calculated for $C_{23}H_{48}N_5O_2$ $[M+H]^+$ 426.3808; found 426.3807.

***N*^{1}-(12-azidododecyl)- *N*^{1}-methylpentane-1,5-diamine (4.04c)**

Compound **4.04c** was obtained according to the procedure described for compound **4.04a**. Colorless oil (2.4 g, 95%). ^{1}H NMR (300 MHz, DMSO-*d*$_6$) δ 3.27 (t, *J* = 6.8 Hz, 2H), 2.81 – 2.74 (m, 2H), 2.48 (dq, *J* = 3.1, 1.5 Hz, 4H), 2.41 (s, 3H), 1.70 – 1.39 (m, 6H), 1.36 – 1.17 (m, 20H). ^{13}C NMR (75 MHz, DMSO-*d*$_6$) δ 55.4, 51.0, 48.6, 40.7, 39.0, 38.9, 32.8, 31.0, 29.4, 28.9, 28.6, 26.8, 26.5, 26.3, 26.2, 25.7, 23.7, 23.2. HRMS (ESI) m/z: calculated for $C_{18}H_{40}N_5$ $[M+H]^+$ 326.3284; found 326.3288.

N-(6-azidohexyl)-2-(3-((2-methylthiazol-4-yl)ethynyl)phenoxy)acetamide (4.15a)

Compound **4.15a** was subjected to general procedure 1. Offwhite solid, 78%. ^{1}H NMR (300 MHz, $CDCl_3$) δ 7.37 (s, 1H), 7.30 – 7.24 (m, 1H), 7.20 (dt, *J* = 7.7, 1.3 Hz, 1H), 7.09 (ddd, *J* = 2.7, 1.4, 0.4 Hz, 1H), 6.90 (ddd, *J* = 8.1, 2.7, 1.2 Hz, 1H), 6.54 (br s, 1H), 4.47 (s, 2H), 3.33 (td, *J* = 7.1, 6.0 Hz, 2H), 3.23 (t, *J* = 6.8 Hz, 2H), 2.72 (s, 3H), 1.81 (br s., 1H), 1.63 – 1.48 (m, 4H), 1.44 – 1.27 (m, 3H). ^{13}C NMR (75 MHz, $CDCl_3$) δ 167.7, 165.8, 156.9, 136.5, 129.8, 125.6, 124.1, 122.6, 117.6, 115.4, 88.0, 83.9, 67.4, 51.3, 38.8, 29.4, 28.7, 26.3, 19.1. HRMS (ESI) m/z: calculated for $C_{20}H_{24}N_5O_2S$ $[M+H]^+$ 398.1651; found 398.1637.

N-(5-((12-azidododecyl)(methyl)amino)pentyl)-2-((5-((2-methylthiazol-4-yl)ethynyl)pyridin-3-yl)oxy)acetamide (4.19e)

Compound **4.19e** was subjected to general procedure 1. Offwhite solid, 69%. ^{1}H NMR (300 MHz, $CDCl_3$) δ 8.44 (d, *J* = 1.6 Hz, 1H), 8.29 (d, *J* = 2.9 Hz, 1H), 7.43 (s, 1H), 7.33 (dd, *J* = 2.9, 1.6 Hz, 1H), 6.55 (t, *J* = 6.2 Hz, 1H), 4.50 (s, 2H), 3.34 (q, *J* = 7.0 Hz, 2H), 3.22 (t, *J* = 7.0 Hz, 2H), 2.72 (s, 3H), 2.30 (dt, *J* = 8.2, 5.4 Hz, 4H), 2.19 (s, 3H), 1.64 – 1.54 (m, 4H), 1.52 – 1.39 (m, 2H), 1.39 – 1.18 (m, 20H). ^{13}C NMR (75 MHz, $CDCl_3$) δ 166.7, 152.7, 145.9, 138.0, 123.5, 123.1, 120.2, 87.1, 84.7, 67.5, 57.8, 57.5, 51.4, 42.1, 39.1, 29.8 – 29.3 (wide peak), 29.1, 28.8, 27.5, 27.1, 26.8, 26.7, 24.7, 21.0, 19.3, 14.1. HRMS (ESI) m/z: calculated for $C_{31}H_{48}N_7O_2S$ $[M+H]^+$ 582.3590; found 582.3596.

N-(5-((12-azidododecyl)(methyl)amino)pentyl)-2-(3-((2-methylthiazol-4-yl)ethynyl)phenoxy)acetamide (4.19f)

Compound **4.19f** was subjected to general procedure 1. Offwhite solid, 75%. ^{1}H NMR (300 MHz, $CDCl_3$) δ 7.37 (s, 1H), 7.31 – 7.25 (m, 1H), 7.21 (dt, *J* = 7.6, 1.3 Hz, 1H), 7.11 – 7.08 (m, 1H), 6.91 (ddd, *J* = 8.1, 2.6, 1.2 Hz, 1H), 6.55 (t, *J* = 5.9 Hz, 1H), 4.47 (s, 2H), 3.39 – 3.29 (m, 2H), 3.23 (t, *J* = 7.0 Hz, 2H), 2.73 (s, 3H), 2.30 (ddd, *J* = 7.8, 6.5, 3.6 Hz, 4H), 2.19 (s, 3H), 1.64 – 1.40 (m, 6H), 1.38 – 1.20 (m, 20H). ^{13}C NMR (75 MHz, $CDCl_3$) δ 167.6, 165.7, 156.9, 136.6, 129.7, 125.6, 124.0, 122.5, 117.6, 115.5, 115.4, 88.1, 83.8, 67.4, 57.8, 57.5, 51.4, 42.2, 39. 1, 29.6, 29.5, 29.4, 29.4, 29.1, 28.8, 27.5, 27.1, 26.8, 26.7, 24.7, 19.2, 14.2. HRMS (ESI) m/z: calculated for $C_{32}H_{49}N_6O_2S$ [M+H]$^+$ 581.3638; found 581.3651.

N-(2-(2-(2-(2-azidoethoxy)ethoxy)ethoxy)ethyl)-2-((5-((2-methylthiazol-4-yl)ethynyl)pyridin-3-yl)oxy)acetamide (**4.17c**)

Compound **4.17c** was subjected to general procedure 1. Offwhite solid, 65%. ^{1}H NMR (300 MHz, $CDCl_3$) δ 8.40 (d, *J* = 1.6 Hz, 1H), 8.30 (d, *J* = 2.9 Hz, 1H), 7.45 (s, 1H), 7.36 (dd, *J* = 2.9, 1.6 Hz, 1H), 7.07 (br s., 1H), 4.53 (s, 2H), 3.67 – 3.57 (m, 14H), 3.35 (t, *J* = 5.6 Hz, 2H), 2.73 (s, 3H). ^{13}C NMR (75 MHz, $CDCl_3$) δ 167.1, 166.4, 153.1, 145.2, 137.6, 126.8, 125.6, 123.7 (d, *J* = 18 Hz), 120.4, 87.2, 84.6, 70.6, 70.6, 70.5, 70.3, 69.9, 69.5, 67.5, 50.6, 38.9, 19.2. HRMS (ESI) m/z: calculated for $C_{21}H_{27}N_6O_5S$ [M+H]$^+$ 475.1764; found 475.1756.

N-(17-azido-3,6,9,12,15-pentaoxaheptadecyl)-2-((5-((2-methylthiazol-4-yl)ethynyl)pyridin-3-yl)oxy)acetamide (**4.17d**)

Compound **4.17d** was subjected to general procedure 1. Offwhite solid, 54%. ^{1}H NMR (300 MHz, $CDCl_3$) δ 8.41 (d, *J* = 1.6 Hz, 1H), 8.30 (d, *J* = 2.9 Hz, 1H), 7.43 (s, 1H), 7.35 (dd, *J* = 2.9, 1.6 Hz, 1H), 7.14 (br s., 1H), 4.52 (s, 2H), 3.66 – 3.50 (m, 22H), 3.34 (t, *J* = 5.6 Hz, 2H), 2.72 (s, 3H). ^{13}C NMR (75 MHz, $CDCl_3$) δ 167.0, 166.1, 153.0, 145.5, 137.9, 135.9, 123.4 (d, *J* = 9.9 Hz), 120.2, 87.1, 84.7, 70.6, 70.6, 70.5, 70.5, 70.5, 70.4, 70.3, 69.9, 69.6, 67.5, 50.6, 38.9, 19.2. HRMS (ESI) m/z: calculated for $C_{25}H_{35}N_6O_7S$ [M+H]$^+$ 563.2288; found 563.2297.

N-(4-(2-((5-hydroxy-1,2,3,4-tetrahydronaphthalen-2-yl)(propyl)amino)ethyl)phenyl)-3-(1-(12-(methyl(5-(2-((5-((2-methylthiazol-4-yl)ethynyl)pyridin-3-yl)oxy)acetamido)pentyl)amino)dodecyl)-1H-1,2,3-triazol-4-yl)propanamide (**4.20c**)

Compound **4.20c** was subjected to general procedure 2. White solid, 46%. LC-HRMS: t_R=6.78 min (10–100% MeCN, 15 min run), purity 96.21%. HRMS (ESI) m/z: calculated for $C_{57}H_{81}N_9O_4S$ [M+2H]$^{2+}$ 493.8061; found 493.8052.

N-(4-(2-((5-hydroxy-1,2,3,4-tetrahydronaphthalen-2-yl)(propyl)amino)ethyl)phenyl)-3-(1-(8-(methyl(5-(2-(3-((2-methylthiazol-4-yl)ethynyl)phenoxy)acetamido)pentyl)amino)octyl)-1H-1,2,3-triazol-4-yl)propanamide (**4.20d**)

Compound **4.20d** was subjected to general procedure 2. White solid, 51%. LC-HRMS: t_R=6.56 min (10–100% MeCN, 15 min run), purity 99.86 %. HRMS (ESI) m/z: calculated for $C_{54}H_{74}N_8O_4S$ [M+2H]$^{2+}$ 465.2771; found 465.2751. Calculated for $C_{54}H_{73}N_8O_4S$ [M+H]$^+$ 929.5475; found 929.5485.

N-(4-(2-((5-hydroxy-1,2,3,4-tetrahydronaphthalen-2-yl)(propyl)amino)ethyl)phenyl)-3-(1-(10-(methyl(5-(2-(3-((2-methylthiazol-4-yl)ethynyl)phenoxy)acetamido)pentyl)amino)decyl)-1H-1,2,3-triazol-4-yl)propanamide (**4.20e**)

Compound **4.20e** was subjected to general procedure 2. White solid, 57%. LC-HRMS: t_R=6.80 min (10–100% MeCN, 15 min run), purity 94.16 %. HRMS (ESI) m/z: calculated for $C_{56}H_{78}N_8O_4S$ $[M+2H]^{2+}$ 479.2927; found 479.2912. Calculated for $C_{56}H_{77}N_8O_4S$ $[M+H]^+$ 957.5788; found 957.5829.

N-(4-(2-((5-hydroxy-1,2,3,4-tetrahydronaphthalen-2-yl)(propyl)amino)ethyl)phenyl)-3-(1-(12-(methyl(5-(2-(3-((2-methylthiazol-4-yl)ethynyl)phenoxy)acetamido)pentyl)amino)dodecyl)-1H-1,2,3-triazol-4-yl)propanamide (**4.20f**)

Compound **4.20f** was subjected to general procedure 2. White solid, 49%. LC-HRMS: t_R=7.11 min (10–100% MeCN, 15 min run), purity 93.69 %. HRMS (ESI) m/z: calculated for $C_{58}H_{82}N_8O_4S$ $[M+2H]^{2+}$ 493.3084; found 493.3036. Calculated for $C_{58}H_{81}N_8O_4S$ $[M+H]^+$ 985.6101; found 985.6149.

N-(5-((12-(4-((2-methoxy-4-((4-(2-methoxyphenyl)piperazin-1-yl)methyl)phenoxy)methyl)-1H-1,2,3-triazol-1-yl)dodecyl)(methyl)amino)pentyl)-2-((5-((2-methylthiazol-4-yl)ethynyl)pyridin-3-yl)oxy)acetamide (**4.21e**)

Compound **4.21e** was subjected to general procedure 2. White solid, 43%. LC-HRMS: t_R=6.86 min (10–100% MeCN, 15 min run), purity 84.61 %. HRMS (ESI) m/z: calculated for $C_{53}H_{75}N_9O_5S$ $[M+2H]^{2+}$ 474.7800; found 474.7725. Calculated for $C_{53}H_{74}N_9O_5S$ $[M+H]^+$ 948.5534; found 948.5563.

N-(5-((12-(4-((2-methoxy-4-((4-(2-methoxyphenyl)piperazin-1-yl)methyl)phenoxy)methyl)-1H-1,2,3-triazol-1-yl)dodecyl)(methyl)amino)pentyl)-2-(3-((2-methylthiazol-4-yl)ethynyl)phenoxy)acetamide (**4.21f**)

Compound **4.21f** was subjected to general procedure 2. White solid, 61%. LC-HRMS: t_R=7.14 min (10–100% MeCN, 15 min run), purity 84.89 %. HRMS (ESI) m/z: calculated for $C_{54}H_{76}N_8O_5S$ $[M+2H]^{2+}$ 474.2824; found 474.2807.

N-(6-(4-((2-methoxy-4-((4-(2-methoxyphenyl)piperazin-1-yl)methyl)phenoxy)methyl)-1H-1,2,3-triazol-1-yl)hexyl)-2-((5-((2-methylthiazol-4-yl)ethynyl)pyridin-3-yl)oxy)acetamide (**4.16b**)

Compound **4.16b** was subjected to general procedure 2. White solid, 55%. LC-HRMS: t_R=7.24 min (10–100% MeCN, 15 min run), purity 89.88 %. HRMS (ESI) m/z: calculated for $C_{41}H_{50}N_8O_5S$ $[M+2H]^{2+}$ 383.1806; found 383.1803. Calculated for $C_{41}H_{49}N_8O_5S$ $[M+H]^+$ 765.3540; found 765.3564.

N-(4-(2-((5-hydroxy-1,2,3,4-tetrahydronaphthalen-2-yl)(propyl)amino)ethyl)phenyl)-3-(1-(6-(2-(3-((2-methylthiazol-4-yl)ethynyl)phenoxy)acetamido)hexyl)-1H-1,2,3-triazol-4-yl)propanamide (**4.16a**)

Compound **4.16a** was subjected to general procedure 2. White solid, 46%. LC-HRMS: t_R=7.49 min (10–100% MeCN, 15 min run), purity 80.18 %. HRMS (ESI) m/z: calculated for $C_{46}H_{57}N_7O_4S$ $[M+2H]^{2+}$ 401.7090; found 401.7073. Calculated for $C_{46}H_{56}N_7O_4S$ $[M+H]^+$ 802.4114; found 802.4108.

N-(6-(4-((2-methoxy-4-((4-(2-methoxyphenyl)piperazin-1-yl)methyl)phenoxy)methyl)-1H-1,2,3-triazol-1-yl)hexyl)-2-(3-((2-methylthiazol-4-yl)ethynyl)phenoxy)acetamide (**4.16c**)

Compound **4.16c** was subjected to general procedure 2. White solid, 65%. LC-HRMS: t_R=7.56 min (10–100% MeCN, 15 min run), purity 89.99 %. HRMS (ESI) m/z: calculated for $C_{42}H_{51}N_7O_5S$ $[M+2H]^{2+}$ 382.6830; found 382.6814. Calculated for $C_{42}H_{50}N_7O_5S$ $[M+H]^+$ 764.3594; found 764.3611.

N-(17-(4-((2-methoxy-4-((4-(2-methoxyphenyl)piperazin-1-yl)methyl)phenoxy)methyl)-1H-1,2,3-triazol-1-yl)-3,6,9,12,15-pentaoxaheptadecyl)-2-((5-((2-methylthiazol-4-yl)ethynyl)pyridin-3-yl)oxy)acetamide (**4.18d**)

Compound **4.18d** was subjected to general procedure 2. White solid, 59%. LC-HRMS: t_R=7.03 min (10–100% MeCN, 15 min run), purity 75.07 %. HRMS (ESI) m/z: calculated for $C_{47}H_{62}N_8O_{10}S$ $[M+2H]^{2+}$ 465.2149; found 465.2128. Calculated for $C_{42}H_{50}N_7O_5S$ $[M+H]^+$ 929.4231; found 929.4214.

N-(4-(2-((5-hydroxy-1,2,3,4-tetrahydronaphthalen-2-yl)(propyl)amino)ethyl)phenyl)-3-(1-(1-((5-((2-methylthiazol-4-yl)ethynyl)pyridin-3-yl)oxy)-2-oxo-6,9,12,15,18-pentaoxa-3-azaicosan-20-yl)-1H-1,2,3-triazol-4-yl)propanamide (**4.22a**)

Compound **4.22a** was subjected to general procedure 2. White solid, 47%. LC-HRMS: t_R=7.03 min (10–100% MeCN, 15 min run), purity 91.52 %. HRMS (ESI) m/z: calculated for $C_{51}H_{68}N_8O_9S$ $[M+2H]^{2+}$ 484.2409; found 484.2378.

N-(2-(2-(2-(2-(4-((2-methoxy-4-((4-(2-methoxyphenyl)piperazin-1-yl)methyl)phenoxy)methyl)-1H-1,2,3-triazol-1-yl)ethoxy)ethoxy)ethoxy)ethyl)-2-((5-((2-methylthiazol-4-yl)ethynyl)pyridin-3-yl)oxy)acetamide (**4.18c**)

Compound **4.18c** was subjected to general procedure 2. White solid, 56%. LC-HRMS: t_R=7.00 min (10–100% MeCN, 15 min run), purity 82.61%. HRMS (ESI) m/z: calculated for $C_{43}H_{54}N_8O_8S$ $[M+2H]^{2+}$ 421.1887; found 421.1826. Calculated for $C_{43}H_{53}N_8O_8S$ $[M+H]^+$ 841.3707; found 841.3729.

N-(4-(2-((5-hydroxy-1,2,3,4-tetrahydronaphthalen-2-yl)(propyl)amino)ethyl)phenyl)-3-(1-(1-((5-((2-methylthiazol-4-yl)ethynyl)pyridin-3-yl)oxy)-2-oxo-6,9,12-trioxa-3-azatetradecan-14-yl)-1H-1,2,3-triazol-4-yl)propanamide (**4.22b**)

Compound **4.22b** was subjected to general procedure 2. White solid, 53%. LC-HRMS: t_R=6.65 min (10–100% MeCN, 15 min run), purity 91.17%. HRMS (ESI) m/z: calculated for $C_{47}H_{60}N_8O_7S$ $[M+2H]^{2+}$ 440.2147; found 440.2118. Calculated for $C_{47}H_{59}N_8O_7S$ $[M+H]^+$ 879.4221; found 879.4232.

N-(4-(2-((5-hydroxy-1,2,3,4-tetrahydronaphthalen-2-yl)(propyl)amino)ethyl)phenyl)-3-(1-(1-(3-((2-methylthiazol-4-yl)ethynyl)phenoxy)-2-oxo-6,9,12,15,18-pentaoxa-3-azaicosan-20-yl)-1H-1,2,3-triazol-4-yl)propanamide (**4.22c**)

Compound **4.22c** was subjected to general procedure 2. White solid, 60%. LC-HRMS: t_R=7.12 min (10–100% MeCN, 15 min run), purity 90.88 %. HRMS (ESI) m/z: calculated for $C_{52}H_{69}N_7O_9S$ $[M+2H]^{2+}$ 483.7433; found 483.7411. Calculated for $C_{52}H_{68}N_7O_9S$ $[M+H]^+$ 966.4799; found 966.4840.

N-(4-(2-((5-hydroxy-1,2,3,4-tetrahydronaphthalen-2-yl)(propyl)amino)ethyl)phenyl)-3-(1-(1-(3-((2-methylthiazol-4-yl)ethynyl)phenoxy)-2-oxo-6,9,12-trioxa-3-azatetradecan-14-yl)-1H-1,2,3-triazol-4-yl)propanamide (**4.22d**)

Compound **4.22d** was subjected to general procedure 2. White solid, 53%. LC-HRMS: t_R=7.05 min (10–100% MeCN, 15 min run), purity 85.91%. HRMS (ESI) m/z: calculated for $C_{48}H_{61}N_7O_7S$ $[M+2H]^{2+}$ 439.7171; found 439.7152.

S5

Chromatographic analyses

LC-MS analyses were carried out on a Waters Alliance 2695 XE separation Module by using a Phenomenex Kinetex EVO C18, 5µm 100x2.1mm and a gradient system of HCOOH in H_2O (0.1 %, v/v)/HCOOH in MeCN (0.1%, v/v) at a flow rate of 0.6 $mLmin^{-1}$, 100:0 to 0:100 (0 to 100 % MeCN) in 15 minutes. High-resolution spectra were recorded on a Waters LCT Premier XE Mass spectrometer and a 2996 Photodiode Array Detector, range 220 nm-400 nm.

Blank

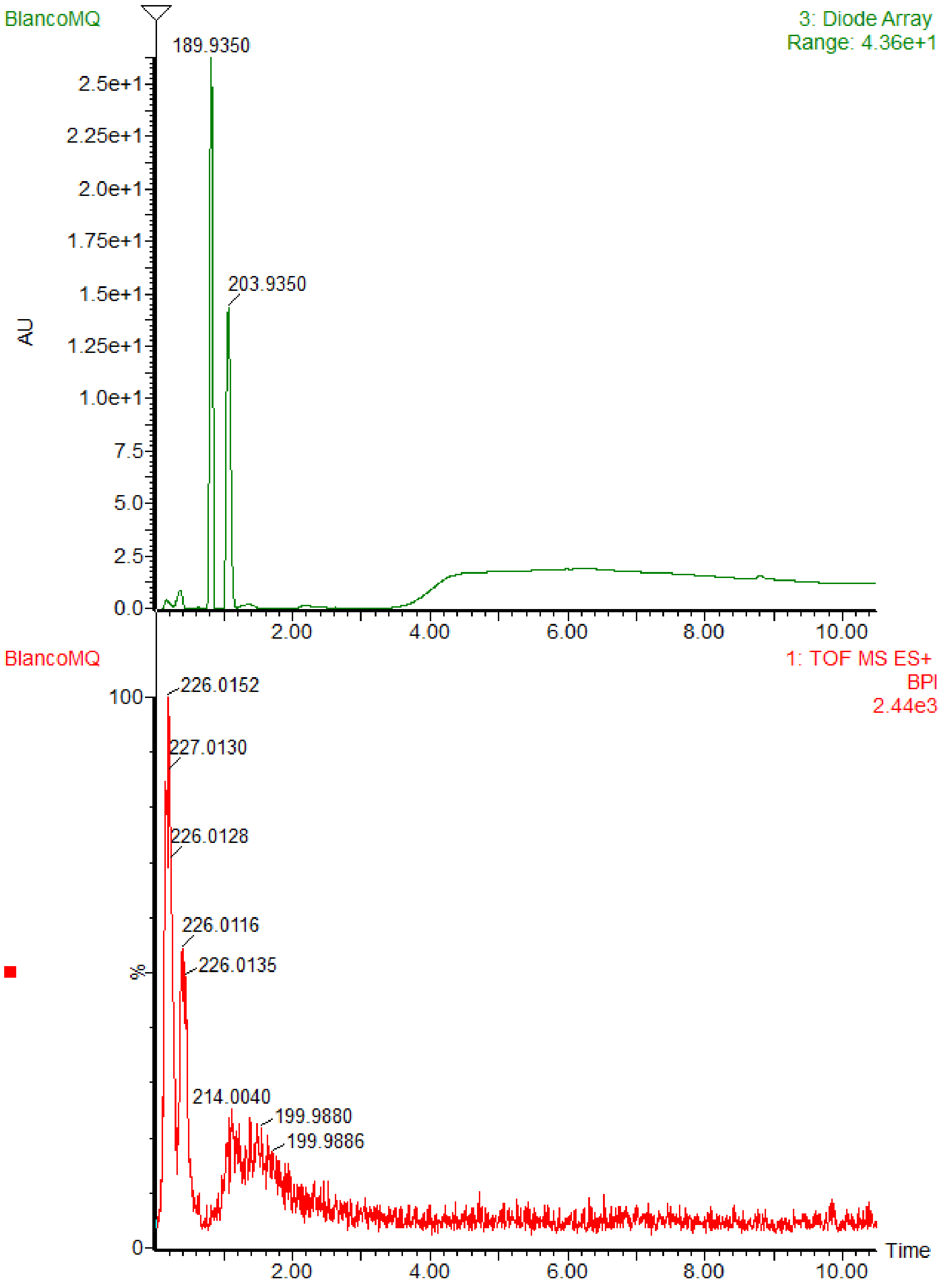
BlancoMQ
3: Diode Array
Range: 4.36e+1
AU
189.9350
203.9350
2.5e+1
2.25e+1
2.0e+1
1.75e+1
1.5e+1
1.25e+1
1.0e+1
7.5
5.0
2.5
0.0
2.00
4.00
6.00
8.00
10.00
BlancoMQ
1: TOF MS ES+
BPI
2.44e3
%
100
0
226.0152
227.0130
226.0128
226.0116
226.0135
214.0040
199.9880
199.9886
2.00
4.00
6.00
8.00
10.00
Time

Compound **4.16**

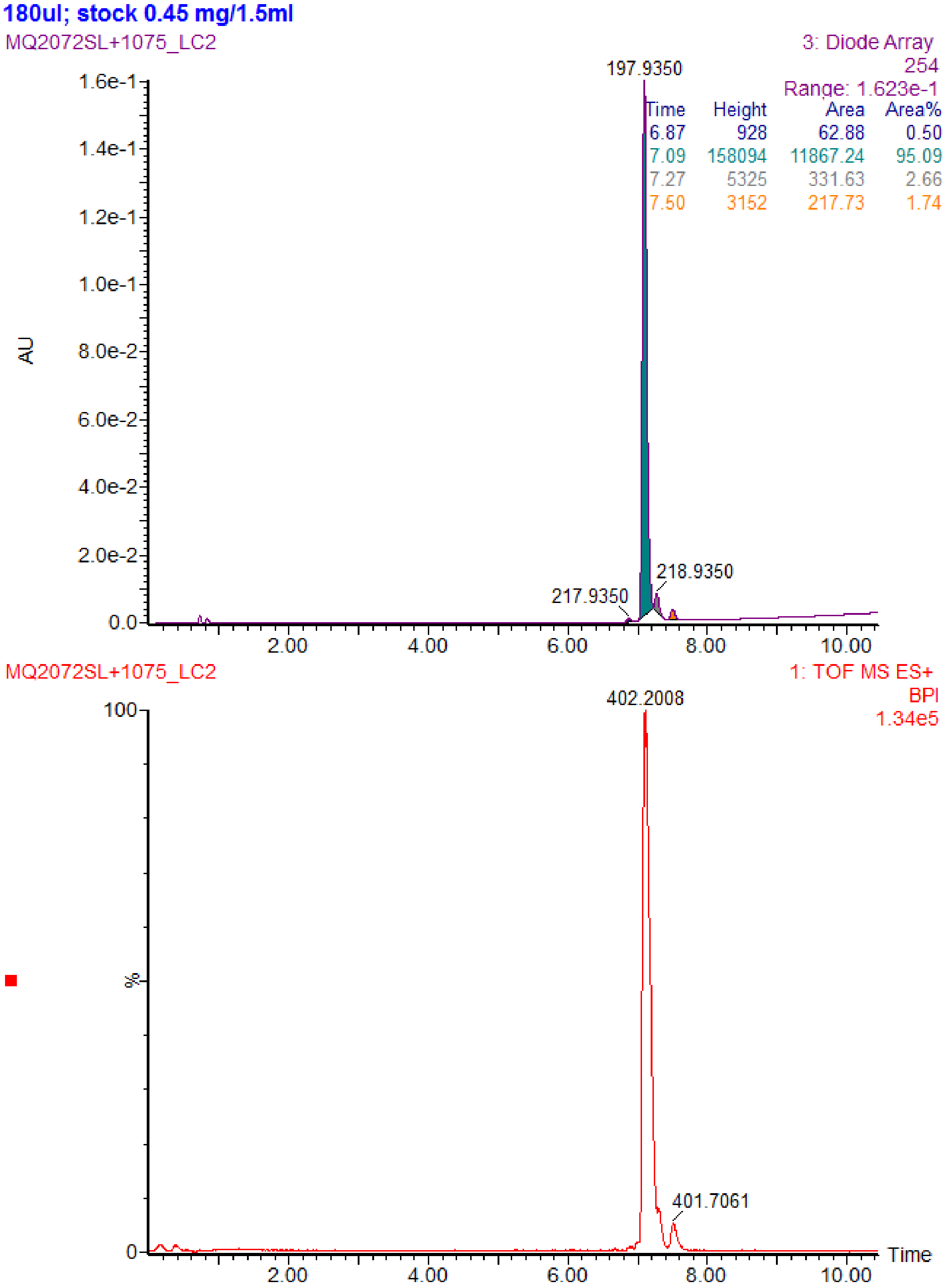

Compound **4.20a**

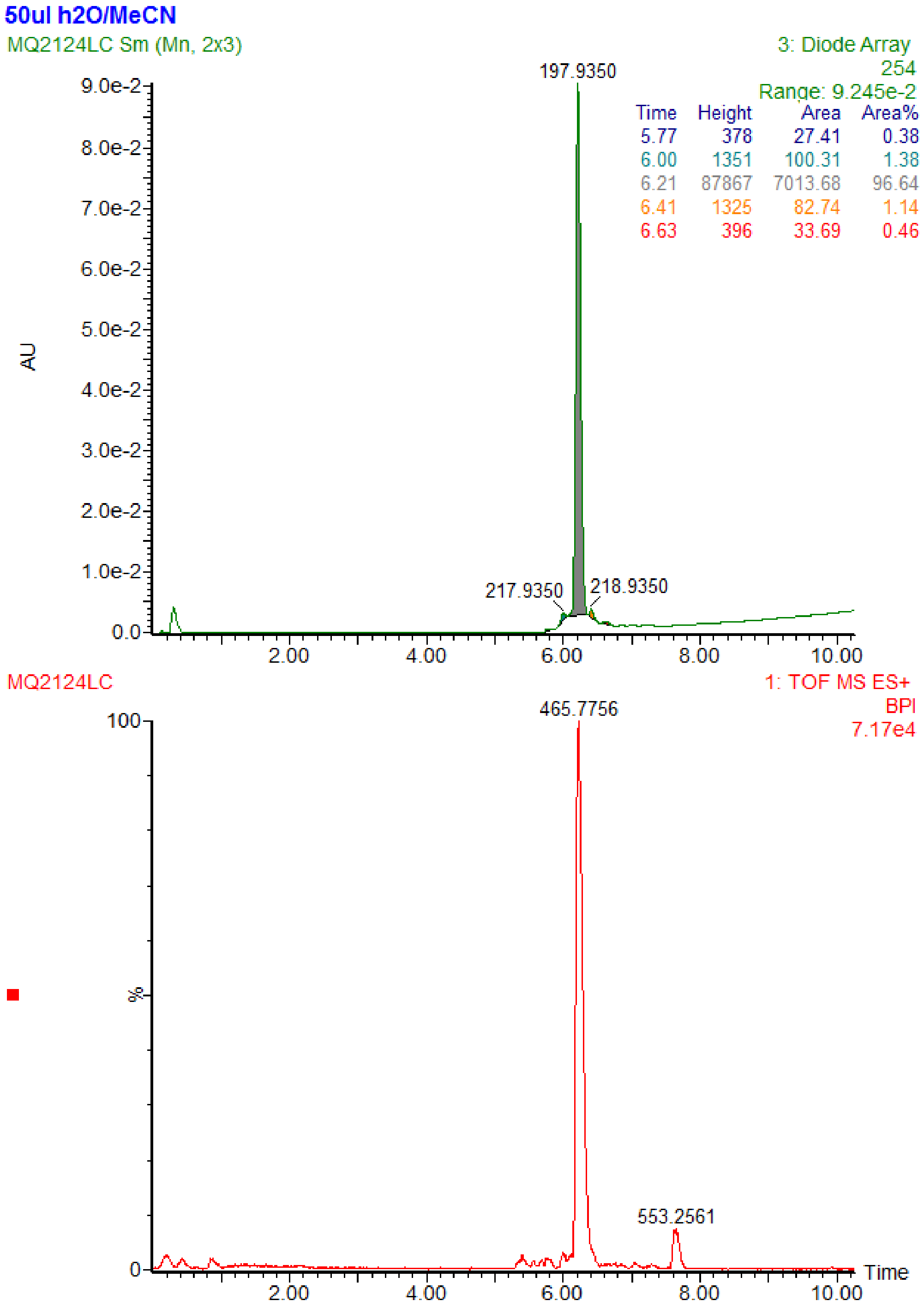

Compound **4.21a**

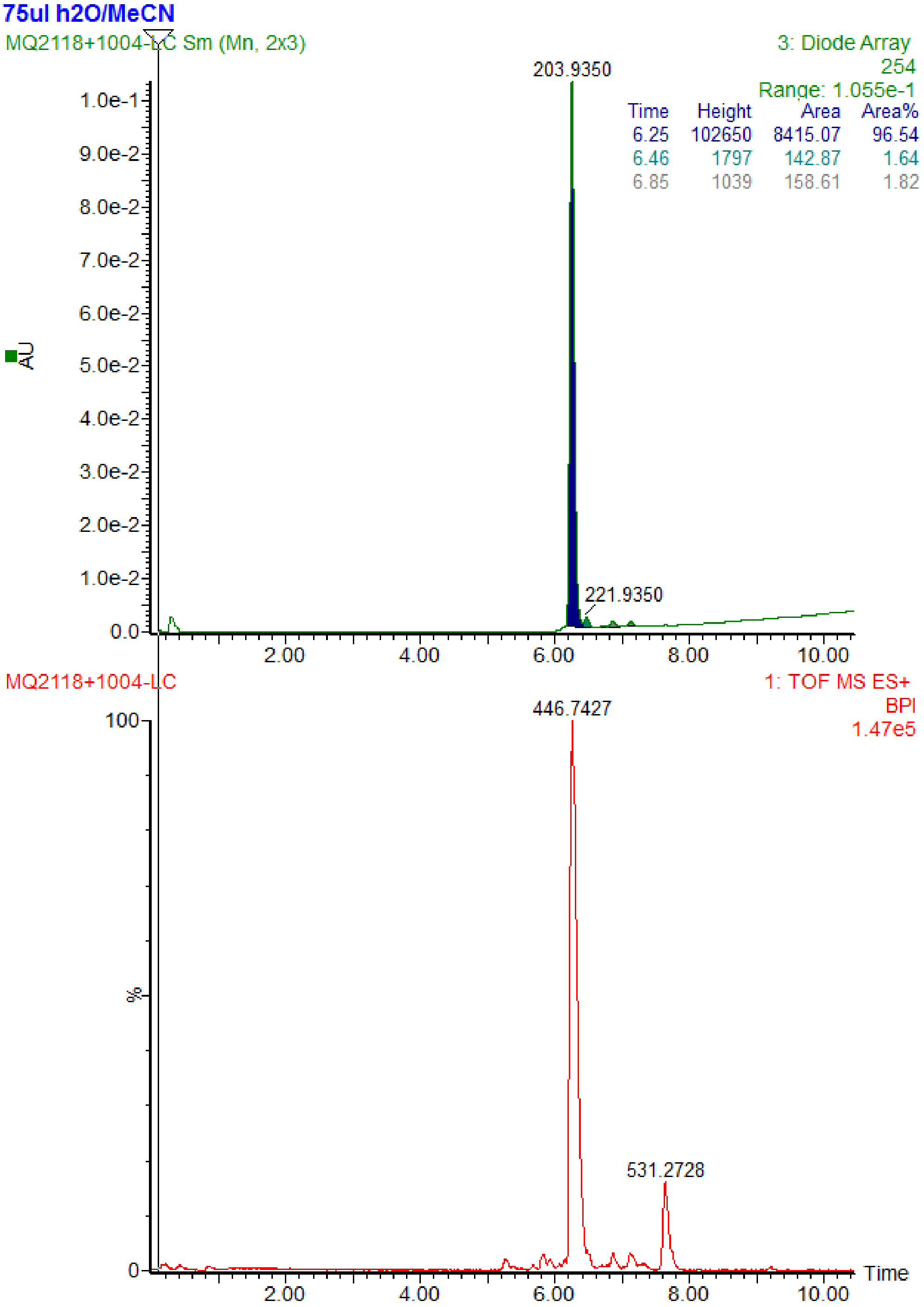

Compound **4.21c**

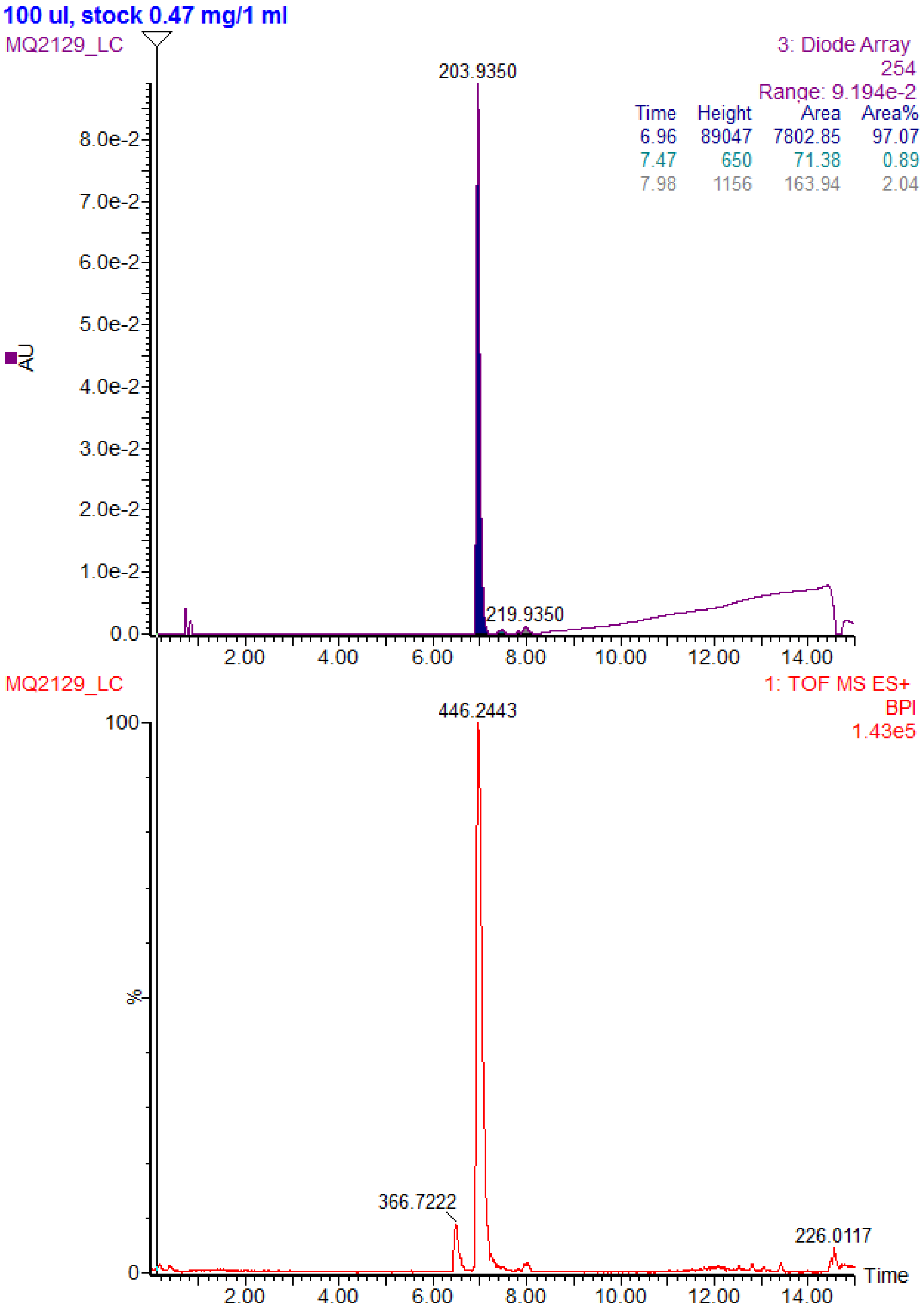

Time	Height	Area	Area%
6.96	89047	7802.85	97.07
7.47	650	71.38	0.89
7.98	1156	163.94	2.04

Compound **4.18a**

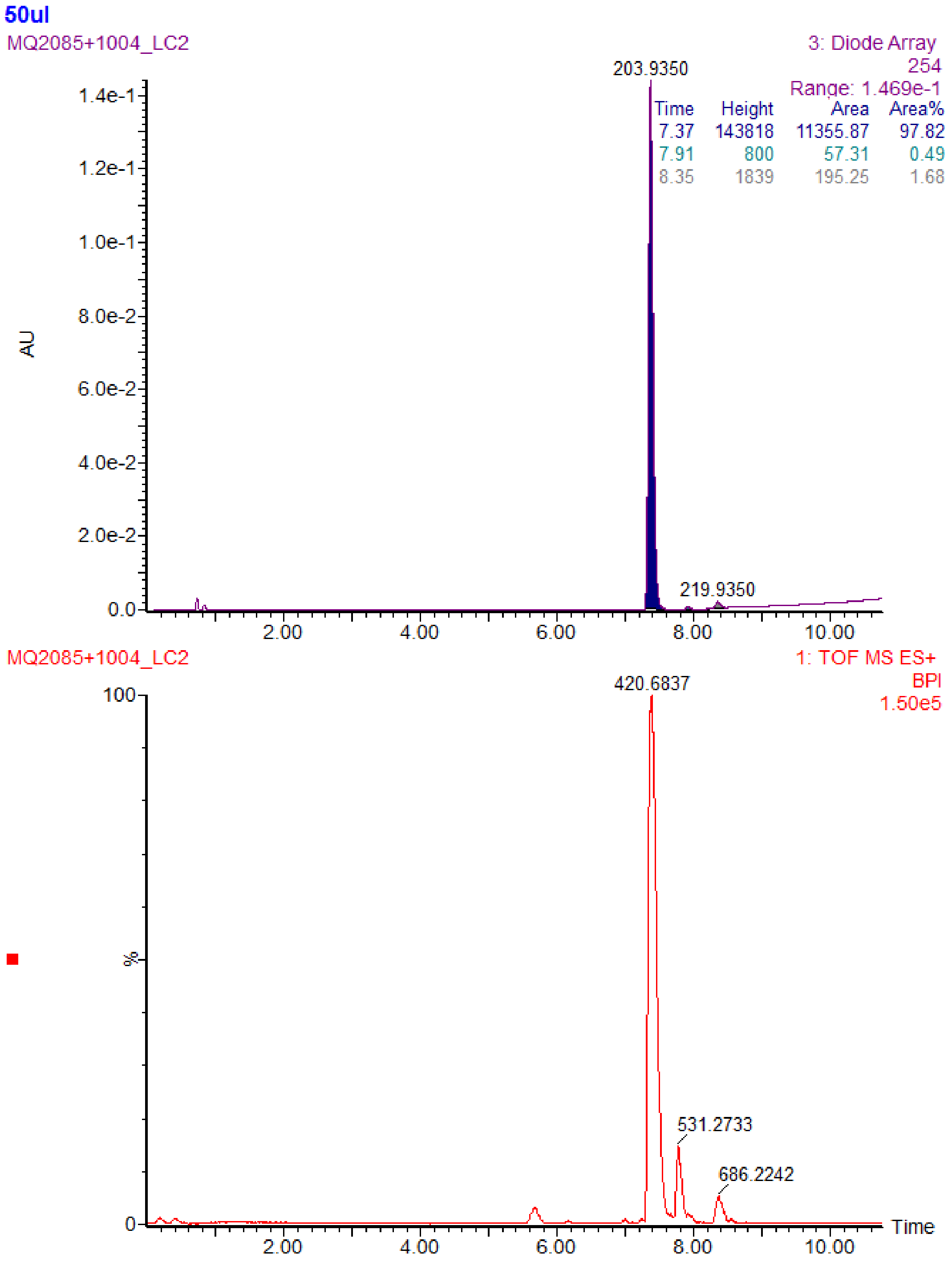

Time	Height	Area	Area%
7.37	143818	11355.87	97.82
7.91	800	57.31	0.49
8.35	1839	195.25	1.68

S6

NMR spectra

The ^{1}H NMR and ^{13}C NMR spectra of compound **4.20a** are given below.

Compound **4.20a**

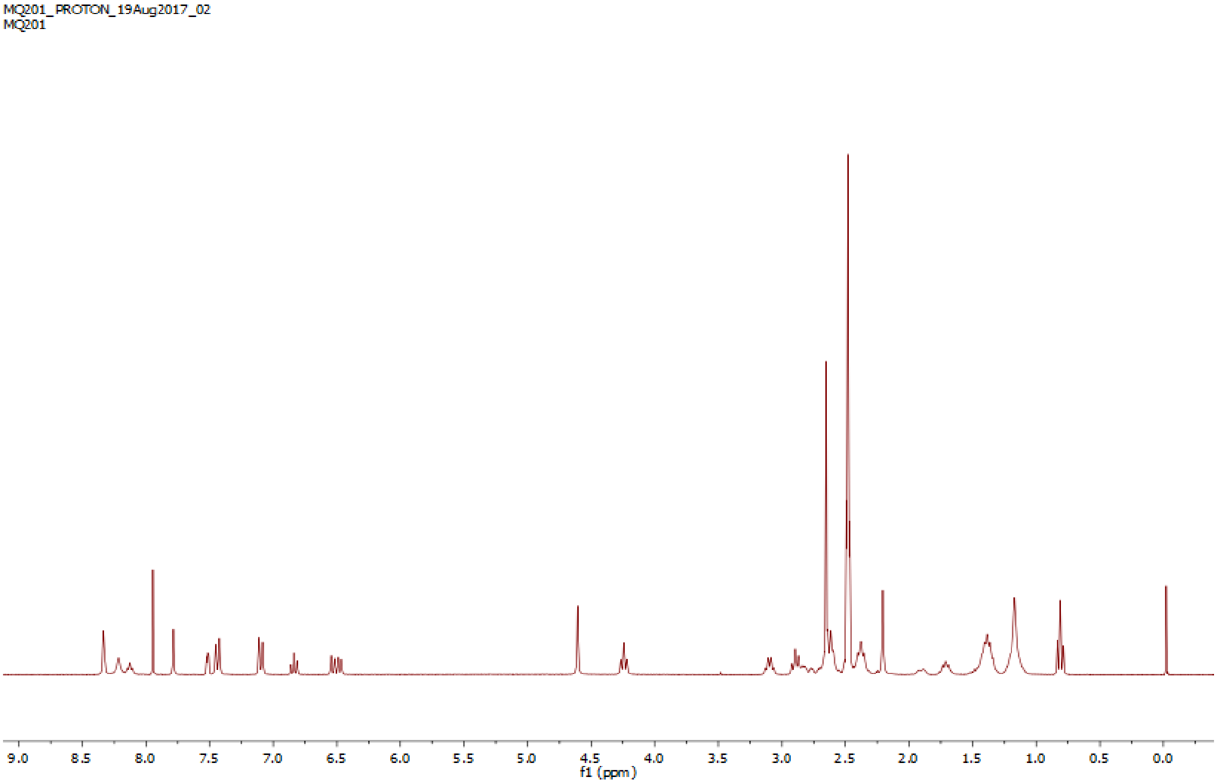

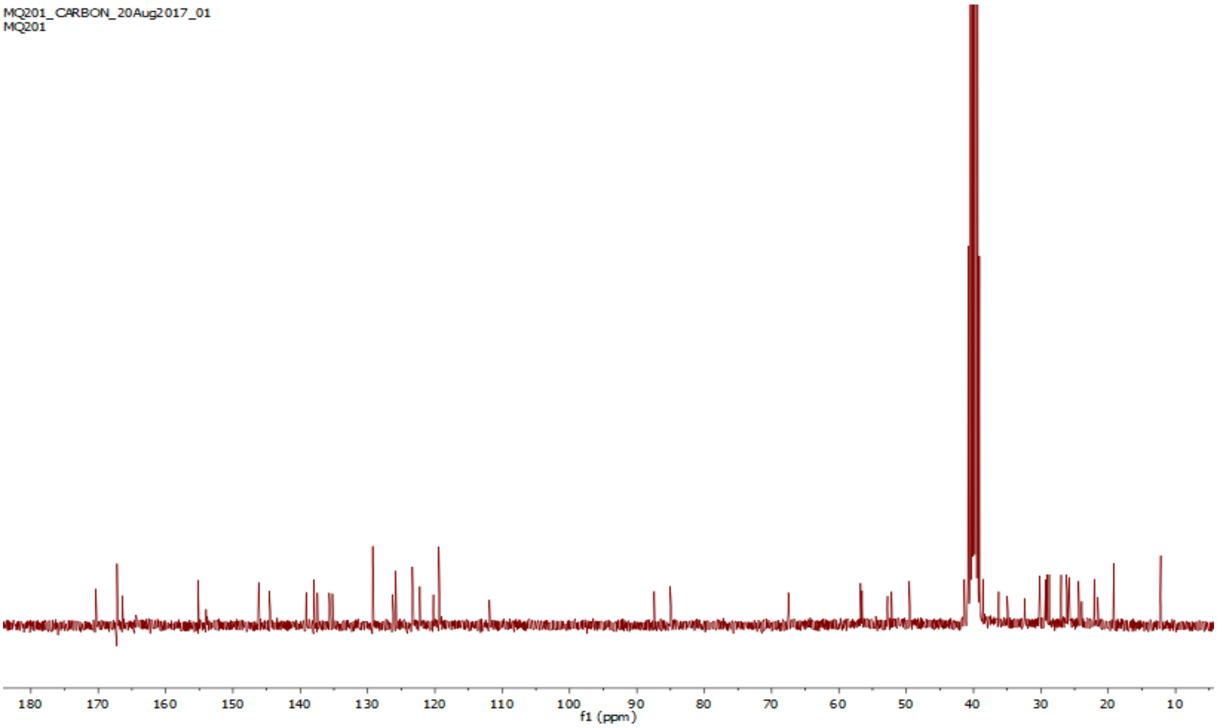

CHAPTER V

Synthesis and biological evaluation of fluorescent ligands targeting the metabotropic glutamate 5 receptor

Víctor Fernandez Dueñas performed all the biological assays under supervision of Prof. Francisco Ciruela (Universitat de Barcelona). Dr. Martijn Risseeuw synthesized the BODIPY dye reagents.

V. SYNTHESIS AND BIOLOGICAL EVALUATION OF FLUORESCENT LIGANDS TARGETING THE METABOTROPIC GLUTAMATE 5 RECEPTOR

V.1. Abstract

In this study, we described the design and synthesis of a series of fluorescent mGluR5 ligands based on BODIPY fluorophores. The preliminary evaluation via NanoBRET suggests that all the fluorescent ligands are able to bind to the mGluR5. In addition, the affinity of compound **5.03** to mGluR5 seems modestly higher than that of **5.10** in the saturation assay. Hence, **5.03** could be a promising tool for further investigating D_2R-mGluR5 dimerization at the surface of living cells by NanoBRET.

V.2. Introduction

The metabotropic glutamate receptors (mGluRs) constitute a family of G-protein coupled receptors (GPCR) in the mammalian central nervous system (CNS) and are characterized by the presence of large, extracellular, N-terminal orthosteric binding domains, which are activated by L-glutamate [1][2][3]. Group I mGluRs (mGluR1 and mGluR5) are principally localized postsynaptically and are extensively distributed in many brain regions, including the hippocampus, thalamic nuclei, and spinal cord. Stimulation of mGluR5 leads to phosphoinositide (PI) hydrolysis and formation of two intracellular second messengers: inositol triphosphate (IP3), which induces intracellular Ca^{2+} release, and diacylglycerol (DAG), which stimulates protein kinase C activity (PKC), via Gq protein coupling to phospholipase C [3][4][5].

Fluorescently labeled ligands have proven their utility as pharmacological tools to study receptor localization, trafficking, and signaling processes via fluorescence imaging [6]. They are also employed in fluorescent binding assays to study ligand/receptor interactions [6]. In such competition assays, fluorescent ligands offer advantages over radioligands, which suffer from health risks and legal and disposal costs.

V.3. Design of fluorescent mGluR5 ligands

Boron dipyrromethene (BODIPY) is a fluorescent dye with diverse properties, such as photochemical stability, high molar absorptivity, high fluorescence quantum yield, and the fact that its fluorescence property can be altered by varying the substitution pattern on the core and the flanking pyrroles. Alkyne functionalized BODIPY dyes can be used to fluorescently label an azido functionalized ligand in a chemo selective manner employing the copper-catalyzed azide–alkyne cycloaddition (CuAAC) reaction [7]. Here we exploited alkyne functionalized BODIPY (496/503) and BODIPY (573/607) to construct a small set of fluorescent mGluR5 ligands (Figure 1). Towards this end, we employed the earlier synthesized MTEP derivatives and linkers as used for the bivalent D_2R-mGluR5 ligands. These fluorescent ligands were tested by NanoBRET. NanoBRET is a relatively new bioluminescence resonance energy transfer (BRET) variant for the analysis of protein-protein interactions, which was developed by Promega by combining an extremely bright luciferase (Nanoluc) with BRET to increase detection sensitivity and dynamic range over current BRET technologies [8].

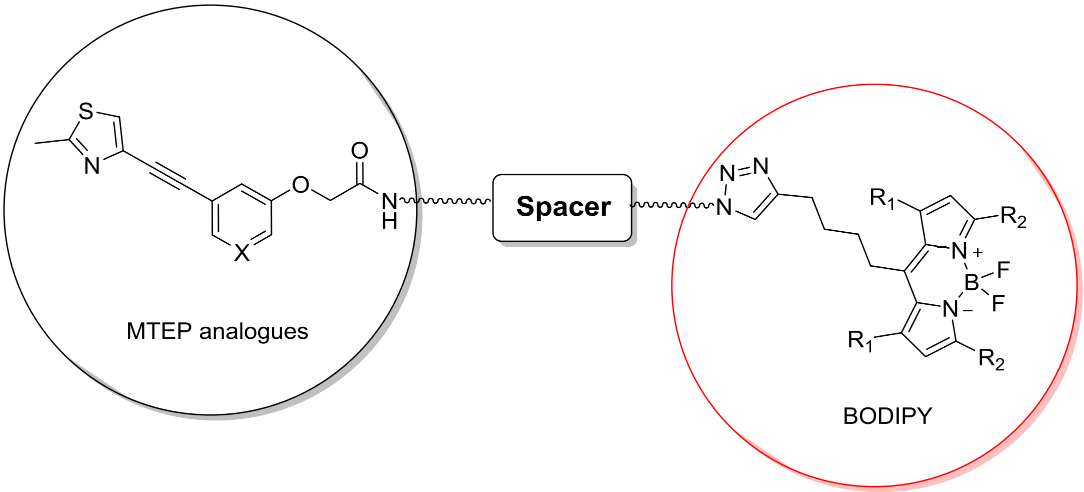

Figure 1. Designed fluorescent mGluR5 ligands based on BODIPY

V.4. Results and discussion

V.4.1. Chemistry

V.4.1.1 Synthesis of fluorescent mGluR5 ligands

The fluorescent ligands were generated by first condensing the mGluR5 carboxylate derivatives with different spacers in the presence of the coupling agent EDC and triethylamine to yield the six intermediate azides, which were described in Chapter IV. The synthesis of the fluorescent ligands was accomplished by reacting each of these azides with both alkyne modified BODIPY green and BODIPY red through CuAAC (Scheme 1). This afforded a concise series of twelve mGluR5 fluorescent ligands.

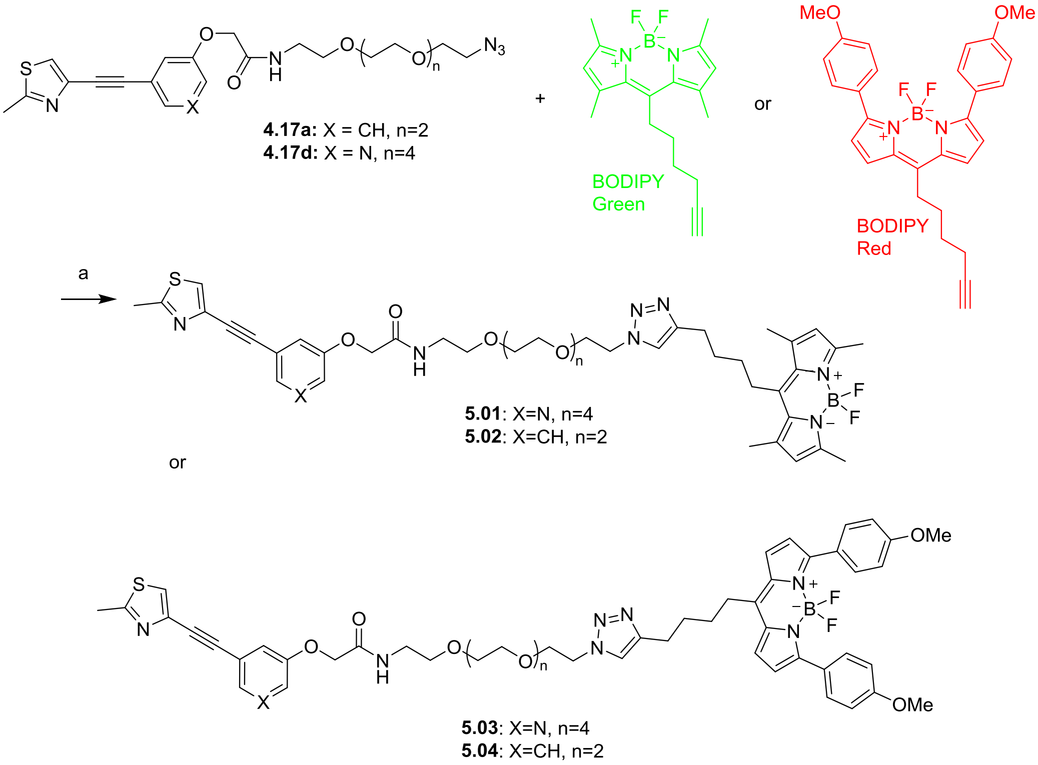
4.17a: X = CH, n=2
4.17d: X = N, n=4
+
BODIPY Green
or
BODIPY Red
a
or
5.01: X=N, n=4
5.02: X=CH, n=2
5.03: X=N, n=4
5.04: X=CH, n=2

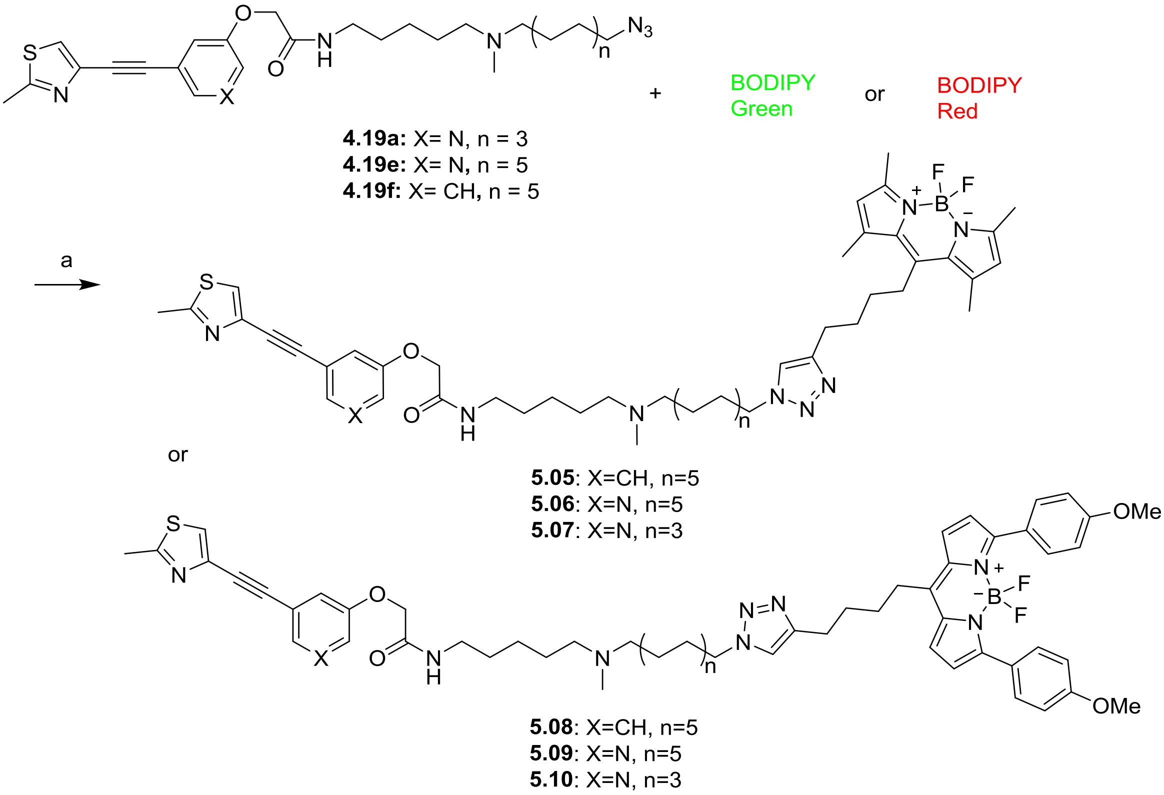
4.19a: X= N, n = 3
4.19e: X= N, n = 5
4.19f: X= CH, n = 5
+
BODIPY Green
or
BODIPY Red
a
or
5.05: X=CH, n=5
5.06: X=N, n=5
5.07: X=N, n=3
5.08: X=CH, n=5
5.09: X=N, n=5
5.10: X=N, n=3

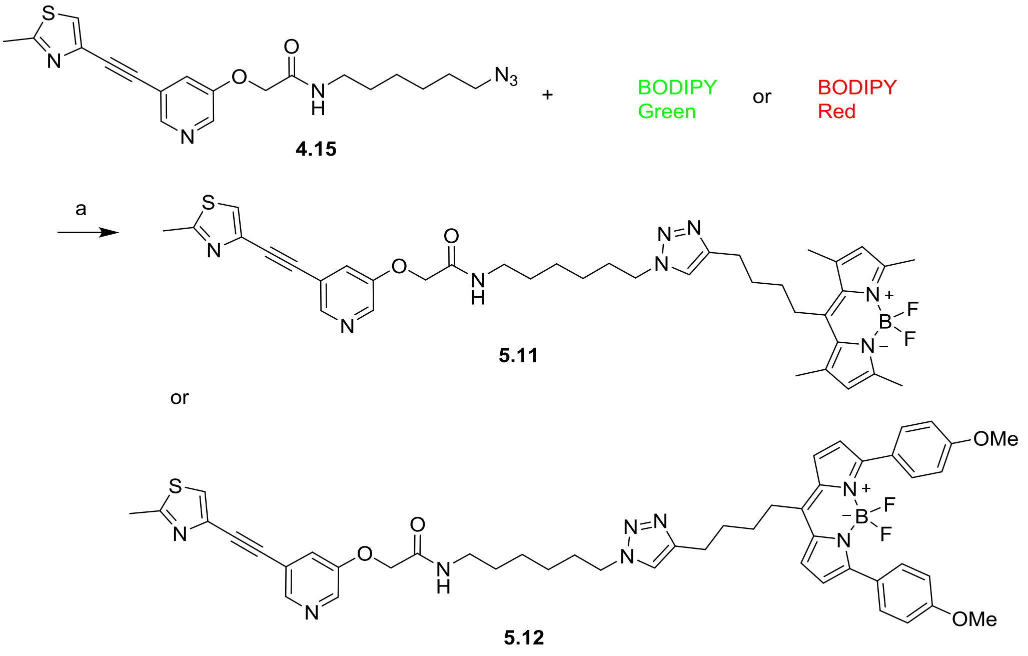

Scheme 1. Reagents and conditions: a) sodium ascorbate, $CuSO_4$, triethylamine, tris[(1-benzyl-1,2,3-triazol-4-yl)methyl]amine, dimethylformamide.

V.4.2. Preliminary evaluation of the synthesized fluorescent mGluR5 ligands

V.4.2.1 Characterization of fluorescent properties

We first determined the excitation and emission spectra of the fluorescent mGluR5 ligands. All BODIPY green labeled ligands exhibited comparable spectral separation (10 nm) between excitation and emission wavelength (Figure 2). Interestingly, spectral separation exceeding more than 30 nm was achieved for the three measured BODIPY red labeled ligands, with **5.03** even displaying spectral separation of 40 nm.

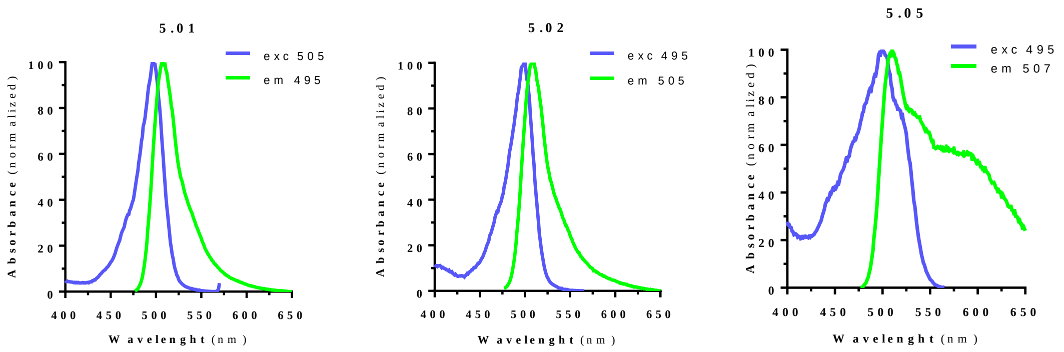

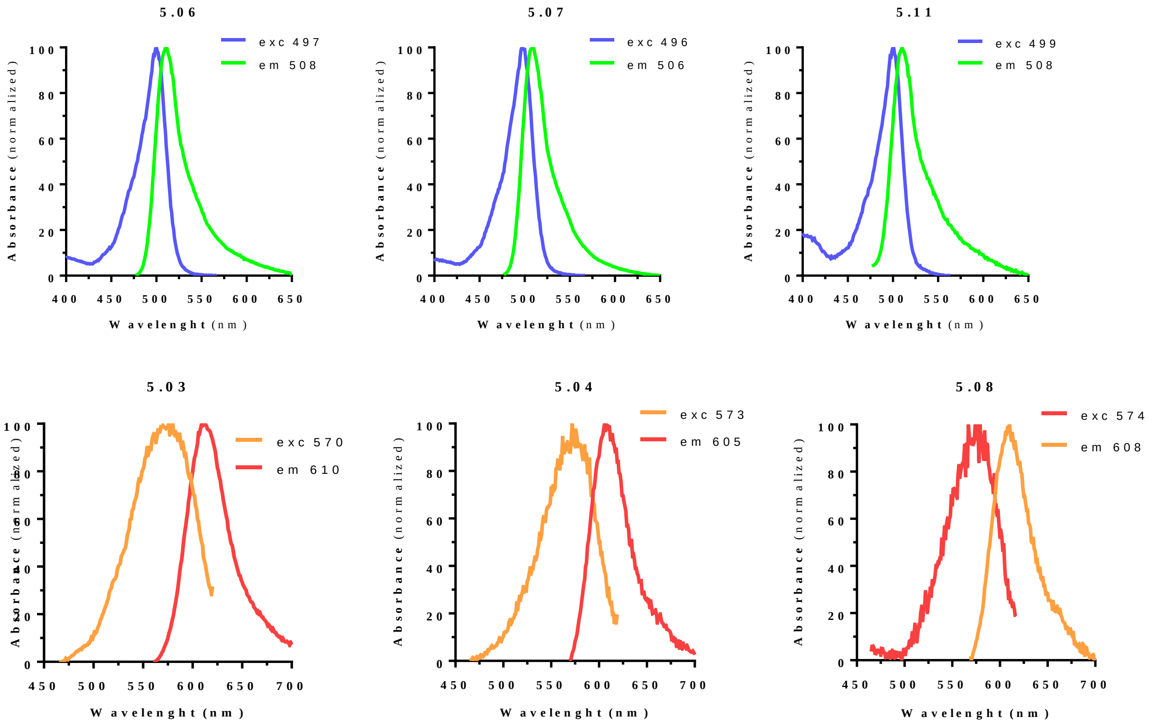

Figure 2. Excitation and emission wavelength for the mGluR5 fluorescent ligands.

Next, we tested the emission intensity for all the BODIPY labeled ligands. Compound **5.01** (Figure 3) showed higher emission intensity than the other BODIPY green labeled ligands. Within the red labeled ligands compounds **5.03** and **5.10** displayed the highest emission intensity. Of note, compounds **5.01** and **5.03** share the same length and composition of spacer (PEG$_6$).

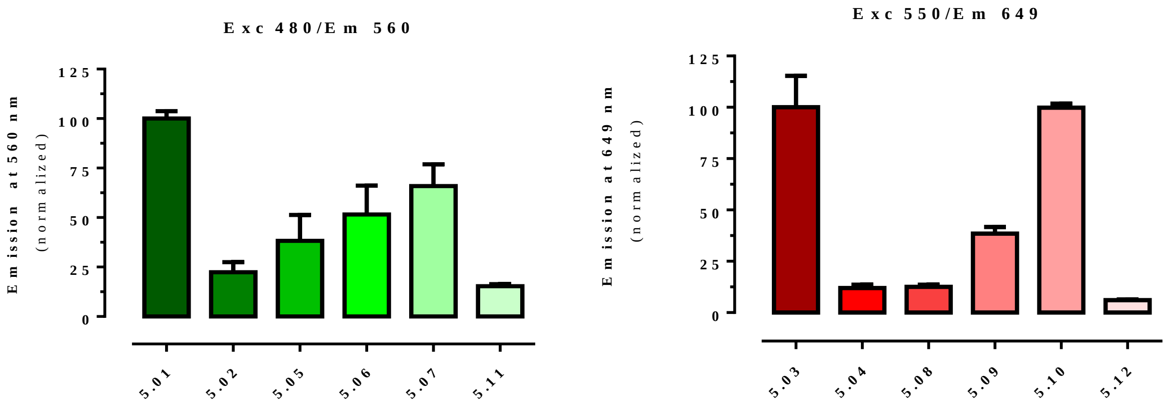

Figure 3. Relative emission at 560 nm or 649 nm of a 10 µM solution of the different BODIPY-conjugates in 0.05% DMSO upon excitation at 480 nm or 550 nm, respectively. This value is somehow related to the quantum yield of each fluorophore.

V.4.2.2 Fluorescent mGluR5 ligands in the NanoBRET assay

Using a mGluR5 that is tagged at its N-terminus with a small, bright Nanoluciferase as a luminescent donor we evaluated the intensity of the NanoBRET signal upon incubation with the different synthesized fluorescent mGluR5 ligands as acceptors. This signal originates from the bioluminescence resonance energy transfer between the NanoLuc and BODIPY labeled ligand in the presence of coelenterazine.[8]

First a binding assay was performed to assess the ability of the fluorescent mGluR5 ligands (10 µM) to generate NanoBRET signals. BODIPY green labeled compounds had a comparable signal at 554 nm except for **5.02** and **5.11**, which gave a considerably lower NanoBRET signal. Amongst the BODIPY red labeled ligands, compound **5.03** exhibited the highest efficacy to generate NanoBRET signal at 610 nm.

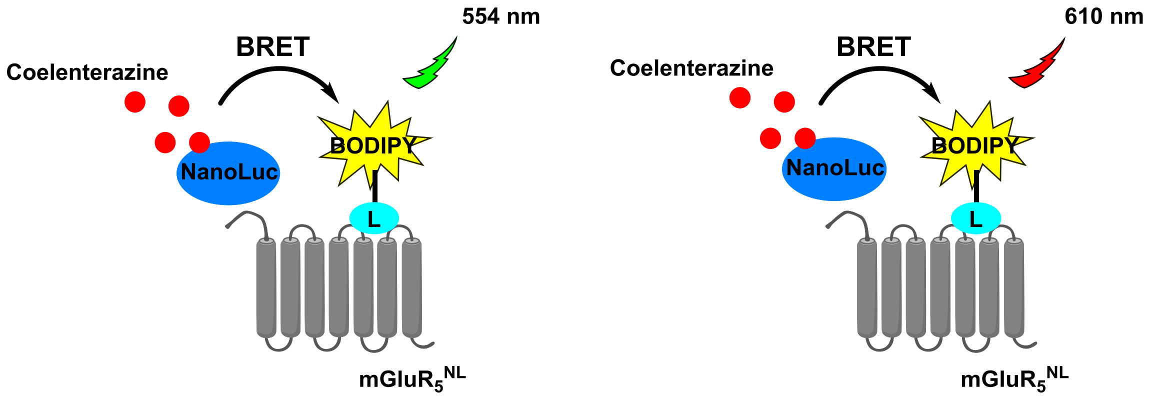

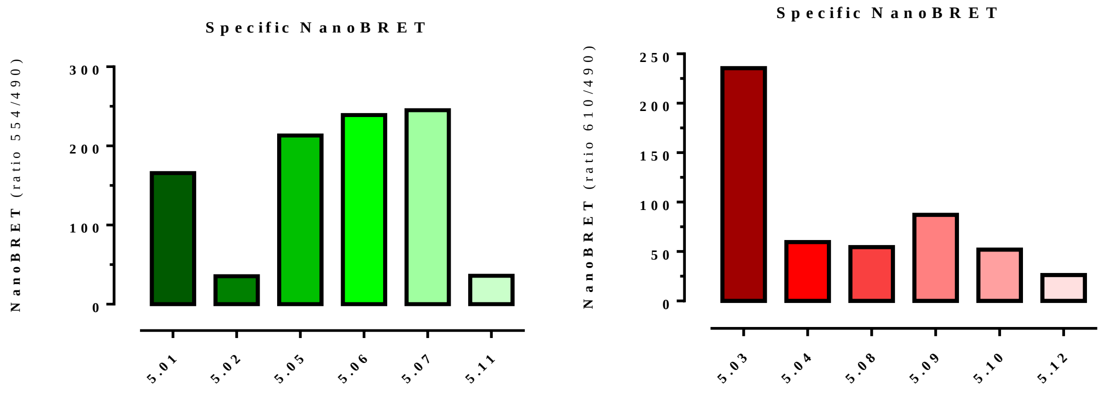

Figure 4. Represents the binding of 10 µM of each ligand to mGluR5^{NL} (a single concentration binding assay). Binding conditions: HEK-293 transiently transfected with mGluR5^{NL} were incubated with 10 µM fluorescent ligands in the absence or presence of 100 µM MTEP during 1h at 22°C.

Subsequently, a saturation assay was performed to assess the binding affinity of fluorescent ligands to mGluR5. Preliminary results indicate that the binding affinity of compound **5.03** (0.84 ± 0.74 µM) is modestly higher than that of **5.10** (1.4 ± 1.2 µM). However, the Bmax values for these two compounds are reversed. In addition, we also tested the expression of the receptor mGluR5^{NL}, which was constructed in HEK 293T cells.

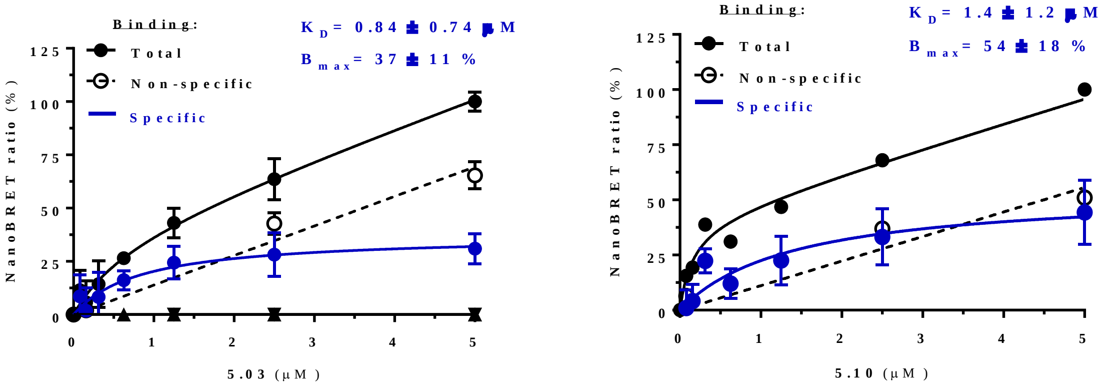

Figure 5. Saturation binding assay for the fluorescent mGluR5 ligands via NanoBRET.

V.5. Conclusion

In summary, we have designed and synthesized twelve novel fluorescent mGluR5 ligands based on BODIPY fluorophores. The preliminary biological assessment via NanoBRET indicates that all the fluorescent ligands are capable of binding to the mGluR5. Furthermore, although the saturation assay needs to be optimized, the affinity of compound **5.03** to mGluR5 seems modestly higher than that of **5.10**. Therefore, **5.03** could be a promising tool for investigating D$_2$R-mGluR5 dimerization at the surface of living cells by NanoBRET (Figure 6).

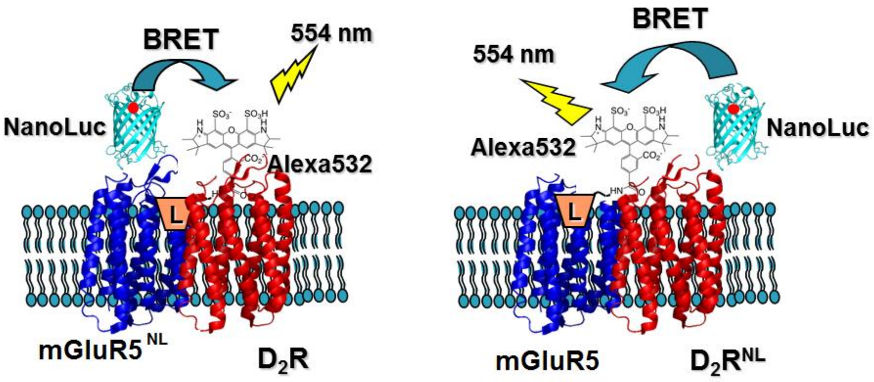

Figure 6. A NanoBRET approach will be used to assess mGluR5-D$_2$R oligomerization.

V.6. Experimental

V.6.1 Chemistry

All reactions described were performed under an N_2 atmosphere and at ambient temperature unless stated otherwise. All regents and solvents were purchased from Sigma-Aldrich (Diegem, Belgium), Fisher Scientific (Merelbeke, Belgium), TCI Europe (Zwijndrecht, Belgium) or Apollo Scientific (Bredbury, Stockport, United Kingdom) and used as received. NMR solvents were acquired from Eurisotop (Saint-Aubin, France). Reactions were monitored by TLC analysis using TLC aluminium sheets (Macherey-Nagel, Alugram Sil G/UV254) with detection by spraying with a solution of $(NH_4)_6Mo_7O_{24}\cdot 4H_2O$ (25 gL^{-1}) and $(NH_4)_4Ce(SO_4)_4\cdot 2H_2O$ (10 gL^{-1}) in H_2SO_4 (10 % aq.) followed by charring or an aqueous solution of $KMnO_7$ (20 gL^{-1}) and K_2CO_3 (10 gL^{-1}) or an ethanolic solution of ninhydrin (2 gL^{-1}) and acetic acid (1% v/v) followed by charring. Solution pH values were estimated using universal indicator paper (Merck). Silica gel column chromatography was performed using a Grace Reveleris X2 system and the corresponding silica gel cartridges. ESI-HRMS spectra were measured with a Waters LCT Premier XE Mass spectrometer calibrated using leucine enkephalin as an external standard. ^{1}H- and ^{13}C-APT-NMR spectra were recorded with a Varian Mercury-300BB (300/75 MHz) spectrometer. Chemical shifts are given in ppm (δ) relative to tetramethylsilane as an internal standard (^{1}H NMR) or the NMR solvent (^{13}C NMR). Coupling constants are given in Hertz (Hz). Weak signals in ^{13}C NMR are indicated as (w). LC-MS analyses were carried out on a Waters AutoPurification System equipped with PDA and ESI-MS detection and using a Waters CORTECS C18 Column (4.6×100 mm, 2.7µm) and a water/acetonitrile/formic acid linear gradient system at a flow rate of 1.44 $mLmin^{-1}$.

General procedure 1: Copper mediated azide-alkyne cycloaddition.

To a solution of the intermediate azide (1.0 eq.) in dimethylformamide (0.1 M) was added the alkyne (1.5 eq.), sodium ascorbate (1.0 eq., 0.5 M), $CuSO_4$ (0.2 eq., 0.05 M), triethylamine (3.0 eq.) and a catalytic amount of tris[(1-benzyl-1,2,3-triazol-4-yl)methyl]amine. The reaction mixture was stirred overnight at room temperature in the dark under an argon atmosphere. The solvent was evaporated under reduced pressure and the residue was redissolved in water and extracted with CH_2Cl_2. Then combined organic fractions were pooled, washed with brine and dried over Na_2SO_4. The crude compound was purified by silica gel chromatography ($NH_4OH/MeOH/CH_2Cl_2$, 1:5:94 v/v/v) to give the final compound as a white solid.

N-(17-(4-(4-(5,5-difluoro-1,3,7,9-tetramethyl-5H-4λ^4,5λ^4-dipyrrolo[1,2-c:2',1'-f][1,3,2]diazaborinin-10-yl)butyl)-1H-1,2,3-triazol-1-yl)-3,6,9,12,15-pentaoxaheptadecyl)-2-((5-((2-methylthiazol-4-yl)ethynyl)pyridin-3-yl)oxy)acetamide (**5.01**)

Compound **5.01** was subjected to general procedure 1. Brown semi-solid, 42%.

LC-HRMS: t_R=6.77 min (10–100% MeCN, 15 min run), purity 92.98 %.

HRMS (ESI) m/z: calculated for $C_{44}H_{59}BF_2N_8O_7S$ $[M+2H]^{2+}$ 446.2138; found 446.2120. Calculated for $C_{44}H_{58}BFN_8O_7S$ $[M-F+H]^{2+}$ 436.2113; found 436.2084. Calculated for $C_{44}H_{58}BF_2N_8O_7S$ $[M+H]^+$ 891.4204; found 891.4258.

5,5-difluoro-1,3,7,9-tetramethyl-10-(4-(1-(1-(3-((2-methylthiazol-4-yl)ethynyl)phenoxy)-2-oxo-6,9,12-trioxa-3-azatetradecan-14-yl)-1H-1,2,3-triazol-4-yl)butyl)-5H-4λ^4-dipyrrolo[1,2-c:2',1'-f][1,3,2]diazaborinin-5-uide (**5.02**)

Compound **5.02** was subjected to general procedure 1. Brown semi-solid, 48%.

LC-HRMS: t_R=7.92 min (10–100% MeCN, 15 min run), purity 95.49 %.

HRMS (ESI) m/z: calculated for $C_{41}H_{51}BF_2N_7O_5S$ $[M+H]^+$ 802.3733; found 802.3759.

N-(17-(4-(4-(5,5-difluoro-3,7-bis(4-methoxyphenyl)-5H-4λ^4,5λ^4-dipyrrolo[1,2-c:2',1'-f][1,3,2]diazaborinin-10-yl)butyl)-1H-1,2,3-triazol-1-yl)-3,6,9,12,15-pentaoxaheptadecyl)-2-((5-((2-methylthiazol-4-yl)ethynyl)pyridin-3-yl)oxy)acetamide (**5.03**)

Compound **5.03** was subjected to general procedure 1. Blue solid, 48%.

LC-HRMS: t_R=7.99 min (10–100% MeCN, 15 min run), purity 95.44 %.

HRMS (ESI) m/z: calculated for $C_{54}H_{63}BF_2N_8O_9S$ $[M+2H]^{2+}$ 524.2244; found 524.2223. Calculated for $C_{54}H_{62}BFN_8O_9S$ $[M-F+H]^{2+}$ 514.2219; found 514.2209.

N-(2-(2-(2-(2-(4-(4-(5,5-difluoro-3,7-bis(4-methoxyphenyl)-5H-4λ^4,5λ^4-dipyrrolo[1,2-c:2',1'-f][1,3,2]diazaborinin-10-yl)butyl)-1H-1,2,3-triazol-1-yl)ethoxy)ethoxy)ethoxy)ethyl)-2-(3-((2-methylthiazol-4-yl)ethynyl)phenoxy)acetamide (**5.04**)

Compound **5.04** was subjected to general procedure 1. Blue solid, 52%.

LC-HRMS: t_R=7.62 min (10–100% MeCN, 15 min run), purity 96.84 %.

HRMS (ESI) m/z: calculated for $C_{51}H_{56}BF_2N_7O_7S$ $[M+2H]^{2+}$ 479.7006; found 479.6974. Calculated for $C_{51}H_{55}BF_2N_7O_7S$ $[M+H]^+$ 958.3939; found 958.3953.

N-(5-((12-(4-(4-(5,5-difluoro-1,3,7,9-tetramethyl-5H-4λ^4,5λ^4-dipyrrolo[1,2-c:2',1'-f][1,3,2]diazaborinin-10-yl)butyl)-1H-1,2,3-triazol-1-yl)dodecyl)(methyl)amino)pentyl)-2-(3-((2-methylthiazol-4-yl)ethynyl)phenoxy)acetamide (**5.05**)

Compound **5.05** was subjected to general procedure 1. Brown semi-solid, 41%.

LC-HRMS: t_R=6.79 min (10–100% MeCN, 15 min run), purity 97.85 %.

HRMS (ESI) m/z: calculated for $C_{51}H_{73}BF_2N_8O_2S$ $[M+2H]^{2+}$ 455.2813; found 455.2817. Calculated for $C_{51}H_{72}BFN_8O_2S$ $[M-F+H]^{2+}$ 445.2788; found 445.2754. Calculated for $C_{51}H_{72}BF_2N_8O_2S$ $[M+H]^+$ 909.5560; found 909.5597.

5,5-difluoro-1,3,7,9-tetramethyl-10-(4-(1-(12-(methyl(5-(2-((5-((2-methylthiazol-4-yl)ethynyl)pyridin-3-yl)oxy)acetamido)pentyl)amino)dodecyl)-1H-1,2,3-triazol-4-yl)butyl)-5H-5λ^4-dipyrrolo[1,2-c:2',1'-f][1,3,2]diazaborinin-4-ium (**5.06**)

Compound **5.06** was subjected to general procedure 1. Brown semi-solid, 39%.

LC-HRMS: t_R=6.14 min (10–100% MeCN, 15 min run), purity 90.67 %.

HRMS (ESI) m/z: calculated for $C_{50}H_{72}BF_2N_9O_2S$ $[M+2H]^{2+}$ 455.7787; found 455.7772. Calculated for $C_{50}H_{71}BFN_9O_2S$ $[M-F+H]^{2+}$ 445.7764; found 445.7726. Calculated for $C_{50}H_{71}BF_2N_9O_2S$ $[M+H]^+$ 910.5501; found 910.5561.

N-(5-((8-(4-(4-(5,5-difluoro-1,3,7,9-tetramethyl-5H-4λ^4,5λ^4-dipyrrolo[1,2-c:2',1'-f][1,3,2]diazaborinin-10-yl)butyl)-1H-1,2,3-triazol-1-yl)octyl)(methyl)amino)pentyl)-2-((5-((2-methylthiazol-4-yl)ethynyl)pyridin-3-yl)oxy)acetamide (**5.07**)

Compound **5.07** was subjected to general procedure 1. Brown semi-solid, 36%.

LC-HRMS: t_R=4.71 min (10–100% MeCN, 15 min run), purity 88.11%.

HRMS (ESI) m/z: calculated for $C_{46}H_{64}BF_2N_9O_2S$ $[M+2H]^{2+}$ 427.7476; found 427.7487. Calculated for $C_{46}H_{63}BFN_9O_2S$ $[M-F+H]^{2+}$ 417.7451; found 417.7420. Calculated for $C_{46}H_{63}BF_2N_9O_2S$ $[M+H]^+$ 854.4880; found 854.4893.

N-(5-((12-(4-(4-(5,5-difluoro-3,7-bis(4-methoxyphenyl)-5H-4λ^4,5λ^4-dipyrrolo[1,2-c:2',1'-f][1,3,2]diazaborinin-10-yl)butyl)-1H-1,2,3-triazol-1-yl)dodecyl)(methyl)amino)pentyl)-2-(3-((2-methylthiazol-4-yl)ethynyl)phenoxy)acetamide (**5.08**)

Compound **5.08** was subjected to general procedure 1. Blue solid, 46%.

LC-HRMS: t_R=9.53 min (10–100% MeCN, 15 min run), purity 85.42 %.

HRMS (ESI) m/z: calculated for $C_{61}H_{77}BF_2N_8O_4S$ $[M+2H]^{2+}$ 533.2919; found 533.2914. Calculated for $C_{61}H_{76}BFN_8O_4S$ $[M-F+H]^{2+}$ 523.2893; found 523.2885.

N-(5-((12-(4-(4-(5,5-difluoro-3,7-bis(4-methoxyphenyl)-5H-4λ^4,5λ^4-dipyrrolo[1,2-c:2',1'-f][1,3,2]diazaborinin-10-yl)butyl)-1H-1,2,3-triazol-1-yl)dodecyl)(methyl)amino)pentyl)-2-((5-((2-methylthiazol-4-yl)ethynyl)pyridin-3-yl)oxy)acetamide (**5.09**)

Compound **5.09** was subjected to general procedure 1. Blue solid, 39%.

LC-HRMS: t_R=6.86 min (10–100% MeCN, 15 min run), purity 90.79 %.

HRMS (ESI) m/z: calculated for $C_{60}H_{76}BF_2N_9O_4S$ $[M+2H]^{2+}$ 533.7895; found 533.7896. Calculated for $C_{60}H_{75}BFN_9O_4S$ $[M-F+H]^{2+}$ 523.7870; found 523.7874.

N-(5-((8-(4-(4-(5,5-difluoro-3,7-bis(4-methoxyphenyl)-5H-4λ^4,5λ^4-dipyrrolo[1,2-c:2',1'-f][1,3,2]diazaborinin-10-yl)butyl)-1H-1,2,3-triazol-1-yl)octyl)(methyl)amino)pentyl)-2-((5-((2-methylthiazol-4-yl)ethynyl)pyridin-3-yl)oxy)acetamide (**5.10**)

Compound **5.10** was subjected to general procedure 1. Blue solid, 37%.

LC-HRMS: t_R=5.93 min (10–100% MeCN, 15 min run), purity 82.47 %.

HRMS (ESI) m/z: calculated for $C_{56}H_{68}BF_2N_9O_4S$ $[M+2H]^{2+}$ 505.7582; found 505.7570. Calculated for $C_{56}H_{67}BFN_9O_4S$ $[M-F+H]^{2+}$ 495.7557; found 495.7557.

N-(6-(4-(4-(5,5-difluoro-1,3,7,9-tetramethyl-5H-4λ^4,5λ^4-dipyrrolo[1,2-c:2',1'-f][1,3,2]diazaborinin-10-yl)butyl)-1H-1,2,3-triazol-1-yl)hexyl)-2-((5-((2-methylthiazol-4-yl)ethynyl)pyridin-3-yl)oxy)acetamide (**5.11**)

Compound **5.11** was subjected to general procedure 1. Brown semi-solid, 41%.

LC-HRMS: t_R=6.08 min (10–100% MeCN, 15 min run), purity 98.75 %.

HRMS (ESI) m/z: calculated for $C_{38}H_{46}BFN_8O_2S$ $[M-F+H]^{2+}$ 354.1796; found 354.1721. Calculated for $C_{38}H_{46}BF_2N_8O_2S$ $[M+H]^+$ 727.3519; found 727.3538.

N-(6-(4-(4-(5,5-difluoro-3,7-bis(4-methoxyphenyl)-5H-4λ^4,5λ^4-dipyrrolo[1,2-c:2',1'-f][1,3,2]diazaborinin-10-yl)butyl)-1H-1,2,3-triazol-1-yl)hexyl)-2-((5-((2-methylthiazol-4-yl)ethynyl)pyridin-3-yl)oxy)acetamide (**5.12**)

Compound **5.12** was subjected to general procedure 1. Blue solid, 45%.

LC-HRMS: t_R= 7.32 min (10–100% MeCN, 15 min run), purity 81.53 %.

HRMS (ESI) m/z: calculated for $C_{48}H_{51}BF_2N_8O_4S$ $[M+2H]^{2+}$ 442.1902; found 442.1881. Calculated for $C_{48}H_{50}BF_2N_8O_4S$ $[M+H]^+$ 883.3731; found 883.3779.

V.6.2 Spectra

The fluorescent ligands were re-suspended in DMSO, to a final concentration of 20 mM. Next, a working solution of 10 µM was prepared and dispensed (100 µL) into a 96-wells plate. The protocols for excitation and emission spectra were selected in the CLARIOstar plate reader (BMG Labtech, Durham, NC, USA).

V.6.3 Relative emission

The relative emission of the different ligands was assessed by exciting the fluorophores at the wavelength corresponding to the excitation peak. Accordingly, a working solution of 10 µM was prepared and dispensed (100 µL) into a 96-wells plate. Then, BODIPY green compounds were excited at 480-10 nm and emission read at 560-20 nm; while BODIPY red compounds were excited at 550-10 nm and emission read at 650-20 nm, using the CLARIOstar plate reader (BMG Labtech).

V.6.4 Single binding NanoBRET assay

The NanoBRET assay was performed on transfected ($mGlu_5R^{NL}$) HEK 293T cells. In brief, cells were re-suspended in HBSS, and seeded into poli-ornitine coated white 96-well plates. After 24 hours, cells were challenged with the fluorescent ligands and the plate returned to 37°C for 1 h. Finally, *h*-Coelenterazine (Life Technologies Corp) was added at a final concentration of 5 µM, and readings were performed after 5 min using a CLARIOstar plate reader (BMG Labtech). The donor and acceptor emission was measured at 490-10 nm and 560-80 for the BODIPY green compounds and 650-80 nm for the BODIPY red compounds, respectively. The raw NanoBRET ratio was calculated by dividing the 560 nm or 650 nm emission by the 490 nm emission. Results were expressed as a percentage of the maximum signal obtained (mBU; miniBRET Units).

V.6.5 Saturation binding NanoBRET assay

The NanoBRET assay was performed on transfected ($mGlu_5R^{NL}$) HEK 293T cells. In brief, cells were re-suspended in HBSS, and seeded into poli-ornitine coated white 96-well plates. After 24 hours, cells were challenged with/without the non-labelled $mGlu_5R$ selective allosteric antagonist (MTEP) and incubated for 1 h at 37°C. Subsequently, the increasing concentrations of the fluorescent ligands (**5.03** and **5.10**) were added and the plate returned to 37°C for 1 h. Finally, *h*-Coelenterazine (Life Technologies Corp) was added at a final concentration of 5 μM, and readings were performed after 5 min using a CLARIOstar plate reader (BMG Labtech). The donor and acceptor emission was measured at 490-10 nm and 650-80 nm, respectively. The raw NanoBRET ratio was calculated by dividing the 650 nm emission by the 490 nm emission. Results were expressed as a percentage of the maximum signal obtained (mBU; miliBRET Units).

References

[1] Bräuner-Osborne, H.; Egebjerg, J.; Nielsen, E. O.; Madsen, U.; Krogsgaard-Larsen, P. Ligands for glutamate receptors: design and therapeutic prospects. *J. Med. Chem.* **2000**, *43*, 2609-2645.

[2] Roppe, J. R.; Wang, B.; Huang, D.; Tehrani, L.; Kamenecka, T.; Schweiger, E. J.; Anderson, J. J.; Brodkin, J.; Jiang, X.; Cramer, M.; Chung, J.; Reyes-Manalo, G.; Munoz, B.; Cosford, N. D. 5-[(2-Methyl-1,3-thiazol-4-yl)ethynyl]-2,3'-bipyridine: a highly potent, orally active metabotropic glutamate subtype 5 (mGlu5) receptor antagonist with anxiolytic activity. *Bioorg. Med. Chem. Lett.* **2004**, *14*, 3993-3996.

[3] Pin, J. P.; Acher, F. The metabotropic glutamate receptors: structure, activation mechanism and pharmacology. *Curr. Drug Targets CNS Neurol. Disord.* **2002**, *1*, 297-317.

[4] Conn, P. J.; Pin, J. P. Pharmacology and functions of metabotropic glutamate receptors. *Annu. Rev. Pharmacol. Toxicol.* **1997**, *37*, 205-237.

[5] Cosford, N. D.; Tehrani, L.; Roppe, J.; Schweiger, E.; Smith, N. D.; Anderson, J.; Bristow, L.; Brodkin, J.; Jiang, X.; McDonald, I.; Rao, S.; Washburn, M.; Varney, M. A. 3-[(2-Methyl-1,3-thiazol-4-yl)ethynyl]-pyridine: a potent and highly selective metabotropic glutamate subtype 5 receptor antagonist with anxiolytic activity. *J. Med. Chem.* **2003**, *46*, 204-206.

[6] Ciruela, F.; Jacobson, K. A.; Fernández-Dueñas, V. Portraying G Protein-Coupled Receptors with Fluorescent Ligands. *ACS Chem. Biol.* **2014**, *9*, 1918−1928.

[7] Verdoes, M.; Hillaert, U.; Florea, B. I.; Sae-Heng, M.; Risseeuw, M. D.; Filippov, D. V.; van der Marel, G. A.; Overkleeft, H. S. Acetylene functionalized BODIPY dyes and their application in the synthesis of activity based proteasome probes. *Bioorg. Med. Chem. Lett.* **2007**, *17*, 6169-6171.

[8] Machleidt, T.; Woodroofe, C. C.; Schwinn, M. K.; Méndez, J.; Robers, M. B.; Zimmerman, K.; Otto, P.; Daniels, D. L.; Kirkland, T. A.; Wood, K. V. NanoBRET--A Novel BRET Platform for the Analysis of Protein-Protein Interactions. *ACS Chem. Biol.* **2015**, *10*, 1797-1804.

V.7. Supporting Information

V.7. 1. Generation of a mGlu$_5$ receptor NanoLuc

Figure 1 clearly shows a protein concentration-dependent expression of mGluR5^{NL} in HEK 293T cells.

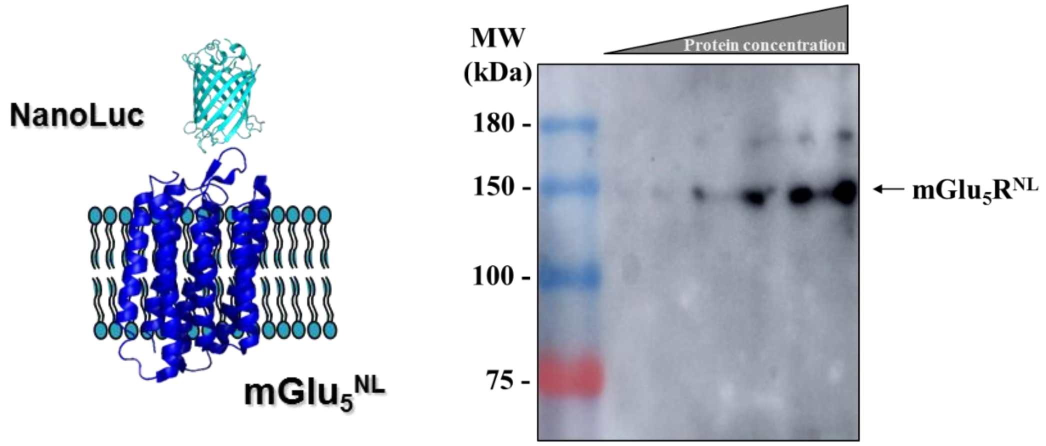

Figure 1. Expression of the mGluR$_5^{NL}$ construct in HEK293T cells.

Gel electrophoresis and immunoblotting

Total membrane extracts from transiently transfected HEK-293T cell were prepared as previously described.[1],[2] Protein concentration was determined using the BCA protein assay kit (Thermo Fisher Scientific, Inc., Rockford, IL, USA).

Extracts were analyzed by sodium dodecyl sulfate–polyacrylamide gel electrophoresis (SDS/PAGE) using 7% polyacrylamide gels. Separated proteins were transferred to polyvinylidene difluoride (PVDF) membranes using a semi-dry transfer system (Bio-Rad, Hercules, CA, USA), immunoblotted with the indicated antibody and then with the horseradish peroxidase (HRP)-conjugated corresponding secondary antibody. The immunoreactive bands were developed using a chemiluminescent detection kit (Thermo Fisher Scientific, Waltham, MA, USA) and detected with an Amersham Imager 600 (GE Healthcare Europe GmbH, Barcelona, Spain).[3]

V.7. 2. Chromatographic analyses

LC-MS analyses were carried out on a Waters Alliance 2695 XE separation Module by using a Phenomenex Kinetex EVO C18, 5μm 100x2.1mm and a gradient system of HCOOH in H_2O (0.1 %, v/v)/HCOOH in MeCN (0.1%, v/v) at a flow rate of 0.6 $mLmin^{-1}$, 100:0 to 0:100 (0 to 100 % MeCN) in 15 minutes. High-resolution spectra were recorded on a Waters LCT Premier XE Mass spectrometer and a 2996 Photodiode Array Detector, range 220 nm-400 nm.

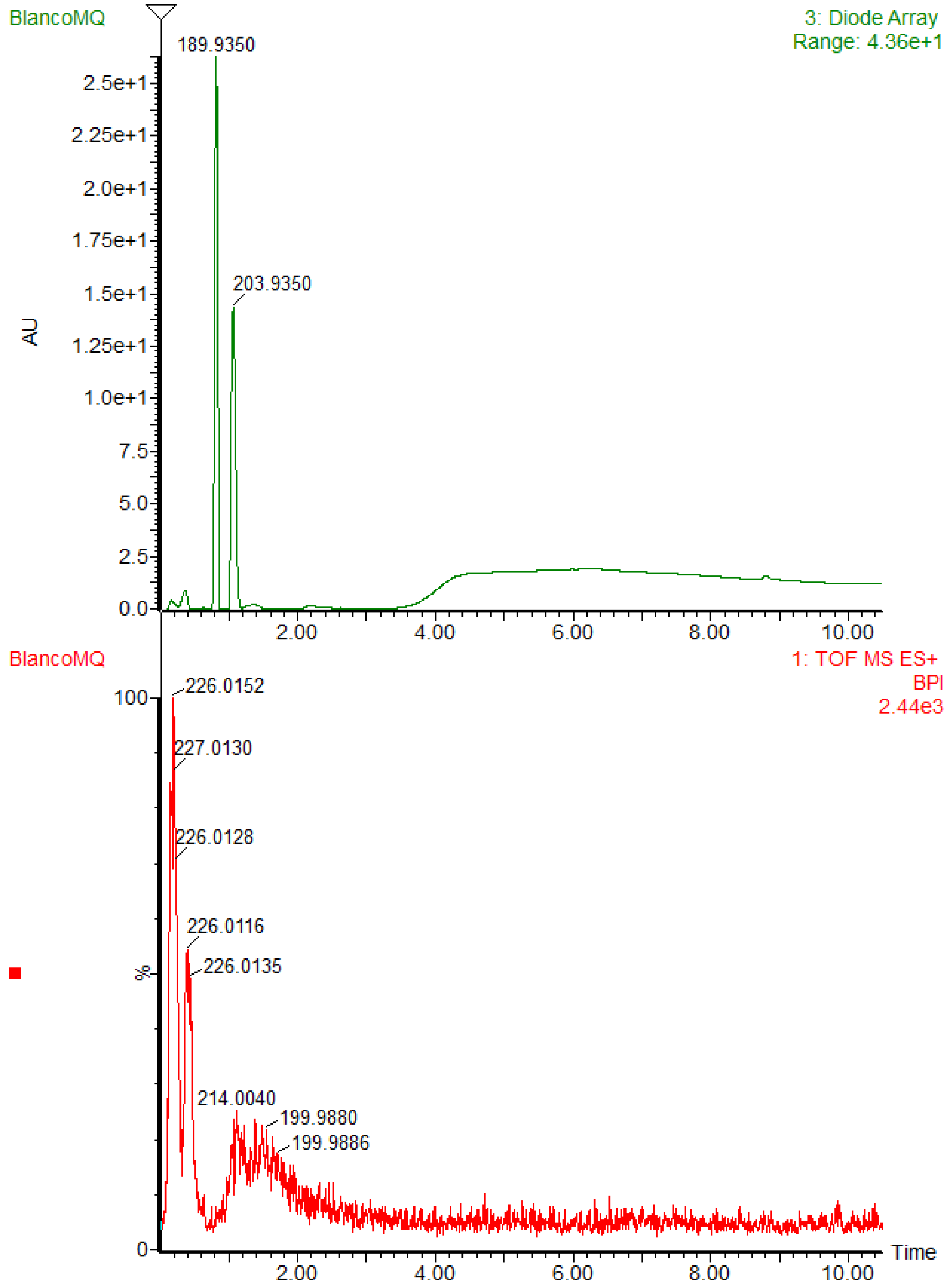
BlancoMQ
3: Diode Array
Range: 4.36e+1
189.9350
203.9350
AU
2.5e+1
2.25e+1
2.0e+1
1.75e+1
1.5e+1
1.25e+1
1.0e+1
7.5
5.0
2.5
0.0
2.00
4.00
6.00
8.00
10.00
BlancoMQ
1: TOF MS ES+
BPI
2.44e3
100
226.0152
227.0130
226.0128
226.0116
226.0135
%
214.0040
199.9880
199.9886
0
Time
2.00
4.00
6.00
8.00
10.00

Compound **5.02**

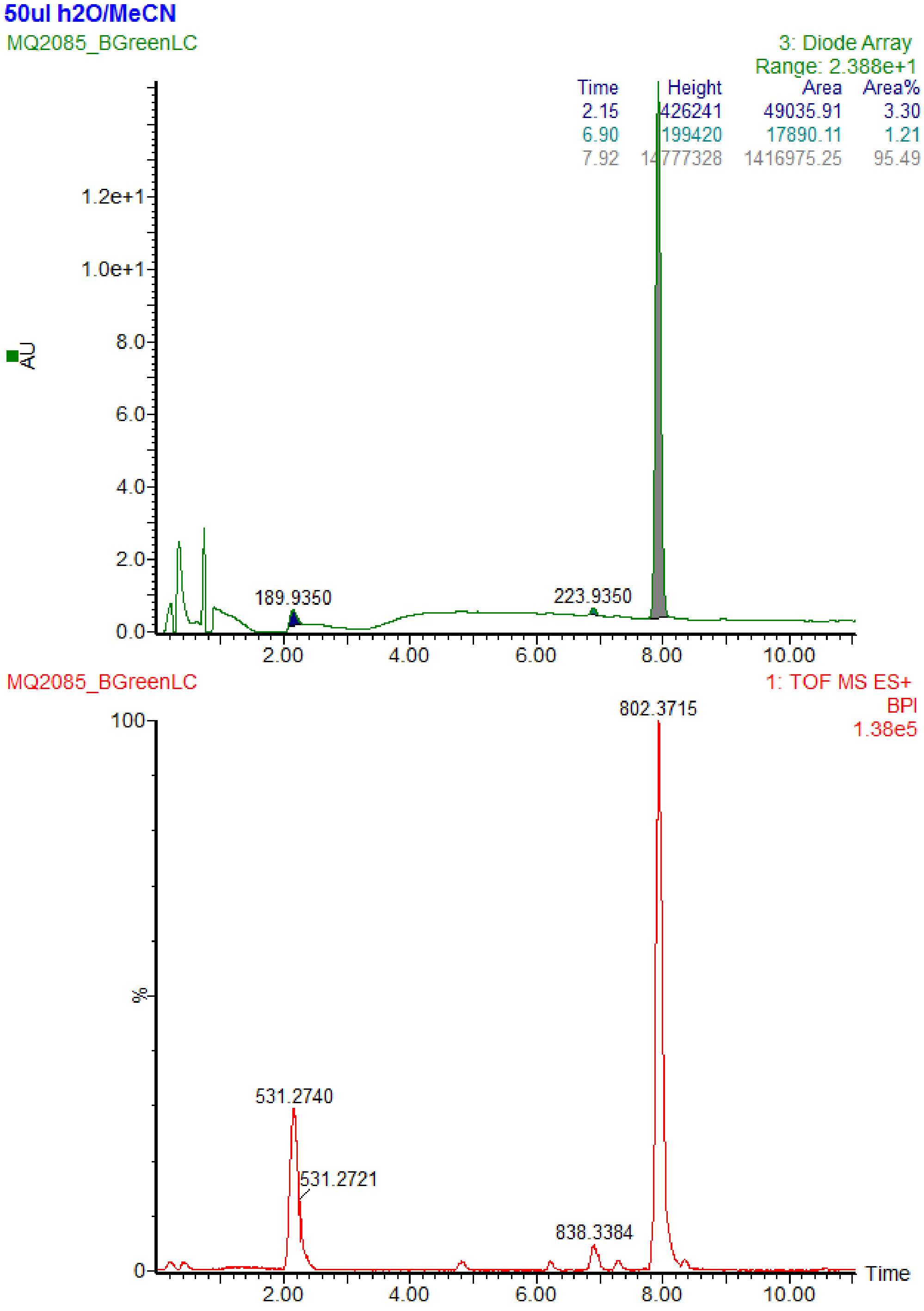

Time	Height	Area	Area%
2.15	426241	49035.91	3.30
6.90	199420	17890.11	1.21
7.92	14777328	1416975.25	95.49

Compound **5.03**

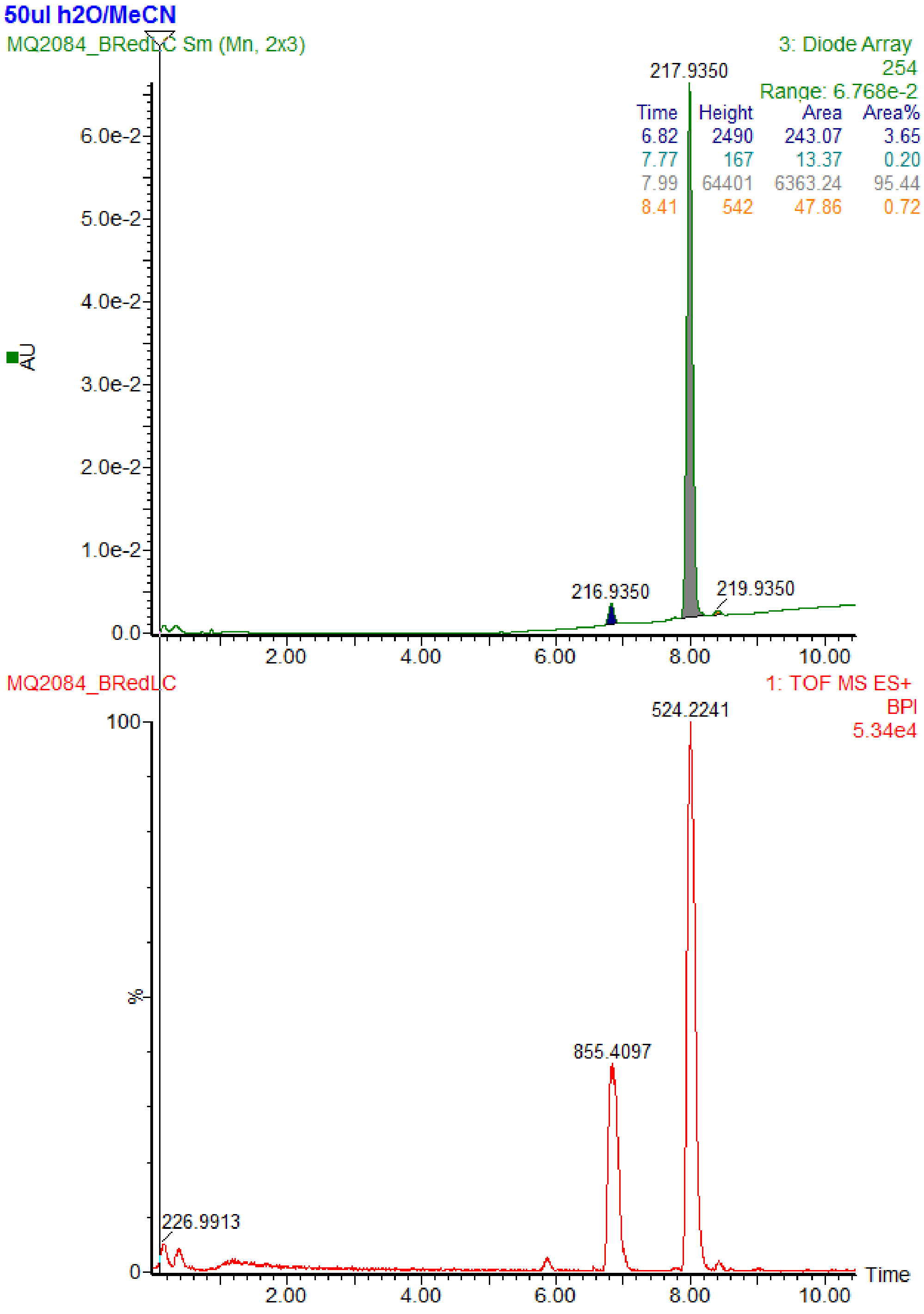

Compound **5.04**

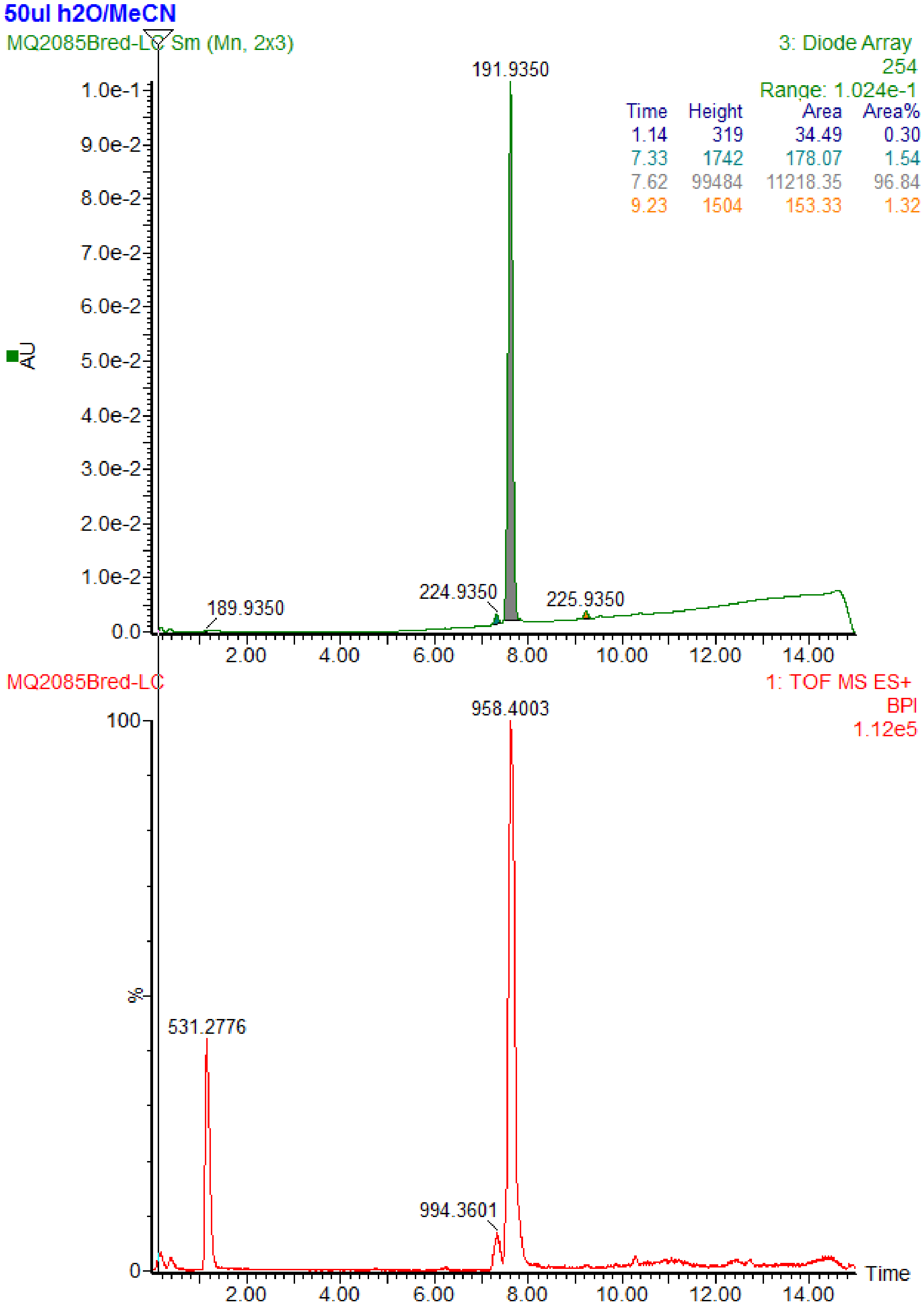

Time	Height	Area	Area%
1.14	319	34.49	0.30
7.33	1742	178.07	1.54
7.62	99484	11218.35	96.84
9.23	1504	153.33	1.32

Compound **5.05**

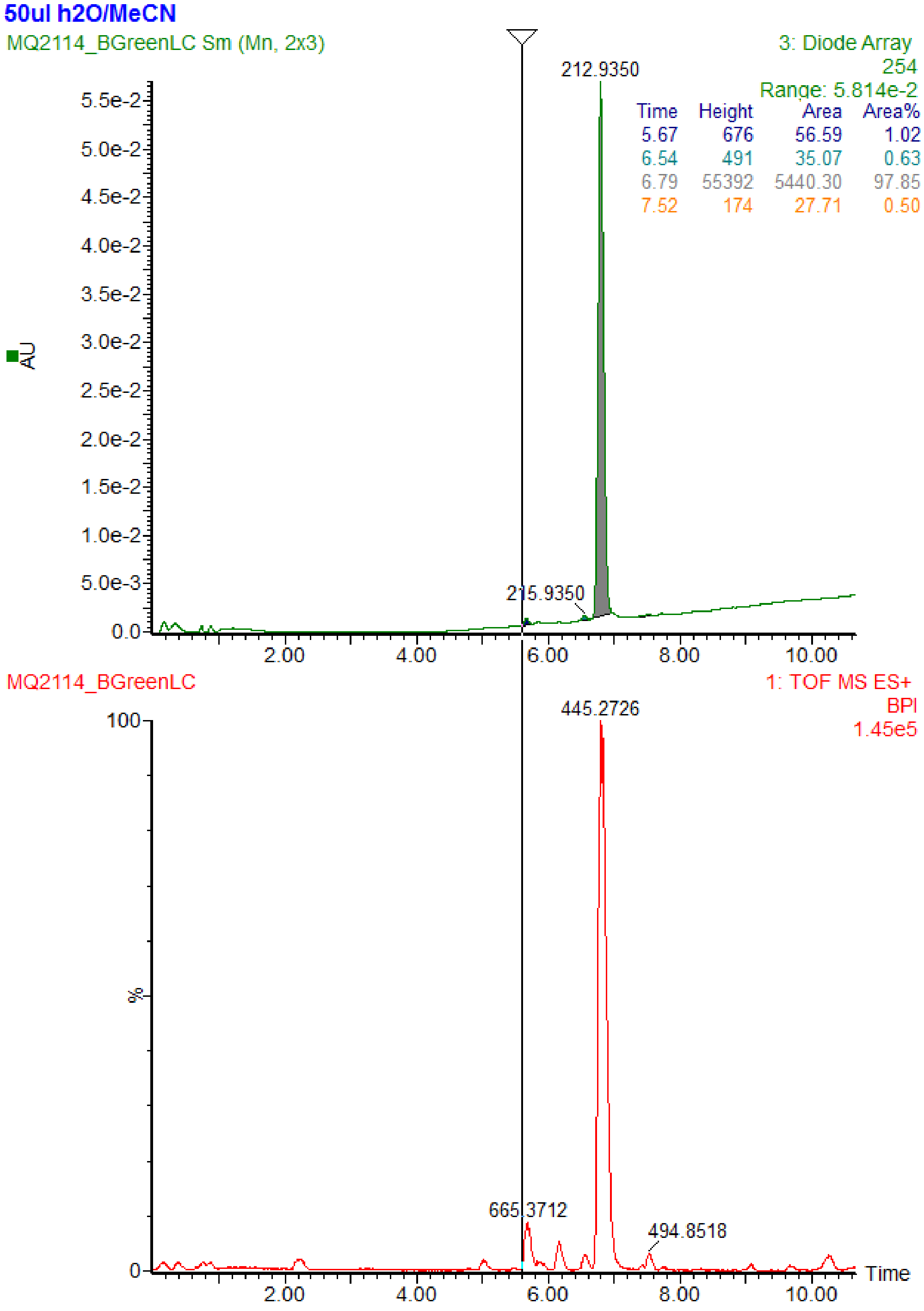

Time	Height	Area	Area%
5.67	676	56.59	1.02
6.54	491	35.07	0.63
6.79	55392	5440.30	97.85
7.52	174	27.71	0.50

Compound **5.11**

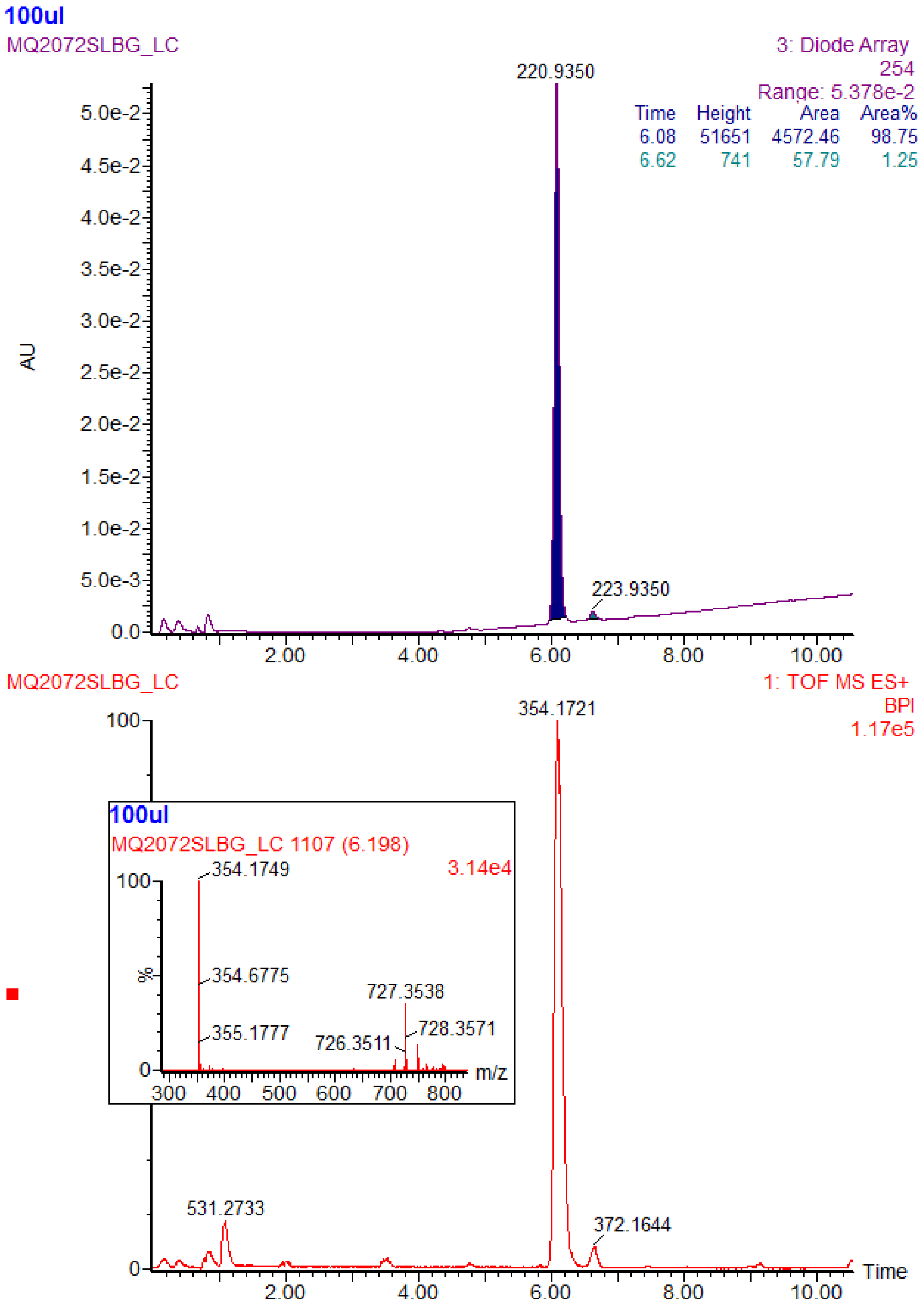

Reference

[1] Burgueno, J.; Blake, D. J.; Benson, M. A.; Tinsley, C. L.; Esapa, C. T.; Canela, E. I; Penela, P.; Mallol, J.; Mayor, F. Jr.; Lluis, C.; Franco, R.; Ciruela, F. The adenosine A2A receptor interacts with the actin-binding protein alpha-actinin. *J. Biol Chem.* **2003**, *278*, 37545–37552.

[2] Morató, X.; López-Cano, M.; Canas, P. M.; Cunha, R. A.; Ciruela, F. Brain membrane fractionation: An ex vivo approach to assess subsynaptic protein localization. *J. Vis. Exp.* **2017**; doi: 10.3791/55661.

[3] Morató, X.; Borroto-Escuela, D. O.; Fuxe, K.; Fernández-Dueñas, V.; Ciruela, F. Co-immunoprecipitation from brain. *Neuromethods*. **2016**, *110*, 19–30.

CHAPTER VI

General conclusion

VI. GENERAL CONCLUSION

Firstly, we designed and synthesized a series of novel heterobivalent ligands based on the chemical structure of two distinct D_2-likeR ligands and a µOR agonist, as well as a µOR antagonist. The ketone group from HM and NTX was converted to the corresponding 6'-*R*-amino derivatives **3.02a** and **3.02b** to allow coupling with the linker via an amide bond. As D_2-likeR ligands we used the antagonist 1,4-DAP and agonist 5-OH-DPAT that were equipped with an appropriate alkyne, which allowed facile connection to the azido group on the PEG linker via a copper-catalyzed azide–alkyne cycloaddition (CuAAC) reaction. The dimeric D_2-likeR-µOR ligands were constructed around PEG spacers of variable length that were equipped with a carboxylic acid on one and an azide on the other end (Figure 1). The use of PEG linkers precludes cumulative incremental increases in hydrophobicity that would occur upon homologation if an alkyl chain were employed. The choice of the position and nature of the attachment points for linking the two pharmacophore units to the spacer relied on two criteria: the feasibility of the chemical modification and the compatibility of the modification with the biological activity of the pharmacophore.

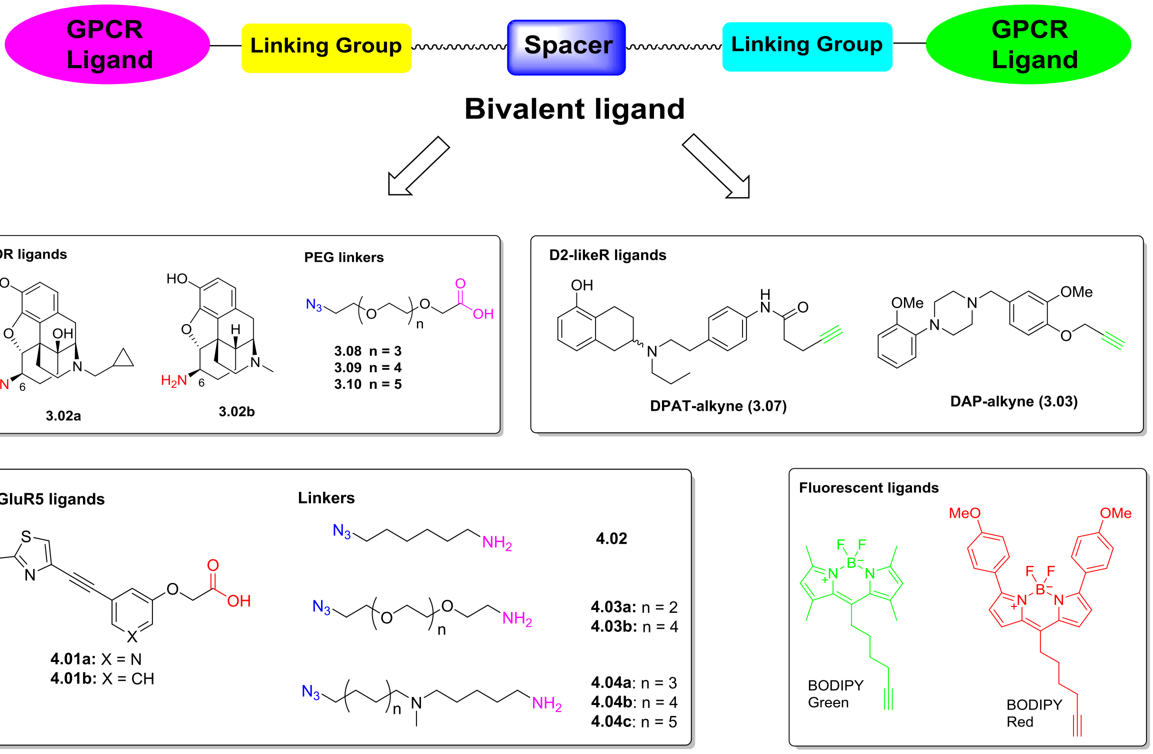
GPCR Ligand
Linking Group
Spacer
Linking Group
GPCR Ligand
Bivalent ligand
µOR ligands
3.02a
3.02b
PEG linkers
3.08 n = 3
3.09 n = 4
3.10 n = 5
D2-likeR ligands
DPAT-alkyne (3.07)
DAP-alkyne (3.03)
mGluR5 ligands
4.01a: X = N
4.01b: X = CH
Linkers
4.02
4.03a: n = 2
4.03b: n = 4
4.04a: n = 3
4.04b: n = 4
4.04c: n = 5
Fluorescent ligands
BODIPY Green
BODIPY Red

Figure 1. Schematic overview of strategies, monovalent ligands and spacers with appropriate ligation handles.

Ligation of µOR ligands did not perturb the affinity for µOR. µOR bivalent ligands derived from the HM agonist are still capable of activating the µOR signaling pathway as demonstrated by β-arrestin2 recruitment. Furthermore, bivalent ligand **3.12d** containing the shortest linker (18-atom) showed excellent potency and high efficacy both in β-arrestin2 recruitment for µOR and MAPK-P for D_4R. On the other hand, ligation of D_2-likeR ligands negatively influenced the affinity for D_2R and D_4R in a competition experiment with [^{3}H]spiperone. However, a biphasic competition-binding curve was observed for **3.12d** to D_4R-µOR, which indicates a bivalent binding mode. Hence, compound **3.12d** could bridge the D_4R-µOR heterodimer.

Unexpectedly, we were unable to identify bivalent ligands that show a biphasic binding mode or a significant increase in affinity for cells expressing both the D_2R and the µOR, compared to cells that only express D_2R. This indicates that none of the bivalent ligands is capable of binding both receptors simultaneously, possibly owing to a suboptimal length or nature of the selected linkers, which, however, were based on the spacers of class A GPCR bivalent ligands. On the other hand it cannot be excluded that subtle differences such as differences in the dissociation rate of the ligands remain undetected by comparing equilibrium dissociation constants. In a study investigating adenosine A_3 receptors, it was found that ligand binding kinetics is found to be influenced in membrane microdomains as a consequence of receptor dimerization.

While future studies may try to address these shortcomings, the current study already gives access to the monomeric ligands that are equipped with appropriate ligation handles to construct second-generation bivalent ligands with alternative spacers. In conclusion, the present results provide useful insights into development of new bivalent ligands as tools to investigate the µOR-D_4R heterodimer.

In order to overcome the above shortcomings, we have designed and synthesized twenty four potential heterobivalent ligands of D_2-likeR and mGluR5 using three different types of linkers, as described in Chapter IV. As depicted in Figure 1, bivalent ligands were derived from the selective and potent noncompetitive mGluR5 antagonist 3-[(2-methyl-4-thiazolyl)ethynyl]pyridine (MTEP). As D_2-likeR ligands we used the previously synthesized antagonist 1,4-DAP and the agonist 5-OH-DPAT with an alkyne ligation handle. Bivalent ligands were built with three different types of spacers of variable length (PEG, polyalkyl and tertiary amine liners) with a primary amine on one and an azide on the other end (Figure 1).

Ligation of D_2-likeR ligands showed that bivalent ligands with PEG (PEG_4 and PEG_6) and hexamethylene linkers exhibit relatively low affinity for D_4R, contrary to bivalent ligands with alkylamine spacers, while all can still activate the D_4R. Interestingly, we identified a bivalent ligand with a 20-atom alkylamine spacer (**4.20a**) that showed 4-fold affinity increase for the D_2R in cells expressing both the D_2R and the mGluR5, compared to cells only expressing D_2R, suggesting that **4.20a** could bridge the D_2R and mGluR5 receptors. On the other hand, ligation of mGluR5 ligands reveals that **4.20a** shows 5-fold higher affinity for D_2R-mGluR5 compared to its corresponding monovalent ligand **4.19a**, which further supports the bridging hypothesis. Furthermore, **4.20a** displays 4- and 7-fold higher potency compared to the monomeric compounds **3.07** and **4.19a** as determined in MAPK-P for D_2R-

mGluR5, respectively. Interestingly, **4.20a** inhibits the forskolin stimulated cAMP formation with a 4-fold higher potency compared to the monovalent agonist **3.07** in the coexpressing cells, indicating that the bivalent binding requires a lower receptor occupation to exert signaling.

Overall, the length and composition of the linker between the two receptor pharmacophores affected binding affinity and potency both at the D_2-likeR and the mGluR5. Compound **4.20a** could be a promising molecular probe to further investigate the protein-protein interaction of D_2-likeR and mGluR5.

To further study the ligand-receptor interaction, we synthesized twelve novel fluorescent mGluR5 ligands based on alkyne functionalized BODIPY fluorophores (Figure 1) that were used to fluorescently label an azido functionalized mGluR5 negative allosteric modulator in a chemoselective manner employing CuAAC reaction. The preliminary biological results indicate that all the fluorescent ligands are capable of binding to the mGluR5 via NanoBRET. Although the saturation assay needs to be optimized, the affinity of compound **5.03** to mGluR5 is modestly higher than that of **5.10**. Therefore, **5.03** could be a promising fluorescent ligand for the further study and an in-depth evaluation is still going on.

In summary, we successfully synthesized the bivalent ligands with different length and composition of spacers to bridge the D_4R-μOR and D_2R-mGluR5 heterodimers, respectively. Although radioligand binding assays indicate that we did not identify a bivalent ligand with an optimal spacer to bridge the D_2R-μOR dimer, all tested ligands could still activate or block the signaling pathway as determined in the MAPK-P assay and β-arrestin2 recruitment. In the article on the successful PEG-conjugated bivalent melanocortin ligands, the nature of the ligands (although also targeting class A GPCRs) themselves is also very hydrophilic (such as peptide). Maybe in our case, characterized by two relatively hydrophobic pharmacophores, the PEG-linker is less suitable.

CHAPTER VII

Broader international context, relevance & future perspectives

VII. BROADER INTERNATIONAL CONTEXT, RELEVANCE, AND FUTURE PERSPECTIVES

VII.1. Marketed small-molecule drugs targeting GPCRs

Rhodopsin-like G protein-coupled receptors (12%), ion channels (19%), protein kinases (10%) and nuclear hormone receptors (3%) account for almost half of all human protein drug targets (Figure 1a). Due to the variable number of approved drugs per target family, these privileged target families are responsible for the therapeutic effect of 70% of small-molecule drugs, while 33% of small-molecule drugs modulate GPCRs.[1]

The highly biased distribution in successfully ‘drugged’ protein families is reflected in the biased distribution of bioactivity data in the ChEMBL database when considered at the target class level (Figure 1b). Figure 1b demonstrates that the discovery-phase investment in rhodopsin-like GPCRs has paid off so far, with the proportion of approved drugs being slightly higher than that of compounds in ChEMBL targeting this family.[1]

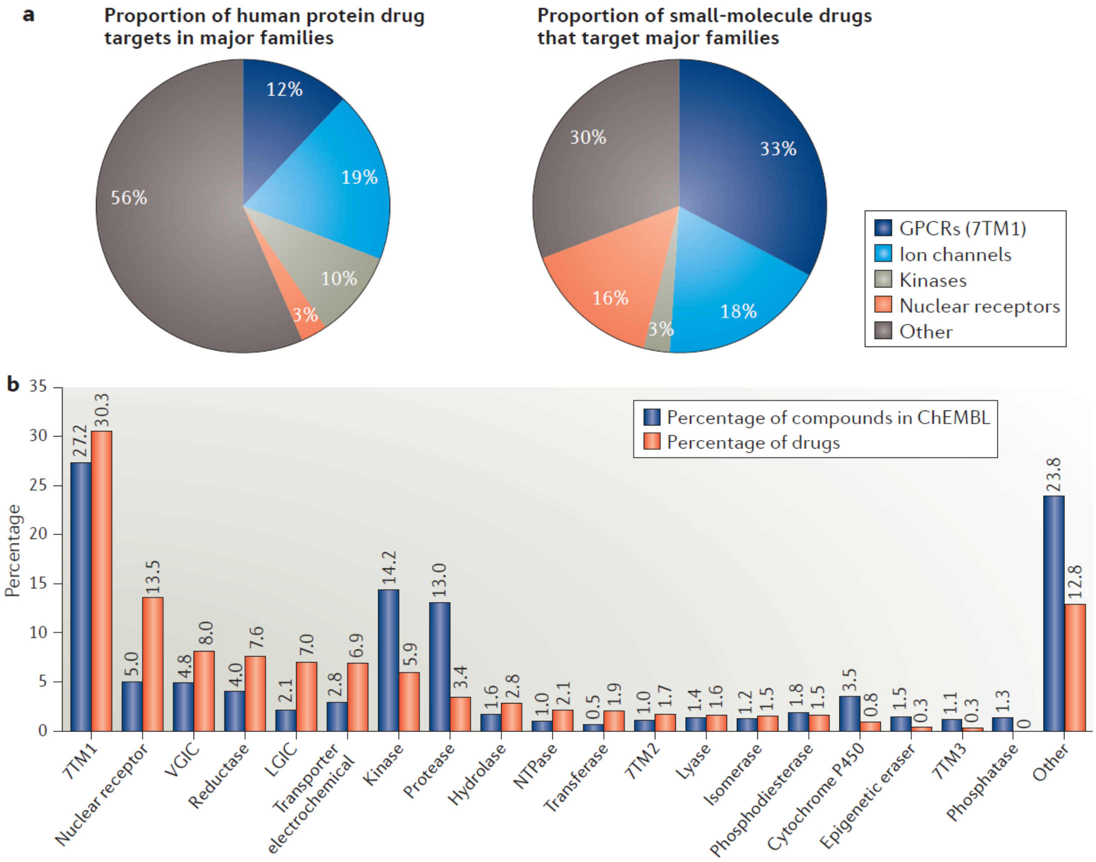

Figure 1. Major protein families as drug targets.[1] **a.** Distribution of human drug targets by gene family (left pie chart) and distribution by the fraction of drugs targeting those families (right pie chart). **b.** Clinical success of

privileged protein family classes. Distribution of non-approved compounds in ChEMBL 20 (extracted from the medicinal chemistry literature, with bioactivity tested against human protein targets) per family class, and distribution of approved drugs (small molecules and biologics) per human protein family class. 7TM, seven transmembrane family; GPCR, G protein-coupled receptor; LGIC, ligand-gated ion channel; NTPase, nucleoside triphosphatase; VGIC, voltage-gated ion channel.

VII.2. Bivalent ligands: tools par excellence to study receptor dimers

GPCRs are a remarkably multifaceted family of transmembrane proteins that exert a variety of physiological effects. Although family A GPCRs are able to operate as monomers, there is increasing evidence that dimerization (or oligomerization) represents a fundamental aspect of GPCR function, trafficking and pharmacology. Hence, it has been suggested that GPCR dimers may represent crucial new molecular targets for bivalent and/or dimer-selective ligands. Bivalent GPCR ligands are single chemical entities designed to selectively interact with binding sites of two separate GPCRs. The increased interest for targetting GPCR dimers with bivalent ligands stems from the superior potency and safety profiles one may achieve as compared with single target agents. Hitherto, bivalent ligands have been utilized mainly as pharmacological tools to investigate GPCR dimerization in vitro and in vivo as discussed in Chapter I.2.[2][11]

Gmeiner et al.[103] reported bivalent 1,4-DAP and/or aminoindane ligands with various types of spacers, including PEG, polyalkyl and ferrocene spacers, targeting dopamine receptors.[2-5] Bivalent ligands with an optimal spacer displayed higher Hill slopes than the monomeric ligand **1.20** for the human D_{2short} receptor (see Chapter I Figure 26).

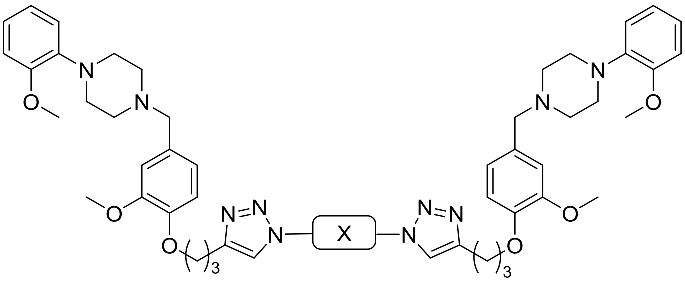

1.21a: X = $(CH_2)_8$, $n_H = 2.0$;
7.01: X = $CH_2(CH_2OCH_2)_2CH_2$, $n_H = 1.0$

Figure 2. Bivalent D_2R ligands with different kinds of linkers.[5]

As described in chapter I, Portoghese et al.[6][12] synthesized homo- and hetero-bivalent ligands of opioid receptors that exhibited in vitro and in vivo properties that differ from those of the corresponding monovalent ligands. Their pioneering work demonstrated that spinal administration of bivalent ligands capable of bridging the GPCR dimers, may lead to superior drug candidates for the treatment of chronic, intractable pain.

While successful bivalent ligands have been constructed targeting dopamine or opioid receptor dimers, we are the first to report bivalent ligands targeting heterodimeric dopamine (D_2-like) and opioid (μ) receptors.[13] Heterodimerization of D_2R–μOR and D_4R–μOR was formerly suggested by co-immunoprecipitation (co-IP) and bioluminescence resonance energy transfer (BRET) studies in mammalian transfected cells, but further substantiated with our newly synthesized bivalent ligands.

Indeed, bivalent ligand **3.12d** (Figure 3) shows a biphasic binding curve for μOR–D_4R and a 170-fold increased “bivalent affinity” for the D_4R/μOR heterodimer compared to that for the D_4R. Unfortunately, no bivalent interaction D_2R-μOR dimers seems to take place with any of the synthesized ligands, which warrants further optimization with regard to pharmacophore selection, attachment point, length and nature of the spacer. Furthermore, alternative assays (besides radioactive ligand binding) might be explored to assess if the bivalent D_2R-μOR ligands effectively bridge the GPCR dimers. Together, these results indicate that the D_4R and μOR form heterodimers that could become a new therapeutic targets, e.g. for the treatment of addiction and chronic pain.

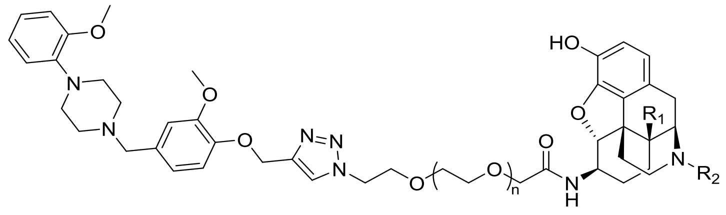

3.12d: n=3, R_1=H, R_2=CH_3

Figure 3. Structure of bivalent ligand **3.12d**.

While the group of Portoghese developed bivalent ligands targeting the mGluR5 and μOR heterodimer,[14] we further corroborated the existence of heteromers of mGluR5 and D_2R, which may represent new targets for the treatment of locomotion, neuropsychiatric disorders, and drug addiction. Bivalent ligand **4.20a** (Figure 4), consisting of a mGluR5 negative allosteric modulator (NAM) connected to the previously used D_2R-ligand via a 20-atom alkylamine spacer showed 4-fold increased affinity for the D_2R in cells expressing both the D_2R and the mGluR5, compared to cells singly expressing D_2R. Likewise, it demonstrated significantly higher affinity and potency for D_2R-mGluR5 compared to its monovalent prcursor **4.19a**. Interestingly, **4.20a** inhibits the forskolin stimulated cAMP formation with a 4-fold higher potency than the monovalent agonist **3.07** in coexpressing cells, indicating that the bivalent binding requires a lower receptor occupation to exert signaling. Overall, compound **4.20a** could be a promising molecular probe to further investigate the protein-protein interaction of D_2R and mGluR5, e.g. in native tissues.

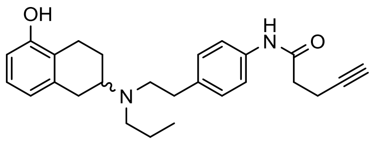

DPAT-alkyne (3.07)

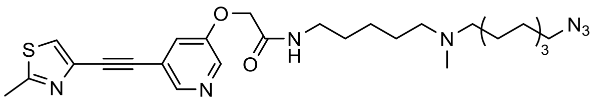

4.19a

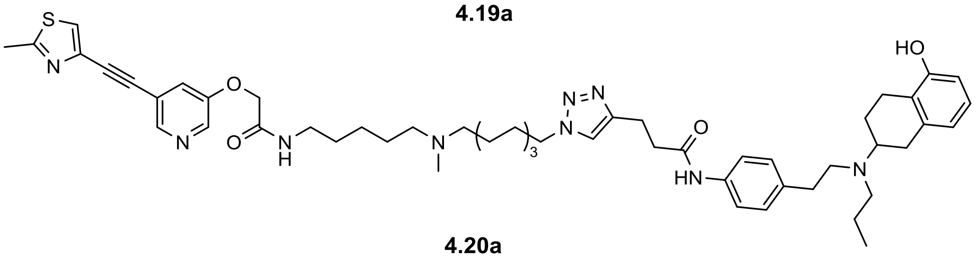

4.20a

Figure 4. Structure of bivalent ligand **4.20a**.

VII.3. From bivalent ligands to drug-like compounds targeting dimeric receptors

VII.3.1. Disadvantages of bivalent ligands

The potential of bivalent ligands as possible therapeutics, as opposed to mere pharmacological tools, remains a topic of discussion.[15] Some obvious hurdles exist in the development of bivalent ligands as drugs, including potential absorption, distribution, metabolism, and excretion (ADME) issues, their unlikeliness to cross the blood–brain barrier, and other issues. These issues are related to some general unfavorable physicochemical properties, particularly their high molecular weight, which does not fit Lipinski's rule of 5 and hence limits the future use of bivalent ligands as potential drugs. Although these barriers seems insurmountable, bivalent ligands may potentially become useful therapeutics by alternative/advanced administration routes, or by converting them into integrated dual acting ligands (see Chapter VII.3.2). More success, however, is expected from "drug-like" compounds that selectively bind and modulate altered binding pockets, which may originate from receptor heteromerization (see Chapter VII.3.3).

VII.3.2. From bivalent ligands to integrated dual acting ligands

A relatively new offshoot from the "classical" bivalent ligands are the so-called integrated dual acting ligands. These molecules are potentially able to interact at two binding sites of a heterodimer simultaneously, possibly resulting in improved subtype selectivity, higher binding affinity, boosted or modified functional activity, and reduced dependence on multiple drug administration regimens.[16]

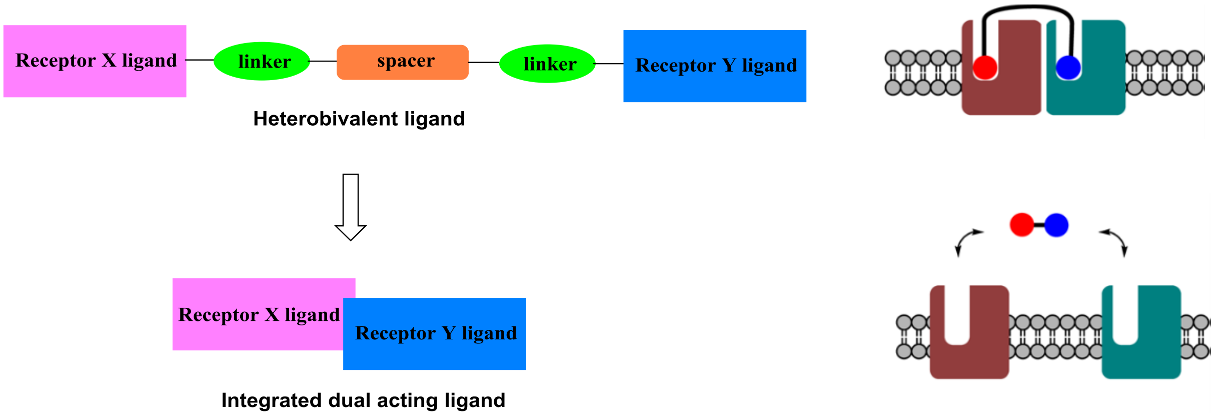
Receptor X ligand
linker
spacer
linker
Receptor Y ligand
Heterobivalent ligand
Receptor X ligand
Receptor Y ligand
Integrated dual acting ligand

Figure 5. (left) Schematic representation of a heterobivalent ligand and integrated dual acting ligand consisting of a receptor X and a receptor Y ligand. (right) Schematic examples of a heterobivalent ligand binding to a heterodimer and an integrated dual acting ligand acting at the two orthosteric sites of two different types of receptor monomers.

Jörg et al. pioneered this concept by converting classical heterobivalent ligands consisting the D_2R agonist ropinirole and the $A_{2A}R$ antagonist ZM 241385 into a so-called integrated and more drug-like dual acting ligand (Figure 6), which maintained the potency of the original pharmacophores at both receptors ($A_{2A}R$ and D_2R).[16] Furthermore, preliminary tests suggest that the integrated dual acting ligand is capable of crossing the blood–brain barrier contrary to the original heterobivalent ligands.

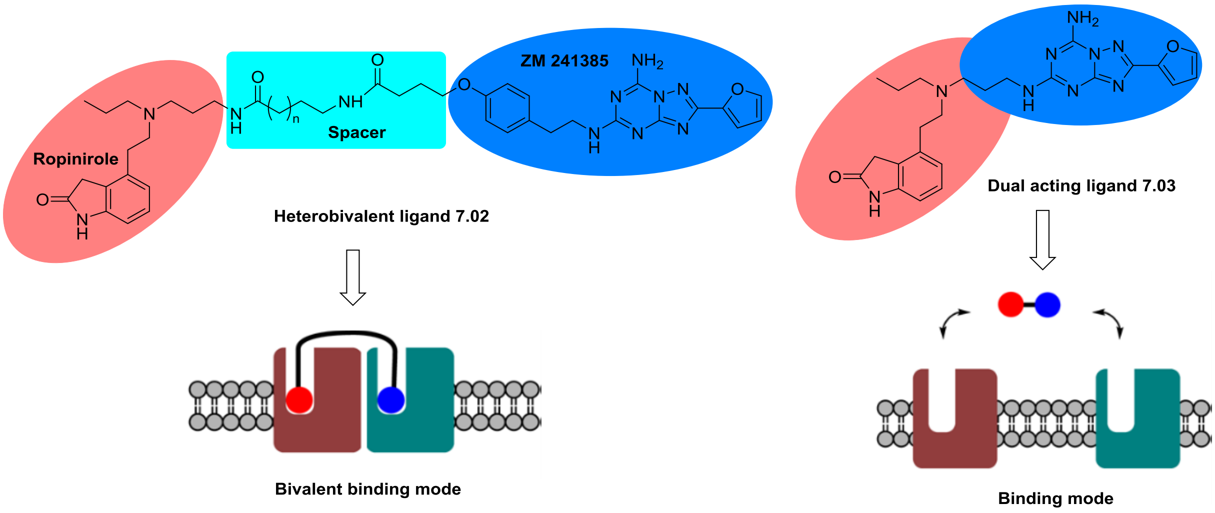
Ropinirole
Spacer
ZM 241385
Heterobivalent ligand 7.02
Dual acting ligand 7.03
Bivalent binding mode
Binding mode

Figure 6. An example of the conversion of a “classical” heterobivalent ligand incorporating the pharmacophores ropinirole and ZM 241385 into an integrated dual acting ligands without the tyramine moiety originally present in ZM 241385.

It is noteworthy that the paradigm of “multiple ligand” approach is not new and many of the drugs originating from screening in animal models, were later found to modulate different targets.[17] Notable examples are the clinically used neuroleptics, which obviously do not obey to the “one-target, one-disease” approach that dominated the pharmaceutical industry for a long time.

VII.3.3. Towards drug-like compounds that selectively activate heterodimeric receptors

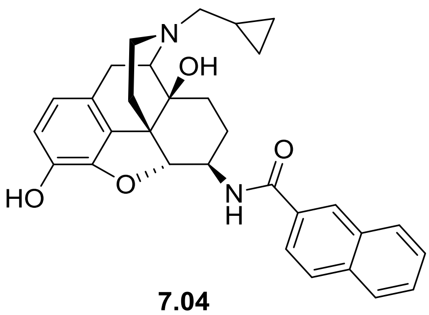

7.04

Figure 7. Molecular structure of *N*-naphthoyl-β-naltrexamine (NNTA).[18]

While the integrated dual acting ligands described in VII.3.2 still share structural similarities with the monovalent ligands that target both protomers, one step further would be the identification of “monovalent-like” ligands that selectely target heterodimeric receptors. Yekkirala et al. [19] discovered that N-naphthoyl-β-naltrexamine (NNTA) (Figure 7) selectively activates heteromeric μ/κ-opioid receptors in HEK-293 cells. In a competition binding assay using [^{3}H]diprenorphine, NNTA was found to bind with very high affinity to cells that express μ- (K_i = 0.077 pM) or κ- (K_i = 0.084 pM) opioid receptors. Interestingly, NNTA was found to be a potent antagonist in cells singly expressing μ-opioid receptor, but an exceptionally potent agonist in cells coexpressing μ/κ-opioid receptors. In the mouse tail-flick assay, NNTA exhibited potent antinociceptive activity. Furthermore, it did not produce significant physical dependence in mice. Taken together, this study afforded important proof-of-concept that it is possible to identify small molecules that selectively activate heteromeric receptors. In this particular case this might lead to the development of new potent analgesics with fewer deleterious side effects.

VII.4. Future Perspectives

In this PhD thesis, we successfully designed and synthesized bivalent D_2-likeR-μOR and D_2R-mGluR5 ligands and identified **3.12d** and **4.20a**, which might be used as molecular probes to further investigate D_4R/μOR and D_2R/mGluR5 heteromers, respectively.

As mentioned before, we observed a biphasic competition binding curve for compound **3.12d** in cells coexpressing D_4R and μOR, which is indicative of a bivalent binding mode. To further validate this, we should perform an additional assay to confirm that addition of a μOR ligand converts the observed biphasic binding curve to a monophasic curve. Molecular modeling studies could further assist in rationalizing the S.A.R. observed with the different bivalent ligands and assist in optimizing their structure.

In our study on D$_2$R-mGluR5 bivalent ligands, **4.20a** showed higher affinity and potency in D$_2$R-mGluR5 coexpressing cells than the corresponding monomeric compounds. However, preliminary data indicate that the poor water-solubility of **4.20a** precludes reliable in vivo studies. Hence, the design bivalent D$_2$R/mGluR5 ligands with enhanced water-solubility is desirable.

Furthermore to further validate the bridging binding mode of bivalent ligands consisting of an agonist and an antagonist described in this thesis, additional assessment of receptor internalization may be the most valuable approach as illustrated by a study of Daniels et al.[20] These authors discovered a bivalent ligand (**7.09**, Figure 8) composed of a μOR agonist and a δOR antagonist.

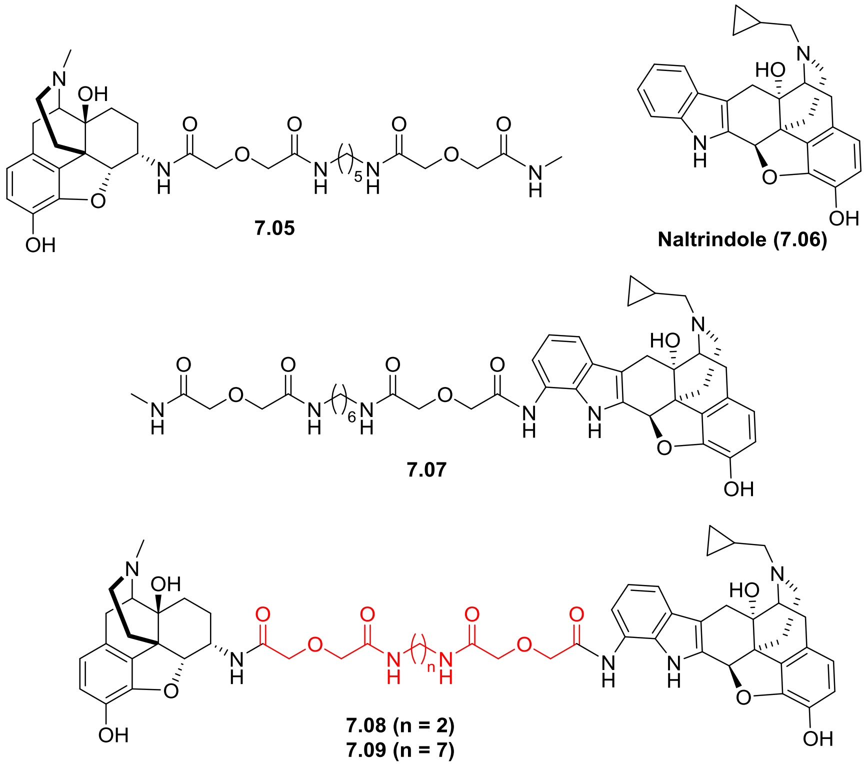

Figure 8. Structures of bivalent ligands (**7.08** and **7.09**), monovalent ligands (**7.05** and **7.07**), and naltrindole (**7.06**).

This bivalent ligand (**7.09**) was shown to inhibit endocytosis of the heteromeric receptors in HEK-293 cells, contrary to **7.08** and monomeric μOR agonist **7.05**.[21] The concept is illustrated in Figure 9.

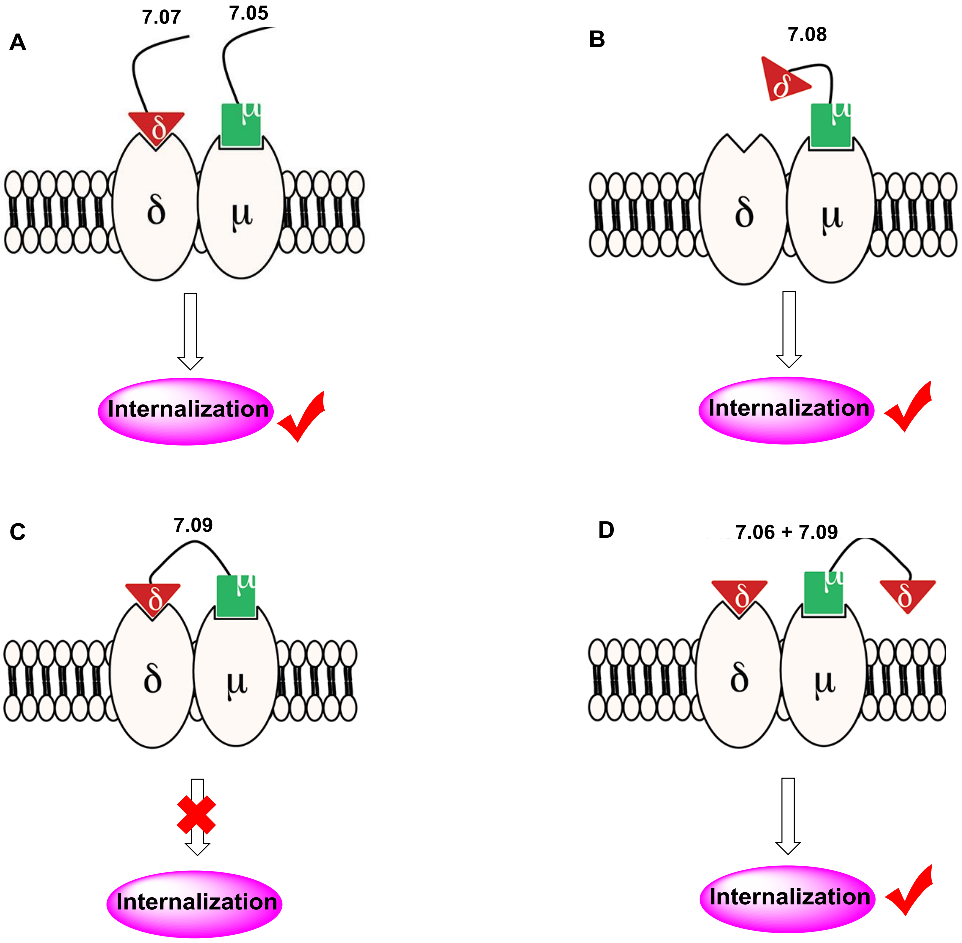

Figure 9. Effect of **7.06** (NTI) on trafficking of μ-δ heterodimer by **7.09**. A cartoon illustrating the effect of delta antagonist on the disruption of bridging protomers in the μ-δ heterodimer.

Also Le Naour et al. assessed the absence of receptor internalization in HEK293 cells for bivalent ligands containing both a μOR agonist and a CB1 antagonist.[22]

Very recently, Lensing et al. elegantly showed that bivalent ligands may induce biased signaling. They constructed a so-called biased unmatched bivalent ligand (BUmBL) targeting melanocortin receptor homodimers.[23] UmBLs also consist of an agonist (His-DPhe-Arg-Trp, **7.10**) and an antagonist (His-DNal(2')-Arg-Trp, **7.11**) pharmacophore connected via various spacers. A selected BUmBL of the human melanocortin-4 receptor (hMC4R) exhibited biased agonism. It potently activated cAMP production (EC_{50} = 1.9–5.9 nM), but minimally stimulated β-arrestin recruitment (⩽55% maximum signal at 10 μM). From a medicinal chemistry perspective, this example demonstrates that targeting receptor dimers may become an attractive approach to induce biased signaling.

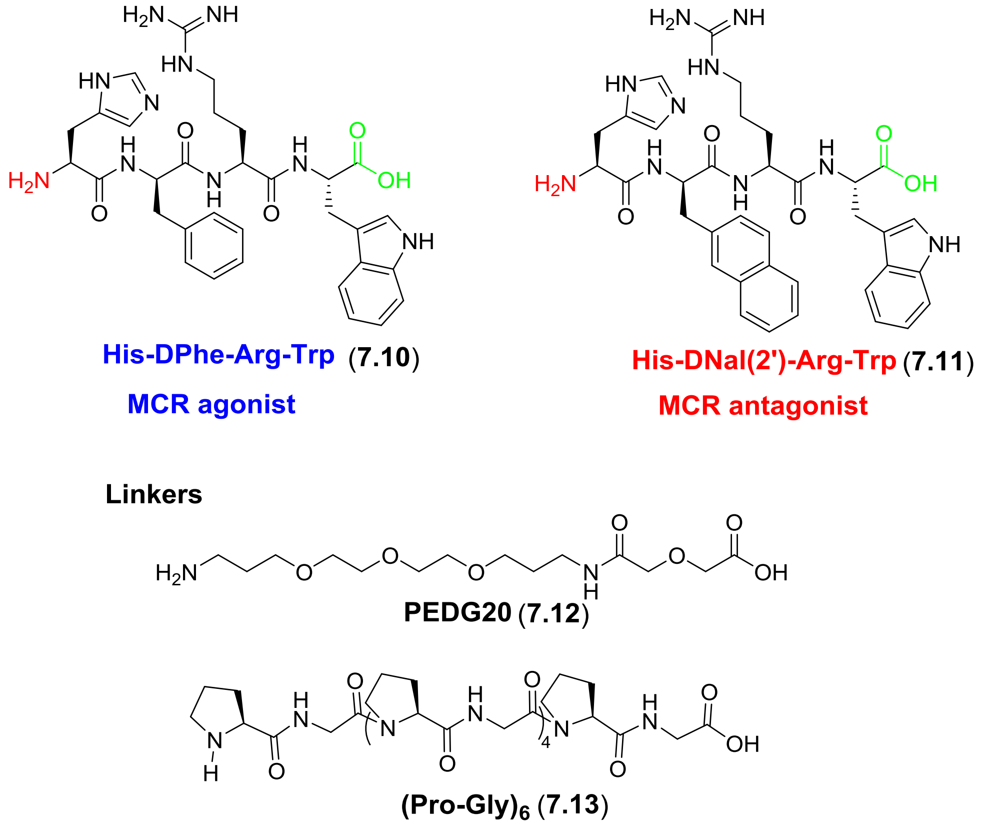

His-DPhe-Arg-Trp (**7.10**)
MCR agonist

His-DNal(2')-Arg-Trp (**7.11**)
MCR antagonist

PEDG20 (**7.12**)

(Pro-Gly)$_6$ (**7.13**)

Figure 10. MCR agonist and antagonist pharmacophores and selected linkers used to construct the bivalent MCR ligands. Red amine and green carboxylic acid represent the attachment points for the linkers.

The cartoon below (Figure 11) explains this concept.[23] Monomeric agonists (blue circle) bind both receptors and activate the cAMP as well as the β-arrestin signal transduction pathway (Figure 11A). Homobivalent agonists (blue circle coupled with black spacer) induce similar signaling (Figure 11B). BUmBLs comprising of an agonist (blue) and an antagonist (red) lead to biased signaling by agonizing the cAMP signaling pathway and antagonizing β-arrestin recruitment upon binding to the asymmetrically signaling homodimer (Figure 11C).

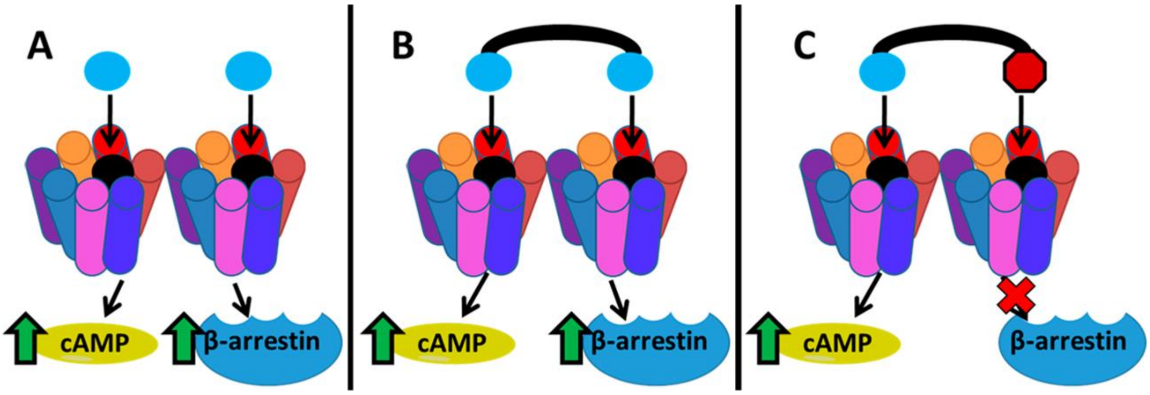

Figure 11. A cartoon illustrating the interaction of ligands with asymmetrically signaling melanocortin homodimers.[23]

These results warrant further assessment of the bivalent ligands synthesized in this thesis to induce biased signaling. In Chapter V, we successfully synthesized a series of fluorescent mGluR5 ligands. Preliminary pharmacological evaluation showed that although the saturation assay via NanoBRET needs to be optimized, the affinity of the red-labeled **5.03** to mGluR5 seems modestly higher than that of **5.10**. Therefore, **5.03** could become a promising tool for investigating D_2R-mGluR5 dimerization at the surface of living cells by NanoBRET.

To better understand the receptor-receptor interaction, the classical approaches such as ligand-induced FRET, BRET or biased signaling and internalization studies are warranted to further assess the correlation of bivalent ligands bridging GPCR dimers, as employed for opioid receptors by Portoghese et al.

Finally, the construction of bivalent ligands **7.14** comprising a D_2R agonist and muscarinic M_1 antagonist (Figure 12) is in progress and successful bivalent ligands may be assessed for reducing locomotion symptoms in Parkinson’s disease. The above mentioned internalization will be applied to study whether these bivalent ligands can bridge the D_2R/M_1R heterodimers.

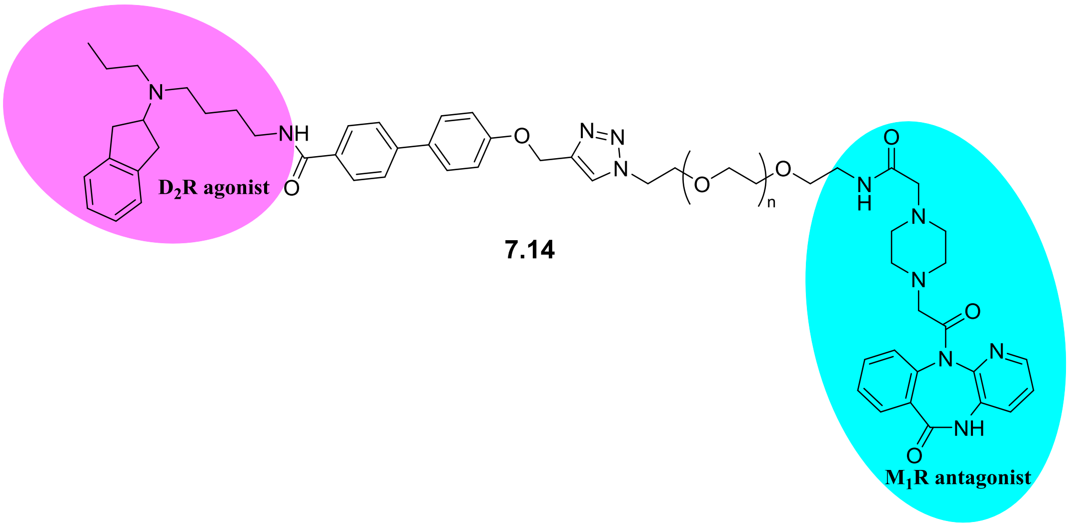

7.14

Figure 12. Design of bivalent ligands consisting of a D_2R agonist and M_1R antagonist.

References

[1] Santos, R.; Ursu, O.; Gaulton, A.; Bento, A. P.; Donadi, R. S.; Bologa, C. G.; Karlsson, A.; Al-Lazikani, B.; Hersey, A.; Oprea, T. I.; Overington, J. P. A comprehensive map of molecular drug targets. *Nat. Rev. Drug Discov.* **2017**, *16*, 19-34.

[2] Huber, D.; Hubner, H.; Gmeiner, P. 1,1′-Disubstituted ferrocenes as molecular hinges in mono- and bivalent dopamine receptor ligands. *J. Med. Chem.* **2009**, *52*, 6860−6870.

[3] Kuhhorn, J.; Gotz, A.; Hubner, H.; Thompson, D.; Whistler, J.; Gmeiner, P. Development of a bivalent dopamine D2 receptor agonist. *J. Med. Chem.* **2011**, *54*, 7911−7919.

[4] Huber, D.; Lober, S.; Hubner, H.; Gmeiner, P. Bivalent molecular probes for dopamine D2-like receptors. *Bioorg. Med. Chem.* **2012**, *20*, 455−466.

[5] Kuhhorn, J.; Hubner, H.; Gmeiner, P. Bivalent dopamine D2 receptor ligands: synthesis and binding properties. *J. Med. Chem.* **2011**, *54*, 4896−4903.

[6] Zheng, Y.; Akgün, E.; Harikumar, K. G.; Hopson, J.; Powers, M. D.; Lunzer, M. M.; Miller, L. J.; Portoghese, P. S. Induced association of mu opioid (MOP) and type 2 cholecystokinin (CCK2) receptors by novel bivalent ligands. *J. Med. Chem.* **2009,** *52*, 247–258.

[7] Yekkirala, A. S.; Kalyuzhny, A. E.; Portoghese, P. S. An immunocytochemical-derived correlate for evaluating the bridging of heteromeric mu-delta opioid protomers by bivalent ligands. *ACS Chem. Biol.* **2013**, *8*, 1412−1416.

[8] Le Naour, M.; Akgün, E.; Yekkirala, A.; Lunzer, M. M.; Powers, M. D.; Kalyuzhny, A. E.; Portoghese, P. S. Bivalent ligands that target μ opioid (MOP) and cannabinoid1 (CB1) receptors are potent analgesics devoid of tolerance. *J. Med. Chem.* **2013**, *56*, 5505−5513.

[9] Akgün, E.; Javed, M. I.; Lunzer, M. M.; Smeester, B. A.; Beitz, A. J.; Portoghese, P. S. Ligands that interact with putative MOR-mGluR5 heteromer in mice with inflammatory pain produce potent antinociception. *Proc. Natl. Acad. Sci. USA.* **2013**, *110*, 11595-11599.

[10] Akgün, E.; Javed, M. I.; Lunzer, M. M.; Powers, M. D.; Sham, Y. Y.; Watanabe, Y.; Portoghese, P. S. Inhibition of Inflammatory and Neuropathic Pain by Targeting a Mu Opioid Receptor/Chemokine Receptor5 Heteromer (MOR-CCR5). *J. Med. Chem.* **2015**, *58*, 8647−8657.

[11] Daniels, D. J.; Lenard, N. R.; Etienne, C. L.; Law, P. Y.; Roerig, S. C.; Portoghese, P. S. Opioid-induced tolerance and dependence in mice is modulated by the distance between pharmacophores in a bivalent ligand series. *Proc. Natl. Acad. Sci. U S A.* **2005**, *102*, 19208-19213.

[12] Portoghese, P. S.; Akgün, E.; Lunzer, M. M. Heteromer Induction: An Approach to Unique Pharmacology? *ACS Chem. Neurosci.* **2017**, *8*, 426−428.

[13] Qian, M.; Vasudevan, L.; Huysentruyt, J.; Risseeuw, M. D. P.; Stove, C.; Vanderheyden, P. M. L.; Van Craenenbroeck, K.; Van Calenbergh, S. Design, synthesis and biological evaluation of

bivalent ligands targeting dopamine D2-like receptors and the μ-opioid receptor. *ChemMedChem* **2018**, *13,* 944 – 956.

[14] Akgün, E.; Javed, M. I.; Lunzer, M. M.; Smeester, B. A.; Beitz, A. J.; Portoghese, P. S. Ligands that interact with putative MOR-mGluR5 heteromer in mice with inflammatory pain produce potent antinociception. *Proc. Natl. Acad. Sci. USA.* **2013**, *110*, 11595-11599.

[15] Shonberg, J.; Scammells, P. J;. Capuano, B. Design strategies for bivalent ligands targeting GPCRs. *ChemMedChem* **2011**, *6,* 963 – 974.

[16] Jörg, M.; May, L. T.; Mak, F. S.; Lee, K. C. K.; Miller, N. D.; Scammells, P. J.; Capuano, B. Synthesis and Pharmacological Evaluation of Dual Acting Ligands Targeting the Adenosine A_{2A} and Dopamine D_2 Receptors for the Potential Treatment of Parkinson's Disease. *J. Med. Chem.* **2015**, *58*, 718−738.

[17] Morphy, R.; Rankovic, Z. Designed multiple ligands. An emerging drug discovery paradigm. *J. Med. Chem.* **2005**, *48,* 6523-6543.

[18] Li, G.; Aschenbach, L. C.; Chen, J.; Cassidy, M. P.; Stevens, D. L.; Gabra, B. H.; Selley, D. E.; Dewey, W. L.; Westkaemper, R. B.; Zhang, Y. Corrections to design, synthesis, and biological evaluation of 6α- and 6β-N-heterocyclic substituted naltrexamine derivatives as μ opioid receptor selective antagonists. *J. Med. Chem.* **2009**, *52,* 1416–1427.

[19] Yekkirala, A. S.; Lunzer, M. M.; McCurdy, C. R.; Powers, M. D.; Kalyuzhny, A. E.; Roerig, S. C.; Portoghese, P. S. N-naphthoyl-β-naltrexamine (NNTA), a highly selective and potent activator of μ/κ-opioid heteromers. *Proc. Natl. Acad. Sci. U S A.* **2011**, *108,* 5098-5103.

[20] Daniels, D. J.; Lenard, N. R.; Etienne, C. L.; Law, P. Y.; Roerig, S. C.; Portoghese, P. S. Opioid-induced tolerance and dependence in mice is modulated by the distance between pharmacophores in a bivalent ligand series. *Proc. Natl. Acad. Sci. U. S. A.* **2005**, *102*, 19208−19213.

[21] Yekkirala, A. S.; Kalyuzhny, A. E.; Portoghese, P. S. An immunocytochemical-derived correlate for evaluating the bridging of heteromeric mu-delta opioid protomers by bivalent ligands. *ACS Chem. Biol.* **2013**, *8*, 1412−1416.

[22] Le Naour, M.; Akgün, E.; Yekkirala, A.; Lunzer, M. M.; Powers, M. D.; Kalyuzhny, A. E.; Portoghese, P. S. Bivalent ligands that target μ opioid (MOP) and cannabinoid1 (CB1) receptors are potent analgesics devoid of tolerance. *J. Med. Chem.* **2013**, *56*, 5505−5513.

[23] a) Lensing, C. J.; Freeman, K. T.; Schnell, S. M.; Adank, D. N.; Speth, R. C.; Haskell-Luevano, C. An in vitro and in vivo investigation of bivalent ligands that display preferential binding and functional activity for different melanocortin receptor homodimers. *J. Med. Chem.* **2016**, *59*, 3112−3128. b) Lensing, C. J.; Freeman, K. T.; Schnell, S. M.; Speth, R. C.; Zarth, A. T.; Haskell-Luevano, C. Developing a biased unmatched bivalent ligand (BUmBL) design strategy to target the GPCR homodimer allosteric signaling (cAMP over β‑arrestin 2 recruitment) within the melanocortin receptors. *J. Med. Chem.* DOI: 10.1021/acs.jmedchem.8b00238. Published date: April 18, **2018**.

Dankwoord – Acknowledgements

Dankwoord ─ Acknowledgements

Here I would like to take this opportunity to thank all people who helped and supported me in the last four years. First of all, I would express my sincere gratitude to my promoter Prof. Serge Van Calenbergh, for providing me an opportunity to carry out my PhD study under his supervision in the Laboratory for Medicinal Chemistry. Thank you, Serge. I still remember the first day when I went to your office. We discussed my PhD research topics and I asked whether it would be possible to evaluate the final compounds by myself. I often cursed myself for asking this question, especially during tough times. But you always supported and encouraged me. Thank you very much, Serge.

Next, I would like to thank my co-promoter Prof. Kathleen Van Craenenbroeck for believing in me and accepting me as her student in the L-GEST-laboratory of toxicology. She taught me how to survive in the tissue culture room, how to use the machines in the lab and how to perform almost all the experiments hand by hand. Thank you so much, Kathleen. In the beginning I only knew some concepts of radioligand binding and functional assays. By joining your laboratory, I learned a lot from you and all the other colleagues. Now I would say proudly I am not only a chemist but also a pharmacologist.

I thank research collaborators, Lakshmi Vasudevan (L-GEST of UGent) for the evaluation of β-arre2 recruitment for μOR; Prof. Francisco Ciruela (University of Barcelona) for assessing the mGluR5 fluorescent ligands by NanoBRET. I also thank Prof. Patrick Vanderheyden (VUB) for fruitfully discussing the radioligand binding assays. I thank Izet for checking the purity of all my final compounds by LC-MS.

I am grateful to colleagues and friends, for being kind and helpful in all aspects. I thank you, Izet, Martijn, Annelies Van Hoeck, Nora, Kiran, Dries, René Chofor, Arno, Joren, Lijun, Fabian, Jonas, Charlotte, Jakob, Yanlin, Cai and Bram from the Laboratory for Medicinal Chemistry and Kamila, Elise (also, thanks for translating summary in Dutch), René Crans, Lakshmi, An, Karen, Annelies Cannaert, Jolien and Prof. Christophe Stove from the L-GEST-Laboratory of Toxicology.

I am deeply thankful to all my family members, for their affection, encouragement and advices at all times. I thank all those, who contributed in their own way during these years of my life.

Finally, I would thank China Scholarship Council (CSC) for financially supporting my PhD study at UGent.

APPENDIX

Scientific curriculum vitae

Scientific curriculum vitae

Name: Mingcheng Qian

Date of birth: September 18, 1988

Nationality: Chinese

E-mail: mqian2014@gmail.com & qmc2010@163.com

EDUCATION

2013 – Present	Ghent University (UGent), Belgium
	PhD Pharmaceutical Sciences
	Thesis title: Synthesis and biological evaluation of novel bivalent GPCR ligands
2010 – 2013	China Pharmaceutical University
	Master of Science in Medicinal Chemistry
2006 – 2010	Jiangsu Normal University
	Bachelor of Science in Biotechnology

RESEARCH FELLOWSHIP

2013 – 2017	PhD Grant from China Scholorship Council

SUPERVISION OF STUDENT

February 2018 – July 2018: Master Student Debora Gagliardini (University of Camerino)

Thesis title: Synthesis and preliminary evaluation of bivalent ligands to study M1-D2 and D2-D2 dimeric receptors.

PUBLICATIONS

- Synthesis and biological evaluation of fluorescent ligands targeting the metabotropic glutamate 5 receptor

  Manuscript in preparation

- Synthesis toward bivalent ligands for the dopamine D_2 and metabotropic glutamate 5 receptors

  Qian, M.; Wouters, E.; Dalton, J. A. R.; Risseeuw, M. D. P.; Crans, R. A. J.; Stove, C.; Giraldo, J.; Van Craenenbroeck, K.; Van Calenbergh, S. *J. Med. Chem.* **2018**, *61*, 8212−8225.

- Design, synthesis and biological evaluation of bivalent ligands targeting Dopamine D_2-like receptors and μ opioid receptor

  Qian, M.; Vasudevan, L.; Huysentruyt, J.; Risseeuw, M. D. P.; Stove, C.; Vanderheyden, P. M. L.; Van Craenenbroeck, K.; Van Calenbergh, S. *ChemMedChem* **2018**, *13*, 944 – 956.

CONFERENCES

- 54th International Conference on Medicinal Chemistry (RICT 2018, Interfacing Chemical Biology and Drug Discovery)

Strasbourg, France, July 4-6, 2018

Poster presentation: Biological evaluation of novel bivalent ligands targeting the dopamine D2 and metabotropic glutamate 5 receptors

- 28th Conference of European Comparative Endocrinologists

Leuven, Belgium, August 21-25, 2016

Poster presentation: Biological evaluation of bivalent ligands for dopamine D_2-like receptors and the μ opioid receptor

- 13th Chemistry Conference for Young Scientists (ChemCYS)

Blankenberge, Belgium, March 16-18, 2016

Poster presentation: Study of the cross-talk between the dopamine D_2-like receptors and the μ opioid receptor

- Annual One-Day Meeting on Medicinal Chemistry of SRC & KVCV (MedChem 2014)

  Braine-L'Alleud, Belgium, November 21, 2014

- Mini-Symposium ADME Profiling

  Leuven, Belgium, March 12, 2014

- Chemistry Conference for Young Scientists (ChemCYS)

  Blankenberge, Belgium, February 27-28, 2014

Overview of synthesized compounds

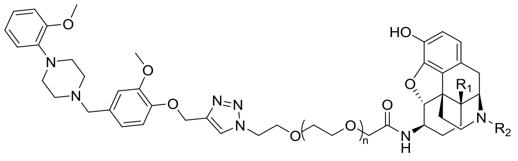

3.12a: n=3, R_1=OH, R_2=CH_2cPr
3.12b: n=4, R_1=OH, R_2=CH_2cPr
3.12c: n=5, R_1=OH, R_2=CH_2cPr
3.12d: n=3, R_1=H, R_2=CH_3
3.12e: n=4, R_1=H, R_2=CH_3
3.12f: n=5, R_1=H, R_2=CH_3

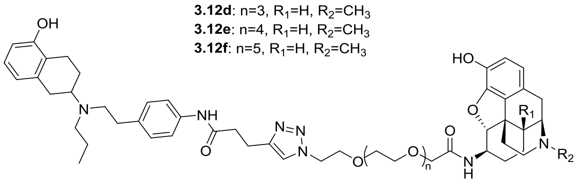

3.13a: n=3, R_1=OH, R_2=CH_2cPr
3.13b: n=4, R_1=OH, R_2=CH_2cPr
3.13c: n=5, R_1=OH, R_2=CH_2cPr
3.13d: n=3, R_1=H, R_2=CH_3
3.13e: n=4, R_1=H, R_2=CH_3
3.13f: n=5, R_1=H, R_2=CH_3

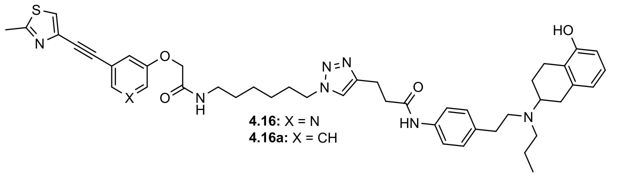

4.16: X = N
4.16a: X = CH

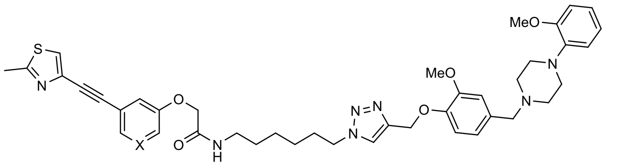

4.16b: X = N
4.16c: X = CH

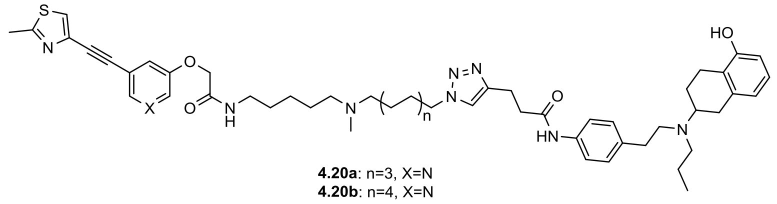

4.20a: n=3, X=N
4.20b: n=4, X=N
4.20c: n=5, X=N
4.20d: n=3, X=CH
4.20e: n=4, X=CH
4.20f: n=5, X=CH

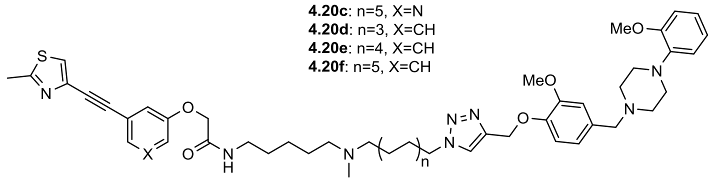

4.21a: n=3, X=N
4.21b: n=4, X=N
4.21c: n=3, X=CH
4.21d: n=4, X=CH
4.21e: n=5, X=N
4.21f: n=5, X=CH

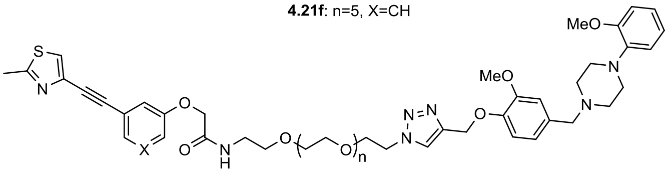

4.18a: n=2, X=CH
4.18b: n=4, X=CH
4.18c: n=2, X=N
4.18d: n=4, X=N

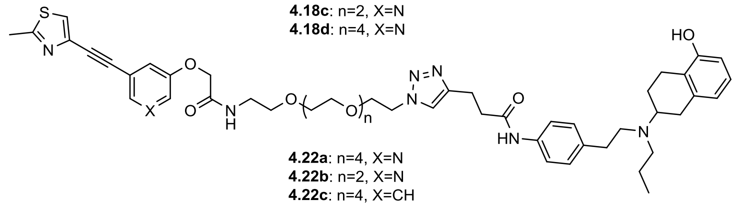

4.22a: n=4, X=N
4.22b: n=2, X=N
4.22c: n=4, X=CH
4.22d: n=2, X=CH

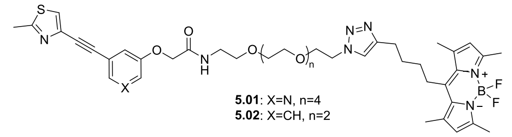

5.01: X=N, n=4
5.02: X=CH, n=2

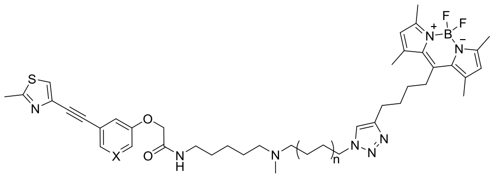

5.05: X=CH, n=5
5.06: X=N, n=5
5.07: X=N, n=3

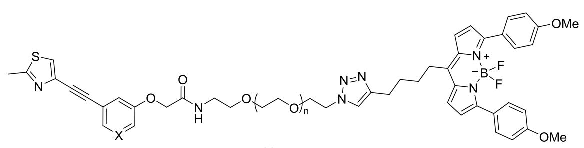

5.03: X=N, n=4
5.04: X=CH, n=2

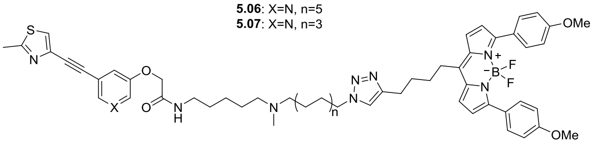

5.08: X=CH, n=5
5.09: X=N, n=5
5.10: X=N, n=3

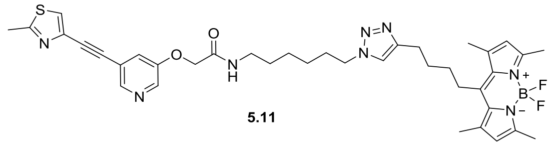

5.11

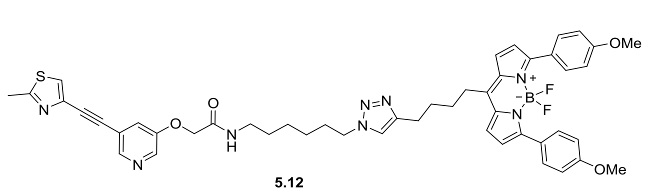

5.12